Foot and ankle functional morphology in anthropoid primates and Miocene hominoids

---

A Dissertation Presented to

the Faculty of the Graduate School

at the University of Missouri

In Partial Fulfillment of the Requirements

for the Degree Doctor of Philosophy

By:

Sharon Kuo

Dr. Carol V. Ward, Dissertation Supervisor

May 2020

Approval Page

The undersigned, appointed by the dean of the Graduate School, have examined the dissertation entitled:

Foot and ankle functional morphology in anthropoid primates and Miocene hominoids

Presented by Sharon Kuo, a candidate for the degree of doctor of philosophy, and hereby certify that, in their opinion, it is worthy of acceptance.

_____

Professor Carol Ward

_____

Professor Kevin Middleton

_____

Professor Casey Holliday

_____

Professor Trent Guess

_____

Professor Nicholas Gidmark

Acknowledgments

First, I would like to thank Carol Ward for admitting me into this program and for your constant support over the past five years. Your enthusiasm for research and belief in your students are unparalleled and I am so lucky to have you in my corner. To the rest of my committee (Kevin Middleton, Casey Holliday, Trent Guess, Nick Gidmark): thank you for greatly improving this dissertation and for your patience throughout this process. In particular, thanks to Kevin for reminding me that it would all be ok and for always answering my stupid questions without making me feel stupid. Nick, I cannot thank you enough for always answering my XROMM questions over the years and for your constant support, beginning with the early phases of this project.

This dissertation would not have been possible without the significant efforts of other people. To the Ross Lab at the University of Chicago, particularly Callum Ross, Michael Granatosky, and Myra Laird, thank you so much for working tirelessly on the XROMM data that made up a significant portion of this dissertation. To Biren Patel, Caley Orr, Sergio Almécija, Jerry DeSilva, and Ellie McNutt: thank you for your generosity with your scan data. I would like to give credit to Morgan Alwell for her help in cleaning the tarsal scans. I owe many thanks to the MU Life Sciences Fellowship for supporting me during my PhD and for Debbie Allen for being so helpful and for feeding all the Life Sciences Fellows. Thank you to Jerry DeSilva for getting me interested in research and for the continued lessons on feet and functional morphology over the years.

The stellar IA faculty offered invaluable expertise and advice, as well as constant emotional support. Ian George, Henry Tsai, Elizabeth Moffett, Amanda Smolinsky, Sarah Peacock, and Kaleb Sellers: thank you for showing me what successful graduate students

look like when I first got here. To Emily Middleton and Faye McGechie, thank you for the insightful conversations, constant support, and truly heartwarming friendship. Sean Greer and Mel Boeyer, thanks for being familiar faces in this program and for being my oldest friends at Mizzou. I am so glad to have some of my Mercyhurst family here with me. Spiro Sullivan, Emily Lessner, and Austin Lawrence, thanks for your friendship and the numerous conversations that helped me in my research and in life. Ian Cost (and your better half), thanks for the nerdy science conversations, constant pep talks, confidence boosters when I didn't really deserve them, and random bird identifications. Saturday morning study breakfasts at the Cost house helped make Columbia feel like home.

Outside of IA, many people got me through my PhD. There are too many people to thank individually in this regard, so to all of you, thanks for being there for me to talk about things other than school, for reminding me that the world outside of this program indeed still exists, for being my travel buddies and pen pals, for editing (especially Luke A.), for telling me to calm down whenever I needed to, and for sending papers that I didn't have access to but didn't have time to ILL over the years. To Gracie Humaita and the Black Sheep, thank you for saving what is left of my sanity and also pulling me back into the world outside of this dissertation. Thank you to Ashley Hammond and KFFS for swooping in while I was in the darkest dissertation depths to remind me of why I love this field and the people with whom I am lucky enough to share it.

To my family, thank you for forgiving missed events, trips, and phone calls so that I could finish this program and for your undying support. I couldn't have done this without you.

Table of Contents

List of Figures

List of Tables

Abstract

Locomotion is essential for survival in many taxa. It also varies greatly among organisms, including primates. Studying locomotor diversity in extant and fossil primates requires an understanding of form-function relationships. This is particularly true in the foot and ankle, as the foot directly contacts the substrate and tarsals are well-represented in the fossil record. Morphological differences alone provide limited aid when inferring locomotion from fossil tarsals in the absence of *in vivo* biomechanical consideration. This dissertation takes a three-step approach to analyze both *in vivo* rotations in the foot and ankle as well as morphological variation in tarsal form in extant anthropoid primates and Miocene hominoids and will provide important new data from a poorly understood anatomical region.

The amount of talocrural, subtalar, and transverse tarsal rotations among the tibia, calcaneus, and navicular were visualized and quantified during the gait cycles using biplanar fluoroscopy and 3D scans of marked bones, a method known as x-ray reconstruction of moving morphology (XROMM) in rhesus macaques (*Macaca mulatta*). This study supported previous hypotheses that the midfoot break occurs distal to the cuboid, demonstrated the predominance of plantarflexion/dorsiflexion at the talocrural joint on a flat surface, quantified conjunct rotation at the subtalar joint, showed evidence that the transverse tarsal joint does not function as a single joint complex.

Geometric morphometric techniques were used to describe and quantify shape differences in isolated tarsals of extant anthropoid primates. PCA and M/ANOVA analyses were run on a Procrustes-fit landmarks taken on broad range of anthropoid tali

(n = 241), calcanei (n = 230), cuboids (n = 282), and naviculars (n = 254). In addition to the typical geometric morphometric techniques, the interlandmark distances that accounted for the greatest amount of variation in this sample were isolated and plotted against centroid size. Phylogenetically controlled generalized least squares analysis revealed which of these measurements were related to locomotion. The relative orientation of the posterior subtalar facet on the talus, talar neck length, calcaneal tuber height, calcaneal anterior length, cuboid length, and navicular anteroposterior length were the morphologies that best separated based on differences in locomotion.

The same landmarks were taken on 16 Miocene hominoid tarsals in order to infer foot function based on tarsal form. The geometric morphometric technique of the extant sample allowed for subsetted analyses for incomplete fossils. Early Miocene taxa *Ekembo, Proconsul,* and *Rangwapithecus* shared common bony features that suggest that they were generally above branch quadrupeds. *Nacholapithecus* showed a mixed or varied locomotor behavior. *Oreopithecus* was shown to not be bipedal, as previously hypothesized, but rather was suspensory.

This dissertation provided the first ever quantification of intertarsal and talocrural rotations in anthropoid primate feet and ankles and an analysis of how rotations within and among joints are related. It also provided a quantification of shape differences in tarsals of extant anthropoid primates and fossil Miocene hominoids. Together, the *in vivo* biomechanics and morphometrics provide insight into form function relationships as well as a foundation for future studies of primate locomotor diversity.

Chapter 1: Introduction

Locomotion in Extant Anthropoid Primates

Anthropoid primates (Old World monkeys, New World monkeys, and apes) display a diverse array of locomotor repertoires (Fleagle 1984; Hunt et al., 1996). Understanding the evolution of this locomotor diversity is intertwined with understanding the evolution of the clade, which involves reconstructing locomotor adaptations of fossil taxa. Locomotion is one of the most important aspects of survival and it varies greatly among taxa (Alexander, 1982; Biewener & Patek, 2018). As a result, understanding the mechanisms and diversity of locomotion among living and fossil taxa has been one of the largest research interests in biology (Muybridge, 1887; Alexander, 1982; Taylor et al., 2010). The different ways in which organisms interact with their environment and how that has changed over time with varying selective pressures on locomotion, especially in our own evolutionary history and that of our closest living relatives is of particular importance. The evolution of suspensory locomotion in anthropoid primates, as well as the changing way in which primate taxa interact with their environment are of particular interest in the primate fossil record. Because many fossil hominoids have no living analogs, reconstructing locomotor behavior requires careful consideration of the functional anatomy of each joint complex (Rose, 1993). Sound locomotor reconstructions are critical to interpreting many of the key transitions in hominoid evolutionary history,

not the least of which is the evolution of suspensory locomotion in hominoids or terrestrial bipedality in the hominin lineage.

Why the Foot?

Foot and ankle morphology are useful when interpreting locomotor repertoire in fossil taxa, as feet interact directly with the substrate on which an animal is moving (Vereecke et al., 2005a; Boyer et al., 2013). The orientation and shape of joints are hypothesized to reflect possible movements of the foot and, therefore, how the foot was used (Langdon, 1986). The foot is a complex structure that consists of seven tarsals, five metatarsals, and fourteen phalanges (Figure 1). Despite its importance to locomotion and perhaps due to its complexity, the foot is often understudied, particularly the tarsals (McNutt, 2018). A thorough analysis of tarsal morphology is sorely needed. Not only would such an analysis demonstrate how foot bone morphology reflects locomotion in extant primates, but it would allow us to interpret many tarsal bones known from fossil hominoids and would therefore improve our interpretation of the locomotor repertoires of these fossil taxa (McNutt et al., 2018). A more accurate understanding of the relationship between tarsal form and locomotor behavior is especially important, because tarsal bones are commonly-preserved in the primate fossil record. However, their functional morphology is not well understood in extinct taxa because there are few validated biomechanical models on which to base locomotor interpretations.

Intertarsal Joint Movements

Movements at the intertarsal joints (Figure 2) are hypothesized to vary among anthropoids to reflect their suspensory, quadrupedal, arboreal and/or terrestrial locomotor specializations (Gebo, 1989). Below branch suspensory locomotion is hypothesized to be facilitated by more intertarsal mobility (Close et al., 1967), leading to more inversion (facing the sole of the foot medially, Figure 3) than during terrestrial locomotion (Holowka et al., 2017). The subtalar and transverse tarsal joints of the foot, which are comprised of the talus, calcaneus, cuboid, and navicular (Figure 2; Figure 4) are thought to be primarily responsible for inversion, eversion (Figure 3), and midfoot flexibility associated with suspensory locomotion (Manter, 1941; Close et al., 1967; Holowka et al., 2017).

To date, however, we do not fully understand the precise movements that occur at these joints during a stride cycle and how these movements differ among individuals and among taxa. This deficit is partially due to the difficulty in quantifying tarsal movements and relative positions during locomotion to relate this information to bone morphology. By evaluating morphological variation among anthropoids at these intertarsal joints and using *in vivo* data to quantify joint rotation, we can understand the foot as a functional unit and unite form and function to fossils. Comparative studies are limited in their utility without testing the functional models on which these inferences are based. This dissertation aims to study both morphology and *in vivo* locomotion in extant anthropoids to provide a validated basis for making inferences about the positional repertoire of fossil taxa.

Tarsal Functional Morphology in Extant Anthropoid Primates

By far, the most thoroughly-studied primate locomotion is that of modern humans. Although human locomotion differs significantly from non-human primate locomotion, movements at the ankle and intertarsal joints are best understood in *Homo sapiens*.

Talocrural Joint

The talocrural joint, or the joint between the tibia/fibula and the talus (Figure 2) is primarily responsible for plantarflexion and dorsiflexion (Figure 3) but also is thought to experience some inversion and eversion (Figure 3) (Wright et al., 1964; Rasmussen & Tovborg-Jenson, 1982; Rome, 1996; Youlatos & Koufos, 2010). In humans, the distal tibia articulates with a relatively flat proximal talar surface, making the long axis of the leg orthogonal to the transverse axis of the foot (Latimer et al., 1987) (Figure 5). Engsberg and Andrews (1987) and Latimer and colleagues (1987) postulated that this roughly orthogonal articulation results in the predominant motion at the talocrural joint to be plantarflexion and dorsiflexion in humans. Engsberg and Andrews (1987) further hypothesized that the predominantly sagittal motion at this joint is beneficial for human bipedal locomotion, where deviation from sagittal movements results in a loss of propulsive efficiency and increases the risk of injury, so much so that excessive mediolateral movement or hyperpronation (the combination of eversion and dorsiflexion, in excess) at this joint is often corrected in shod populations through corrective orthotics. Lewis (1980a) described the proximal articular surface on the talus as convex and broad (Figure 6) and that it forms a trochlea with a shallow depression between the two

trochlear rims (Figure 6). The proximal trochlear surface is continuous with the medial and lateral malleolar surface for the medial tibial malleolus and lateral fibular malleolus, respectively (Figure 7). Latimer et al. (1987) measured 35˚ to 60˚ of excursion between extreme plantarflexion and dorsiflexion in a sample of 40 modern humans using an osteological sample, although previous studies have reported wider ranges of dorsiflexion from 10˚ to 51˚ and plantarflexion from 15˚ to 56˚ (see Rasmussen & Tovborg-Jenson, 1982). Wan and colleagues (2006) found that due to the curved shape of the talar trochlea (Figure 6) and the flat distal tibial articular surface, less than 50% of the articular cartilage of the talus is in contact with the tibia, yet noted that the joint transmits ground reaction forces between two to three times the body weight during locomotion. Motions at this joint establish foot position and it is therefore key during locomotion.

Subtalar Joint

The subtalar joint (Figure 2) is between the talus and calcaneus (Figure 4) (Netter, 2010). Researchers (e.g., Close et al., 1967; Engsberg & Andrews, 1987; Riegger, 1988; Sarrafian, 1993; Leardini et al., 2001) that have studied the subtalar joint have noted that unlike the other joints discussed in this dissertation, the subtalar joint has three articulations between the talus and calcaneus: the anterior, middle, and posterior subtalar joints (Figure 8). These joints, however, are often considered to function together, partially due to the interlocking nature of the talus and calcaneus, particularly by clinicians due to the similarities of the motions that occur at these joints (Rockar, 1995). The posterior articulation between the talus and calcaneus is concave on the talar body and convex on the calcaneal body (Figure 2; Figure 8). The middle subtalar articulation

occurs between the talar neck and the sustentaculum tali, whereas the anterior subtalar joint is located distally (Figure 8), between the inferior aspect of the talar head and the medial aspect of the superior surface of the distal end of the calcaneus (Riegger, 1988; Rockar, 1995). As a result of the multifaceted articulations, motions at the subtalar joint do not strictly align with any cardinal body plane and has been described as "triplanar" (Rockar, 1995), "screw-like" (Manter, 1941), or "about an oblique compromise axis" (Lewis, 1980). The complex motions at this joint have led some, such as Conoy and colleagues (1983) and Parr and colleagues (2012) to consider it an important joint to study when considering substrate use and locomotor differences among animals, particularly primates.

Transverse Tarsal Joint

The transverse tarsal joint complex consists of the talonavicular and calcaneocuboid joints (Figure 2), yet are often considered one joint complex due to their coplanar location and the assumption that they move in conjunction with each other (Manter, 1941; Bojsen-Møller, 1979; Lewis, 1980; Riegger, 1988; Cornwall, 2002). Unlike the functional grouping of the subtalar articulations, however, this joint complex consists of two separate joints that are located between two independent pairs of bones (Figure 2), rather than multiple articulations between two bones (Netter, 2010). The talonavicular joint (Figure 2) is the articulation between the distal end of the head of the talus and the cup-like articulation of the proximal navicular (Figure 9) (Manter, 1941). The calcaneocuboid joint (Figure 2) in humans has been described as "mildly saddle shaped" (Prang, 2016), or "as a sector of one end of an hour-glass shaped surface"

(Bojsen-Møller, 1979). The surfaces of the joint are highly congruent, with a proximal cuboid bony protrusion articulating with a depression in the distal calcaneus (Figure 10). In humans, the transverse tarsal joint, and midfoot in general, are thought to be more stiff in order to increase propulsive efficiency during bipedal locomotion (Elfman & Manter, 1935; Riegger, 1988; DeSilva, 2010; Prang, 2016). Gomberg (1985) has hypothesized that movements at this joint are minimized in order to turn the human foot into a lever during the second half of stance phase. Gomberg (1985) describes motions at the transverse tarsal joint during stance phase in human locomotion: due to the transverse arch, when the foot flattens on the ground, the navicular rotates counterclockwise, while the cuboid rotates clockwise, resulting in opposing rotations at the talonavicular and calcaneocuboid joints. The importance of midfoot stability in humans during bipedal locomotion as well as the midfoot mobility in nonhuman primates (discussed below) make the transverse tarsal joint an important joint complex to investigate further.

Human tarsals are thought to be highly specialized among primates for bipedal locomotion (Elfman & Manter, 1935; Harcourt-Smith & Aiello, 2004; McNutt et al., 2018), and similar degrees of specialization related to locomotion are evident in tarsals across many taxa, including bovids. Bovid limb posture differs markedly from primate limb posture in that bovids are unguligrade, meaning they walk on their toes and their metapodials have become relatively elongated (Gregory, 1912; Webb et al., 1977; Theodor, 2001). Bovid astragalar motion is largely constrained to the sagittal plane, reducing eversion and inversion during locomotion (Barr, 2014). This morphological constraint reflects their predominantly cursorial locomotor behavior (Barr, 2014). Bovids also serve as an example of how tarsal morphology has been used to reconstruct

locomotor differences using differing morphologies on isolated bones. Despite the fact that relatively little movement occurs at the intertarsal joints due to this unique limb posture, bovid tarsals are commonly studied for differences among taxa that move differently (Barr, 2014). Part of their utility is the ability to infer habitat preference from astragalar morphology (Barr, 2014). Bovids that live in open environments rely on cursorial abilities to avoid and evade predators, whereas bovids that live in forested environments have few cursorial needs and therefore display greater ability to walk on variable substrates (Kappelman, 1988; Barr, 2014). Barr (2014) found that cursorial bovids display shorter astragali for faster plantarflexion during rapid movement on open land whereas bovids who live in more forested areas display a longer astragalus to increase power during plantarflexion. Cursorial taxa exhibit greater range of angular excursion to increase stride length and have a larger articular surface area on the proximal trochlea to dissipate loads associated with consistent fast running (Barr, 2014). Morphological distinctions such as these among bovid substrate uses displays the utility in analyzing gross shape differences among taxa that move in different manners. These morphological differences can then be used to reconstruct both the locomotion of extinct bovids in the fossil record and aid in paleoenvironmental reconstructions.

Nonhuman Primate Tarsal Morphological Variation

Outside of humans, primate tarsal morphological variation and how it may relate to locomotor biomechanics is less well-known. Much like how many of the adaptations in human tarsals are thought to facilitate bipedal locomotion in humans and bovid astragali are used to infer locomotor type and environmental preference, tarsal morphology is

thought to reflect how animals negotiate variable substrates across nonhuman primates (Gebo, 1986, 1989; Strasser, 1988; MacLatchy et al., 2000; DeSilva, 2009; Boyer et al., 2013). Taxa with different locomotor emphases are expected to vary in pedal functional morphology (Prost, 1965; Ripley, 1967; Walker, 1974; Dagosto & Gebo, 1998; Byron & Covert, 2004; Holowka et al., 2017). Moving on terminal branches, climbing, and suspensory activities require strong grasping, which in turn involve midfoot flexibility, especially during flexion and inversion (Grand, 1968; Gebo, 1993). Grasping also requires inverted foot postures and increased ranges of motion during inversion and eversion for positioning the foot on variably-oriented and curved substrates (Cartmill, 1974; Langdon, 1986). In contrast, quadrupeds that mainly travel on large-diameter branches or on the ground rely more heavily on effective, lever-like pedal propulsion (Cartmill, 1974), likely related to restricted midfoot flexibility, diminished hallucal prehensile grasp, and tarsal morphology well-suited for longitudinal rather than transverse stresses (Langdon, 1986; Gebo, 1993). To date these hypotheses have not been tested *in vivo* and are based on functional inferences rather than actual locomotion in nonhuman primates. The primate taxa included in this study and their phylogenetic relationships are presented in Figure 11.

Interspecific differences in tarsal position and movement related to grasping and inversion is hypothesized to be evident in the talocrural, subtalar, and transverse tarsal joints (Figure 2).

Primate Comparative Anatomy in the Talocrural Joint

Talocrural joint morphology has been found to differ among taxa with different substrate preferences (Simons et al., 2019). Sondaar and Van der Geer (2002) hypothesized that trapezoidal talar trochleae are related to midfoot flexibility and pedal prehension. They explained that more wedged trochleae allow for more mediolateral movements when the foot is in a plantarflexed position due to the tapering of the talar trochlea posteriorly (Figure 12). The trapezoidal shape of the wedged trochleae allows for adduction and abduction of the foot in plantarflexion (Sondaar and Van der Geer, 2002). The authors note, however, that this morphology leads to instability at the ankle during plantarflexion, which is why they hypothesized that quadrupedal taxa that require stability during plantarflexion possess less wedged, more rectangular trochleae (Figure 12).

Asymmetrical trochlear crests are also thought to reflect habitually inverted foot postures (Figure 13) (Latimer et al., 1987; Dunn et al., 2014; Knigge et al., 2015). As demonstrated by Dunn and colleagues (2014) in gorilla tali, the degree of asymmetry of the talar trochleae was greater in lowland gorillas, which exhibit more arboreal behaviors than their more terrestrial highland counterparts. The authors attribute the difference in morphology to increased foot and ankle inversion in the gorillas that climb more to decrease shearing stresses on the talocrural joint (Dunn et al., 2014), though Strasser (1988) noted that asymmetrical trochleae are also seen in terrestrial cercopithecoids and therefore this pattern requires further study across taxa (Gebo, 1989). In general, terrestrial or leaping taxa are reported to have higher, broader, minimally-wedged trochleae to ensure increased stability during plantarflexion (Langdon, 1986; Strasser, 1988; Gebo et al, 2001; Turley & Frost 2013).

Primate Comparative Anatomy in the Subtalar Joint

The subtalar joint, as previously discussed, is a complex joint with non-sagittal movements that is hypothesized to vary among taxa that locomote differently. Langdon (1986) hypothesized that the long axis of posterior subtalar articulation is more perpendicular to the long axis of the foot in suspensory anthropoid taxa to facilitate a greater degree of rotation at the joint in a transverse plane (Lewis, 1980). The subtalar joint is also hypothesized to be more mediolaterally curved (referred to as L-shaped in Lewis (1980); Figure 14) to allow for more rotation of the talus relative to the calcaneus in more foot postures in suspensory taxa to facilitate transverse rotation of the foot (Lewis, 1980; Langdon, 1986). Most inversion and eversion occurs at the subtalar and transverse tarsal joints, though how much and when in the gait cycle the most inversion and eversion occur requires further *in vivo* study as well as a broad comparative analysis of the morphology at these joints (Manter, 1941; Wright et al., 1964; Close et al., 1967; Lewis, 1980; Sarrafian, 1993).

Primate Comparative Anatomy in the Transverse Tarsal Joint

Both joints that comprise the transverse tarsal joint (i.e., the calcaneocuboid and talonavicular joints) are described as becoming close-packed in extension for stability, particularly in taxa that require more foot propulsion than mobility (Gebo & Schwartz, 2006). The peg-and-socket morphology of the calcaneocuboid joint (Figure 15), wherein the projection of the proximal cuboid that fits into the depression of the distal calcaneus, is hypothesized to allow for increased mobility without dislocation during extreme inversion while grasping small branches (Bojsen-Møller, 1979; Rose, 1986; Gebo, 1993).

The amount of movement that occurs at this joint during locomotion has not been quantified. Movement at the talonavicular joint, however, is hypothesized by Prang (2016) to be more restricted in terrestrial taxa than in suspensory taxa, but this has not been thoroughly explored across anthropoids with different locomotor types. The role of both joint complexes in producing foot inversion and eversion, as well as how much and when in the gait cycle the most inversion and eversion occur and to what degree these joints work as one joint complex all requires further *in vivo* study in addition to a broad comparative analysis of the morphology at these joints (Manter, 1941; Wright et al., 1964; Close et al., 1967; Lewis, 1980).

Reconstructions of Miocene Hominoid Locomotion

Elucidating tarsal functional morphology will provide crucial information for locomotor reconstructions of fossil taxa, particularly Miocene hominoids. Tarsals are frequently preserved in the Miocene hominoid fossil record, when early hominoid locomotor diversity could be explored, but most Miocene hominoid taxa exhibit a combination of bony morphologies not seen in extant taxa, confounding inferences about their locomotor adaptations (Rose, 1993, 1994; Ward, 1998); additionally, some tarsals are often found in isolation. For these reasons, it is necessary to carefully consider the functional implications of morphological variation among extant and fossil taxa to provide accurate locomotor reconstructions for these specimens and the evolution of body form and locomotor adaptation in the fossil specimens that include preserved tarsal elements.

Ekembo heseloni and *Ekembo nyanzae*

The best represented genus in the Early Miocene is *Ekembo* (20-17 Ma) from Kenya (McNulty et al., 2015; Figure 16). These species appear broadly similar postcranially (Rose, 1994), although they differ in body size, with *E. heseloni* estimated to have weighed roughly 10.9 kg and *E. nyanzae* up to 36 kg (Rafferty et al., 1995). *Ekembo nyanzae* and *E. heseloni* had a roughly even intermembral index (i.e., the arms and legs were more even than in suspensory primates), similar to those of a macaque (Figure 16) (Rose, 1994; Dunsworth, 2006), a long, flexible spine (Ward, 1993) and narrow pelvis, though with laterally facing ilia (Ward, 1993). Ward (1993) implies that these morphologies are indicative of a narrow thoracic cage, similar to extant above branch quadrupedal monkeys, even though it lacked a tail (Ward et al., 1991). Unlike extant apes, *Ekembo* displays bony contact between ulna and wrist (Beard et al., 1986; Ward, 2007), suggesting at least some quadrupedal behavior. *Ekembo* is interpreted as a pronograde quadruped, however, Rose (1993) points out that the humeral trochlea is neither strongly spool shaped like an extant hominoid nor cylindrical like an extant monkey. Additionally, the ulnar olecranon process is retroflexed (Rose, 1993), indicating loading similar to that in arboreal quadrupeds. This led Rose (1993) to conclude that the elbow of *Ekembo* appears to be that of a quadruped that is also adapted for loading in a wide range of postures. This locomotor repertoire is unlike that of any living primate, suggesting a more varied locomotor mode including clambering over multiple supports (Beard et al., 1993; Rose, 1994; McNulty et al., 2015). Fortunately, multiple tarsal elements, including a calcaneus from *E. heseloni* (Figure 17) and a talus (Figure 18) and two calcanei (Figures 19-20) from *E. nyanzae* are preserved, which could elucidate the

locomotor behaviors of this genus (DeSilva, 2008), but these pedal specimens have not been analyzed in detail (Dunsworth, 2006).

Proconsul major

Another basal hominoid from the Miocene is *Proconsul major*, known from about 20 Ma in Kenya (McNulty et al., 2015). This taxon is mainly represented by cranial material (Figure 21) (Rafferty et al., 1995; Kelley, 1997; Hill et al., 2013); however, it also has a preserved calcaneus (Figure 22) and talus (Figure 23) (Lewis, 1980b). Previously grouped with the two *Ekembo* species, *Proconsul major* was estimated to be around 75 kg (Rafferty et al., 1995). *P. major* tali and calcanei have been reconstructed as similar to *Ekembo* skeletally (Leakey et al., 1988; Ward, 1998). In fact, the two genera were previously assigned to the same genus, but dietary, ecological, and morphological differences between the specimens found at the two sites have led to the differentiation of *Proconsul* and *Ekembo* (McNulty et al., 2015). In light of this split into two genera, the grouping of locomotor adaptations warrants reevaluation.

Rangwapithecus gordoni

Rangwapithecus gordoni (Figure 24) is another early Miocene hominoid that has an associated calcaneus (Figure 25) and talus (Figure 26) (C. Ward, 1997). This specimen appears to have had a flatter, more wedge-shaped talar trochlea and a flatter anterior talar facet on the calcaneus (DeSilva, 2008), suggesting that it may have engaged in vertical climbing and a more varied locomotor repertoire than *Ekembo* or *Proconsul*, but more

broad comparisons of *R. gordoni* with both extant anthropoid primates as well as other Miocene hominoids is required.

Nacholapithecus kerioi

The middle Miocene is hypothesized to contain more locomotor diversity among hominoids than the early Miocene based on the fossils from this time period (Benefit & McCrossin, 1995). *Nacholapithecus kerioi* (Figure 27) is known from a partial skeleton that dates to 15 Ma from Kenya (Ishida et al., 1999, 2004). Torso structure for *Nacholapithecus* is inferred to be long, narrow, and monkey-like, as in *Ekembo*, with six lumbar vertebrae and no tail, but its limbs differ from both *Ekembo* and extant arboreal quadrupeds (Nakatsukasa et al., 1998; Ishida et al., 1999, 2004; Ward, 2007). The forelimbs are longer than the hind limbs (Figure 27), and the shoulder joint appears to better facilitate abduction related to suspensory locomotion compared to extant monkeys (Nakatsukasa et al., 1998; Ward, 2007). The elbow indicates *that N. kerioi* engaged in forelimb-dominated climbing, but Nakatsukasa and Kunimatsu (2009) argue that the phalanges lack specializations for climbing, such as "pronounced shaft curvature, strong flexor sheath ridges, deep trochlear groove, proximally oriented proximal articular surface of the proximal phalanx" (p. 111). The combination of monkey-like morphology with relatively large upper limbs is not known from any extant primate, therefore no extant model can be used to interpret the locomotion of *N. kerioi*. The skeleton, however, preserves a damaged talus and calcaneus (Figure 28), which can inform its unusual locomotor morphology and function based on whether its foot was more capable of strong pedal grasping and varied foot postures.

Oreopithecus bambolii

From the late Miocene, *Oreopithecus bambolii* (Gervais, 1872) is dated to 9-7 Mya (Köhler & Moyà-Solà, 1997) from Italy and is known from a crushed partial skeleton (Figure 29), as well as from many other isolated postcranial elements (Harrison, 1986; Sarmiento, 1987; Rook et al., 1999). It has a high intermembral index like that of *Pongo* and *Pan*, a short pelvis, a reduced lumbar region (Straus, 1963; Russo & Shapiro, 2013). Notably, *Oreopithecus* has short phalanges compared to extant nonhuman apes (Köhler & Moyà-Solà, 1997). Some (Köhler & Moyà-Solà, 1997; Rook et al., 1999) have postulated that *Oreopithecus* was not ape-like in its locomotion, but rather engaged in bipedality, with evidence of lumbar lordosis, a short ischium, a hominin-like diaphyseal angle of the femur, short phalanges, and a foot that has a medially oriented line of leverage as human-like foot proportions; however, a thorough analysis of tarsals could provide a biomechanically-based reconstruction of its locomotion (McNutt et al., 2018). *Oreopithecus* preserves two calcanei, (Figures 30-31), two tali (Figures 32-33), two cuboids (Figures 34-35), and a navicular (Figure 36).

None of these taxa resembles extant hominoids in all ways, making locomotor reconstructions using analogies difficult. This, in turn, confounds the ability of researchers to reconstruct the locomotor evolution leading to extant apes and hominins. Although Miocene hominoid phylogeny is largely unresolved, the hypothesized phylogenetic positions of the taxa discussed above are presented in Figure 37. Given that several taxa are known postcranially only from tarsal bones, being able to use these to make accurate inferences about their locomotor adaptations is particularly important, which could inform the evolution of locomotion in Miocene hominoids. The research

proposed here will provide a validated framework with which to interpret these fossil foot bones by quantifying how tarsal morphology affects and reflects foot use during *in vivo* locomotion and characterizing variation in tarsal morphology in extant hominoids in 3D.

Visualizing and Quantifying Motion of Intertarsal Joints

Foot bone functional anatomy and tarsal mobility have been assessed to some extent using different methods, although few of these methods have been able to visualize and quantify motion and posture of the individual pedal elements during locomotion *in vivo*. External markers on the foot have been used to study movements in the feet of humans (Leardini et al., 1999, 2007; Hunt et al., 2001; DeSilva, 2008); macaques, and mandrills (DeSilva, 2008); and chimpanzees (DeSilva, 2008; Holowka et al., 2017). External markers allow researchers to track the location of bony morphologies using markers placed on the skin and allow for non-invasive observation of movements *in vivo*, but do not always capture motions such as those at intertarsal joints because these movements are subtle and the skin surrounding these joints do not adhere to the bones well enough to reflect their movements (Cornwall, 2002). Studies based solely on cadaveric or anesthetized specimens (Morton, 1922; Langdon, 1986; Hintermann et al., 1994; Hamel et al., 2004; Holowka & O'Neill, 2013; Greiner & Ball, 2014; DeSilva et al., 2015; Agoada & Kramer, 2019) can offer more precise bony morphology visualization than external markers, since the bones themselves can be visualized, but then do not account for active muscle contraction and natural gait kinematics that occur *in vivo*. Cineradiography can assess motion between tarsals *in vivo* (Thompson et al.,

2014a; Hesse et al., 2015), but limits the ability to quantify motions not restricted to one plane.

X-ray Reconstruction of Moving Morphology (XROMM)

This dissertation will employ x-ray reconstruction of moving morphology (XROMM) to visualize the posture and movement of tarsal bones in live primates moving on different substrates. XROMM is a relatively new, validated technique in the field of vertebrate functional morphology for studying *in vivo* movements of bones that cannot be visualized externally (Brainerd et al., 2010; Gatesy et al., 2010). XROMM uses biplanar fluoroscopy in combination with CT scans of the same individual to track complex, 3D movements in live specimens (Figure 38) and has allowed for the successful visualization and analysis of an array of behaviors that are otherwise difficult or impossible to visualize and quantify *in vivo* in taxa such as frogs (Astley & Roberts, 2012), alligators (Baier & Gatesy, 2013), chukars (Baier et al., 2013), carp (Gidmark et al., 2013, 2014), bass (Camp & Brainerd, 2015), guineafowl (Kambic et al., 2015), pigs (Menegaz et al., 2015), rats (Bonnan et al., 2016), iguanas (Brainerd et al., 2016), and macaques (Orsbon et al., 2018). Marker-based XROMM uses tantalum beads, which are surgically embedded into the specimen's bones, to track the 3D movements of each rigid body while the animal is moving. The 3D positions of the markers are then aligned with a CT rendering of the same bone in order to calculate the movements between elements (Brainerd et al., 2010).

Marker-based 3D XROMM of macaques during locomotion has never been conducted. Two-dimensional variations of this approach have been used by employing

standard plain film radiography or uniplanar cineradiography to assess hip and transverse tarsal kinematics in humans (Jenkins, 1972; Thompson et al., 2014b) and cotton-top tamarins (Hesse et al., 2015). Lundberg (1989) employed a 3D variant *in vivo* in humans, where tantalum markers were placed in live human legs and feet and subjects were asked to stand in different postures while two x-rays were taken at right angles to each other at every 10 degrees of rotation (Lundberg, 1989; Lundberg et al., 1989), but this did not track continuous movement.

XROMM is ideal for studying foot bones because it allows the position and movement of each bone to be visualized during gait. Foot bones are small and complicated in shape, and their motions are not restricted to cardinal planes (Inman, 1976; Lundberg, 1989). Thus, their movement and relative positions cannot be fully evaluated in two dimensions, nor from observing external markers associated with the bones. XROMM allows one to visualize, track, and quantify *in vivo* functionally relevant motions among these small bones, which is necessary to accurately capture how tarsal bones permit and reflect foot postures during locomotion. *In vivo* data provide a necessary test of the models of foot function underlying comparative analyses. However, because of the limited opportunities to visualize and quantify movement of the bones of the foot in live animals, a broader comparative sample is needed. The combination of the quantification of *in vivo* movements and a study of the morphological variation of tarsals allows us to test hypothesized form-function relationships in a wide array of taxa. By combining *in vivo* and comparative approaches, this study provides an informed context into which observed morphological variation among extant anthropoids can be placed,

and can provide a basis for using tarsal morphology to reconstruct foot function in extinct taxa.

This dissertation takes a three-step, novel approach to test the functional models upon which comparative inferences are made by combining osteological morphometric and *in vivo* locomotor data applied to the fossil record and will provide important new data from a poorly understood anatomical region. This project uses biomechanically-informed models of locomotion validated using experimental data in extant primates in conjunction with morphometric data from a broad sample of extant taxa.

The goals of this dissertation are: 1) to quantify motions at the intertarsal and talocrural joints; 2) to identify aspects of morphology that differ among extant primate taxa that differ in size, phylogeny, and locomotion; and 3) to infer locomotor repertoires of Miocene fossil hominoids based on tarsal morphology. This research explores form-function relationships in the foot and ankle and provide the ability to make informed reconstructions about foot function in Miocene fossil hominoids, including the basal hominoids *Proconsul major, Ekembo nyanzae, Ekembo heseloni, Rangwapithecus gordoni;* middle Miocene taxa *Nacholapithecus kerioi* and later Miocene *Oreopithecus bambolii*. These results will also provide a basis for analyzing other fossil anthropoid tarsal elements as well as non-anthropoid morphology in the future.

The following three chapters of this dissertation assess form function relationships in the foot and ankle through the following aims:

Aim 1: Use x-ray reconstruction of moving morphology (XROMM) to visualize and quantify relative motion and position of the tibia, talus, calcaneus, navicular, and cuboid *in vivo* during locomotion in *Macaca mulatta.*

Aim 2: Quantify the shape of the calcaneus, talus, cuboid, and navicular in a broad sample of anthropoid primates to identify osteological correlates of posture and motion at the talocrural, subtalar, and transverse tarsal joints.

Aim 3: Use the osteological correlates of tarsal posture and motion determined by combining results of Aims 1 and 2 to interpret Miocene hominoid tarsals and to reconstruct foot use during locomotion.

Figures and Tables for Chapter 1

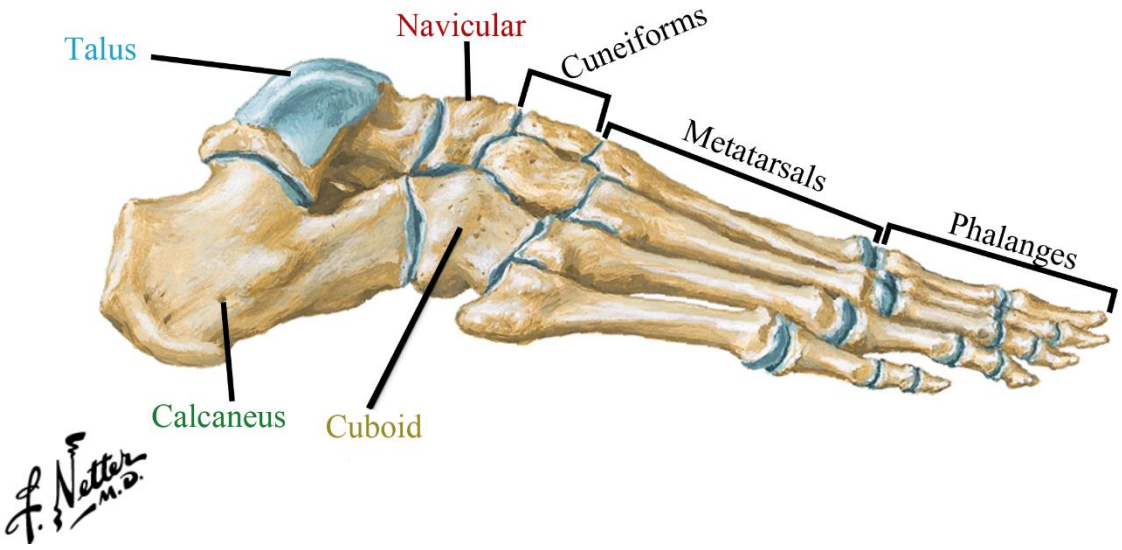

Figure 1: Articulated human (*Homo sapiens*) foot (lateral view). Figure modified from Netter (2010).

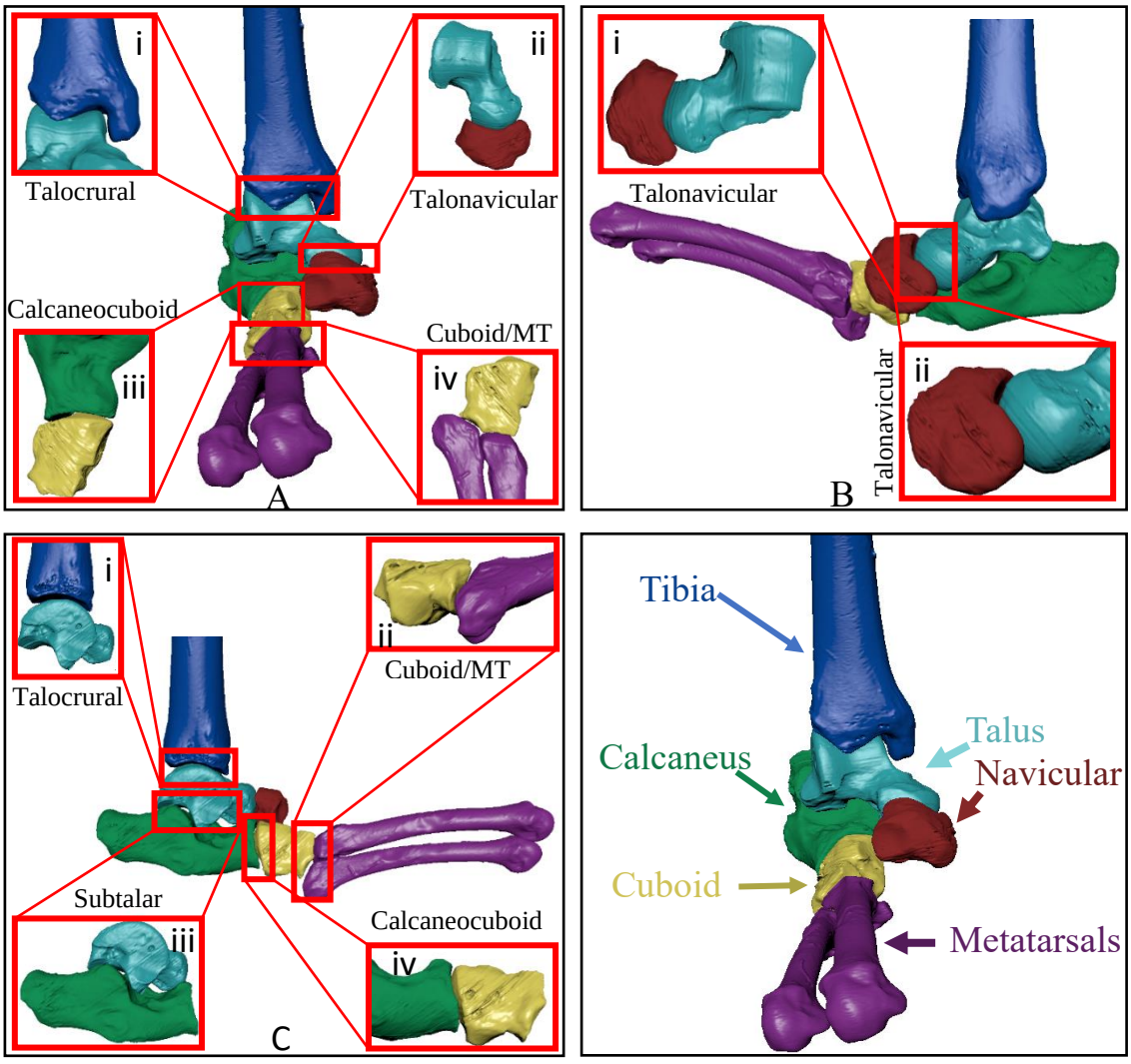

Figure 2: Joints and bones of interest for this study. Anterior (A), medial (B), and lateral (C) views of the tibia (blue), talus (teal), calcaneus (green), navicular (red), cuboid (yellow), and MT4/MT5 (purple) of *Macaca mulatta*. Joints of interest are: talocrural (blue/teal; insets Ai, Ci), subtalar (teal/green; inset Ciii), talonavicular (teal/red; insets Aii, Bi, Bii), calcaneocuboid (green/yellow; insets Aiii, Civ), and cuboid/MT5 (yellow/purple; insets Aiv, Cii).

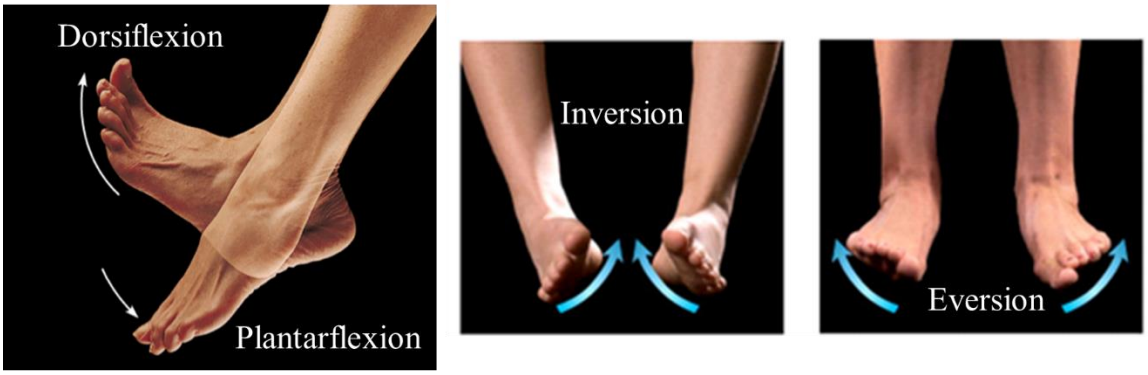

Figure 3: Movements of the foot. Diagram shows movements of the foot discussed in this dissertation. Figures modified from Antranik.org.

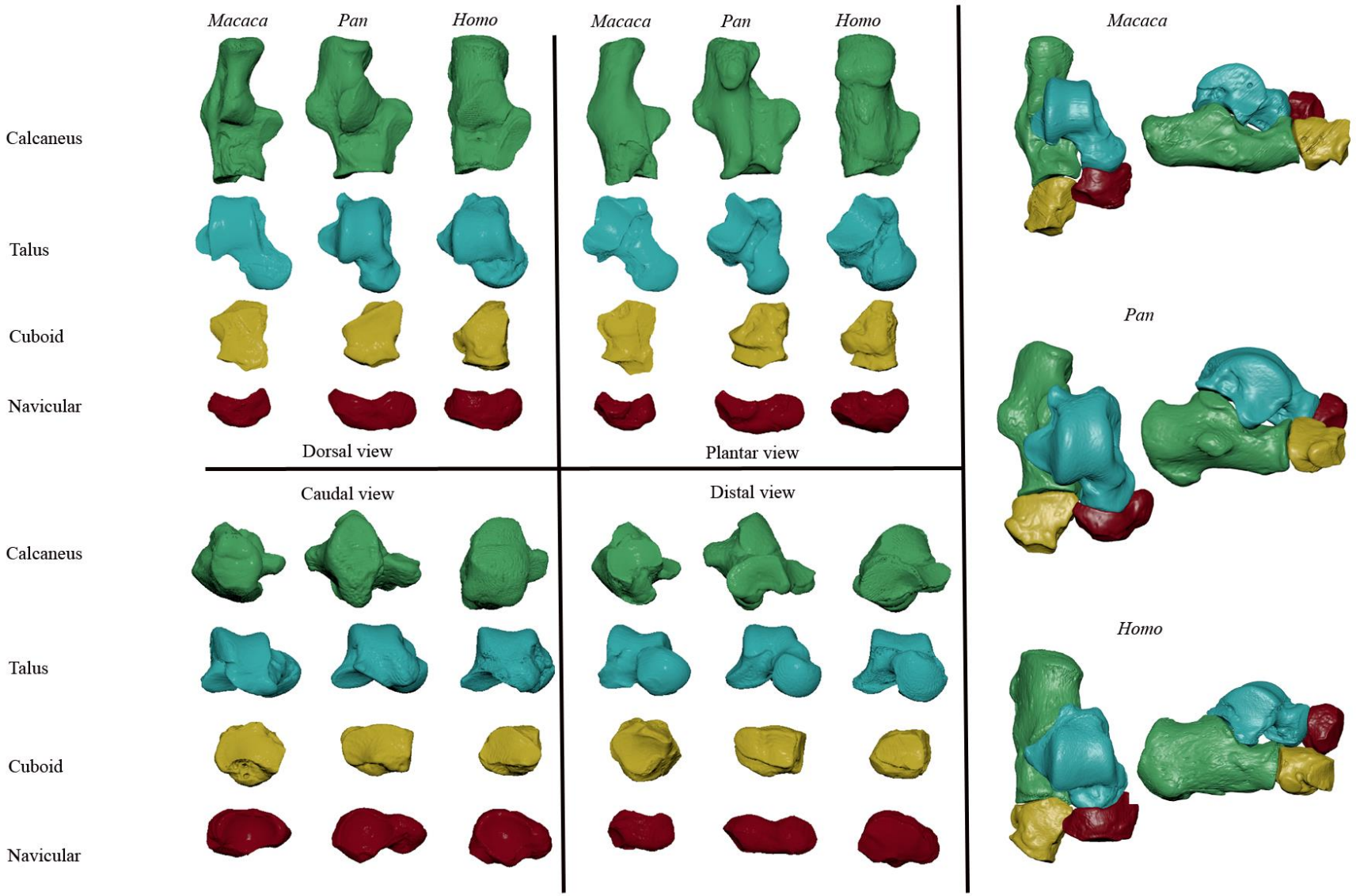
Macaca
Pan
Homo
Macaca
Pan
Homo
Calcaneus
Talus
Cuboid
Navicular
Dorsal view
Plantar view
Caudal view
Distal view
Calcaneus
Talus
Cuboid
Navicular
Macaca
Pan
Homo

Figure 4: Left: Isolated calcanei, tali, cuboids, and naviculars from *Macaca*, *Pan*, and *Homo*. Right: articulated calcaneus, talus, cuboid, and navicular in *Macaca*, *Pan*, and *Homo*. Dorsal view is in the left column, lateral view is in the right column. Isolated calcanei have been scaled by calcaneal length, tali by talar length, cuboids by cuboid length, and naviculars by navicular width.

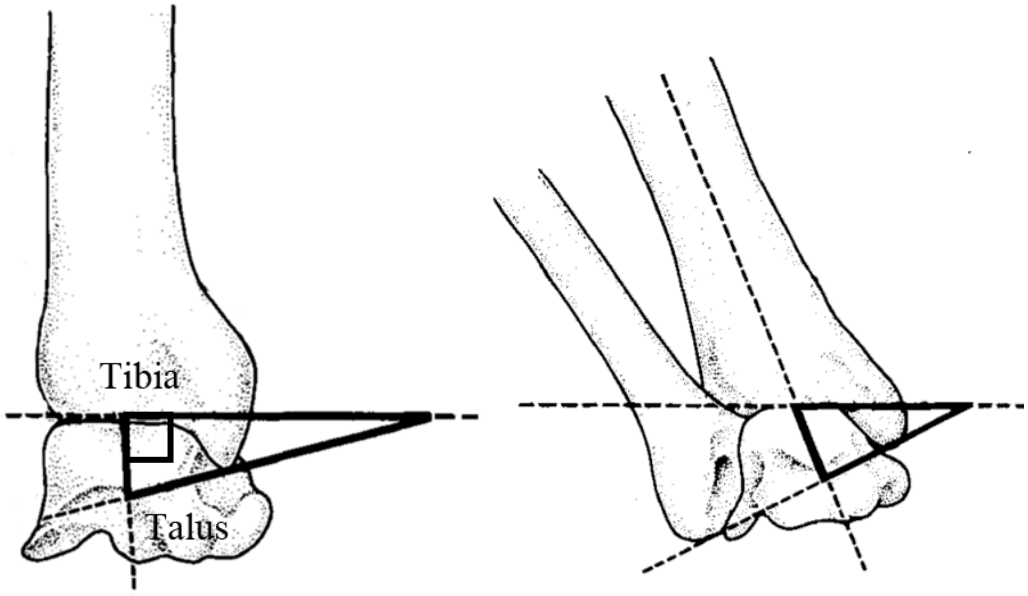

Figure 5: Talocrural joint in *Homo sapiens*, showing the roughly orthogonal human talocrural joint (left) in comparison to a pongid talocrural joint (right), which has a more inverted foot set. Figure modified from Latimer et al., 1987.

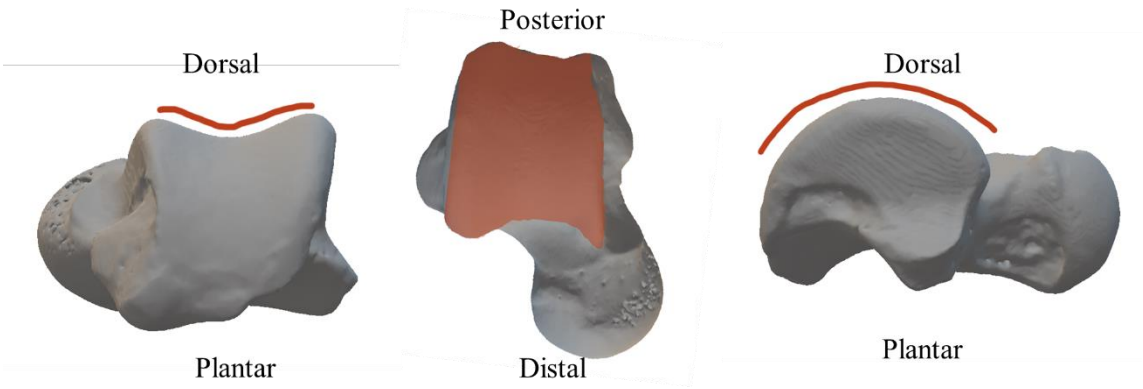

Figure 6: Morphological features of the primate talar trochlea. Left: Talar trochlear articular surface (posterior view, *Cercopithecus ascanius)* showing the trochlear groove. Middle: Talar trochlear articular surface (dorsal view). Right: Lateral view of the talus, showing the convexity of the talar trochlea.

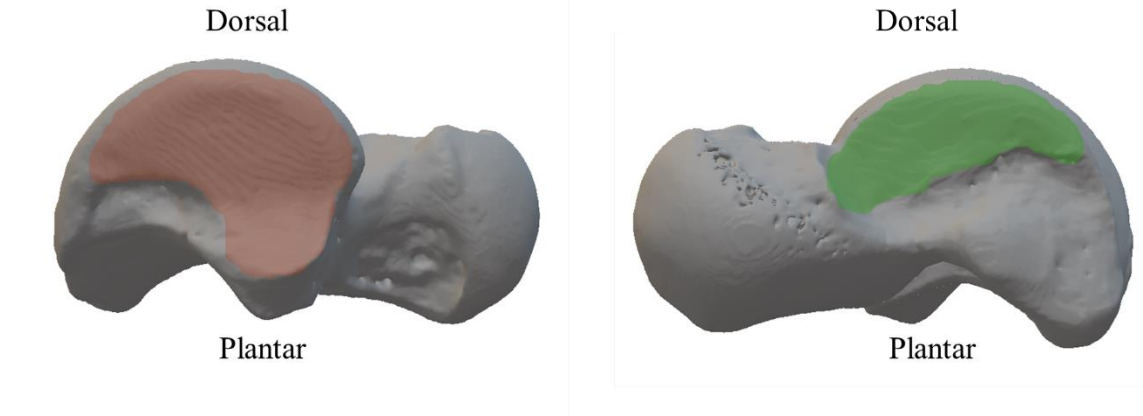

Figure 7: Medial (left, red) and lateral (right, green) malleolar articular surfaces on the talus (*Cercopithecus ascanius* shown as example here).

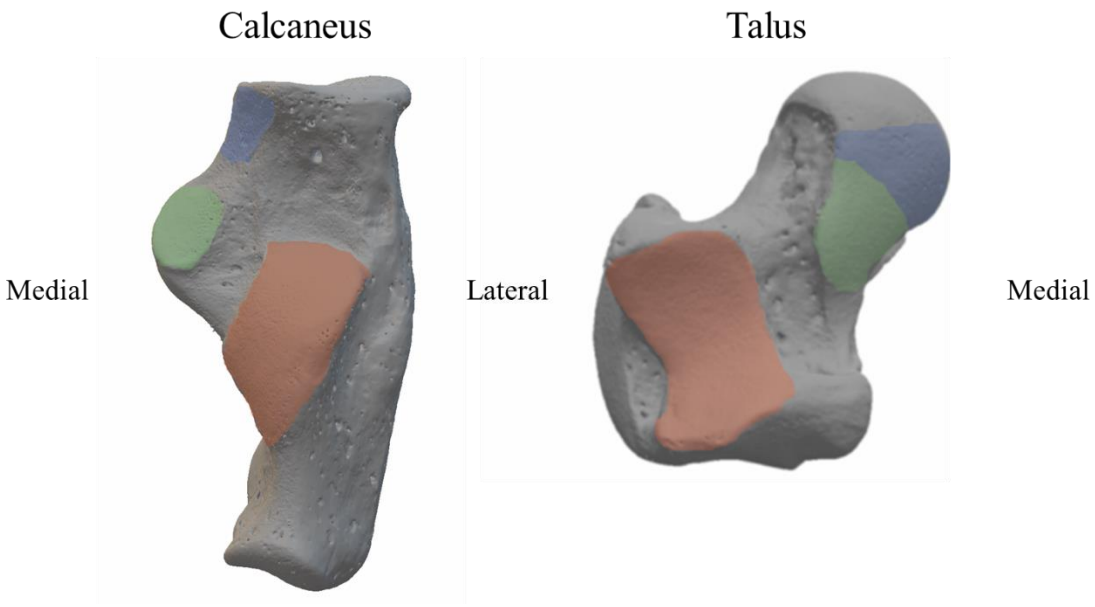

Figure 8: Subtalar articulations on the calcaneus (left, dorsal view) and talus (right, plantar view). Posterior subtalar articular surface colored in red, middle subtalar articular surface in green, anterior subtalar articular surface colored in blue. Shown here in *Cercopithecus ascanius* specimens.

Figure 9: Talonavicular articulations on the talus (left, distal view) and navicular (right, proximal view). Articular surface highlighted in red on both surfaces. Shown here in *Cercopithecus ascanius*.

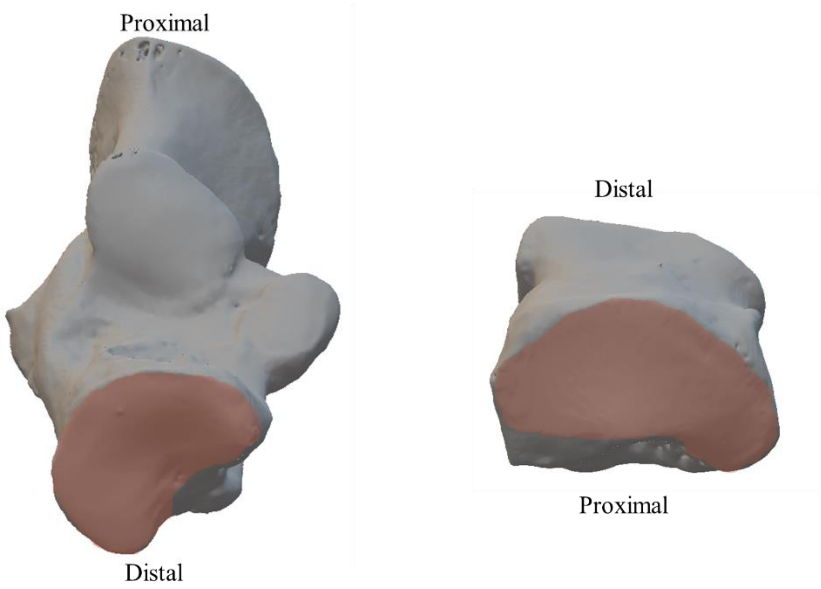

Figure 10: Calcaneocuboid joint articulations on the calcaneus (left, distal view) and cuboid (right, proximal view). Articular surface highlighted in red on both surfaces. Shown here in *Cercopithecus ascanius*.

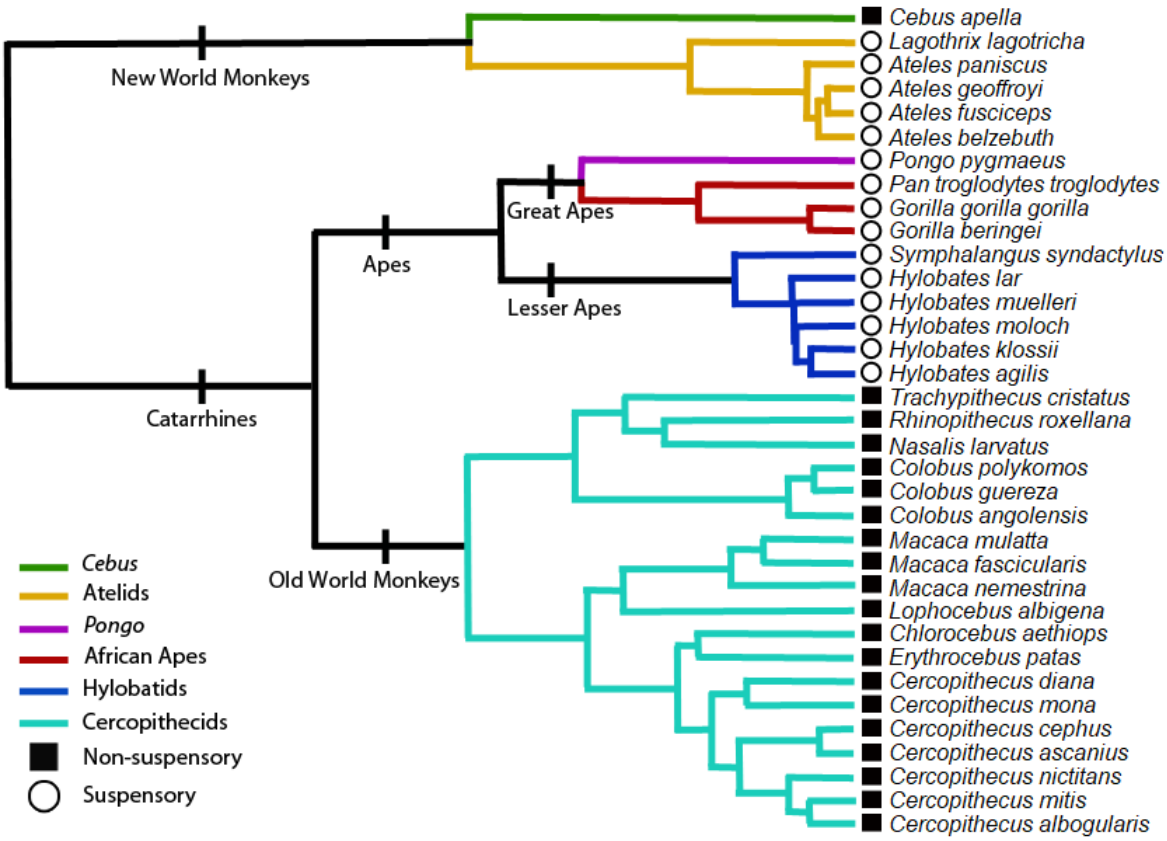

Figure 11: Phylogenetic relationships of the extant sample of anthropoid primates used in this study. Tree modified from 10k Trees (Arnold et al., 2010). Branches are colored by Taxonomic Group, identified in the key. Locomotor category is indicated by a black square non-suspensory) or hollow circle (suspensory).

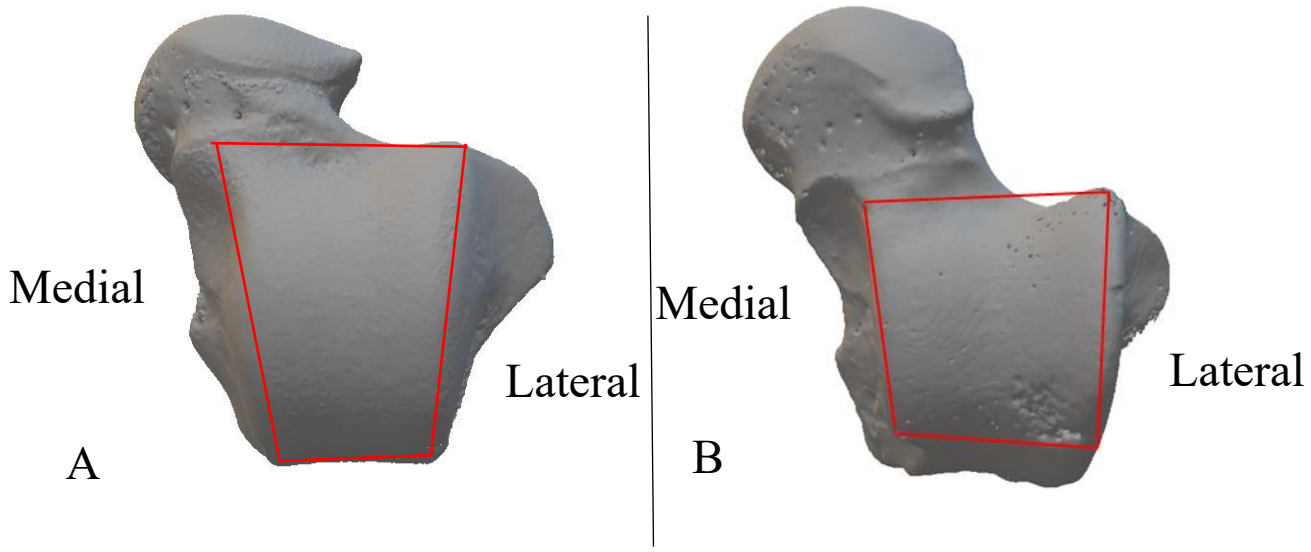

Figure 12: Examples of A) a trapezoidal talar trochlea (*Hylobates klossi*), which tapers posteriorly versus B) a more rectangular talar trochlea (*Cercopithecus mitis*). Note: models are scaled to each other by talar length. Both tali are in dorsal views.

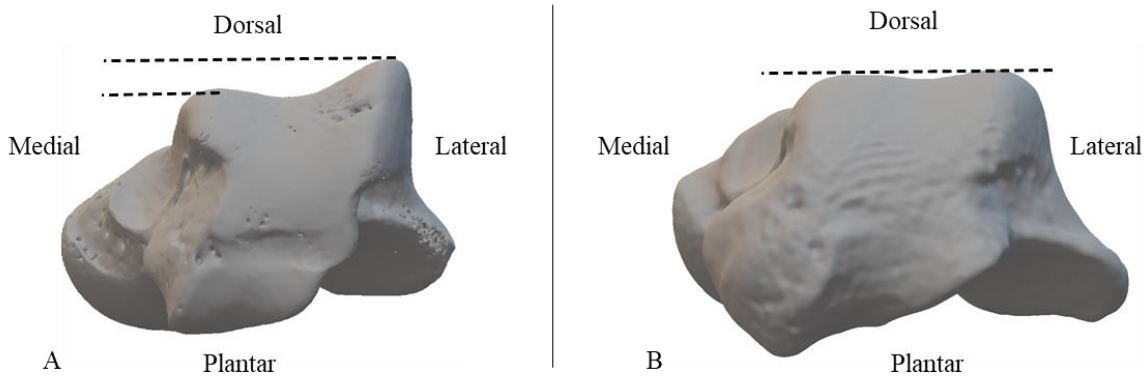

Figure 13: Examples of A) high and asymmetrical talar trochlear crests (*Cercopithecus mitis*) versus B) symmetrical trochlear crests (*Pan troglodytes*). Note: models are scaled to each other by talar height and are positioned to demonstrate trochlear asymmetry, not anatomical orientation. Both tali are in caudal views.

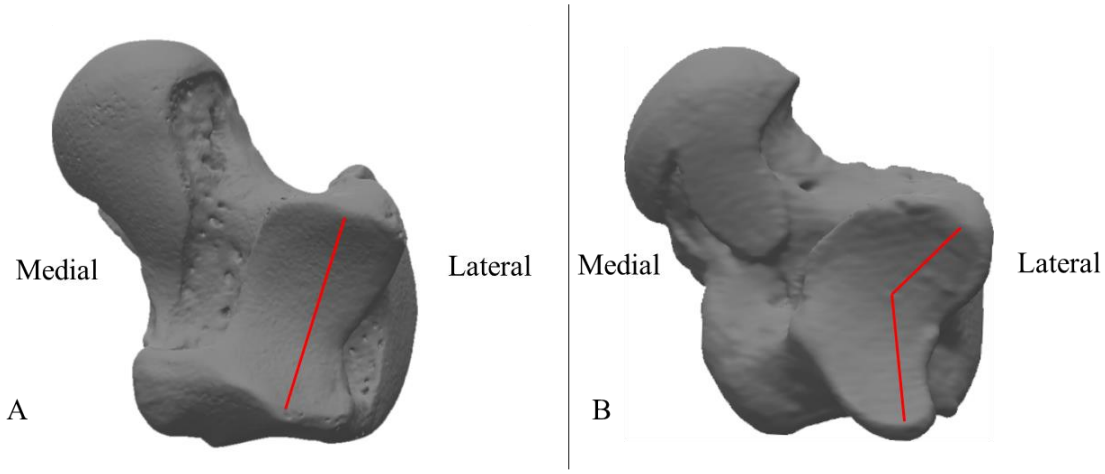

Figure 14: Example of variation in the morphology of the subtalar articular surface in *Cercopithecus alborgularis* (left) and *Pan troglodytes* (right), which is hypothesized to differ between suspensory and non-suspensory taxa. Left tali were scaled to the same length, and thus do not reflect actual talar size relative to each other. Both tali are in plantar views.

A  B 

Figure 15: Examples of A) prominent peg and socket morphology at the calcaneocuboid joint (*Pongo pygmaeus*, plantar view, arrow indicates proximal bony protuberance) versus B) a more planar articulation at the calcaneocuboid joint (*Trachypithecus cristatus* plantar view, arrow indicates proximal bony protuberance). Note: pictures are scaled to each other by cuboid proximodistal length.

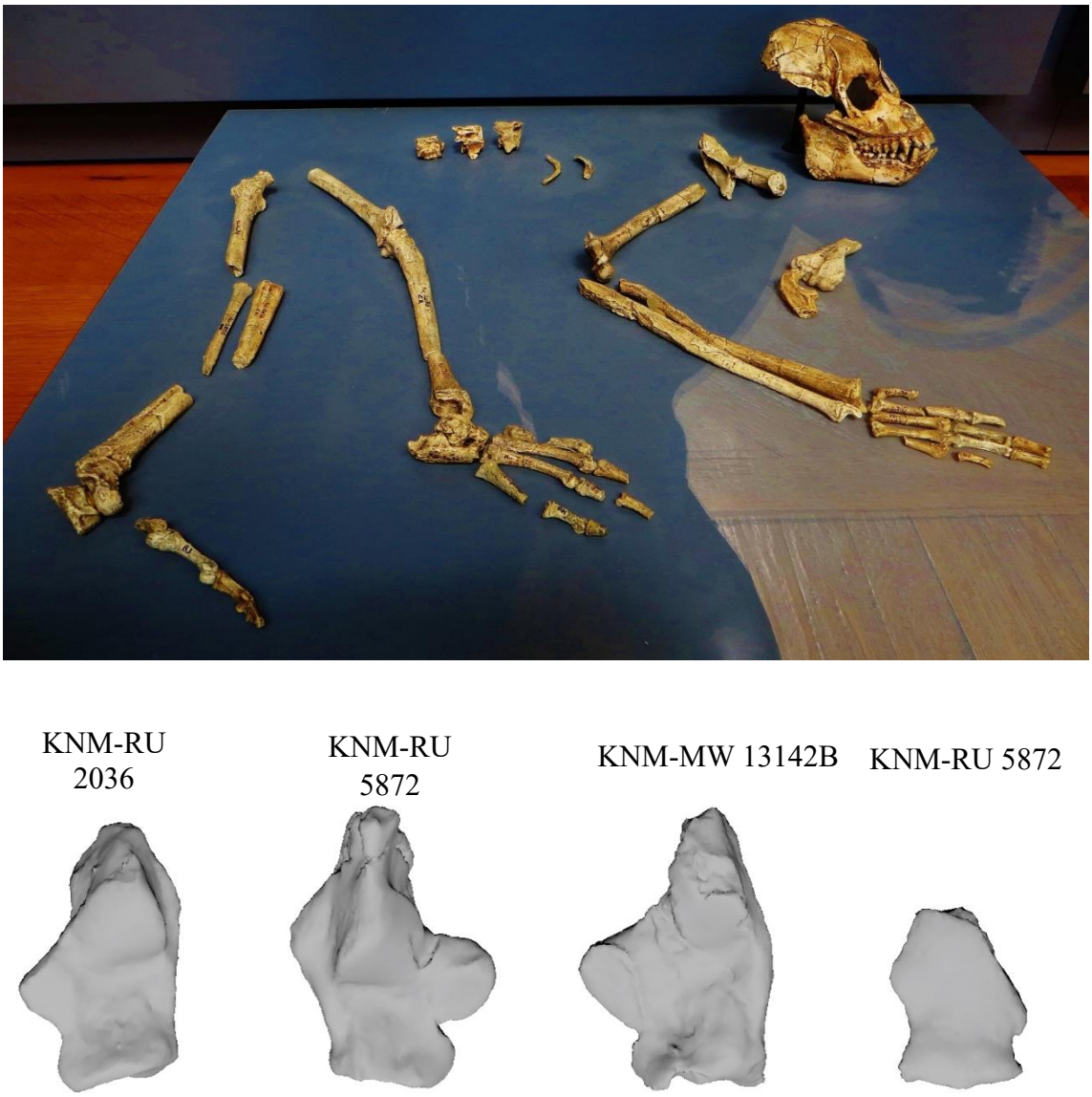

Figure 16: Above: Composite *Ekembo* skeleton. Image from Ghedoghedo https://commons.wikimedia.org/w/index.php?curid=26826777. Below: Isolated *Ekembo* tarsals included in this analysis. All tarsals are in dorsal view.

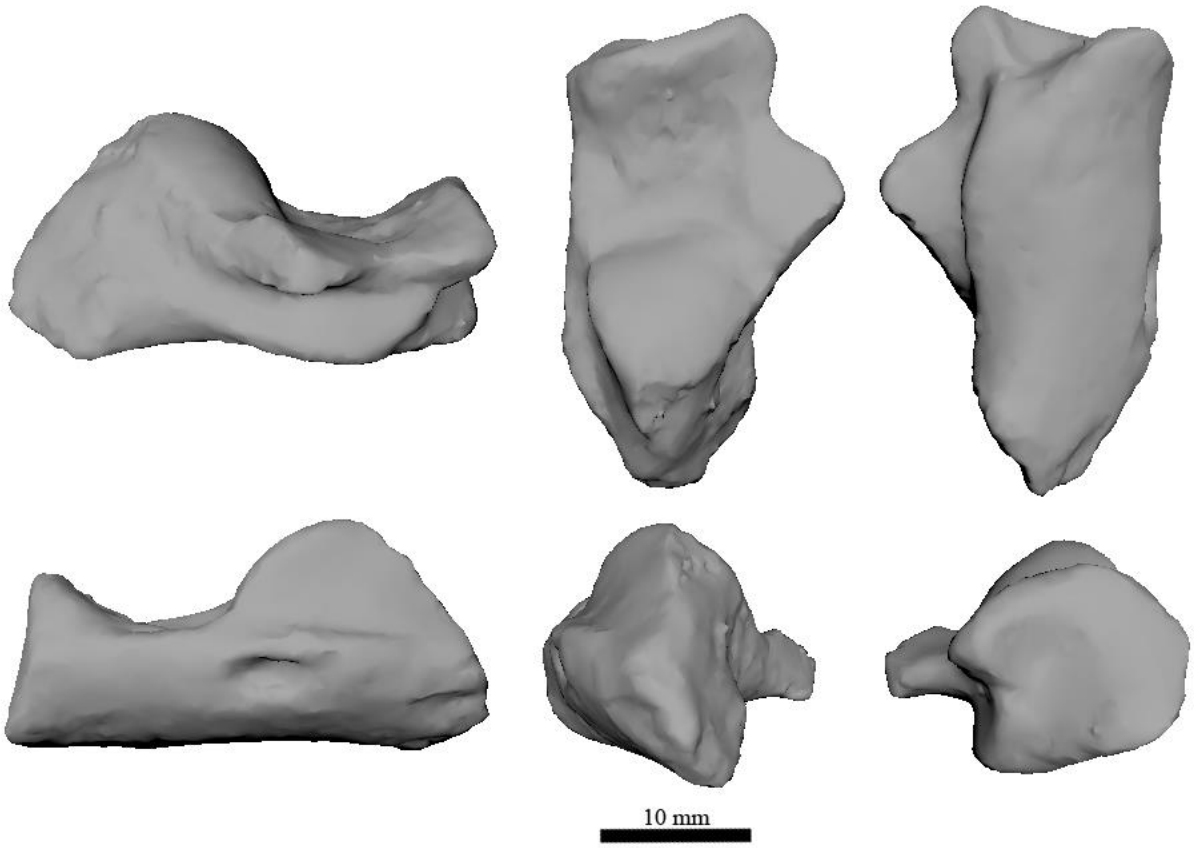

Figure 17: KNM-RU 2036 left calcaneus attributed to *Ekembo heseloni*. Top row views: medial, proximal, plantar. Bottom row views: lateral, caudal, distal.

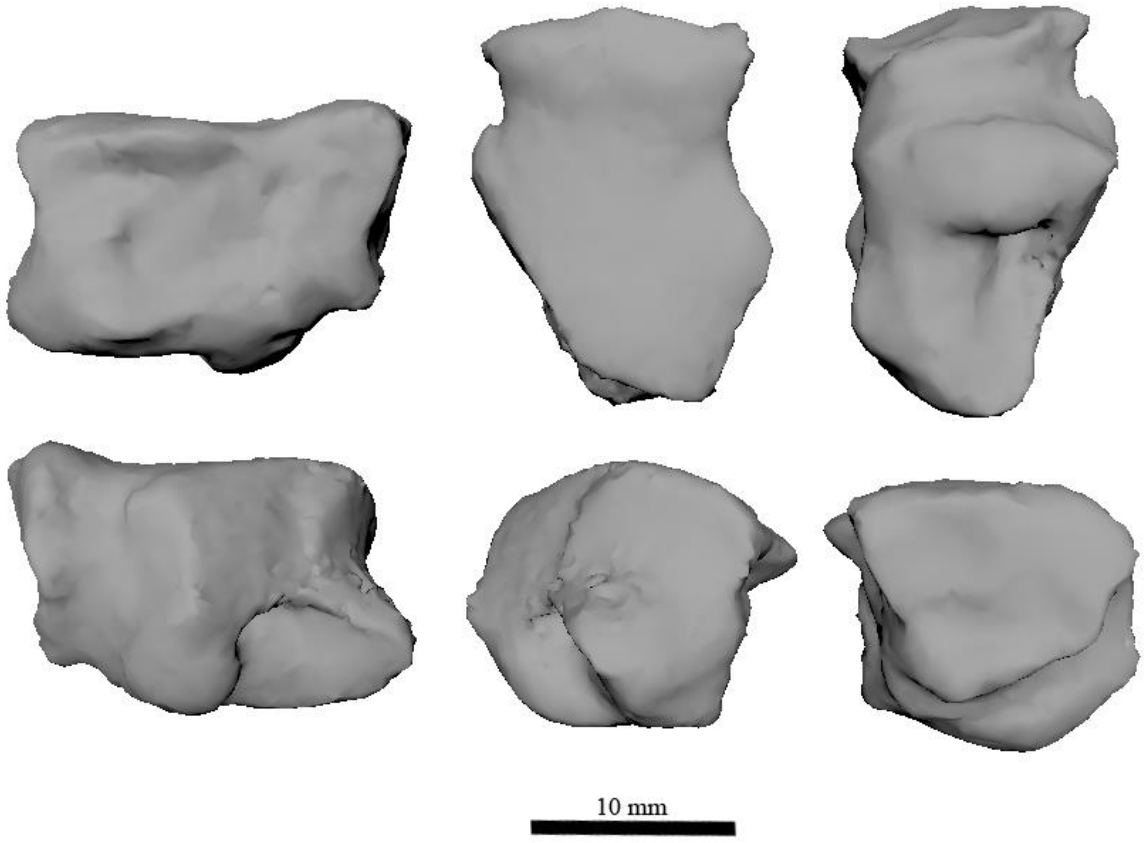

Figure 18: KNM-RU 5872 left cuboid attributed to *Ekembo nyanzae*. Top row views: medial, dorsal, plantar. Bottom row views: lateral, proximal, distal.

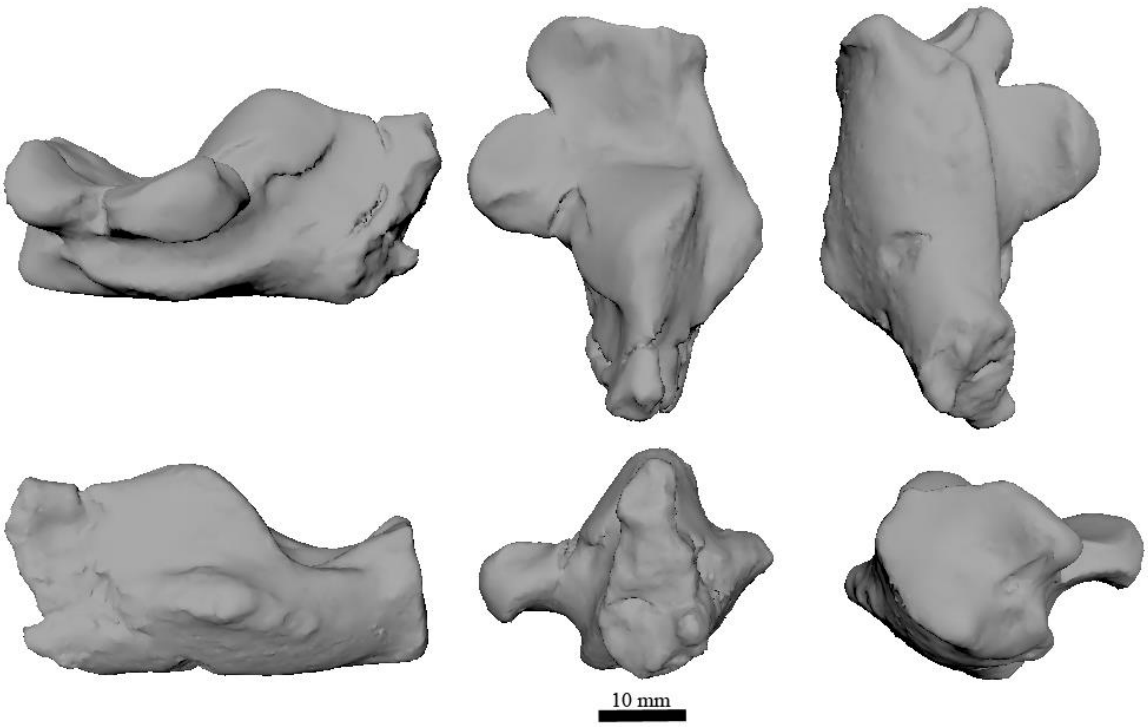

Figure 19: KNM-MW 13142B right calcaneus attributed to *Ekembo nyanzae*. Top row views: medial, proximal, plantar. Bottom row views: lateral, caudal, distal.

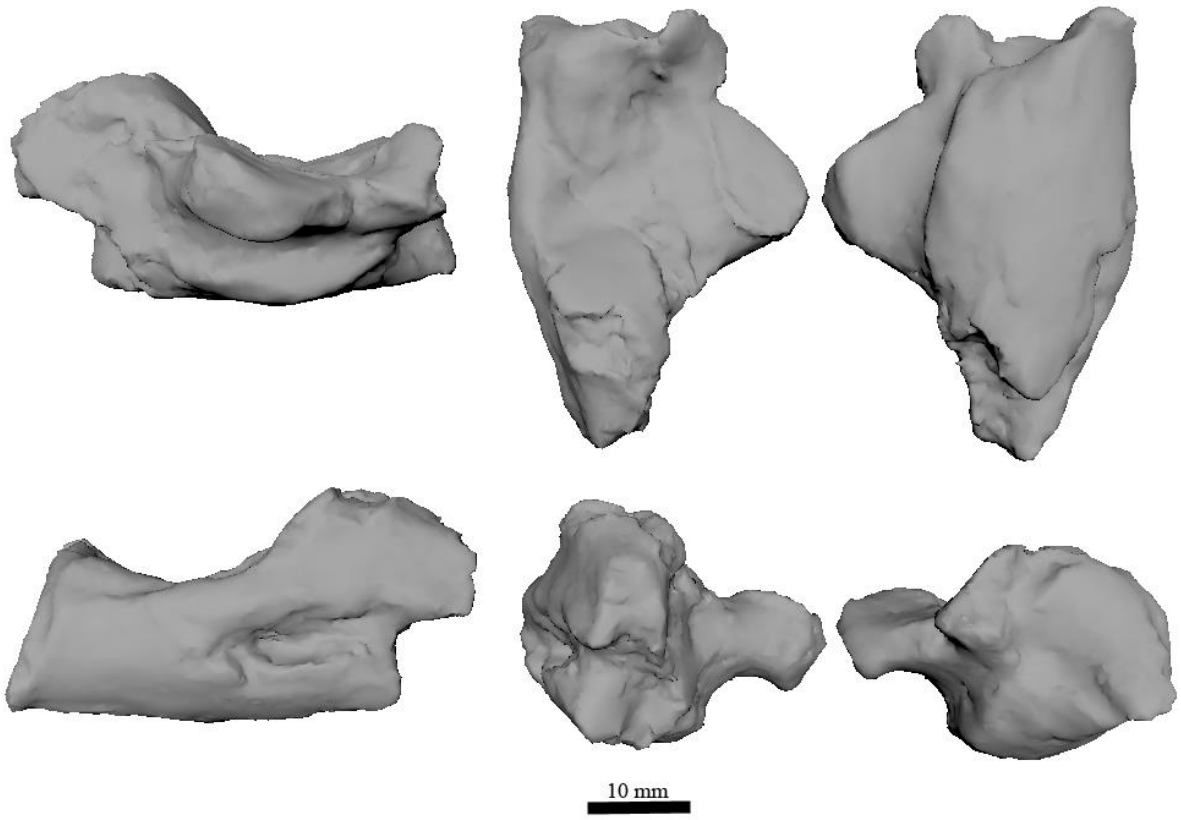

Figure 20: KNM-RU 5872 left calcaneus attributed to *Ekembo nyanzae*. Top row views: medial, proximal, plantar. Bottom row views: lateral, caudal, distal.

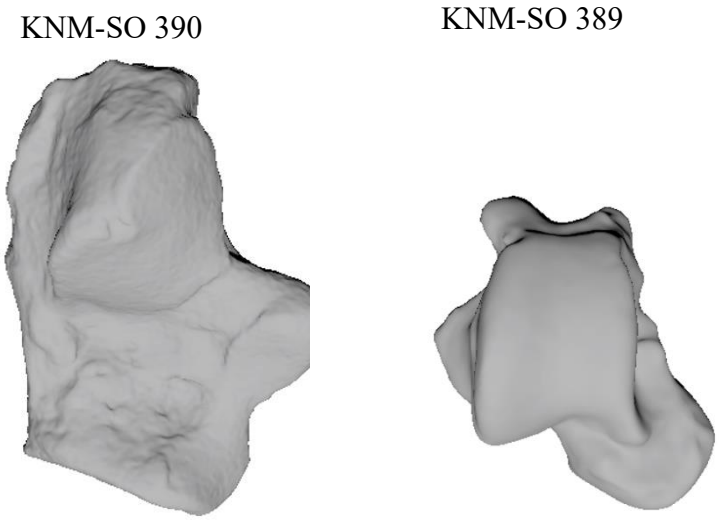

Figure 21: Above: mandibles attributed to *Proconsul major* (occlusal view). Below: Isolated calcaneus (left, dorsal view) and talus (right, dorsal view) attributed to *Proconsul major*.

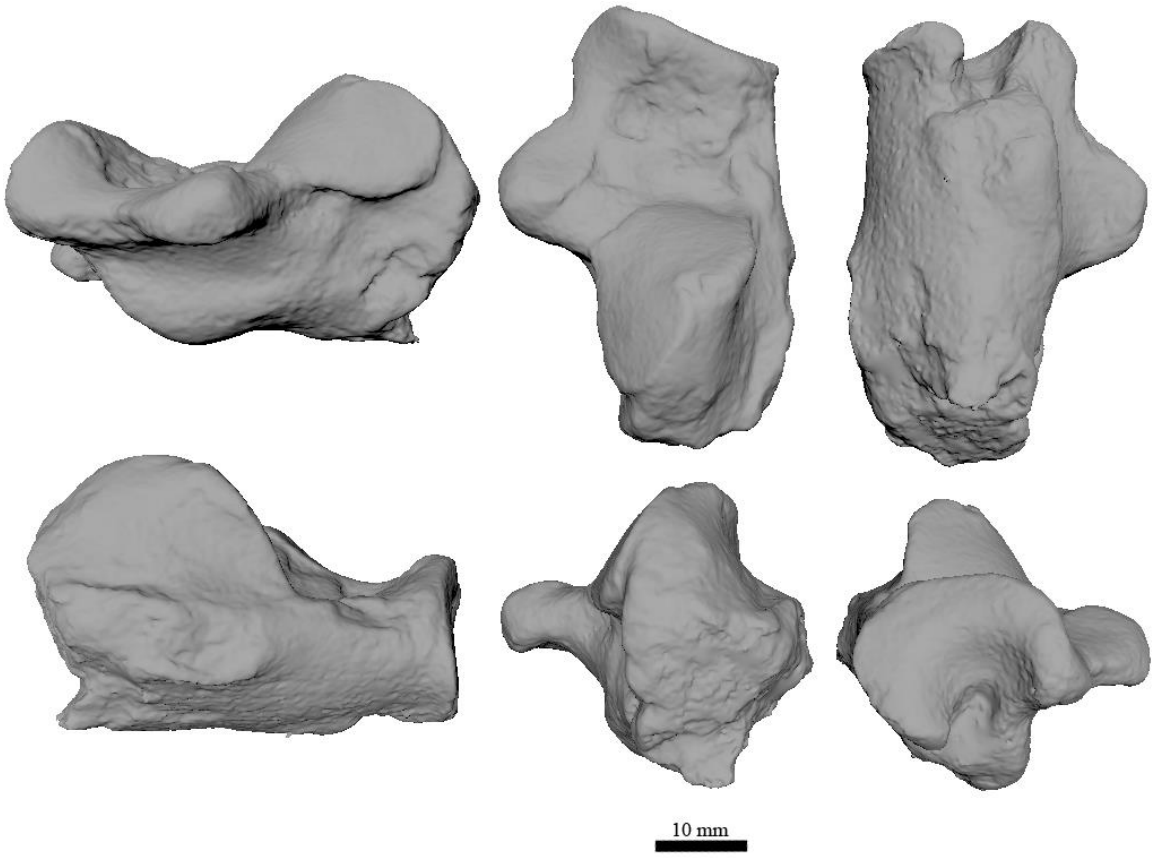

Figure 22: KNM-SO 390 right calcaneus attributed to *Proconsul major*. Top row views: medial, proximal, plantar. Bottom row views: lateral, caudal, distal.

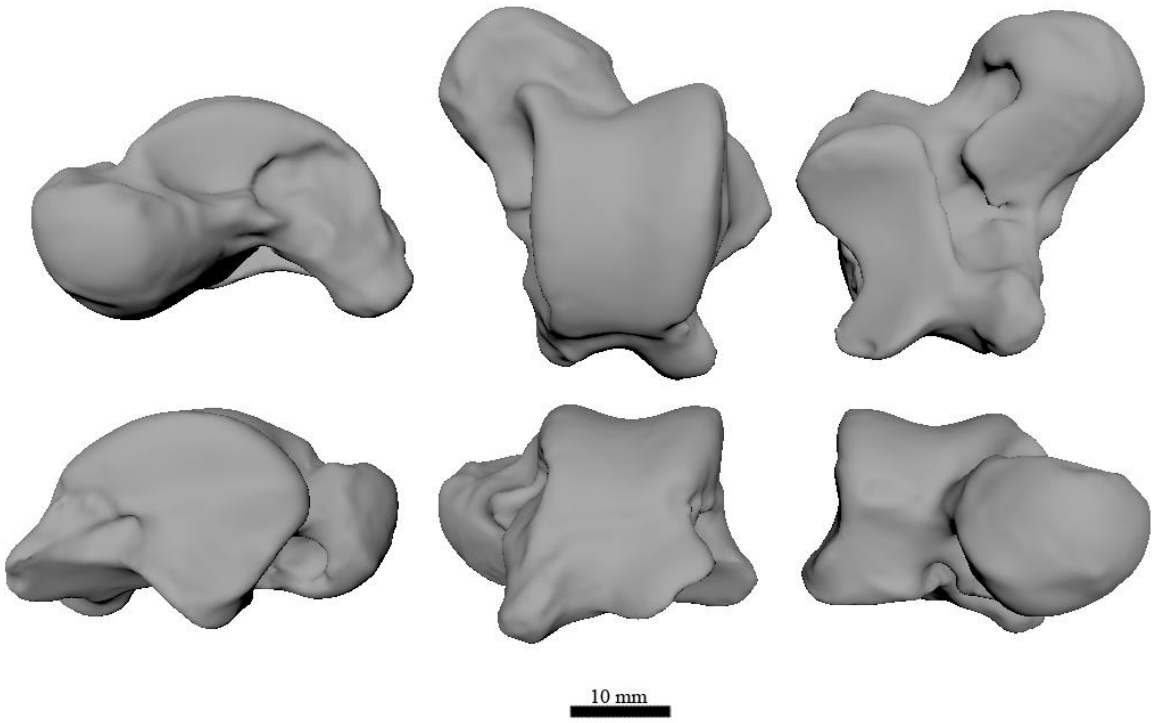

Figure 23: KNM-SO 389 right talus attributed to *Proconsul major*. Top row views: medial, proximal, plantar. Bottom row views: lateral, caudal, distal.

KNM-SO 427 KNM-SO 968

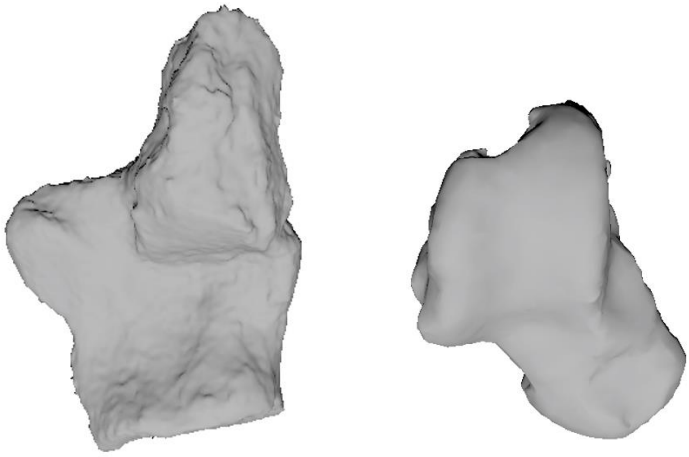

Figure 24: Above: Maxilla (KNM-SO 700, occlusal view), type specimen for *Rangwapithecus gordoni.* Image modified from Puech (2018). Below: Calcaneus (left, dorsal view) and talus (right, dorsal view) attributed to *Rangwapithecus gordoni*.

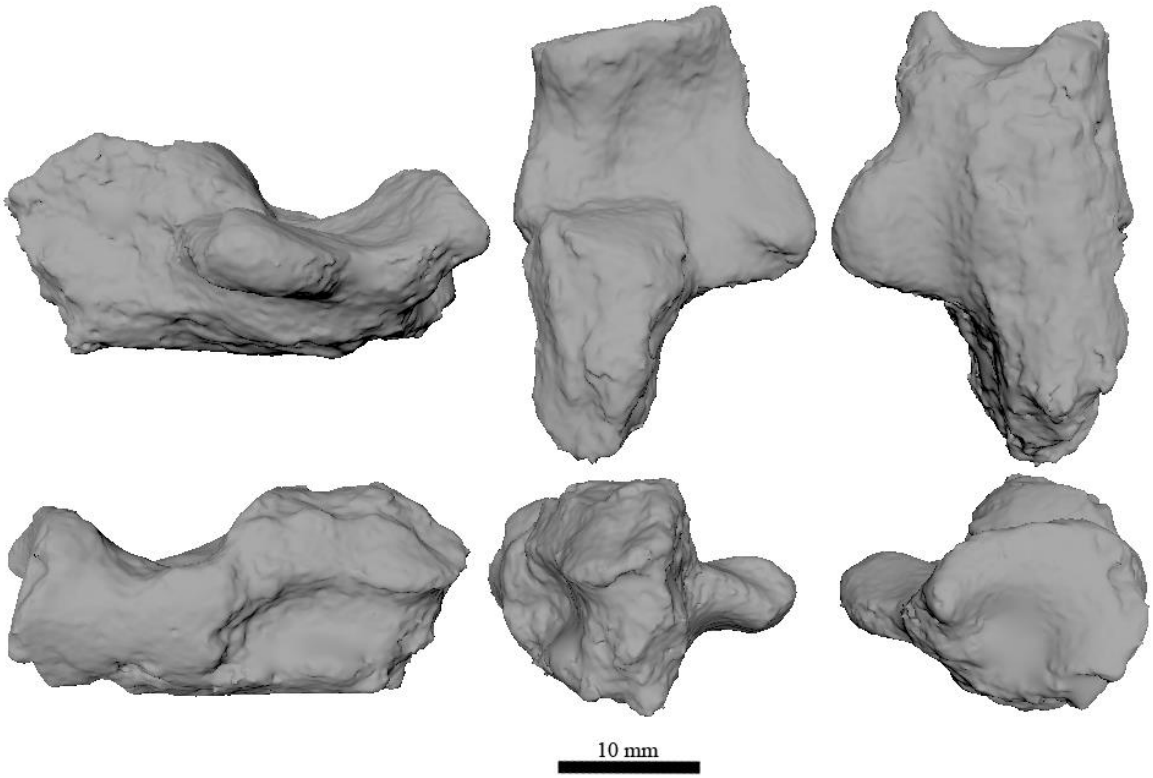

Figure 25: KNM-SO 427 left calcaneus attributed to *Rangwapithecus gordoni*. Top row views: medial, proximal, plantar. Bottom row views: lateral, caudal, distal.

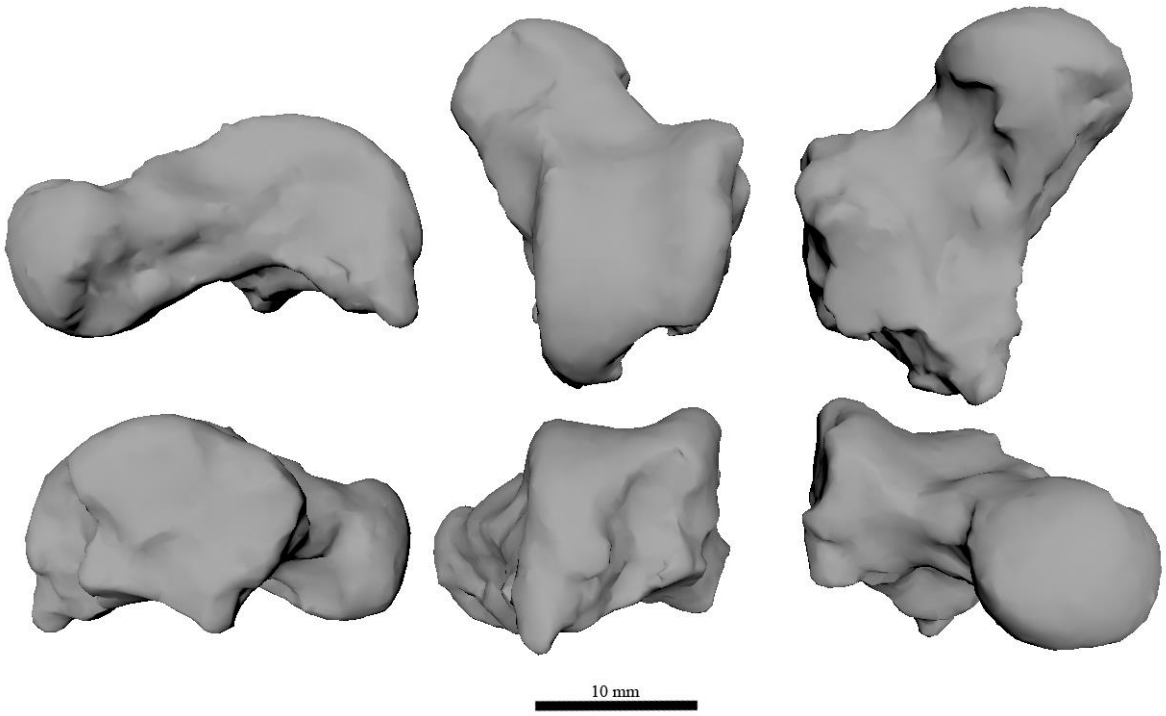

Figure 26: KNM-SO 968 right talus attributed to *Rangwapithecus gordoni*. Top row views: medial, proximal, plantar. Bottom row views: lateral, caudal, distal.

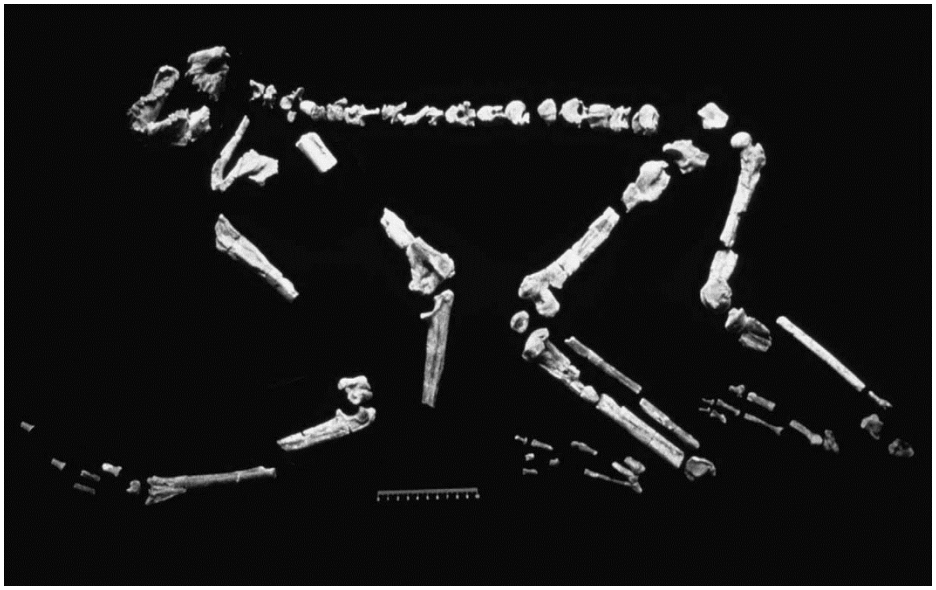

KNM-BG 35250

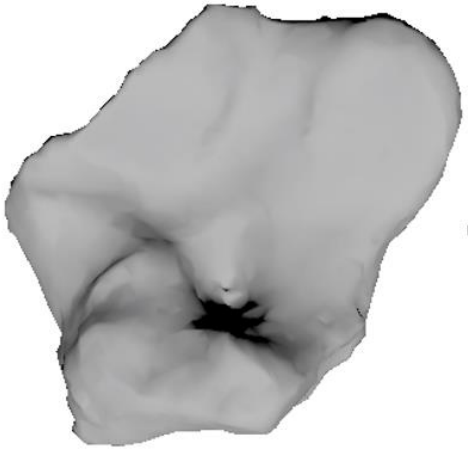

Figure 27: Above: Associated fossilized skeletal remains of *Nacholapithecus kerioi* (KNM-BG 35250). Image taken from Ishida et al. (2004).

Below: Distal calcaneus (dorsal view) attributed to *Nacholapithecus kerioi.*

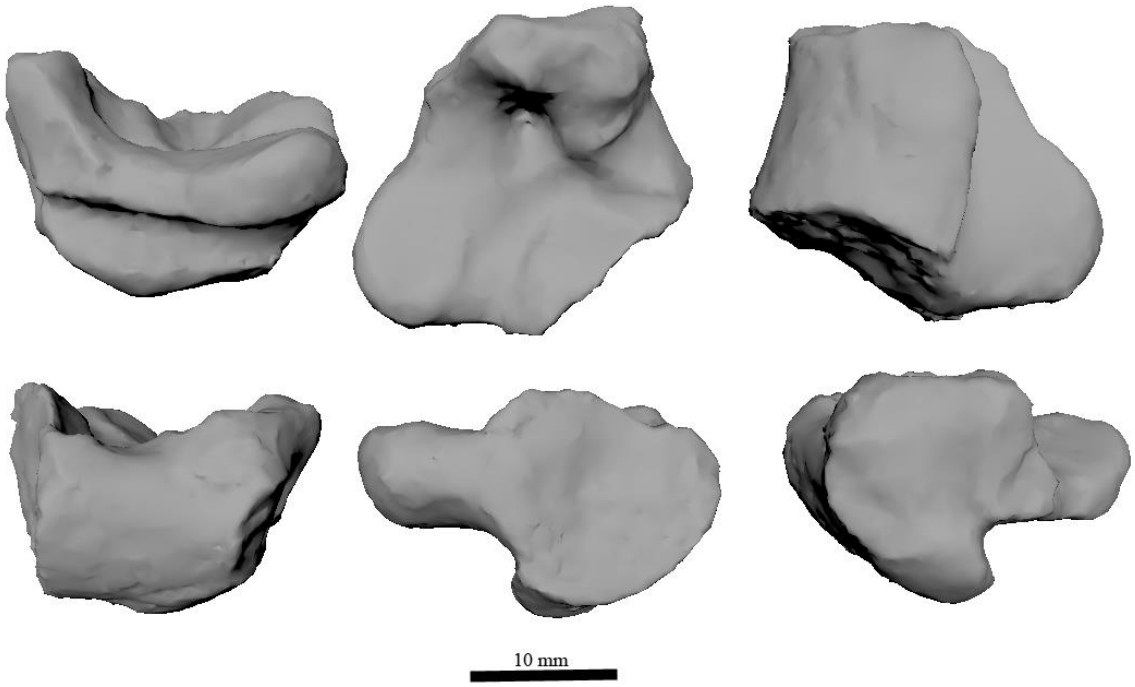

Figure 28: KNM-BG 35250 right calcaneus attributed to *Nacholapithecus kerioi*. Top row views: medial, proximal, plantar. Bottom row views: lateral, caudal, distal.

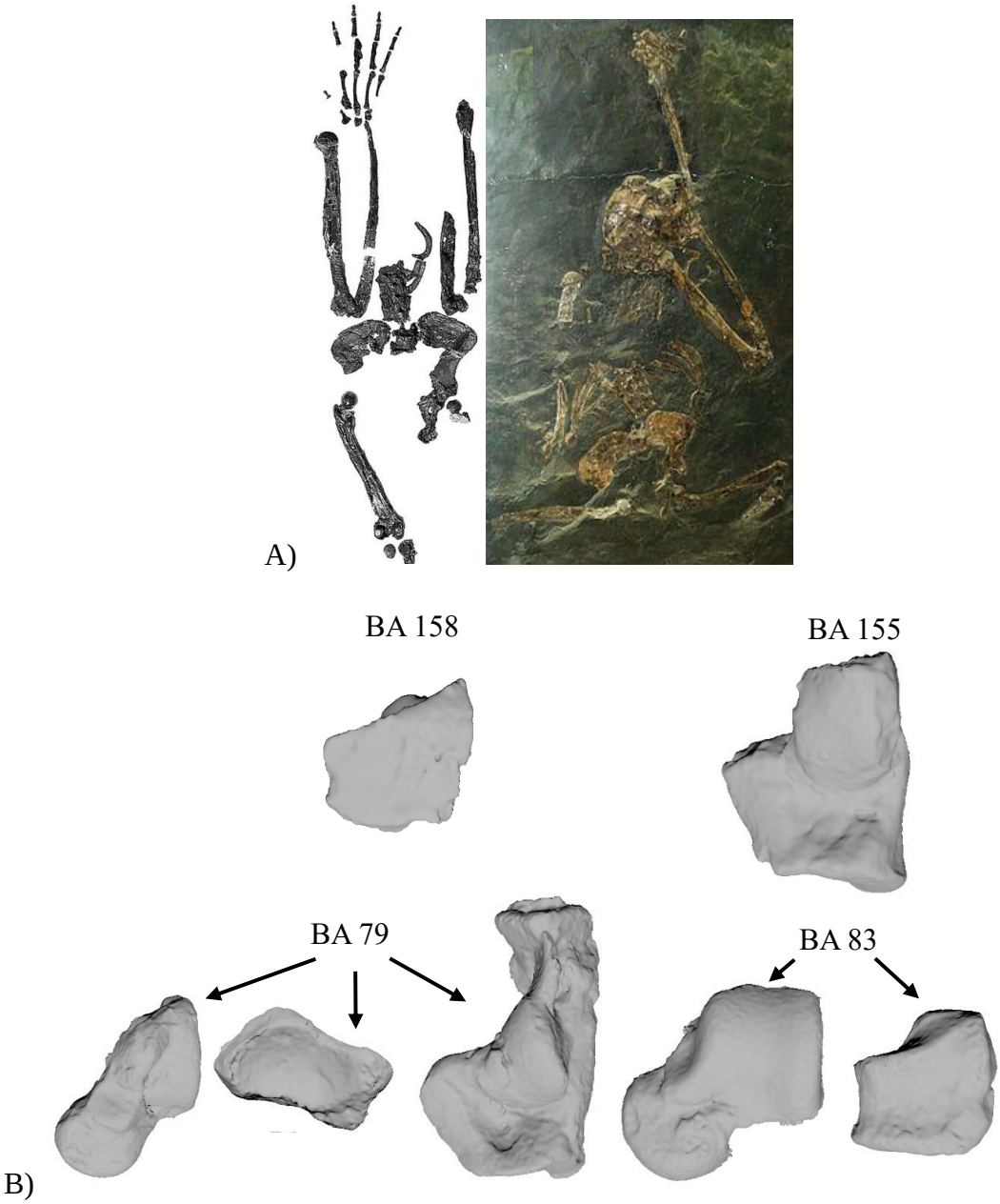

Figure 29: A) Fossilized partial skeleton of *Oreopithecus bambolii* (IGF 11778). Left image is from https://commons.wikimedia.org/wiki/File:Oreopithecus_bambolii_1.JPG. Right image is from Susman (2004). B) Isolated tarsals attributed to *Oreopithecus bambolii*. Top row: cuboid (dorsal view), calcaneus (dorsal view); Bottom row: talus (dorsal view), navicular (proximal view), calcaneus (dorsal view), talus (dorsal view), cuboid (dorsal view).

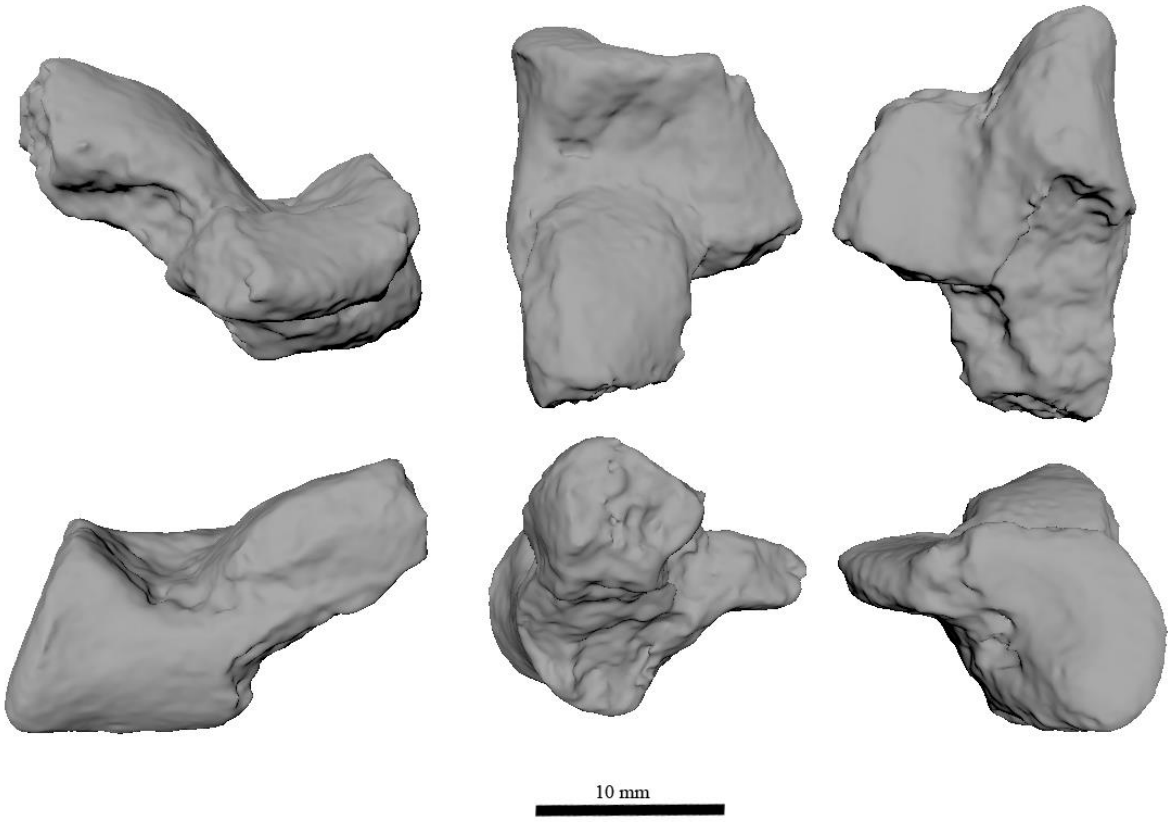

Figure 30: BA 155 left calcaneus attributed to *Oreopithecus bambolii*. Top row views: medial, proximal, plantar. Bottom row views: lateral, caudal, distal.

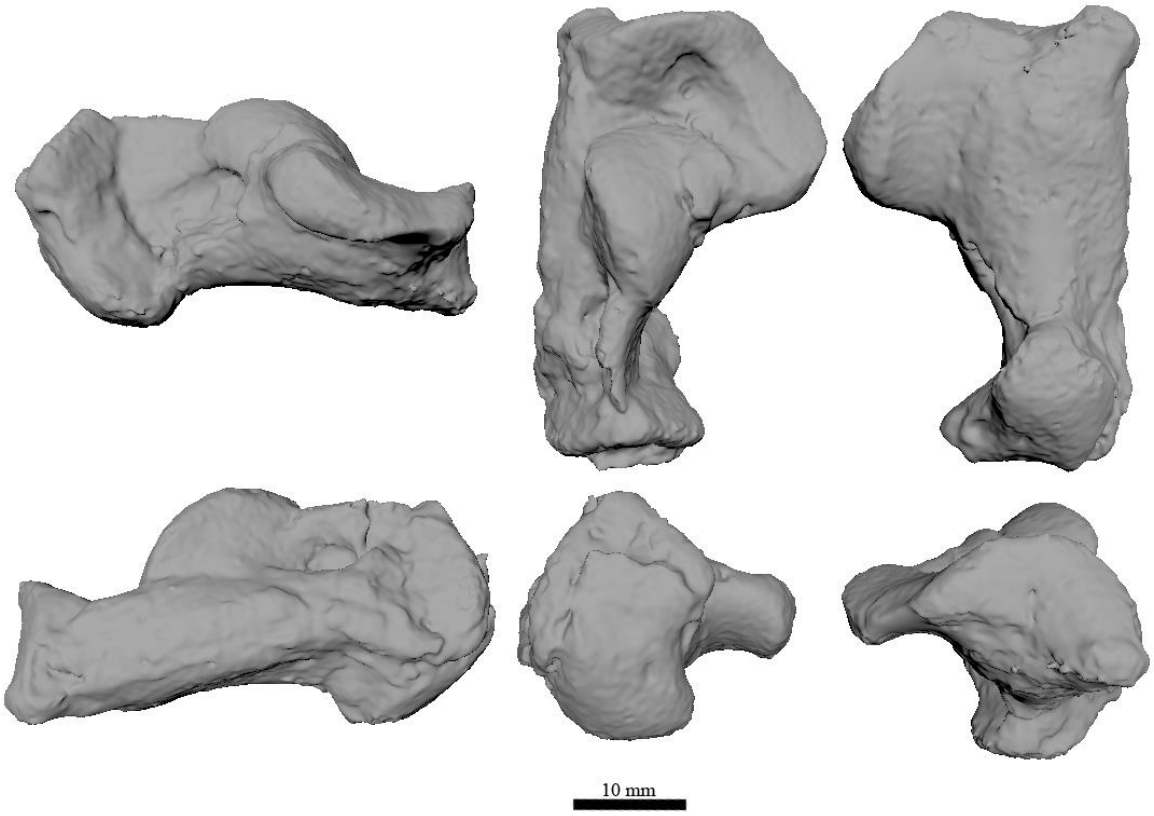

Figure 31: BA 79 left calcaneus attributed to *Oreopithecus bambolii*. Top row views: medial, proximal, plantar. Bottom row views: lateral, caudal, distal.

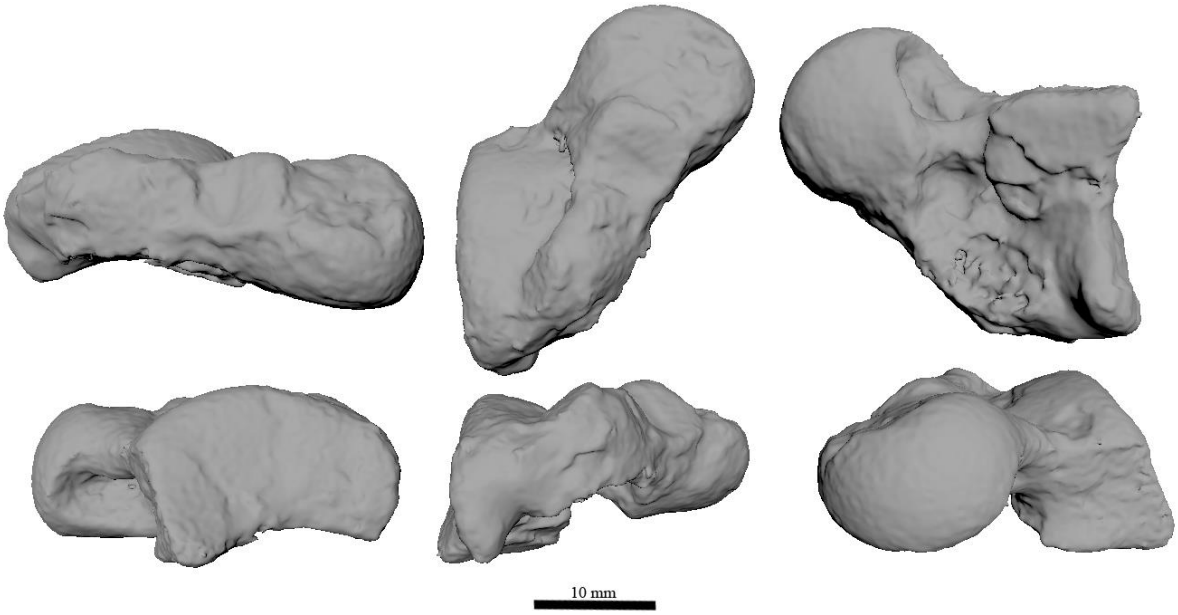

Figure 32: BA 79 left talus attributed to *Oreopithecus bambolii*. Top row views: medial, proximal, plantar. Bottom row views: lateral, caudal, distal.

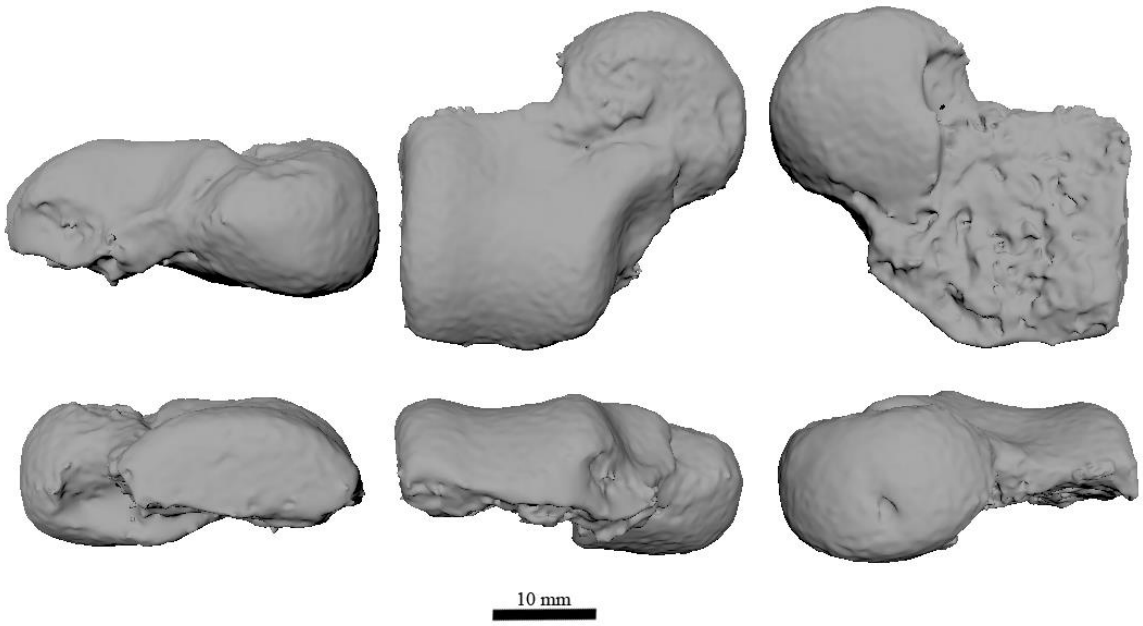

Figure 33: BA 82 left talus attributed to *Oreopithecus bambolii*. Top row views: medial, proximal, plantar. Bottom row views: lateral, caudal, distal.

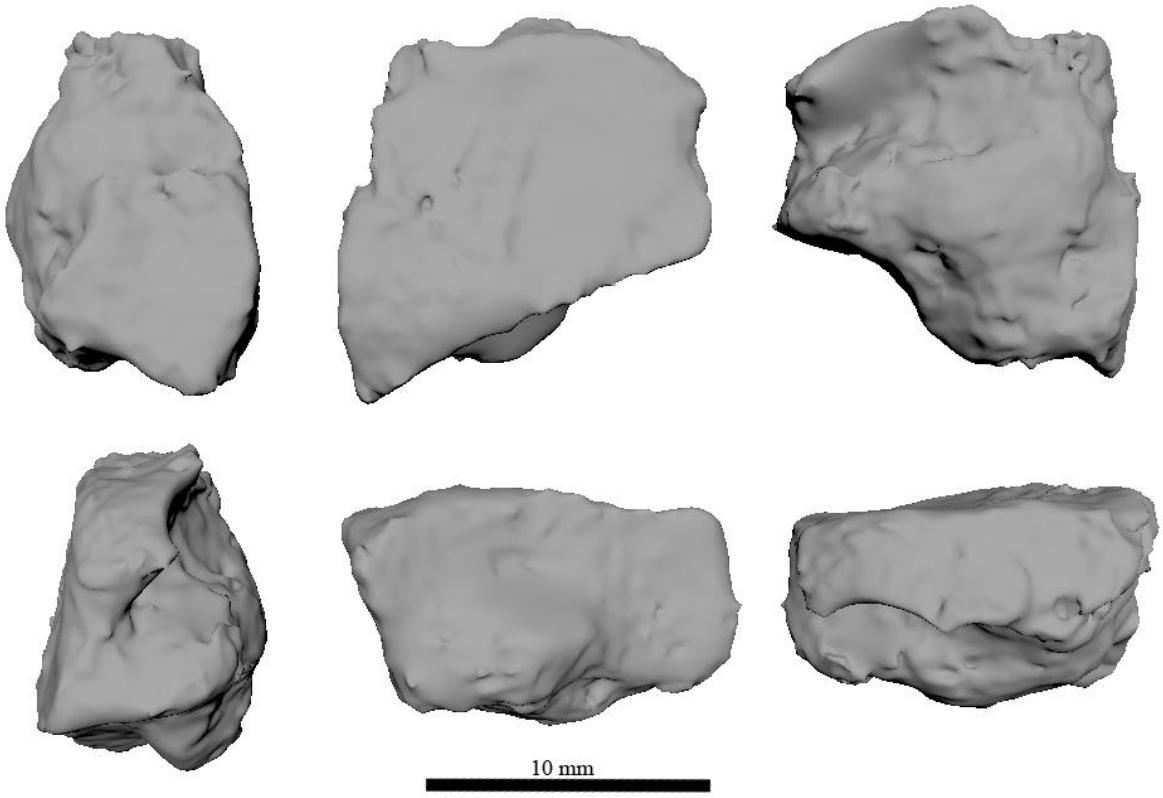

Figure 34: BA 158 right cuboid attributed to *Oreopithecus bambolii*. Top row views: medial, dorsal, plantar. Bottom row views: lateral, proximal, distal.

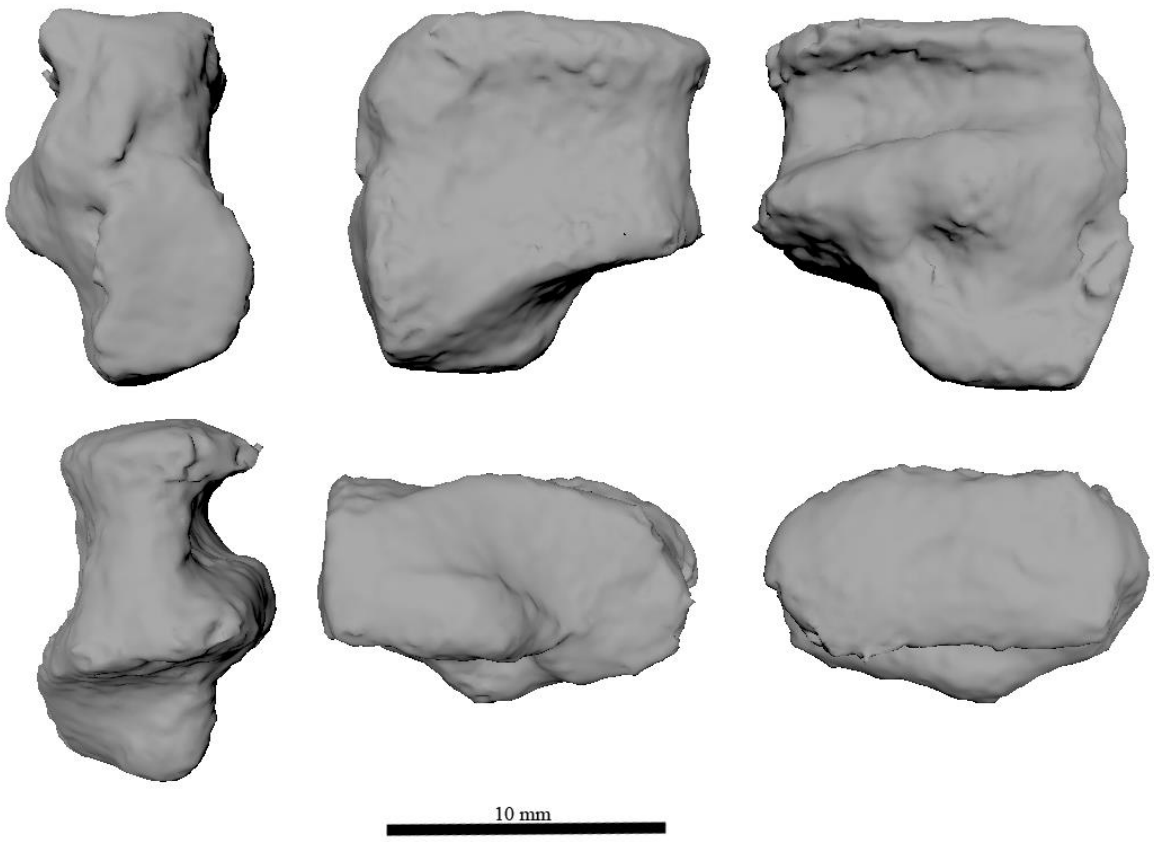

Figure 35: BA 83 right cuboid attributed to *Oreopithecus bambolii*. Top row views: medial, dorsal, plantar. Bottom row views: lateral, proximal, distal.

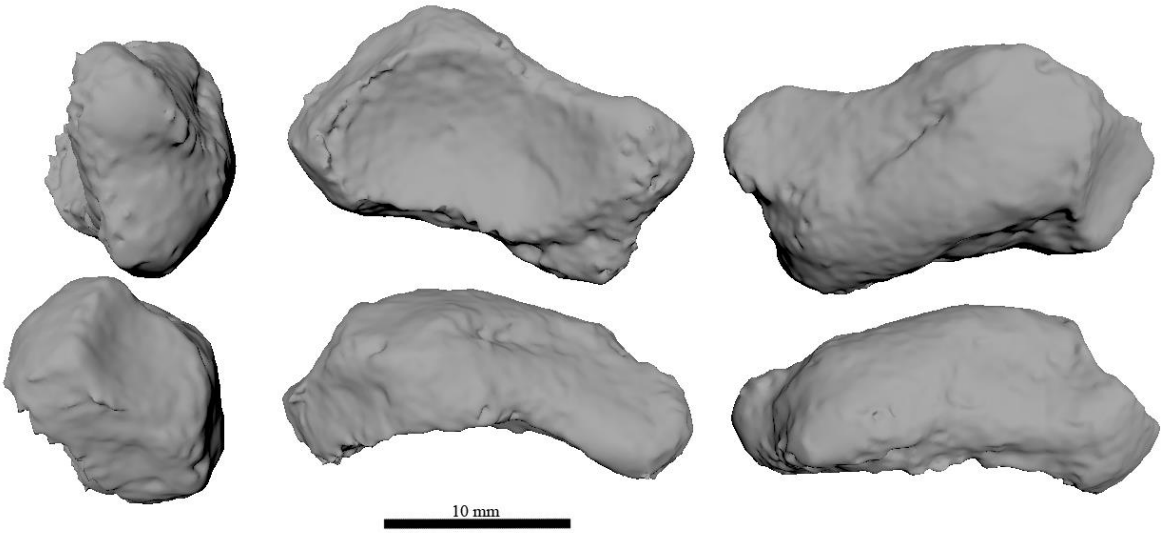

Figure 36: BA 79 left navicular attributed to *Oreopithecus bambolii*. Top row views: medial, proximal, distal. Bottom row views: lateral, dorsal, plantar.

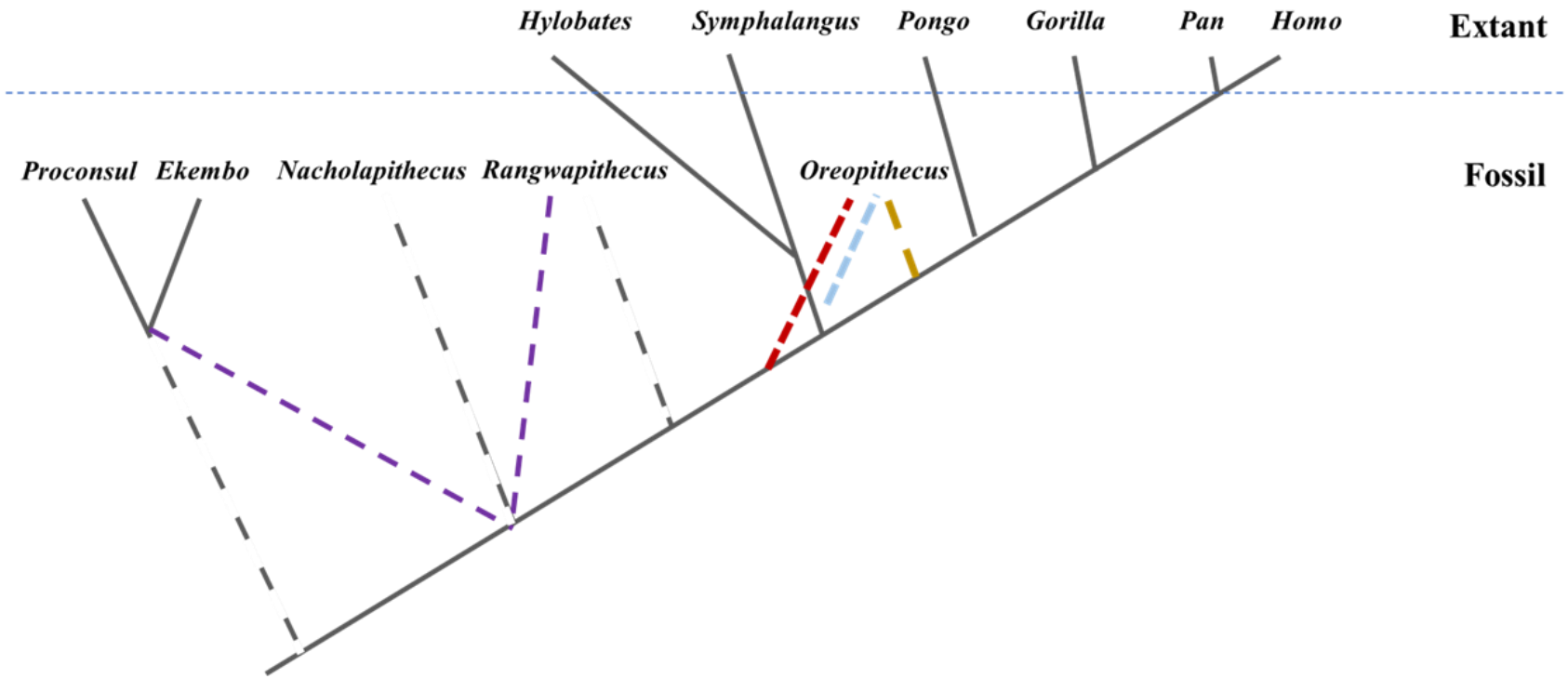

Figure 37: Composite hypothesized phylogeny of fossil hominoids in relation to extant apes. Extant taxa are above the dotted line, whereas fossil taxa are below the dotted line. Extant ape phylogeny is from Perelman et al. (2011). *Proconsul* and *Ekembo* phylogeny based on Nengo et al. (2017) and Rasmussen et al. (2019). *Nacholapithecus* phylogeny based on Nengo et al. (2017). *Rangwapithecus* phylogeny based on Nengo et al. (2017). *Oreopithecus* phylogenetic position based on Young & Maclatchy (2002) (yellow), Begun

(2007) (blue), Thompson & Almécija (2017) (red and yellow), and Nengo et al. (2017) (red). Polytomy of early Miocene hominoids (purple) is based on Ward (pers.comm.).

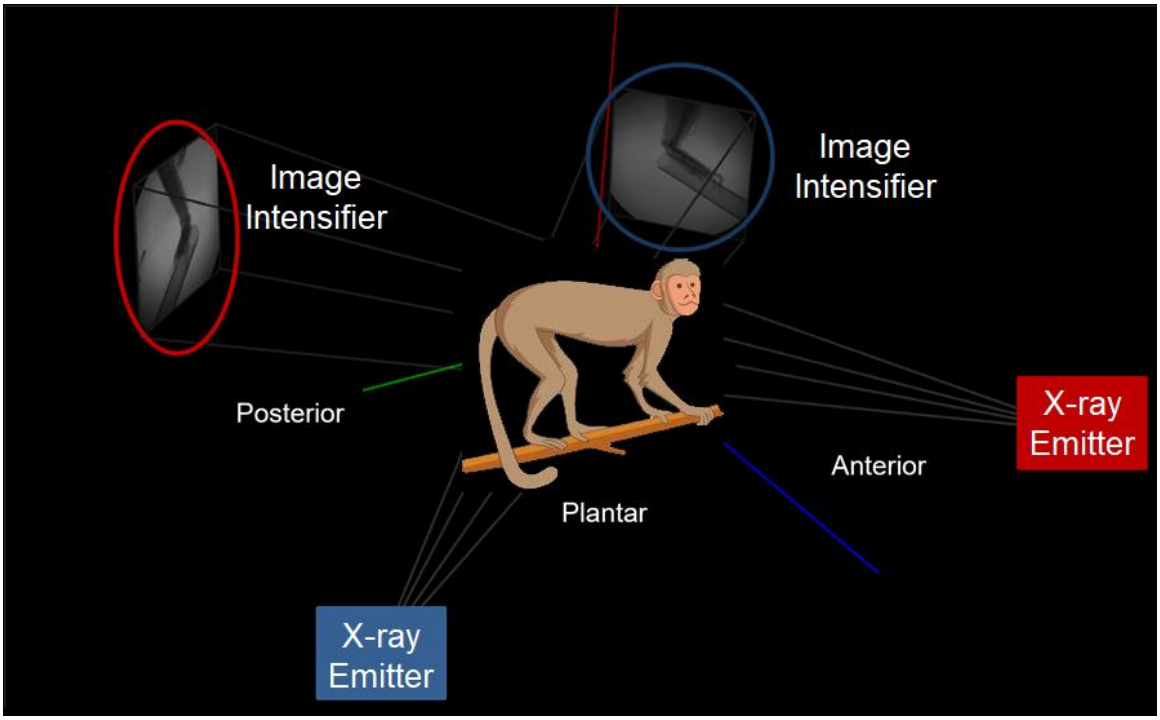

Figure 38: Schematic of XROMM setup. The animal walked between the x-ray emitters and image intensifiers. Each emitter sends x-rays to the corresponding image intensifier on the other side of the animal, producing two sets of 2D images.

Chapter 2: X-ray reconstruction of moving morphology (XROMM) of the talocrural, subtalar, calcaneocuboid, and talonavicular joints in *Macaca mulatta*

Introduction:

Foot Functional Morphology in Anthropoid Primates

Inferring function from form is one of the most important endeavors in biological anthropology, particularly in the interpretation of the fossil record (Morton, 1924; Lewis, 1980a; Langdon, 1986; Gebo, 2010). In order to associate *in vivo* movements with morphological shape variation, one must first understand what motions occur at each joint in question. Primates have a rich locomotor diversity in extant taxa–including such disparate modes as above branch quadrupedalism and brachiation–with similar hypothesized locomotor diversity in the fossil record that warrants further study (Oxnard, 1973; Fleagle, 1984; Gebo, 1986; Rose, 1993; Gebo, 2010). One method to study this locomotor diversity in fossil specimens is to examine the joints of the feet. The bones and joints of the feet are hypothesized to be especially adapted for a given type of locomotion due to the direct interactions between the foot and the substrate (Morton, 1922; Langdon, 1986). In particular, the talocrural, subtalar, calcaneocuboid, and talonavicular joints (Figure 1) are hypothesized to vary among anthropoids to reflect their suspensory, quadrupedal, arboreal and/or terrestrial locomotor specializations (Lewis, 1980b; Latimer et al., 1987).

Tight pedal grasping during arboreal climbing and suspension has been hypothesized to be facilitated by more mobility at the intertarsal joints, leading to more inversion of the foot than during terrestrial locomotion (Close et al., 1967; Inman, 1976; Gebo 2010; Chester et al., 2015; Holowka et al., 2017). Intraspecific differences in tarsal position and movement related to grasping and inversion is predicted to be evident in the talocrural, subtalar, and transverse tarsal joints (Lewis, 1980).

Intertarsal Joint Anatomy

Talocrural Joint

The talocrural joint (Figure 1), or the joint between the tibia/fibula and the talus forms the ankle joint. This study focuses only on the articulation between the talus and tibia. Though primarily responsible for flexion and extension in humans, the talocrural joint also experiences inversion and eversion, particularly in arboreal primates (Wright et al., 1964; Rome, 1996). Latimer et al. (1987) measured 35˚ to 60˚ of excursion between extreme plantarflexion and dorsiflexion in a sample of 40 modern humans using an osteological sample, although previous studies have reported wider ranges of dorsiflexion from 10˚ to 51˚ and plantarflexion 15˚ to 56˚ in cadaveric amputated legs (Rasmussen & Tovborg-Jenson, 1982). As noted by Metz-Schimmerl and colleagues (1994), however, movements of the ankle are difficult to quantify, as many studies use passive range of motion, which “are of questionable reliability” (p.443), or other studies are limited to two dimensions and/or skin markers (Schimmerl et al., 1994). As a result, the range of motion at the talocrural joint requires further study with more precise methods that quantify bony movements rather than using soft tissue or cadaveric proxies.

Subtalar Joint

The subtalar joint, between the talus and calcaneus (Figure 1), consists of the anterior, middle, and posterior subtalar joints but is considered one joint functionally (Lewis 1980; Close et al., 1967; Sarrafian, 1993) and are therefore grouped as one joint in this study. Most inversion and eversion are thought to occur at the subtalar joint, particularly during arboreal locomotion on small-diameter substrates that require tight grasping (Lewis, 1980; Langdon, 1986). However, the degree of inversion/eversion versus plantarflexion/dorsiflexion that occurs at this complex joint and how these two motions occur in conjunction during a step require further *in vivo* study (Manter, 1941; Wright et al., 1964; Close et al., 1967; Lewis, 1980; Sarrafian, 1993). In response to the paucity of data on subtalar range of motion, Beimers and colleagues (2008) used CT imaging to quantify bony movements between the talus and calcaneus. They noted that the talus is particularly difficult to landmark externally and that the complexity of subtalar joint morphology precluded *in vivo* data collection for their study (Beimers et al., 2008). They instead placed subjects in a medical CT scanner with one foot affixed to a footplate that positioned the foot in eight extreme positions to measure the subtalar displacement between these foot postures (Beimers et al., 2008). They found 27˚-50˚ of rotation between the calcaneus and talus between extreme eversion to extreme inversion, but noted the difficulty—and necessity—in quantifying these joints *in vivo*.

Transverse Tarsal Joint

The transverse tarsal joint complex consists of the calcaneocuboid and talonavicular joints (Figure 1), but these two are often considered together as one joint

complex (Manter, 1941; Bojsen-Møller, 1979; Lewis, 1980; Langdon, 1986; Cornwall, 2002). Both joints are described as becoming close-packed in extension for stability, particularly in taxa that require more foot propulsion than mobility (Gebo & Schwartz, 2006). However, the amount of plantarflexion, dorsiflexion, inversion, and eversion that occur at the calcaneocuboid and talonavicular joints during *in vivo* locomotion has not been quantified. The independence in movements, in magnitude, plane, or timing between these two joints during locomotion could challenge the treatment of the transverse tarsal joint as a functionally single joint complex.

The calcaneocuboid joint, the lateral portion of the transverse tarsal joint, is hypothesized to be the location of the midtarsal break, the point where dorsiflexion of the foot occurs during stance phase in non-human primates (Elftman & Manter, 1935). The anatomical location of the midtarsal break, however, has been questioned due to hypothesized inabilities of the calcaneocuboid to excurse to the degree that the primate midfoot dorsiflexes during locomotion (D'Août et al., 2002). Instead, DeSilva (2010) hypothesized that this dorsiflexion actually occurs between the cuboid and fifth metatarsal (MT5). Using a combination of osteological and soft-tissue specimens, radiographs, and externally-observed kinematics, DeSilva (2010) concluded that the majority of midfoot dorsiflexion occurs distal to the cuboid. The use of *in vivo* visualization and quantification of the calcaneocuboid and cuboid/MT5 joints during locomotion would support or refute the midtarsal/midfoot break hypothesis and determine whether the calcaneocuboid joint is responsible for the majority of midfoot dorsiflexion during late midstance.

The talonavicular joint forms the medial half of the transverse tarsal joint, but little is known about the rotations that occur at this joint during locomotion. Movement at the talonavicular joint is hypothesized to be more restricted in terrestrial taxa than in suspensory taxa, but this hypothesis has not been thoroughly explored across anthropoids with different locomotor types (Langdon, 1986). The amount of inversion/eversion and plantarflexion/dorsiflexion that occurs at this joint is unknown but is thought to be related to movement at the calcaneocuboid joint, as both make up the transverse tarsal joint (Lewis, 1980a). As with the subtalar joint, the role of both joints in producing foot inversion and eversion, how much and when in the gait cycle the most inversion and eversion occur, and to what degree these joints work as one joint complex all require further *in vivo* study (Manter, 1941; Wright et al., 1964; Close et al., 1967; Lewis, 1980).

The motions at the calcaneocuboid and talonavicular, however, have also been found to differ from each other. Gomberg (1985) has hypothesized that movements at this joint are minimized to turn the human foot into a lever during the second half of stance phase. Gomberg (1985) describes motions at the transverse tarsal joint during stance phase in human locomotion: due to the transverse arch, when the foot flattens on the ground, the navicular rotates counterclockwise, while the cuboid rotates clockwise, resulting in opposing rotations at the talonavicular and calcaneocuboid joints. The importance of midfoot stability in humans during bipedal locomotion as well as the midfoot mobility in nonhuman primates make the transverse tarsal joint an important joint complex to investigate further. Additionally, the magnitude of motion that occurs at this supposed joint complex was studied in chimpanzees using cineradiography. Thompson and colleagues (2014) found that in the sagittal plane, the talonavicular joint is

more mobile than the calcaneocuboid joint, exhibiting over double the amount of excursion (Thompson et al., 2014).

Evaluating Foot Function in Anthropoid Primates

Motion of intertarsal joints in nonhuman primates has traditionally been difficult to evaluate in 3D (D'Août et al., 2002; DeSilva, 2008; Thompson et al., 2014), despite this information forming the basis of functional models used in studies of primate feet. In order to interpret isolated tarsal bones in the hominoid fossil record, where soft tissues that inform range of motion are absent, we need to understand how the bones are moving during locomotion and which aspects of bone morphology reflect that locomotion. Although we cannot study *in vivo* locomotion in fossil taxa—or even in many extant taxa in a laboratory setting—understanding the precise intertarsal rotations of available extant primates will provide a better appreciation of *in vivo* kinematics, which can be integrated with bone shape for a biomechanically-based interpretation of foot functional morphology.

To date, foot bone functional anatomy and tarsal mobility have been assessed to some extent using methods such as external markers, cadaveric range of motion, and cineradiography. External markers on the foot or external observations of the ankle (Leardini et al., 1999; Hunt et al., 2001; DeSilva, 2008; Channon et al., 2011; Leardini et al., 2007; Griffin et al., 2015; Holowka et al., 2017) allow for non-invasive observation of movements *in vivo*, thereby allowing for a sample of diverse taxa including endangered great apes, but these methods do not always capture subtle motions of each bone, as the bones are covered with soft tissue, limiting the ability to quantify bony movement at

individual joints (Cornwall, 2002). Studies based solely on cadaveric or anesthetized specimens (Morton, 1922; Langdon, 1986; Ouzounian & Shereff, 1989; Hintermann et al., 1994; Hamel et al., 2004; Holowka & O'Neill, 2013; Greiner & Ball, 2014; Thompson et al., 2014a; DeSilva et al., 2015) can offer precise bony morphology visualization but do not account for active muscle contraction and natural gait kinematics that occur *in vivo*. Cineradiography can assess motion between tarsals (Thompson et al., 2014a; Hesse et al., 2015) but limits the ability to quantify motions not restricted to one plane. However, none of these methods has been able to visualize and quantify 3D motion and posture of the individual pedal elements during locomotion *in vivo*.

X-ray Reconstruction of Moving Morphology (XROMM)

X-ray reconstruction of moving morphology (XROMM) is a relatively new, validated technique in vertebrate functional morphology for studying *in vivo* movements that are subtle or otherwise undetectable (Brainerd et al., 2010; Gatesy et al., 2010). XROMM uses biplanar fluoroscopy in combination with CT scans of the same individual to track complex, 3D movements in live specimens (Figure 2) and has allowed for the successful visualization and analysis of an array of behaviors that are otherwise difficult or impossible to visualize and quantify *in vivo* in taxa such as frogs (Astley & Roberts, 2012), alligators (Baier & Gatesy, 2013), chukars (Baier et al., 2013), carp (Gidmark et al., 2013, 2014), bass (Camp & Brainerd, 2015), guineafowl (Kambic et al., 2015), pigs (Menegaz et al., 2015), rats (Bonnan et al., 2016), iguanas (Brainerd et al., 2016), and macaques (Orsbon et al., 2018). Marker-based XROMM uses tantalum beads, which are surgically embedded to track the three-dimensional movements of each rigid body while

the animal is moving, as described by Brainerd and colleagues (2010) and shown in Figure 2.

To date, no other XROMM studies of macaque locomotion have been published. Two-dimensional variations of this approach have been used by employing standard plain film radiography or uniplanar cineradiography to assess hip and transverse tarsal kinematics in chimpanzees (Jenkins, 1972; Thompson et al., 2014) and cotton-top tamarins (Hesse et al., 2015). Thompson and colleagues (2014) studied transverse tarsal joint range of motion during midstance-to-toe-off plantarflexion and found that in anesthetized chimpanzees, the talonavicular joint underwent more plantarflexion than the calcaneocuboid joint. However, the authors admitted that additional motion may occur outside the sagittal plane, which they could not quantify in their uniplanar analysis. Tracking static *in vivo* tarsal position using markers has also been accomplished in humans, where tantalum markers were placed in live human legs and feet and subjects were asked to stand in different postures while two x-rays were taken at right angles to each other at every 10˚ of joint rotation (Lundberg, 1989; Lundberg et al., 1989). Due to the use of plain film radiography, continuous movements were not captured in this study, but through the visualization of tarsals at set points, the authors inferred movement and compared postures on differently inclined surfaces (Lundberg, 1989). Despite these advances in our understanding, no study to date has evaluated continuous, 3D movements of tarsals *in vivo* during anthropoid primate locomotion.

XROMM is ideal for studying foot bones because it allows the position and movement of each bone to be visualized during gait. Tarsals are small and complicated in shape and motion and are difficult to evaluate from observing external markers. The

movements that occur at the talocrural, subtalar, and transverse tarsal joints are often conjunct and non-planar, related to motions at the talocrural joint, and are therefore not adequately captured in uniplanar studies (Inman, 1976; Lundberg, 1989). XROMM is currently the only method that can visualize, track, and quantify *in vivo* the functionally relevant motion among these small bones in 3D. XROMM analytic techniques allow the rotations and translations of bones to be quantified and compared throughout a gait cycle as the animal moves.

The goal of this study is to quantify the degree of rotation about the transverse and long axes of the foot, representing plantarflexion/dorsiflexion and inversion/eversion, respectively, at the talocrural, subtalar, calcaneocuboid, and talonavicular joints in *Macaca mulatta* using markered XROMM and test hypotheses concerning movements at these joints. Based on the foregoing discussion, I have developed five hypotheses regarding motions of the foot joints which can be answered using an XROMM approach: 1) I hypothesize that the location of the midtarsal/midfoot break, or the most lateral instance of foot plantarflexion, occurs at the joint between the cuboid and the fifth metatarsal rather than at the calcaneocuboid joint. 2) I also hypothesize that motion at the talocrural joint on a flat surface would be mainly restricted to plantarflexion and dorsiflexion, with minimal or no inversion or eversion. 3) I hypothesize that inversion and eversion will occur at the subtalar joint. 4) I expect that on a flat surface, there is more plantarflexion and dorsiflexion at the calcaneocuboid and talonavicular joints, since no grasping is occurring. 5) If the transverse tarsal joint is truly a single joint complex, then the movements that occur at these two joints will be correlated with each other both in timing and degree of rotation.

Methods:

Specimens

Two *Macaca mulatta* specimens were used in this study. These monkeys, which have no pathologies or gait abnormalities, were previously used in a feeding study at the University of Chicago by Dr. Callum Ross (NSF MRI-DBI 1338066). All Animal Care and Use Protocols were approved by the University of Chicago (ACUC # 71565, 72351, 72430; PHS # D16-00322-A3523-01). These monkeys were captive-raised adult research specimens. As a result, there are activity and nutrition related differences between these specimens and animals in the wild. In addition, due to the constraints of *in vivo* primate research, only two macaques were used.

Each monkey underwent surgery to have 1 mm non-bioreactive tantalum beads implanted into the cortical bone of the calcaneus, cuboid, and MT5 of monkey 1 and the tibia, calcaneus, talus, cuboid, and navicular of monkey 2 using a 1 mm-diameter mini hand drill. Each bone has at least three markers and care was taken to avoid marker collinearity (Figure 3). Tantalum markers permit the 3D models generated from CT scans to be registered to the video fluoroscopy images (Brainerd et al., 2010). The small size of the drill and beads causes minimal soft tissue damage to the animal and the hole created in the cortical bone is small, thereby allowing for quick healing and minimization of pain associated with the procedure. Each animal was given at least two weeks to recover from the surgery. This marker implantation process has been used in previous studies, including lower limbs of frogs (Astley & Roberts, 2012) and the mandibles of pigs (Menegaz et al., 2015), with negligible effect on performance and, in humans, with reported discomfort ceasing after one week (Lundberg, 1989).

Fluoroscopy

After the animals healed, motion was analyzed using the markered XROMM protocol outlined by Brainerd and colleagues (2010). Two fluoroscopes sent x-rays through the animals into corresponding image intensifiers, which were attached to high speed video cameras, thereby creating two radiographic movies, recorded at 150 f/s (Figures 2-3). The overlapping space between the two sets of fluoroscopes was calibrated using an undistortion grid over the image intensifiers, as well as using a calibration reference point cube, following the procedures outlined by Brainerd et al. (2010).

The macaques were trained to walk in a specially designed treadmill to simulate terrestrial or large-substrate quadrupedalism. The treadmill was placed in a transparent polycarbonate chamber to contain the animal (Figure 4). The monkeys walked in a calibrated space in the field of view of both fluoroscopes for at least 30 steps per day on three different days. Only steps that were visible in both fluoroscope videos were quantified using XROMM (Table 1). The fluoroscopy videos were assessed for digitization clarity and processed in *XMALab1.5.0* (Knörlein et al., 2016), where the 3D positions of the implanted beads were tracked. For Monkey 1 six steps were digitized for motion at the calcaneocuboid and cuboid/MT5 joint (Table 1). For monkey 2, five steps were digitized, but the tibia was not visible through the entire trial in one step, so the talocrural is only represented by four steps in this study. The subtalar, calcaneocuboid, and talonavicular each had five steps tracked and processed (Table 1).

Image Processing

The lower limb of each animal was CT scanned at the University of Chicago using a GE Phoenix v|tome|x s Industrial High-Resolution CT scanner (150 kV, 150 mA for 1000 ms, at 89.4 μm). These scan data were segmented in *Avizo 7.0* to create 3D polygonal models of each bone and the markers (Figure 1). Marker coordinate exporting, rendering, joint rotation quantification, and animation were all performed in *Maya2016* (Autodesk, San Rafael, CA) using a separate MEL-coded plugin specifically for XROMM animation (Brainerd et al., 2010). The 3D positions of each marker were exported from *Maya2016* into individual bone files and imported into *XMALab1.5.0* as rigid body files (n = 4 markers for the talus of Monkey 2; n = 3 markers for the remaining bones). Error was quantified in *XMALab* using mean rigid body error, which calculates the difference between the known 3D distances of the markers from the CT scan and the 3D distances of the marker tracking of the user (Knörlein et al., 2016). The rigid body transformations, resulting from the 3D movements of each point within a rigid body, were then exported from *XMALab* and imported into *Maya2016.* The polygonal models of the tibia, talus, calcaneus, navicular, and cuboid were used to render the 3D coordinates of the rigid bodies within the *in vivo* trials in *Maya2016*.

Joint Rotation Measurement

To quantify rotation between pairs of bones during locomotion, a joint coordinate system was aligned with each of the studied joints from midstance to toe off in *Maya2016* (Brainerd et al., 2010) (Figure 5). The joint coordinate system uses the movements of the proximal and distal elements to calculate the rotation and translation that occurs in the x, y, and z axes between bones. The joint coordinate system was

aligned with the anteroposterior axis of the foot, the mediolateral axis of the foot, and the proximodistal axis of the leg, or dorsoplantar axis of the foot (Figure 5). Kinematic variables of interest for this study were rotation about the long axis, representing inversion/eversion and rotation about the mediolateral axis, representing plantarflexion/dorsiflexion (Figure 5). Directionality of the rotations are determined using the right-hand rule for the joint coordinate axes in Figure 5. Maximum rotations were calculated from each motion (plantarflexion/dorsiflexion, inversion/eversion) for each joint. Maximum rotations were used as a simplified comparison between motions within a joint and between joints because 1) movements may occur at different times of the gait cycle, making comparisons difficult, and 2) because extreme habitual motions at the intertarsal joints drive the variation of bone morphology, which is of interest to this dissertation. As such, the rotation at the maximum excursion in any direction is the most valuable measure in each step. Translation was also calculated for each joint but, as expected, was negligible and is therefore not reported in this study. To assess joint placement error, the maximum rotation in the x, y, and z planes for two joints were each calculated three separate times. The mean maximum rotation and the distance from the mean point were calculated for each rotation in each direction, for each joint.

Analyses

Analytical p-values from a t-test were calculated with randomization in order to compare maximum rotation between joints and among motions within a joint. In addition to visualizing total rotation throughout a step, to explore how closely inversion/eversion and plantarflexion/dorsiflexion were related in each step, maximum rotations were also

explored per step, and Spearman's rank correlation analyses were carried out between both motions in each joint. Similar correlation analyses were carried out between the same motions of the calcaneocuboid and talonavicular joints in order to explore the association of the joints that make up this hypothesized joint complex. To correct for multiple comparisons, the adjusted p-values are reported here using the Benjamini & Hochberg (1995) method ("BH"). All statistical analyses were carried out in *R Statistical Software* (R Core Team 2013). Overlaid polygonal models of the whole foot posture and paired bone positions at midstance and the end of stance phase were created to visualize overall foot postural changes through the step in *Maya* by importing two copies of the foot scan from Monkey 2, aligning one with the first frame and the other with the last frame of animation. The whole models were then aligned at the tibiae to show relative change position of the foot and the same procedure was carried out for each joint studied. In the individual joint overlays, the proximal element was always aligned to itself to visualize the displacement of the distal element.

Results:

Error Measures

Rigid body error, or difference between the known 3D distances of the markers from the CT scan and the 3D distances of the marker tracking calculated in *XMALab* determined for each bone in each trial for both monkeys (Table 2). All rigid body errors were less than 1 mm, with the exception of error measurements on the calcaneus of Monkey 1 in trials 4 and 5, which were both 1.1 mm. Error associated with joint axis placement was also assessed. Mean joint axis error for the three trials of the two joints in

the error study was 2.3˚. As such, any maximum rotations below 2.3˚ is considered indistinguishable from joint placement error in this study.

Midfoot Break

Rotation about the transverse axis was calculated between the cuboid and calcaneus, as well as between the cuboid and MT5, to evaluate the location of the midtarsal/midfoot break, as hypothesized by DeSilva (2010). Significantly more dorsiflexion occurred at the cuboid/MT5 joint in the six steps analyzed than dorsiflexion at the calcaneocuboid joint ($p = 0.006$). This finding indicates that dorsiflexion in the lateral midfoot region mostly takes place at the tarsometatarsal (cuboid/MT5) joint (Figure 6; Table 3), providing evidence of a midfoot, rather than midtarsal break, and support for Hypothesis 1.

Talocrural Joint

Motion at the talocrural joint was predominately about the transverse axis (plantarflexion/dorsiflexion), though a small amount (up to 6 degrees) of inversion/eversion did occur at this joint (Figures 7 & 8; Table 4). Maximum rotations in plantarflexion/dorsiflexion had a significantly larger range (3˚-26˚) than inversion/eversion rotations, which were restricted to 3˚-6˚ (Figures 7 & 8), and the amount of plantarflexion and dorsiflexion was greater than inversion and eversion ($p = 0.042$). When overlaid (aligned by the tibia), the end position of the talus at the talocrural joint is inverted, indicating that the slight amount of inversion was enough to affect the

posture of the foot (Figure 7). Therefore, Hypothesis 2 that the talocrural joint will undergo minimal inversion is supported.

Subtalar Joint

Unlike the talocrural joint, roughly equal amounts of long axis rotation and transverse axis rotation ($p = 0.44$) occur at the subtalar joint (Figures 9 & 10; Table 4). Both inversion and dorsiflexion appear to gradually increase following midstance, with no sharp incline in any of the recorded steps for either motion (Figure 9). The degree of overall rotation overlaps between long axis rotation and transverse axis rotation (Figure 9) and the means are indistinguishable for the steps analyzed in this study (Figure 10). When maximum rotations were plotted by trial, the plantarflexion/dorsiflexion and inversion/eversion appear to fluctuate in a similar pattern (Figure 15). This provides support for Hypothesis 3, that inversion occurs at the subtalar joint. Maximum rotations about both axes were also highly correlated (Spearman's rho = 0.9; $p = 0.037$), indicating that the joint undergoes plantarflexion/dorsiflexion and inversion/eversion to similar degrees during locomotion. The subtalar joint was the only joint studied with a significant correlation between these two motions (Figure 15). When the end position of the talus and calcaneus were overlaid onto their starting position (aligned by the talus), the calcaneus was inverted and dorsiflexed relative to the talus.

Calcaneocuboid Joint

Movements at the calcaneocuboid joint underwent a mix of inversion and eversion (Figure 11). Additionally, this joint underwent plantarflexion, though not to a

significantly greater extent than the inversion/eversion ($p = 0.72$; Figure 12), thereby failing to reject the null of Hypothesis 4 for the calcaneocuboid joint. The variation in maximum rotations at this joint was high, with plantarflexion increasing more gradually than inversion/eversion (Figure 11; Table 4). There was no significant correlation between the maximum rotations of plantarflexion/dorsiflexion and inversion/eversion at the calcaneocuboid joint ($p = 0.15$) (Figure 15).

Talonavicular Joint

Unlike the calcaneocuboid joint, the talonavicular joint displayed more inversion/eversion than plantarflexion/dorsiflexion ($p = 0.015$) (Figures 13 & 14), unlike predicted in Hypothesis 4. Inversion increased towards the end of the step, whereas the degree of dorsiflexion remained relatively constant throughout the step (Figure 13; Table 4). This inversion can be seen when the position of the talus and navicular at midstance is overlaid with their positions at the end of stance phase (Figure 13). There was no significant correlation between inversion/eversion and plantarflexion/dorsiflexion in the talonavicular joint ($p = 0.25$) (Figure 15).

Transverse Tarsal Joint Complex

Plantarflexion/dorsiflexion and inversion/eversion were also compared between the calcaneocuboid and talonavicular joints in order to determine whether they were correlated. Neither motion revealed a significant correlation ($p = 0.69$ for inversion/eversion and $p = 0.25$ for plantarflexion/dorsiflexion), indicating that these two

joints are not tightly associated in either motion (Figures 16-17) and arguing against their grouping as a single functional joint (Hypothesis 5).

Discussion:

The goal of this study was to quantify maximum dorsiflexion, plantarflexion, inversion, and eversion at the talocrural, subtalar, calcaneocuboid, and talonavicular joints in the foot of macaques during terrestrial locomotion in order to evaluate relative motions within a joint, relative motion between joints, and relative contributions to hypothesized joint complexes. It was hypothesized that 1) the location of the midtarsal/midfoot break occurs at the joint between the cuboid and the fifth metatarsal rather than at the calcaneocuboid joint; 2) that the talocrural joint on a flat surface would mainly be restricted to plantarflexion and dorsiflexion; 3) that the subtalar joint would undergo plantarflexion/dorsiflexion and inversion/eversion; 4) that more plantarflexion and dorsiflexion would occur at the calcaneocuboid and talonavicular joints than inversion and eversion on a flat surface; and 5) that movements of the calcaneocuboid and talonavicular joints will be correlated with each other if the transverse tarsal joint complex is functionally one joint.

Calcaneocuboid Joint and the "Midtarsal Break"

Because the fifth metatarsal was marked with tantalum beads and tracked in Monkey 1, its relative contributions to lateral foot plantarflexion were explored. Plantarflexion at the cuboid/MT5 joint exceeded plantarflexion at both the calcaneocuboid and talonavicular joints, supporting DeSilva's (2010) hypothesis that the

midtarsal break was erroneously hypothesized to occur at the transverse tarsal joint and should instead be considered a midfoot break, located distal to the cuboid rather than proximal.

This finding highlights the importance of precise quantification of the intertarsal movements of the foot and ankle, as data based on external observations alone were unable to aptly pinpoint the location of movements that are thought to be important in the locomotion of primates (Elftman & Manter, 1935; DeSilva & Gill, 2013) but had not been previously confirmed.

Talocrural Joint

As hypothesized, the talocrural joint primarily underwent plantarflexion and dorsiflexion; however, a small amount of inversion was present, even in the ankle of a quadrupedal monkey walking in a straight line on a flat surface. This leads to speculation that inversion would be greater on a small-diameter substrate such as a branch, as arboreality requires the entire foot to be inverted, and the talocrural joint would contribute to this inversion. This also leads suggests that the morphology of the talocrural joint may display adaptations for climbing to allow for such inversion. The talar trochlea is expected to differ between taxa with disparate locomotor repertoires. Highly arboreal taxa are expected to have flat talar trochlea to allow for more mobility during plantarflexion and asymmetrical talar trochleae to place the foot in an inverted position when walking on a small branch or during vertical climbing (Langdon, 1986; Dunn et al., 2014; Knigge et al., 2015). Terrestrial taxa that emphasize stability during plantarflexion/dorsiflexion, on the other hand, are expected to have taller trochleae to

minimize non-parasagittal movements during locomotion (Strasser 1988). Talar trochlear curvature, which is associated with plantarflexion/dorsiflexion would also be expected to vary among taxa that move differently, given the large range of plantarflexion/dorsiflexion that occurs at this joint. A broad morphological study of osteological correlates of locomotor differences is needed to test these hypotheses. Additionally, the large range of plantarflexion/dorsiflexion (23˚ range) was curious, though broader ranges have been measured previous studies of human locomotion (25˚ range in Latimer et al., 1987; 41˚ range in Rasmussen & Tovborg-Jenson, 1982). This may be related to the inability to direct the monkey on a treadmill to 'walk normally' and this study may have captured an aberrant step that would artificially affect how much movement occurred at this joint. Using light camera measurements to standardize the amount of rotation at that joint by how far the monkey moved forward may be informative. More steps analyzed will shed light on whether some of our values are outliers.

Subtalar Joint

Unlike the talocrural joint, the subtalar joint underwent roughly equal inversion/eversion compared to dorsiflexion/plantarflexion (Figure 11). However, this degree of inversion observed in this study is not significantly higher than the other joints quantified in the present study. This is likely because trials were limited to a flat surface, and the subtalar joint is likely more responsible for inversion on curved surfaces (Lewis 1980b). Therefore, I would expect to see more inversion at the subtalar joint on a curved surface than a flat one due to the need for the foot to assume an inverted posture to

effectively grasp a small substrate during locomotion. It appears that on a flat surface, the subtalar joint is only responsible for slightly more inversion than at the other joint studied but still significantly more than the talocrural joint. Maximum plantarflexion/dorsiflexion and inversion/eversion were highly and significantly correlated (Figure 12), and the paired motions follow each other in each step (Figure 10). It appears that plantarflexion/dorsiflexion and inversion/eversion are tightly associated during locomotion and occur equally on a flat surface. I would expect to see a spectrum of morphologies allowing for both motions at the subtalar joint, such as the posterior subtalar articular surface orientation differing among taxa with varying arboreality.

Transverse Tarsal Joint Complex

Close examination of the transverse tarsal joint complex revealed previously unknown kinematics of the joint complex. Although the calcaneocuboid and talonavicular joints rotate in conjunction along with overall movement of the foot, the two joints display independent movements that challenge the treatment of these two joints as a single joint complex in degree and timing of rotation. Contrary to one of the predictions of this study, the talonavicular joint exhibited more inversion than the calcaneocuboid joint during locomotion on a flat surface, likely due to the tibialis posterior muscle tendon puling on the medial navicular tuberosity (Netter, 2010) during plantarflexion, which would pull the bone into inversion, even on a flat surface. Increased inversion occurred later in the second half of late stance phase (Figure 13), whereas there was no such discernable spike in movement at the calcaneocuboid joint (Figure 11).

Furthermore, the correlation between the maximum rotations of the calcaneocuboid and talonavicular joints was not significant, bringing even more doubt to their treatment as one single joint complex. Aside from the physical proximity to each other, the calcaneocuboid and talonavicular joints do not appear to work in conjunction more than one would expect for adjacent joints to interact. Whereas the calcaneocuboid joint displayed equal amounts of inversion/eversion and plantarflexion/dorsiflexion (Figures 11 & 12), the talonavicular joint displayed relatively more inversion in the trials quantified in this study (Figures 13 & 14). Talonavicular inversion also occurred later in the step than did calcaneocuboid inversion/eversion, and later than plantarflexion occurred in both joints. Based on these results, I hypothesize that the talus and navicular would have more osteological correlates of long axis rotation, more so than in the calcaneocuboid joint, which I hypothesize may display more evidence for joint stability when climbing. More eversion may occur in some taxa at the calcaneocuboid joint during vertical climbing, when the tendon of peroneus longus, which runs along the lateral and plantar surfaces of the cuboid (Netter 2010), would be engaged to evert the foot.

Limitations

The results of this study are based on two live laboratory macaques with different body masses. The difference between wild and laboratory macaque hind limb biomechanics and between small and large animals are unknown, particularly in the foot where little previous quantification of joint rotations and translations has been undertaken. Nonetheless, ankle excursion calculations from these trials were similar to kinematics from non-XROMM studies of macaque locomotion (Granatosky et al., 2018).

Additionally, the animals were walking on a treadmill, in an enclosure, and on a leash to ensure the safety of the researchers, staff, and monkeys. This setting obviously does not mirror locomotion in the wild; the compliance of the treadmill, the lack of obstacles or incline change in the treadmill, and the inability to change directions in the enclosure are conditions exclusive to a laboratory setting.

Nevertheless, this study serves as a valuable initial baseline dataset from which to expand investigations considering different substrate sizes and orientations. Understanding how tarsal elements move and are positioned during *in vivo* locomotion is necessary to begin building an informed context to understand extant variation in tarsal bone morphology. Comprehension of locomotion in extant species and accurately inferring function from bone form are imperative for accurately reconstructing foot function in extinct animals.

This study emphasizes the importance of precise joint rotation quantification in the study of functional morphology, particularly in regions such as the foot, which is difficult to examine without 3D x-ray methods such as XROMM. This study represents a preliminary first step in the use of XROMM on primate locomotion, which will provide a biomechanical basis for interpretation of locomotion of both extant and extinct taxa.

Conclusion:

This study is the first to visualize and quantify catarrhine locomotion in 3D using markered XROMM, as well as the first study to assess the 3D joint rotations of the talocrural, subtalar, calcaneocuboid, cuboid/MT5, and talonavicular joints. It provides functional interpretations of previously established joint complexes such as the

midtarsal/midfoot break and the transverse tarsal joint. This study confirmed previous hypotheses that the midfoot break occurs distal to the cuboid though direct measures of intrinsic foot movements. The predominance of plantarflexion/dorsiflexion at the talocrural joint on a flat surface implies that species that mainly engage in propulsive quadrupedalism will have morphologies that emphasize stability in this parasagittal motion. This study also confirmed that on a flat substrate, inversion and eversion occur at the subtalar joint, which was also found to have a strong correlation between different motions at this joint. Evidence of adaptation for extreme inversion and eversion is thus hypothesized to be evident in the subtalar joint in suspensory taxa. The transverse tarsal joint was found to not function as a single joint complex and will thus be treated as two independent joints in further analyses. The results of this study can be applied to a broader morphometrics analysis to assess variation in bony tarsal morphology among a diverse sample of primate taxa. Together, the analysis of form (bony morphometrics) and function (intertarsal joint rotations) will allow for a functional interpretation of Miocene hominoid tarsal morphology.

Figures and Tables for Chapter 2

Figures:

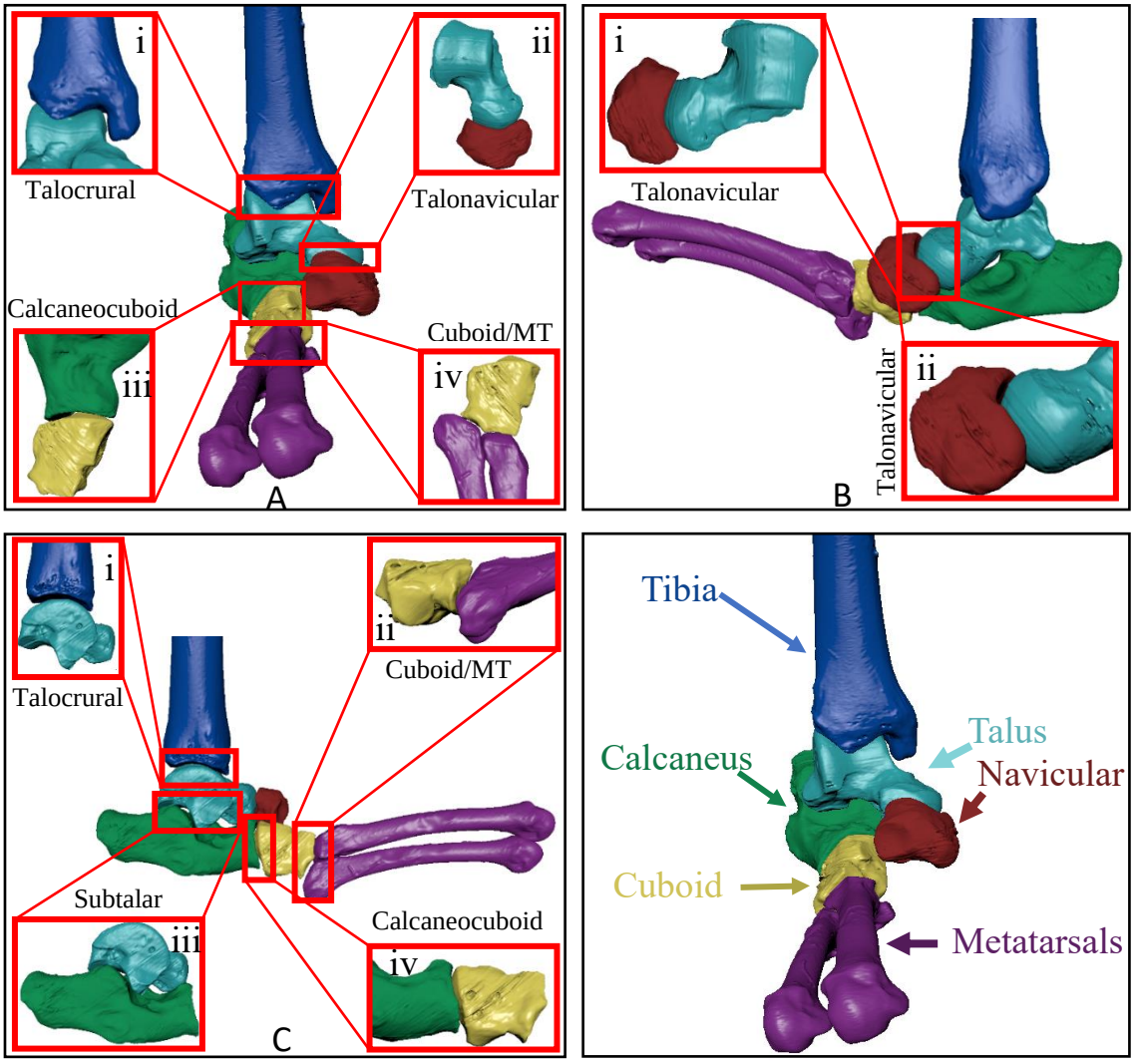

Figure 1: Joints and bones of interest for this study. Anterior (A), medial (B), and lateral (C) views of the tibia (blue), talus (teal), calcaneus (green), navicular (red), cuboid (yellow), and MT4/MT5 (purple) of *Macaca mulatta*. Joints of interest are: talocrural (blue/teal; insets Ai, Ci), subtalar (teal/green; inset Ciii), talonavicular (teal/red; insets Aii, Bi, Bii), calcaneocuboid (green/yellow; insets Aiii, Civ), and cuboid/MT5 (yellow/purple; insets Aiv, Cii).

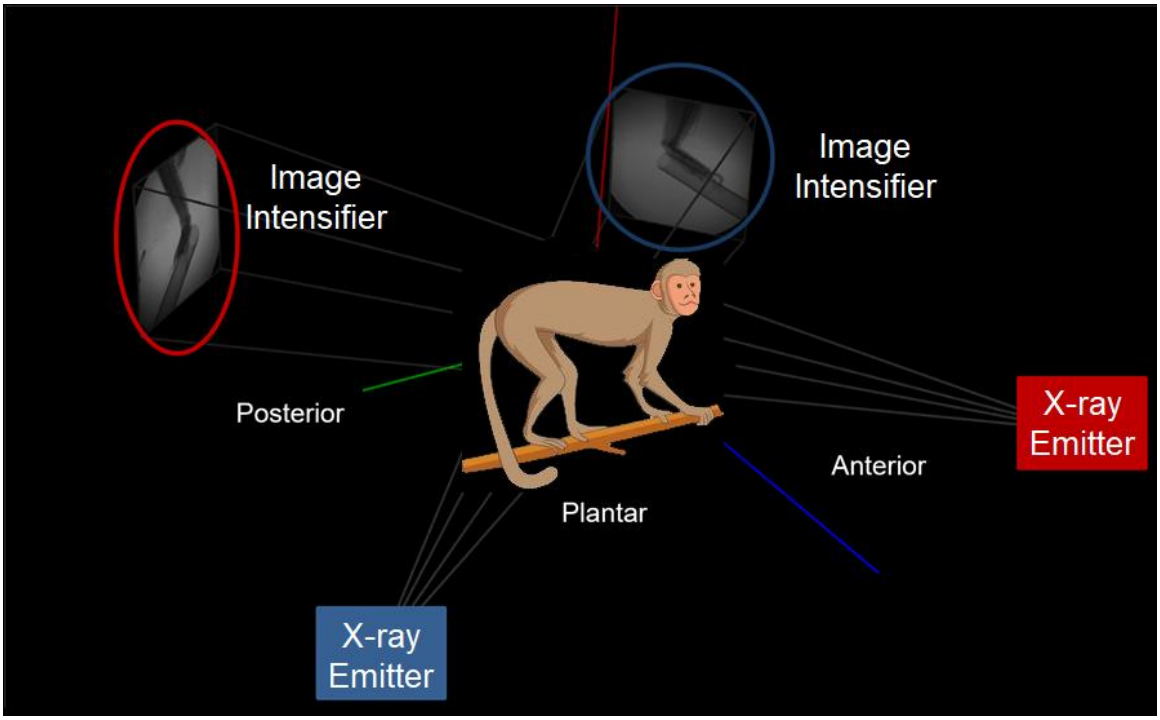

Figure 2: Schematic of XROMM setup. The animal walked between the x-ray emitters and image intensifiers. Each emitter sends x-rays to the corresponding image intensifier on the other side of the animal, producing two sets of 2D images.

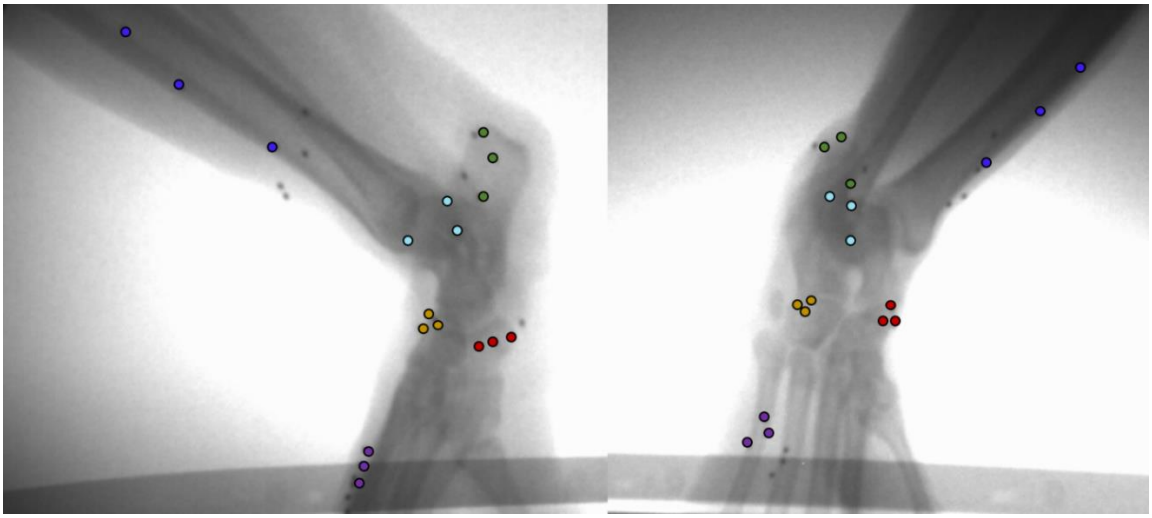

Figure 3: Biplanar fluoroscopy of *Macaca mulatta* specimen during late stance phase. Dots indicate the location of each tantalum bead (n = 3 per bone) embedded in the cortical bone of the animal. Colors correspond with colors used to identify each bone in Figure 1. Additional muscle markers (unspecified black dots) were implanted but were not part of this study.

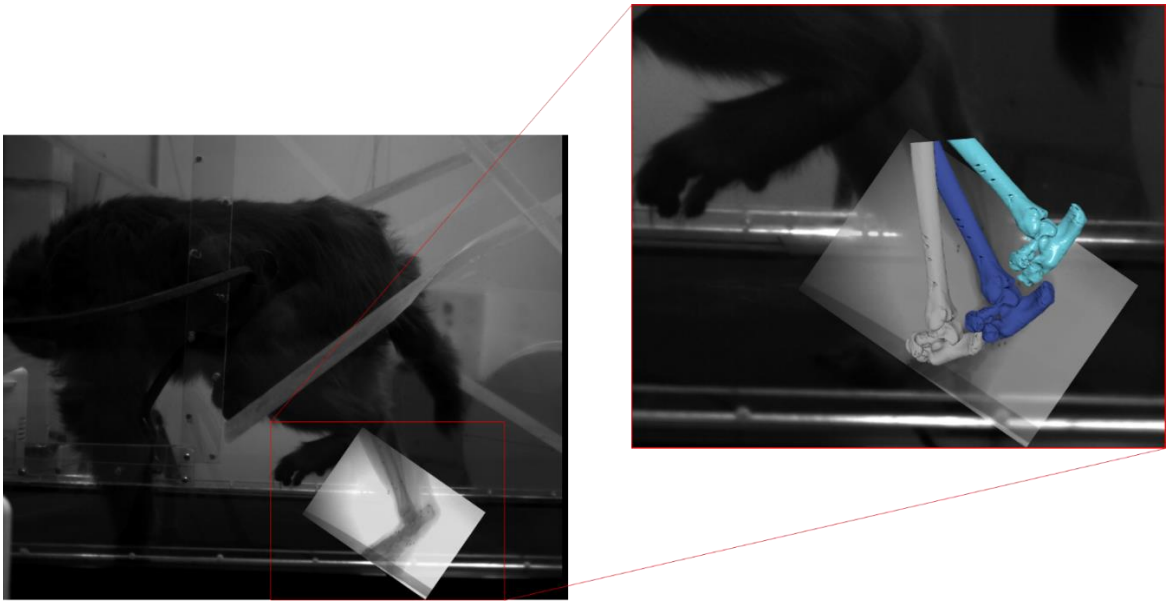

Figure 4: Light video screenshot of *Macaca mulatta* with lateral view fluoroscope image overlaid. Inset: Light video closeup of right marked foot with fluoroscope image and time series of moving bone model overlaid show movement of the marked area over time (grey = midstance; dark blue = late stance phase; light blue = toe off).

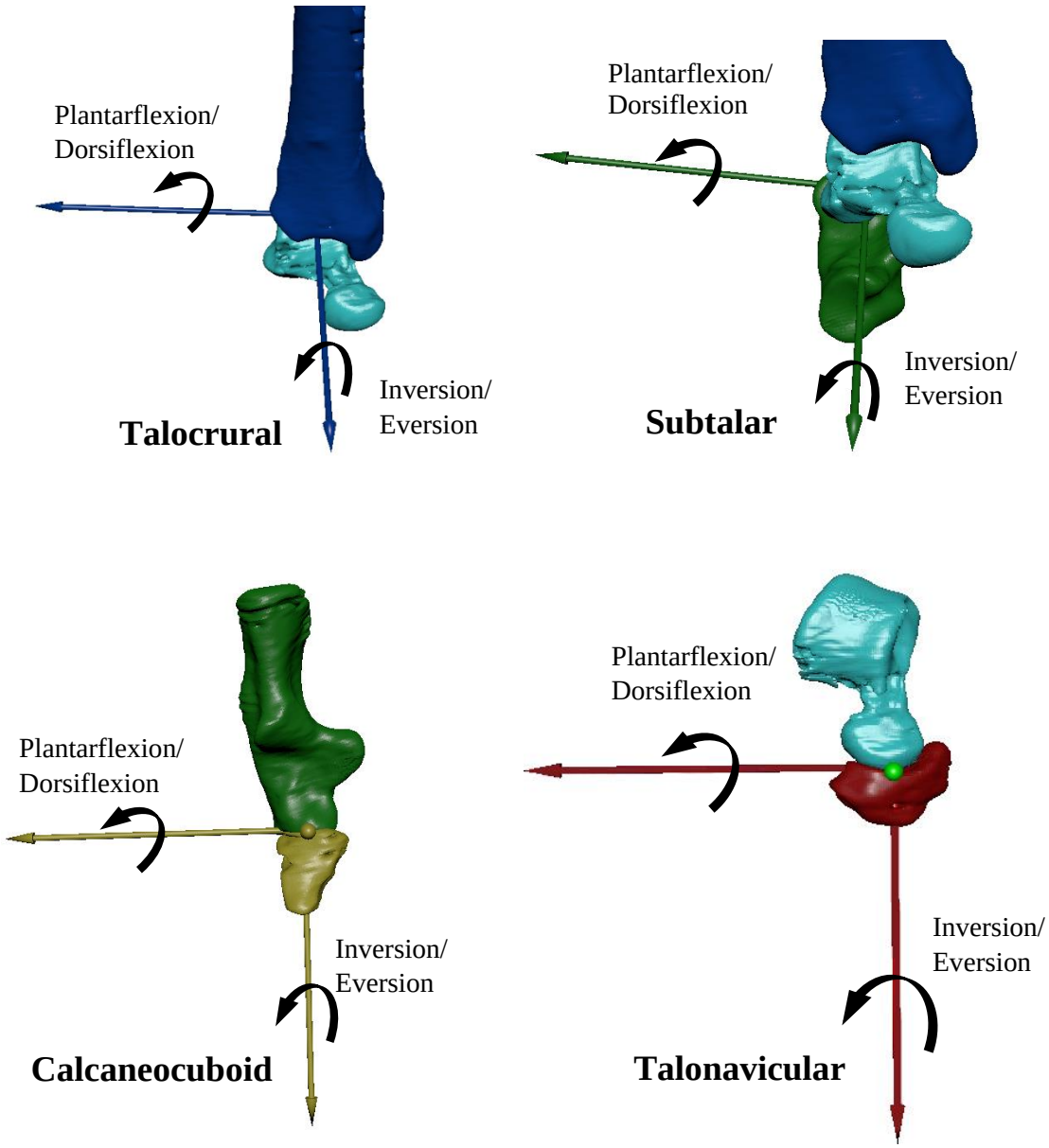

Figure 5: Joint axis placement on the talocrural (top left, anterior view), subtalar (top right, anterior view), calcaneocuboid (bottom left, dorsal view), and talonavicular (bottom right, dorsal view) joints and associated motions.

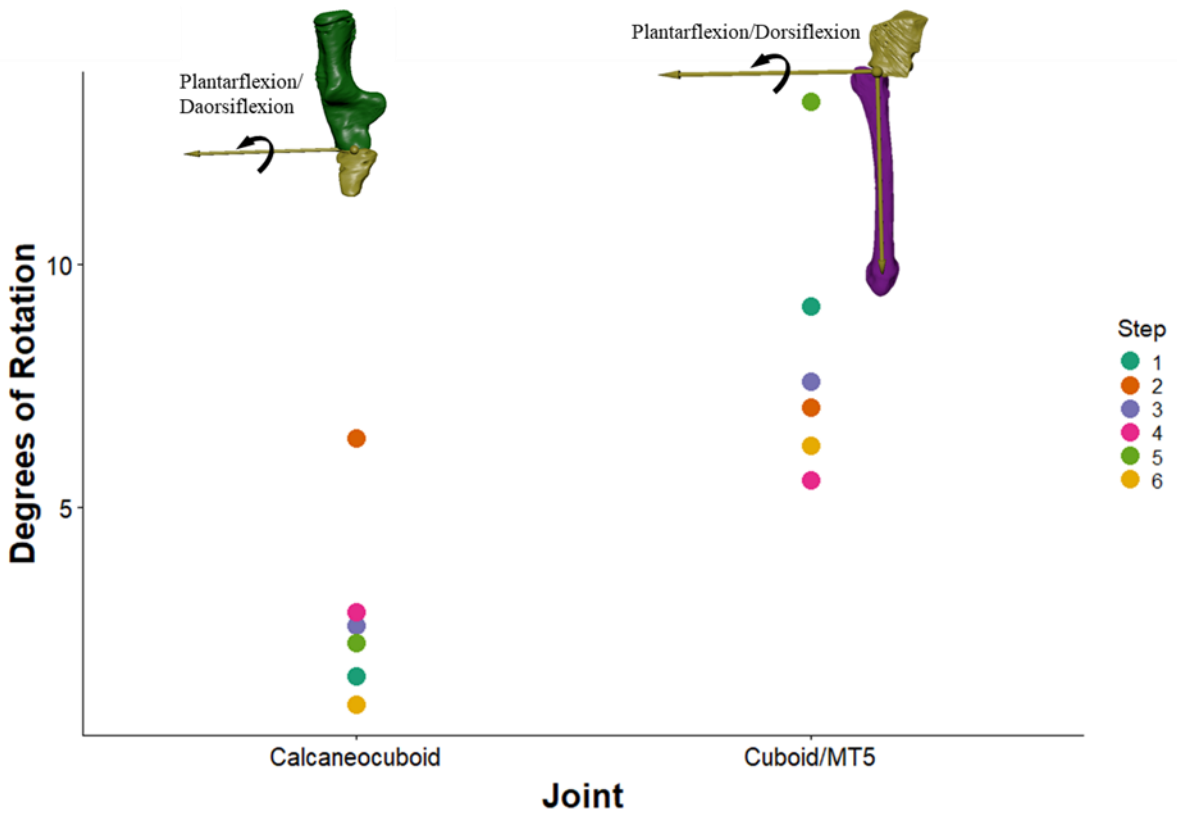

Figure 6: Degree of maximum plantarflexion at the calcaneocuboid and cuboid/MT5 joint in Monkey 1. Data points are colored by step number. Plantarflexion at the cuboid/MT5 joint was significantly higher than plantarflexion at the calcaneocuboid joint ($p < 0.001$).

A

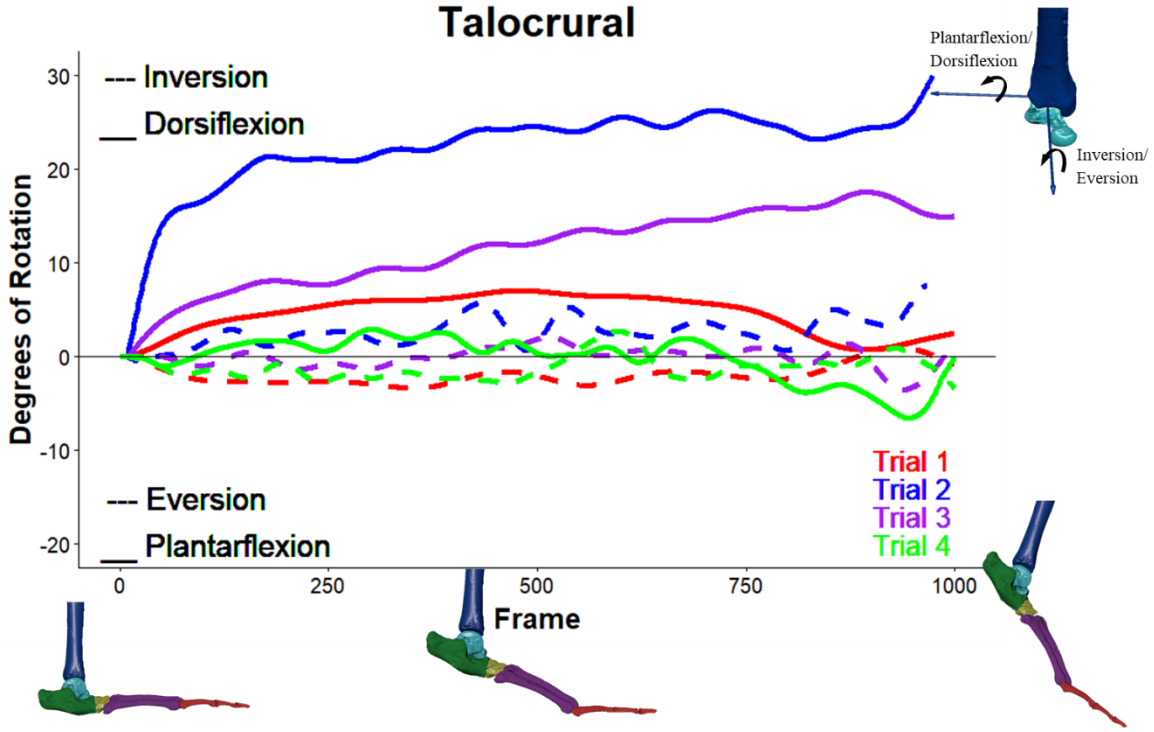

B

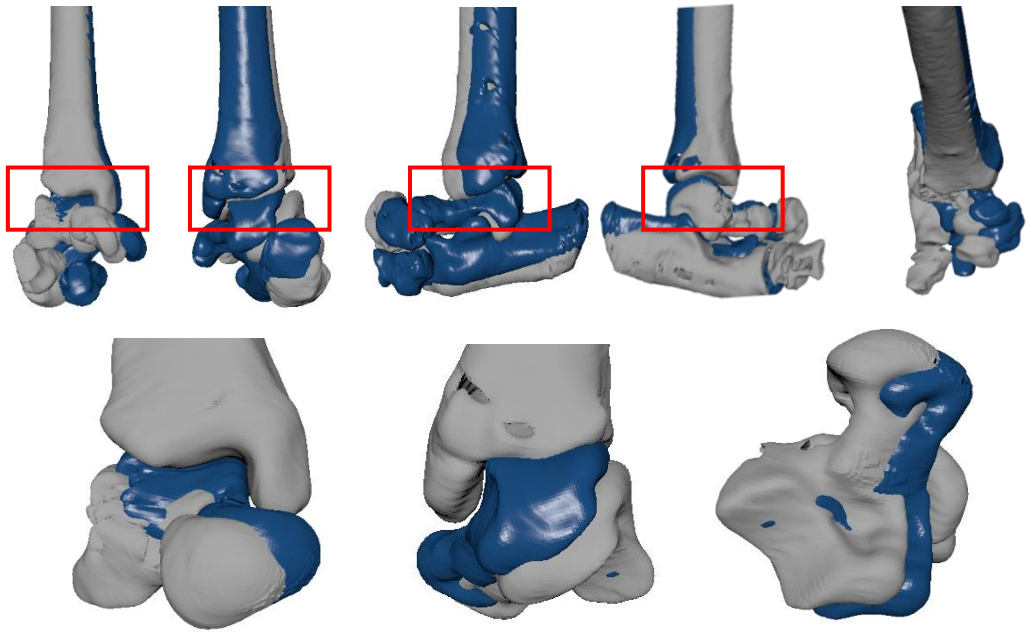

Figure 7: A: Degree of rotation at the talocrural joint. Rotations indicate the talus moving relative to the tibia. Each line represents one motion for one step for one joint. Rotations about the transverse axis (dorsiflexion/plantarflexion) are represented by solid lines,

whereas rotations about the long (AP) axis of the foot (inversion/eversion) are represented by dashed lines. Trials begin at midstance (Frame 0) and end on the end of stance phase.

B: Start (grey) and end (blue) positions of the foot, with detailed views of the position of the talocrural joint, showing the difference in position of the talus relative to the tibia from midstance to the end of stance phase. Top row views from left to right: distal, caudal, medial, lateral, dorsal with the talocrural joint indicated by red rectangles. Bottom row views from left to right: distal, caudal, inferior.

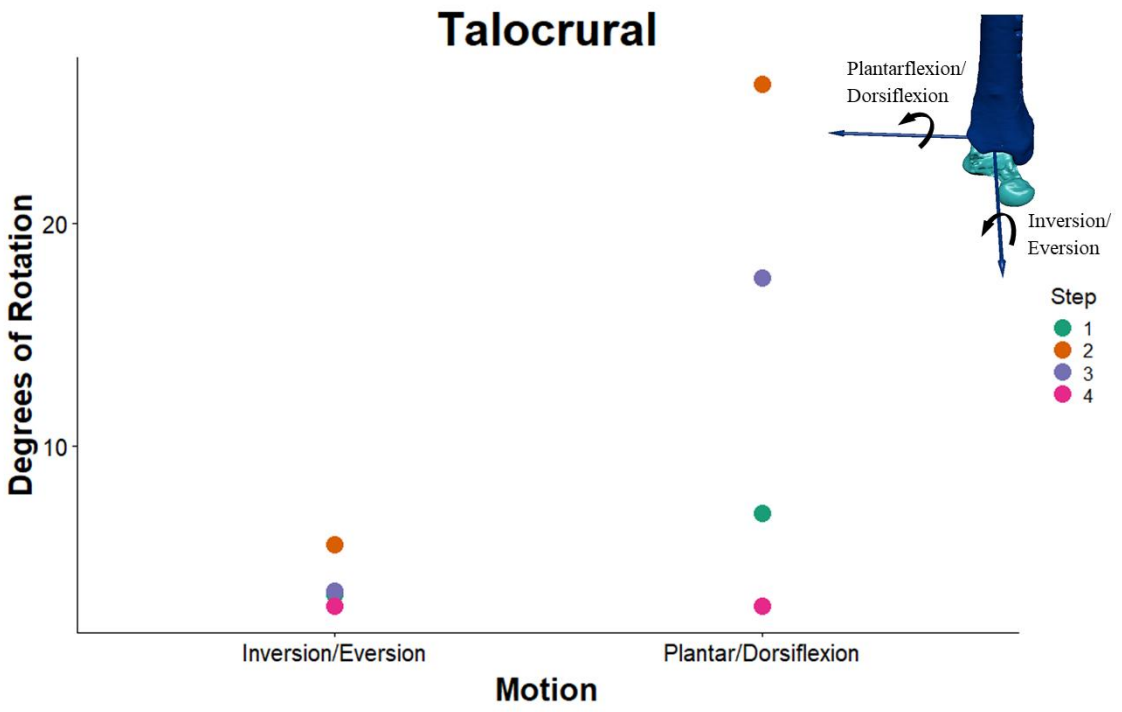

Figure 8: Comparison of maximum rotations about the long axis (inversion/eversion), and about the transverse axis (plantar/dorsiflexion) in the talocrural joint. There was more plantarflexion/dorsiflexion than inversion/eversion at the talocrural joint ($p = 0.042$) and almost no inversion/eversion.

A

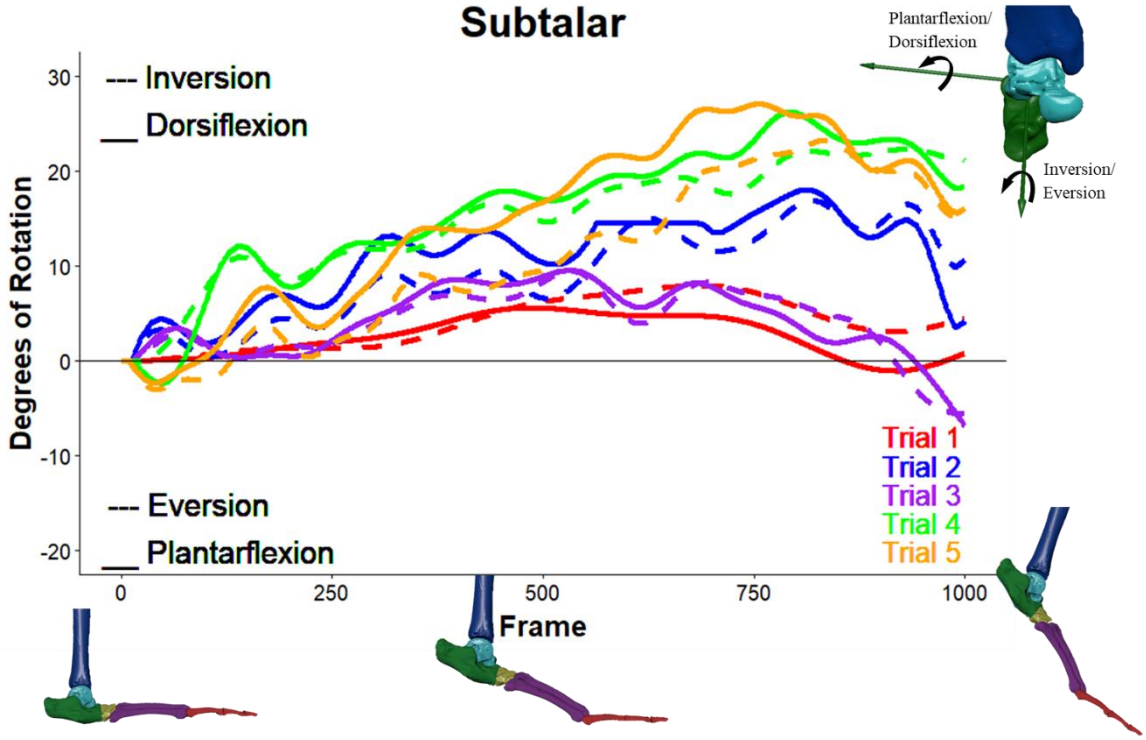

B

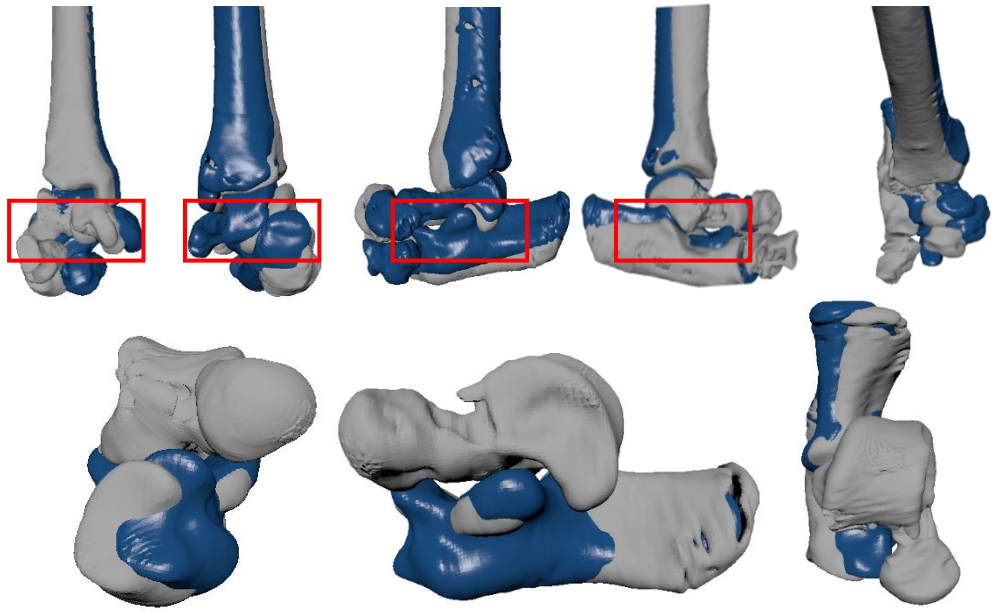

Figure 9: A: Degree of rotation at the subtalar joint. Rotations indicate the calcaneus moving relative to the talus. Each line represents one motion in one step in one joint. Rotations about the transverse axis (dorsiflexion/plantarflexion) are represented by solid

lines, whereas rotations about the long (AP) axis of the foot (inversion/eversion) are a dashed lines. Frames begin at midstance (Frame 0) and end on the end of stance phase.

B: Start (grey) and end (blue) positions of the foot, with detailed views of the position of the subtalar joint, showing the difference in position of the calcaneus relative to the talus from midstance to the end of stance phase. Top row views from left to right: distal, caudal, medial, lateral, dorsal with the subtalar joints indicated by the red rectangles. Bottom row views from left to right: distal, medial, proximal.

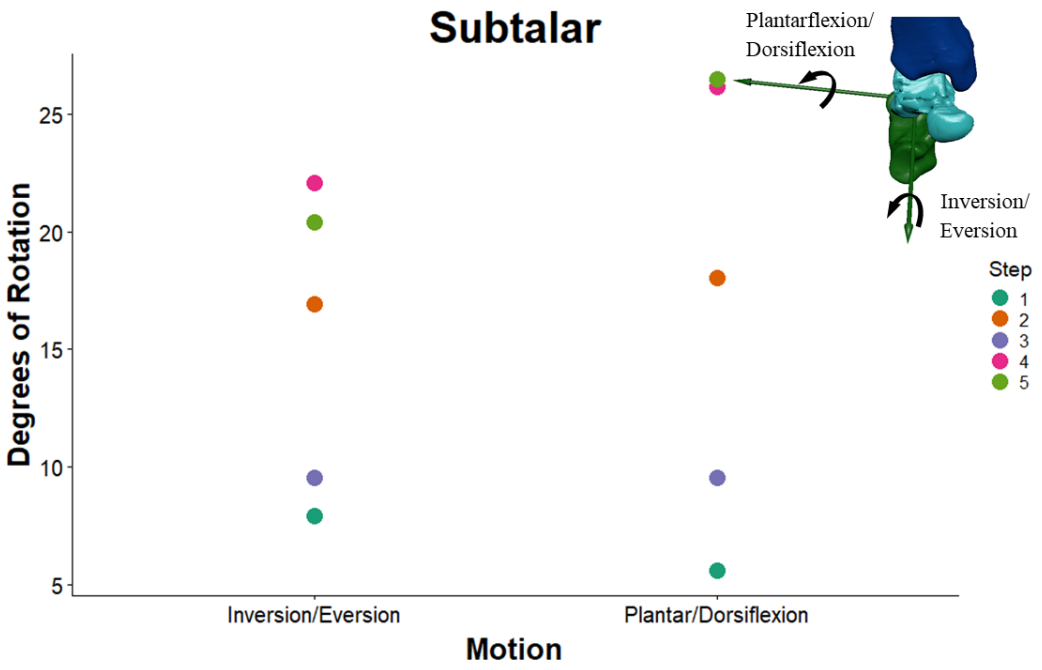

Figure 10: Comparison of maximum rotations about the long axis (inversion/eversion), and about the transverse axis (plantar/dorsiflexion) in the subtalar joint. Motion about the transverse axis and motion about the long axis of the foot did not differ ($p = 0.44$).

A

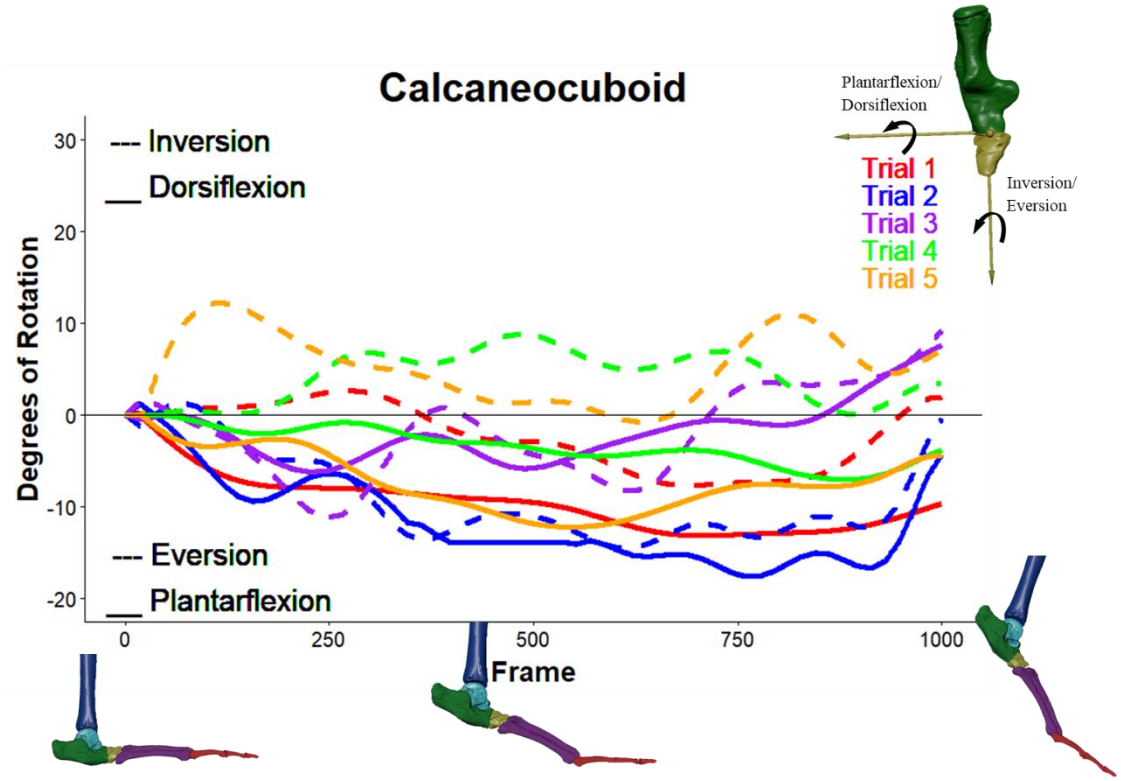

B

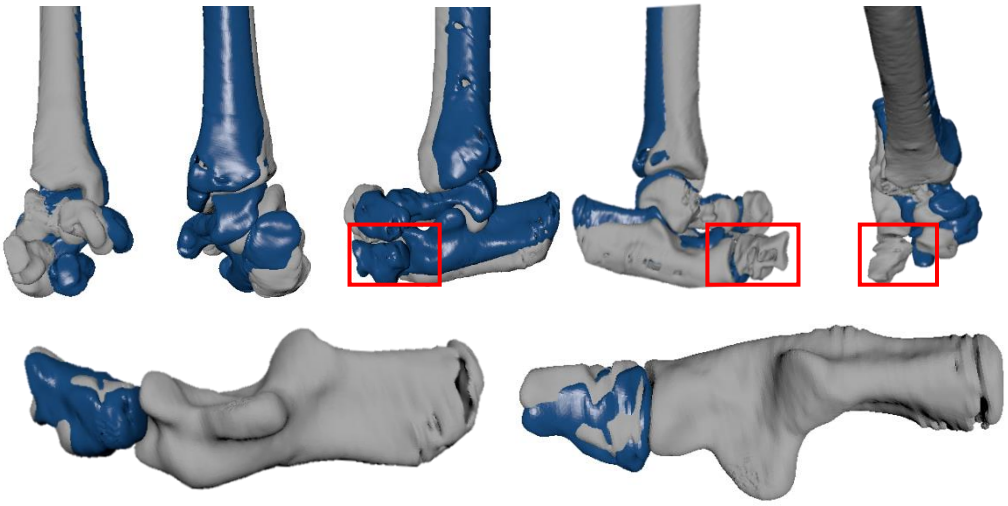

Figure 11: A: Degree of rotation at the calcaneocuboid joint. Rotations indicate the cuboid moving relative to the calcaneus. Each line represents a step in one plane. Rotations about the transverse axis (dorsiflexion/plantarflexion) are solid lines, whereas

rotations about the long (AP) axis of the foot (inversion/eversion) are dashed lines. Frames begin at midstance (Frame 0) and end on the end of stance phase.

B: Start (grey) and end (blue) positions of the foot, with a detailed lateral view of the position of the calcaneocuboid joint, showing the difference in position of the cuboid relative to the calcaneus from midstance to the end of stance phase. Top row views from left to right: distal, caudal, medial, lateral, dorsal with the calcaneocuboid joints indicated by red rectangles. Bottom row views from left to right: medial, proximal.

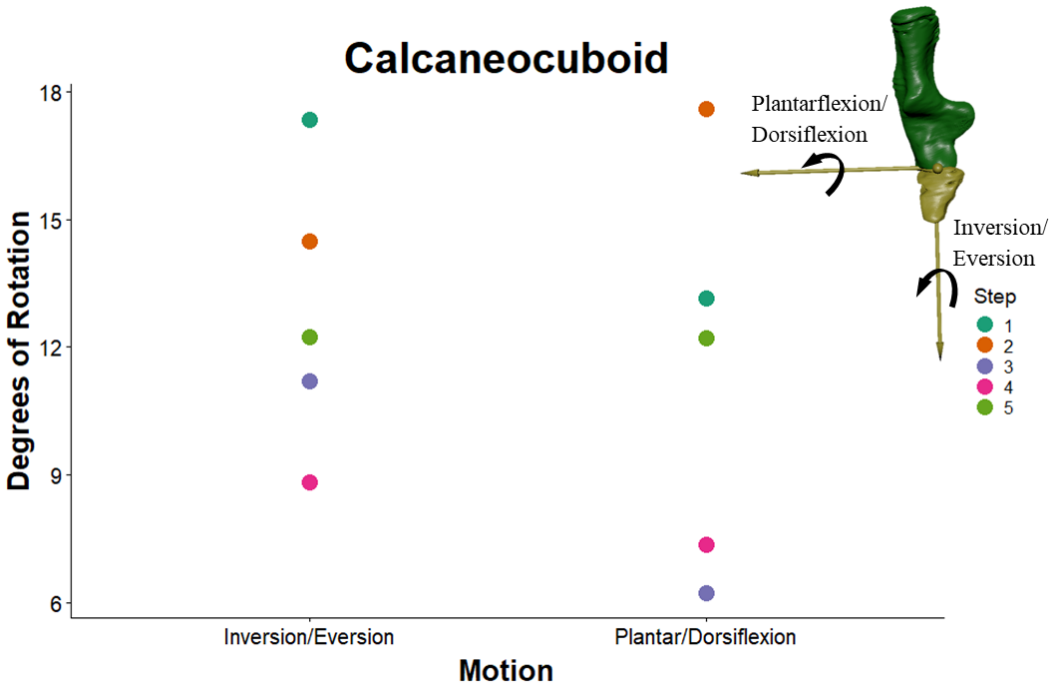

Figure 12: Comparison of maximum rotations about the long axis (inversion/eversion), and about the transverse axis (plantar/dorsiflexion) in the calcaneocuboid joint. The rotations in different motions at this joint did not differ significantly from each other ($p = 0.72$).

A

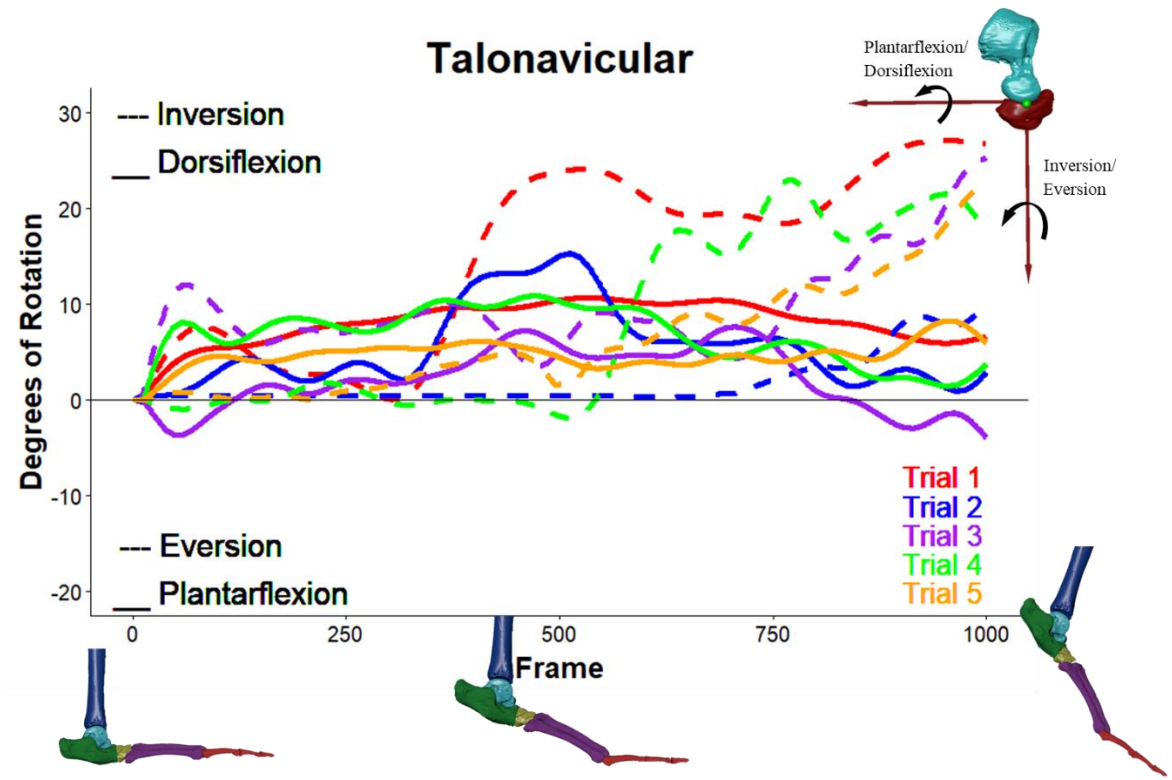

B

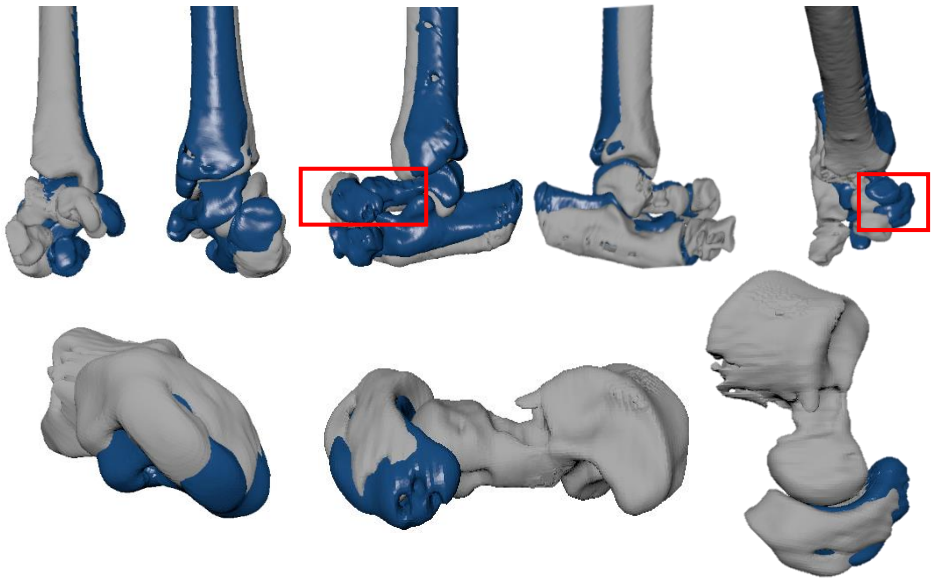

Figure 13: A: Degree of rotation at the talonavicular joint. Rotations indicate the navicular moving relative to the talus. Each line represents a step in one plane. Rotations about the transverse axis (dorsiflexion/plantarflexion) are represented by solid lines,

whereas rotations about the long (AP) axis of the foot (inversion/eversion) are dashed lines. Frames begin at midstance (Frame 0) and end on the end of stance phase.

B: Start (grey) and end (blue) positions of the foot, with a detailed medial view of the position of the talonavicular joint, showing the difference in position of the navicular relative to the talus from midstance to the end of stance phase. Top row views from left to right: distal, caudal, medial, lateral, dorsal with the talonavicular indicated by red rectangles. Bottom row views from left to right: distal, medial, proximal.

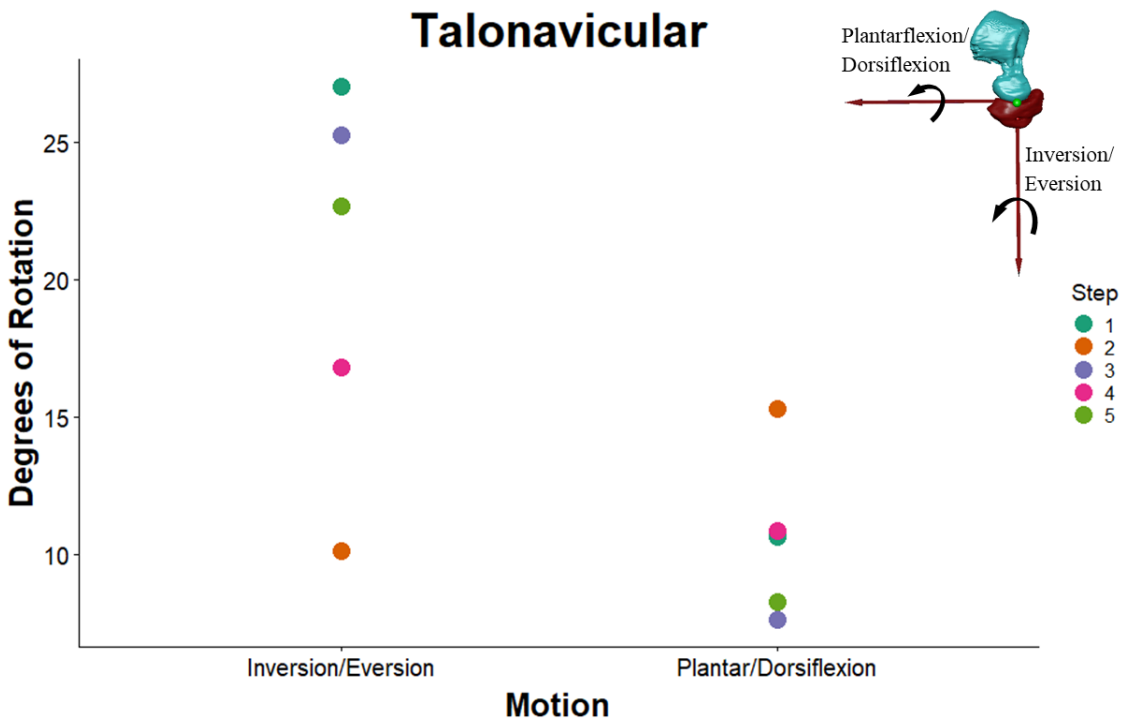

Figure 14: Comparison of maximum rotations about the long axis (inversion/eversion), and about the transverse axis (plantarflexion/dorsiflexion) in the talonavicular joint, colored by trial number. Inversion/Eversion was significantly higher at the talonavicular joint than plantarflexion/dorsiflexion ($p = 0.015$).

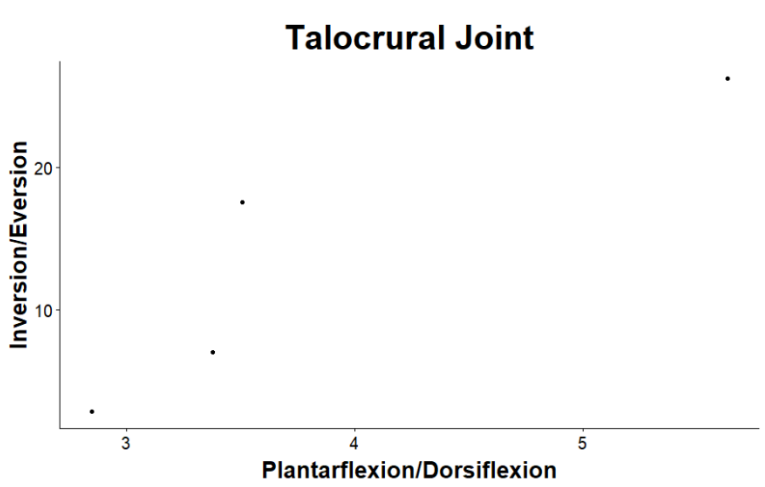
Talocrural Joint
Inversion/Eversion
Plantarflexion/Dorsiflexion
3
4
5
10
20

A

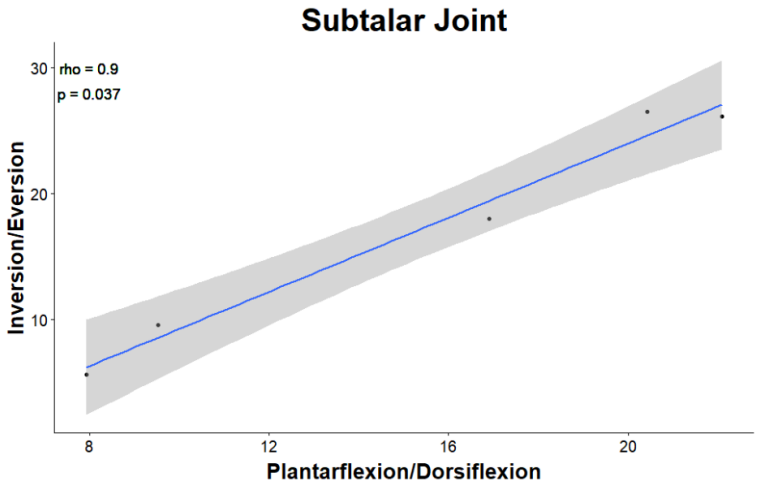
Subtalar Joint
rho = 0.9
p = 0.037
Inversion/Eversion
Plantarflexion/Dorsiflexion
8
12
16
20
10
20
30

B

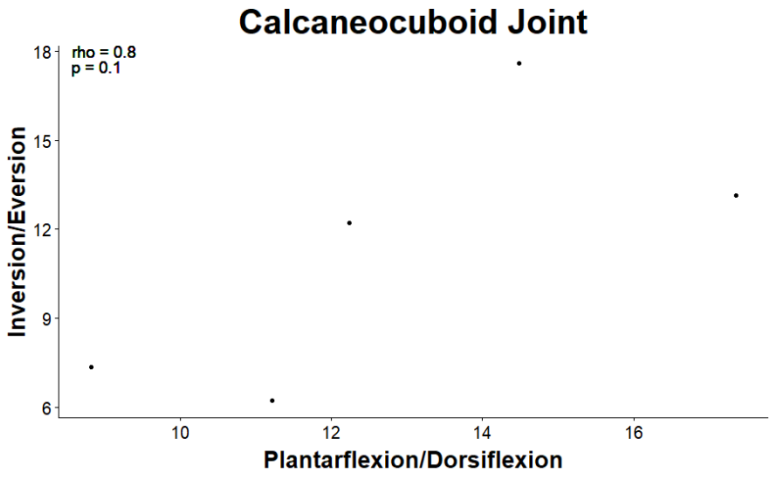
Calcaneocuboid Joint
rho = 0.8
p = 0.1
Inversion/Eversion
Plantarflexion/Dorsiflexion
10
12
14
16
6
9
12
15
18

C

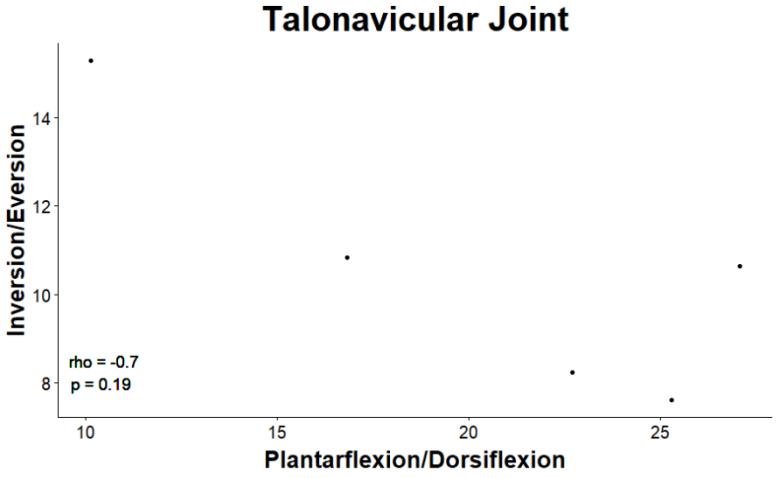
Talonavicular Joint
rho = -0.7
p = 0.19
Inversion/Eversion
Plantarflexion/Dorsiflexion
10
15
20
25
8
10
12
14

D

Figure 15: Maximum rotation (˚) about both axes for each step in the (A) talocrural, (B) subtalar, (C) calcaneocuboid, and (D) talonavicular joints. Only the subtalar joint was had a significant correlation between plantarflexion/dorsiflexion and inversion/eversion.

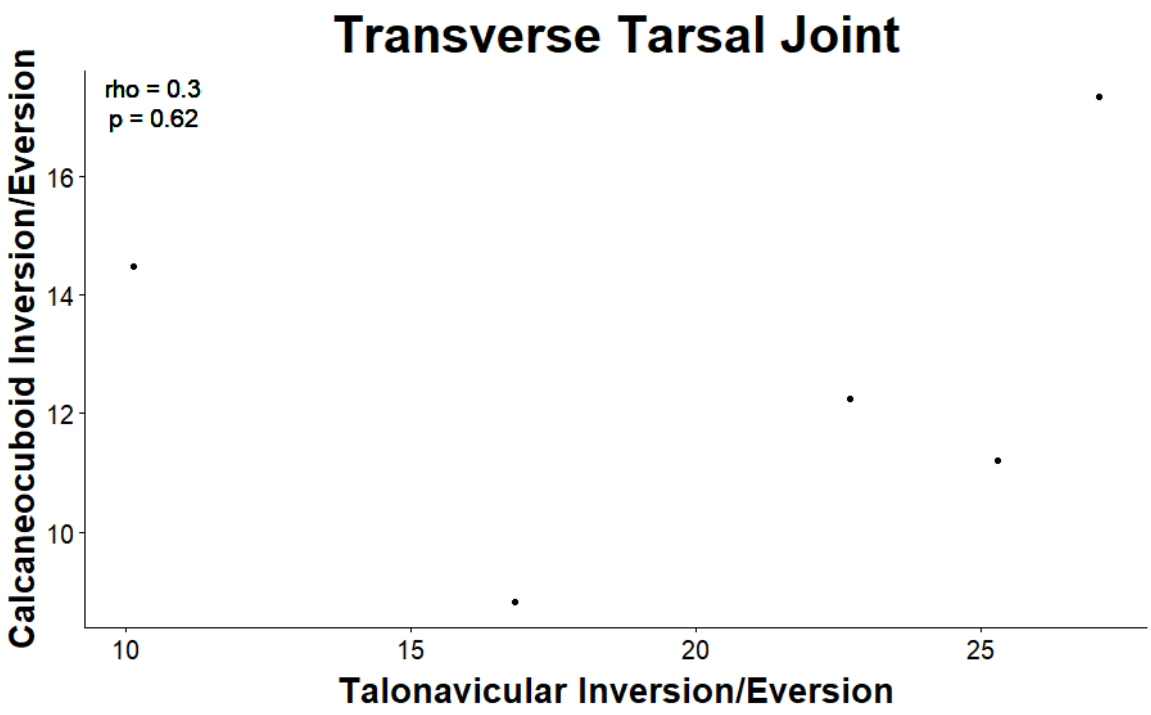

Figure 16: Inversion/eversion maximum rotations (˚) of the calcaneocuboid joint against the talonavicular joint. The correlation of maximum rotations between these two joints was not significant (p = 0.68), indicating that they are not tightly associated in inversion/eversion.

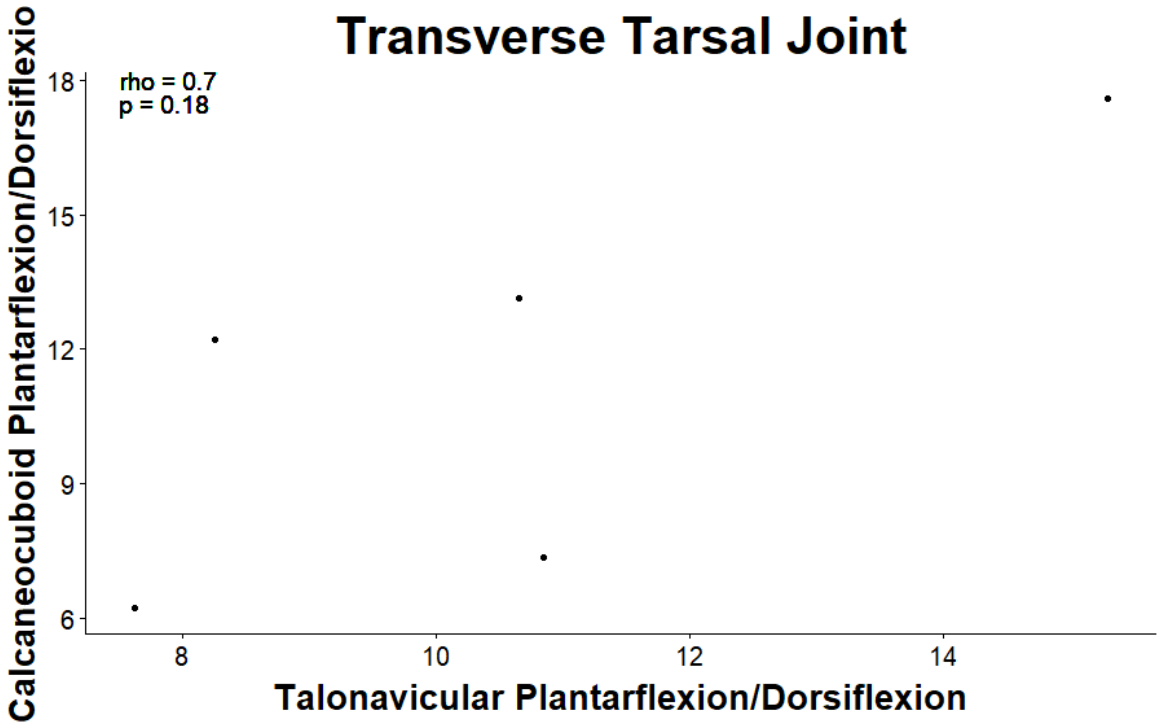

Figure 17: Plantarflexion/dorsiflexion maximum rotations (˚) of the calcaneocuboid joint against the talonavicular joint. The correlation of maximum rotations between these two joints was not significant (p = 0.25), indicating that they are not tightly associated in plantarflexion/dorsiflexion.

Tables:

Table 1: Number of steps analyzed per joint per monkey

Monkey	Joint	n steps
1	Calcaneocuboid	6
	Cuboid/MT5 (Lateral Midfoot)	6
2	Talocrural	4
	Subtalar	5
	Calcaneocuboid	5
	Talonavicular	5

Table 2: Mean rigid body error for each bone for each monkey, trial, and bone studied. Rigid body error is calculated using the total number of markers tracked in each bone and the calculated distance between markers in the CT scan of the marked foot.

Monkey	Trial	Bone	Rigid Body Error (mm)
1	1	Calcaneus	0.88 +/- 0.083
		Cuboid	0.29 +/- 0.054
		MT5	0.91 +/- 0.032
	2	Calcaneus	0.97 +/- 0.11
		Cuboid	0.31 +/- 0.045
		MT5	0.91 +/- 0.056
	4	Calcaneus	1.1 +/- 0.070
		Cuboid	0.31 +/- 0.036
		MT5	0.94 +/- 0.056
	5	Calcaneus	1.1 +/- 0.090
		Cuboid	0.31 +/- 0.045
		MT5	0.97 +/- 0.071
	6	Calcaneus	0.97 +/- 0.060
		Cuboid	0.32 +/- 0.035
		MT5	0.92 +/- 0.034
2	1	Tibia	0.067 +/- 0.037
		Talus	0.086 +/- 0.0349
		Calcaneus	0.79 +/- 0.035

		Cuboid	0.197 +/- 0.055
		Navicular	0.067 +/- 0.024
	2	Tibia	0.060 +/- 0.035
		Talus	0.084 +/- 0.026
		Calcaneus	0.81 +/- 0.060
		Cuboid	0.17 +/- 0.058
		Navicular	0.097 +/- 0.055
	3	Tibia	0.054 +/- 0.027
		Talus	0.076 +/- 0.022
		Calcaneus	0.80 +/- 0.054
		Cuboid	0.16 +/- 0.050
		Navicular	0.086 +/- 0.051
	4	Tibia	0.062 +/- 0.033
		Talus	0.081 +/- 0.025
		Calcaneus	0.79 +/- 0.041
		Cuboid	0.18 +/- 0.047
		Navicular	0.081 +/- 0.031
	5	Tibia	0.067 +/- 0.037
		Talus	0.086 +/- 0.035
		Calcaneus	0.79 +/- 0.035
		Cuboid	0.20 +/- 0.055
		Navicular	0.067 +/- 0.024

Table 3: Maximum plantarflexion at the calcaneocuboid joint and cuboid/MT5 joints in Monkey 1.

Joint	**Trial**	**Max. Rotation (˚)**
Calcaneocuboid	1	1.5
	2	6.4
	3	2.6
	4	2.8
	5	2.2
	6	0.91
Cuboid/MT5	1	9.1
	2	7.1
	3	7.6
	4	5.5
	5	13.4
	6	6.3

Table 4: Maximum inversion/eversion and plantarflexion/dorsiflexion at the talocrural, subtalar, calcaneocuboid, and talonavicular joints in Monkey 2.

Joint	Trial	Motion	Max. Rotation (˚)
Talocrural	1	Plantar/Dorsiflexion	7.0
		Inversion/Eversion	3.4
	2	Plantar/Dorsiflexion	26.2
		Inversion/Eversion	5.6
	3	Plantar/Dorsiflexion	17.5
		Inversion/Eversion	3.5
	4	Plantar/Dorsiflexion	2.9
		Inversion/Eversion	2.9
Subtalar	1	Plantar/Dorsiflexion	5.6
		Inversion/Eversion	7.9
	2	Plantar/Dorsiflexion	18.0
		Inversion/Eversion	16.9
	3	Plantar/Dorsiflexion	9.6
		Inversion/Eversion	9.5
	4	Plantar/Dorsiflexion	26.2
		Inversion/Eversion	22.1
	5	Plantar/Dorsiflexion	26.5
		Inversion/Eversion	20.4
Calcaneocuboid	1	Plantar/Dorsiflexion	13.2
		Inversion/Eversion	17.4
	2	Plantar/Dorsiflexion	17.6
		Inversion/Eversion	14.5
	3	Plantar/Dorsiflexion	6.2
		Inversion/Eversion	11.2
	4	Plantar/Dorsiflexion	7.4
		Inversion/Eversion	8.8
	5	Plantar/Dorsiflexion	12.2
		Inversion/Eversion	12.2
Talonavicular	1	Plantar/Dorsiflexion	10.7
		Inversion/Eversion	27.1
	2	Plantar/Dorsiflexion	15.3
		Inversion/Eversion	10.1
	3	Plantar/Dorsiflexion	7.6
		Inversion/Eversion	25.3
	4	Plantar/Dorsiflexion	10.8
		Inversion/Eversion	16.8
	5	Plantar/Dorsiflexion	8.3
		Inversion/Eversion	22.7

Chapter 3: Morphological variation of the calcaneus, talus, cuboid, and navicular in extant anthropoid primates

Introduction:

Understanding the functional morphology of the foot and ankle allows for the application of what we know about *in vivo* movements to the fossil record, and allows us to study the diversity of extant primate morphological variation. Foot bony morphology is useful when studying locomotion because feet interact directly with the substrate on which an animal is moving (Morton, 1922; Harcourt-Smith, 2002; Boyer et al., 2013). The shape of tarsal bones is hypothesized to reflect possible movements of the foot and, therefore, how the foot was used (Gebo, 1986; D'Août & Aerts, 2008). Understanding how foot bone morphology reflects locomotion in extant primates allows us to improve our knowledge of the locomotor repertoires of extant taxa and apply these findings to fossil taxa.

Movements at the ankle and intertarsal joints are hypothesized to vary among anthropoids and reflect foot use during suspensory, quadrupedal, arboreal and/or terrestrial locomotion. Grasping tightly during climbing and suspension might be facilitated by more intertarsal mobility, leading to more inversion of the foot than occurs during terrestrial locomotion (Close et al., 1967; Inman, 1976; Chester et al., 2015; Holowka et al., 2017; McNutt et al., 2018). The subtalar, calcaneocuboid, and talonavicular joints (Figure 2.1) of the foot are thought to be primarily responsible for inversion, eversion, and midfoot flexibility (Manter, 1941; Close et al., 1967; Holowka et al., 2017). In addition, the orientation of the foot is affected by the talocrural joint (Figure

2.1), mainly in the sagittal plane to allow for postural adaptations for variable substrates (Wright et al., 1964; Lundberg, 1989). These four joints will be the focus of this chapter.

Extant Primate Locomotor Diversity

Anthropoid primates engage in a wide range of locomotor behaviors, making locomotor classification for each species difficult (Prost, 1965; Rose, 1973; Dagosto & Gebo, 1988; Hunt et al., 1996; Schmidt, 2011). Among extant anthropoids, however, there is variation in the degree to which taxa are specialized for positional behaviors that would require different patterns of foot use. Nonhuman anthropoid primates can be divided into four categories: Asian apes, African apes, Old World monkeys, and New World monkeys.

Asian Apes

Asian apes consist of orangutans and hylobatids (gibbons and siamangs). All are accomplished suspensors that rarely travel terrestrially (Fleagle, 1976; Fleagle, 1985; Byron & Covert, 2004). Orangutans engage in slow, orthograde, quadramanous suspensory locomotion, which involves using all four limbs to travel between trees (Thorpe & Crompton, 2006). This type of locomotion allows them to traverse the forest canopies and to obtain fruit (Thorpe & Crompton, 2006). Hylobatids, on the other hand, primarily engage in ricochetal brachiation, or fast, forelimb-dominated swinging below branches (Swartz et al., 1989), but also climb, leap, and walk bipedally when locomoting above branches or when on the ground (Fleagle, 1976). This bipedal locomotion differs from human bipedalism in that the knees and hip are bent, hylobatids do not heel strike,

and the foot is far more compliant than a human or arboreally quadrupedal monkey (Vereecke et al., 2005b; Vereecke & Aerts, 2008). Although both types of locomotion involve below branch suspension, orangutan locomotion requires the feet to grasp small branches and engage in extreme inversion and eversion when traversing between trees, which often involves bridging gaps between terminal branches (Thorpe et al., 2007; Manduell et al., 2012). Inversion is also helpful for orangutans when supporting themselves on horizontal branches or vertical tree trunks for stability (Thorpe & Crompton, 2006). Hylobatids, on the other hand, rely more heavily on their forelimbs for below branch suspension (Vereecke et al., 2005a). Additionally, they do also use their hind limbs to grasp small branches during climbing and jumping, as well as on large branches during bipedal locomotion (Vereecke et al., 2005a).

African Apes

Nonhuman African apes consist of gorillas and chimpanzees (Jungers & Susman, 1984). All gorillas are knuckle walkers when on the ground, meaning they walk with a semiorthograde posture with their fingers flexed such that they walk on their forelimb knuckles, but their hindlimbs engage in plantigrade quadrupedalism—and therefore propulsive plantarflexion—when on the ground (Straus, 1940). However, the amount of arboreal locomotion varies among gorilla taxa (Remis, 2013 Dunn et al., 2014). There are locomotor differences between mountain and lowland gorillas due to habitat and body size differences (Remis, 2013). Mountain gorillas, which are larger than lowland gorillas and are found in areas with fewer and smaller trees, exhibit little to no suspensory behaviors and are largely terrestrial knucklewalkers (Remis, 2013). In addition to

terrestrial knuckle walking, lowland gorillas engage in vertical climbing and suspensory locomotion. (Gebo, 1989; D'Août et al., 2004).

Chimpanzees also exhibit knuckle walking on the ground, but all species within *Pan* engage in suspensory behavior (Pontzer & Wrangham, 2004). Chimpanzees exhibit more suspensory locomotion during ontogeny than in adulthood (Doran, 1997) and bonobos are more arboreal than chimpanzees (Susman, 1987). However, even in adulthood, chimpanzees vertically climb and suspend below branches (Susman, 1984). Vertical climbing in both gorillas and chimpanzees require the foot to be placed and loaded in an inverted posture so that the plantar surface of the foot can press against a vertical substrate. Additionally, chimpanzees and lowland gorillas grasp branches with their hands and feet, requiring them to have feet adapted for inverted foot postures and the ability to grasp small-diameter branches (Gebo, 1992).

Old World Monkeys

Old World monkeys consist of colobines and cercopithecines (Disotell, 1996). Colobines (leaf eating Old World monkeys) are generally arboreal quadrupeds, meaning they walk on top of tree branches and largely remain pronograde for access to food sources (Bennett & Davies, 1994; Kimura, 2002), though some, like *Rhinopithecus* are also adept at walking on the ground (Grueter et al., 2013). Unlike the nonhuman African apes, they do not adopt a knuckle walking posture, but rather the plantar surfaces of all autopodia touch the substrate (Patel, 2010). Some genera, like *Colobus* also leap between trees, which requires strong propulsion and stability during plantarflexion as well as the ability to grasp small branches (Gebo, 1989).

Cercopithecines (cheek-pouched Old World monkeys) engage in arboreal quadrupedalism or terrestrialism, which would emphasize parasagittal motions and require less extreme inversion and eversion than more suspensory taxa (Rollinson & Martin, 1981; Meldrum, 1991). Many cercopithecine monkeys are adept at locomotion in trees and on the ground, engaging in quadrupedalism on either substrate, depending on how open or wooded their environments are (Strasser, 1992; Kimura, 2002; Schmitt, 2003; Gosselin-Ildari, 2013).

Atelines

Atelines (subfamily of New World monkeys) are either suspensory or arboreal quadrupeds, which would require inverted foot postures and midfoot mobility to grasp branches (Grand, 1968; Gebo, 1989; Bergeson, 1998; Cant et al., 2003; Schmitt et al., 2005; Di Fiore & Campbell, 2007). The degree of suspensory locomotion utilized by atelines varies among genera. For example, *Ateles* engages in highly suspensory behaviors, including grasping small branches with all four limbs and their prehensile tail (Mittermeier, 1978; Cant et al., 2001). Other atelines such as *Cebus* and *Sapajus*, on the other hand, are described as "highly quadrupedal" (Gebo, 1992b p.277) with some running and leaping abilities (Wright, 2007).

Primate Foot Use

Although there is considerable locomotor variability among taxa, foot use and the role of pedal morphology in facilitating these behaviors is not well understood. While some work has been done on foot proportions and phalangeal morphology in relation to

grasping (Begun, 1988; Bloch & Boyer, 2002; Almécija et al., 2010; Patel et al., 2015; Young & Heard-Booth, 2016), much less is known about the role of the tarsal skeleton and intertarsal joints. This is unfortunate because tarsals are frequently preserved in the fossil record. Therefore, elucidating tarsal functional morphology will provide an important piece of the puzzle for locomotor reconstructions of fossil taxa.

Tarsal morphology is hypothesized to affect the ability of animals to negotiate variable substrates (Gebo, 1986; Strasser, 1988; Gebo, 1989; MacLatchy et al., 2000; DeSilva, 2009; Boyer et al., 2013). As such, taxa with different locomotor emphases are expected to vary in pedal functional morphology (Prost, 1965; Ripley, 1967; Walker, 1974; Dagosto & Gebo, 1998; Byron & Covert, 2004; Holowka et al., 2017). Moving on terminal branches, climbing, and suspensory activities require strong grasping, which in turn involves midfoot flexibility, especially during flexion and inversion (Grand, 1968; Gebo, 1993). Grasping is also hypothesized to require inverted foot postures and increased ranges of motion during inversion and eversion for positioning the foot on variably-oriented and curved substrates (Cartmill, 1974; Langdon, 1986). In contrast, quadrupeds that mainly travel on large-diameter branches or on the ground rely more heavily on effective, lever-like pedal propulsion (Cartmill, 1974), likely related to restricted midfoot flexibility and tarsal morphology well-suited for longitudinal rather than transverse stresses (Langdon, 1986; Gebo, 1993). These differences in motion are hypothesized to be reflected in the morphology of tarsal bones and to vary among taxa that locomote differently.

The Talocrural, Subtalar, Calcaneocuboid, and Talonavicular Joints

Talocrural Joint

The primary motions at the talocrural joint are flexion and extension (Chapter 2). Plantarflexion is mainly powered by the triceps surae muscles, which attach via the Achilles tendon on the posterior calcaneal tuber (Moore et al., 2011). The ankle lever mechanics for *Macaca mulatta* are displayed in Figure 1. Increasing the in-lever (the distance between the triceps surae insertion and the talocrural joint) will increase the mechanical advantage of the pull of the triceps surae on the calcaneus, increasing the power of plantarflexion at the ankle (Youlatos, 2003). Previous studies comparing calcanei among anthropoid primates have suggested that Cercopithecidae have longer posterior calcanei compared to the rest of anthropoid primates (Gebo, 1989; Youlatos, 2003). As such, taxa that are more reliant upon propulsive plantarflexion when walking on a flat or large-diameter surface are expected to have longer posterior calcanei than those that mainly engage in below branch suspensory locomotion.

The talocrural joint not only affects the orientation of the foot in the sagittal plane through plantarflexion, but also contributes to inversion and eversion (Wright et al., 1964; Lundberg, 1989; Rome, 1996; Chapter 2 of this dissertation). Taxa that are predicted to be especially reliant on midfoot flexibility and pedal prehension (e.g., *Pongo, Ateles*) are hypothesized to have shorter (proximodistally), trapezoidal (proximal view) trochleae (Figure 2), which results in some talar rotation during plantarflexion and dorsiflexion (Langdon, 1986). Less wedged trochleae will decrease the amount of mediolateral movement that occurs at the talocrural joint when the ankle is plantarflexed. However, this morphology has not been quantified among all anthropoids (Langdon,

1986). Asymmetrical trochlear crests (Figure 3) also cause the foot to be more inverted as a result of nonparallel trochlear margins moving along the distal tibial articular surface (Langdon, 1986; Gebo, 1989; Larson & Stern, 2006; Dunn et al., 2014; Knigge et al., 2015). Asymmetrical trochlear crests are also seen in cercopithecoids, which are largely terrestrial or arboreal quadrupedal and therefore this pattern requires further study across taxa (Strasser, 1988). I hypothesize that terrestrial taxa will have higher, more rectangular trochleae that restricts mediolateral movements of the talus during dorsiflexion and plantarflexion to ensure the foot remains stiff during locomotion, and to maintain stability, whereas arboreal taxa will exhibit flatter trochleae allow for more movement of the talus at the talocrural joint (Gebo, 1988; Sondaar & Van der Geer, 2002; Dunn et al., 2014).

Subtalar Joint

The functional subtalar joint consists of the anterior, middle, and posterior subtalar joints (Figure 4) (Close et al., 1967; Sarrafian, 1993). Lewis (1980a & b) hypothesized that the long axis of posterior subtalar articulation to be to be more oblique and L-shaped in suspensory taxa to facilitate a greater degree of rotation at the joint in a transverse plane (Figure 5) (Lewis, 1980a; Lewis, 1980b). The inferior aspect of the talus in suspensory taxa and those that climb vertically is thought to face medially, placing the foot in an inverted posture (Latimer et al., 1987). The resulting foot posture allows for better contact between the foot and a vertical substrate (Latimer et al., 1987; DeSilva, 2009). Terrestrial or arboreal quadrupedal taxa are thought to have inferiorly-oriented subtalar articular surfaces to direct forces associated with locomotion in a sagittal

direction and keep the ankle from exhibiting unnecessary mediolateral motion (Latimer et al., 1987; DeSilva, 2009). Most inversion and eversion occurs at the subtalar and transverse tarsal joints (Chapter 2), though how the morphology at these joints reflects this greater inversion/eversion requires a broad comparative analysis of the morphology at these joints (Manter, 1941; Wright et al., 1964; Close et al., 1967; Lewis, 1980; Sarrafian, 1993). Langdon (1986) also found that suspensory taxa have more oblique posterior subtalar articular surfaces, which would allow for more oblique motions of the calcaneus relative to the talus (Figure 5). These oblique movements would aid in allowing the foot to achieve more varied postures during locomotion on arboreal substrates.

Transverse Tarsal Joint

The transverse tarsal joint complex consists of two separate joints: the calcaneocuboid and talonavicular joints (Manter, 1941; Bojsen-Møller, 1979; Lewis, 1980; Cornwall, 200l; Turley & Frost 2013). In Chapter 2 of this dissertation the treatment of this joint as one complex was questioned, and these joints will be treated separately in this Chapter. In terrestrial taxa, the distal calcaneus and cuboid are close-packed in extension, and movement is restricted at these joints, which reflects stability more than flexibility for grasping during locomotion on terminal branches, leaping, and climbing (Gebo and Schwartz, 2006). A peg and socket morphology at the calcaneocuboid joint (Figure 6) is hypothesized to allow for increased mobility without dislocation during extreme inversion while grasping small-diameter branches (Bojsen-Møller, 1979; Rose, 1986; Gebo & Simons, 1987; Gebo, 1993). Wedged cuboids (Figure

7) are also hypothesized to reflect locomotor differences due to the lateral shift in positioning of the lateral rays in wedged cuboids (Ward, 1997). This repositioning is thought to be more prevalent in suspensory taxa, which would emphasize grasping behaviors (Ward, 1997). I therefore hypothesize that proximal cuboid projection and wedged cuboids will differentiate highly arboreal taxa.

Inversion/eversion at the talonavicular joint is predicted to also be more restricted in terrestrial taxa than in suspensory taxa, though this has not been confirmed across anthropoid taxa. In Asian apes, African apes, atelids, and colobines that leap (e.g., *Colobus*; McGraw, 1998), the talonavicular joint undergoes more rotation and translation than during quadrupedal terrestrial locomotion, which allows for more midfoot movement for below branch suspension, vertical climbing, grasping during locomotion on terminal branches, or grasping during leaping and landing (Langdon, 1986). Greater movement between the talus and navicular may be reflected in the size and shape of both bones, but this has not been thoroughly explored across anthropoids and among different locomotor types. These functional interpretations represent hypothesized postures and movements based on interpretation of bony morphology. Testing these inferences requires the ability to visualize the relative posture and motion among bones of the ankle and tarsus, and then relating this to bone shape. In strepsirrhines, Gebo (1988) found that quadrupedal taxa had longer naviculars, whereas climbing taxa have short naviculars to facilitate more midfoot mobility. A similar trend has been hypothesized in anthropoid primates, where a shorter midfoot allows for conformity on a smaller substrate than a longer midfoot (Figure 8). Gebo (1989) also found that Old World monkeys had a longer navicular, which he attributed to increased quadrupedalism compared to other primates,

particularly apes, which possess a relatively shorter navicular. Gebo noted, however, that Old World monkeys still can and do engage in climbing activities so this morphological difference requires further study. I therefore hypothesize that climbing taxa that rely on grasping of smaller substrates will have a shorter midfoot than taxa that do not have a heavy reliance on grasping small substrates.

This chapter serves to quantify 3D articular surface shape of the calcaneus, talus, cuboid, and navicular in a broad sample of anthropoid primates (Tables 1 & 3) to identify osteological correlates of posture and motion at the talocrural, subtalar, calcaneocuboid, and talonavicular joints. The goal of this chapter is to test hypotheses about functional variation in morphology discussed above about tarsal shape: 1) I hypothesize that the tali of suspensory taxa will be more wedged, 2) have lower trochleae, 3) relatively shorter talar necks, and 4) more oblique subtalar articular surfaces. I hypothesize that on the calcaneus, 5) suspensory taxa will have relatively shorter posterior lengths. I hypothesize that suspensory taxa will have 6) more wedged cuboids, and 7) a more projecting proximal peg and socket on the cuboid. I hypothesize that arboreal taxa will have 8) longer cuboids and 9) longer naviculars. This will be evident in longer posterior calcanei, longer talar necks, and longer (proximodistally) naviculars and cuboids, respectively. I will also explore size and phylogenetic influences, as size affects an animal's locomotion and bony morphology (Fleagle, 1985; Biewener, 1989) and phylogeny likely affects bony morphological differences among these taxa.

Methods:

Samples and Groupings

The study sample comprises of taxa that were chosen to represent an array of locomotor emphases (Figure 9; Tables 1 & 3). Extant anthropoids were grouped into phylogenetic and locomotor groupings of taxa with different emphases in their locomotor repertoires (Table 3). The phylogenetic groups are *Pongo*, which is suspensory; hylobatids (*Hylobates, Symphalangus*) that are specialized for suspension and climbing; African apes (*Gorilla, Pan*) that emphasize climbing and suspension but also rely on terrestrial knuckle walking; atelids (*Ateles, Lagothrix)* engage in suspension and climbing, *Sapajus*, which is an arboreal quadruped, colobines (*Colobus, Nasalis, Rhinopithecus, Trachypithecus*), and cercopithecids (*Erythrocebus*, *Chlorocebus*, *Cercopithecus, Lophocebus, Macaca*) (Table 3). Due to similarities between colobines and cercopithecines, the two groups were combined in this analysis as cercopithecids, which are arboreal and/or terrestrial quadrupeds. All specimens are from non-pathological, skeletally mature individuals.

MicroCT scans of tali, calcanei, cuboids, and naviculars (Table 1) were provided by B. Patel (University of Southern California), C. Orr (University of Colorado Denver), S. Almécija (George Washington University), and W. Jungers (Stony Brook University). Each talus, calcaneus, cuboid, and navicular was segmented out from any other bones in the scan. Monkey tarsals were segmented using MIMICS software (Materialise, Leuven, Belgium) at the University of Colorado-Denver and apes were segmented using *Avizo7* (Thermo Fisher Scientific) at George Washington University. The resulting polygonal models were cleaned using *Geomagic Wrap 2017* (3D Systems, Inc.).

Landmarking

To quantify bone shape, 3D landmarks (modified from Harcourt-Smith, (2002); Figure 10) were placed on the polygonal surface model (Table 2). These landmarks were chosen to capture morphological variation reflecting foot bone posture and joint mobility, as in previous studies of ape tarsals (Harcourt-Smith, 2002). The 3D landmark data were placed on polygonal models using *Checkpoint* software (Stratovan, 2018) and imported into *Morphologika* (O'Higgins & Jones, 1999), *R* (R Core Team, 2014), and *MorphoJ* (Klingenberg & McIntyre, 2016) for visualization and analysis.

To quantify intraobserver error in landmark placement, the talus, calcaneus, cuboid, and navicular of two specimens (one monkey and one ape) were each landmarked three times. The mean point location was calculated from the three trials and the distance from the mean point location was then calculated for each trial. The average distance of those three trials was divided by the number of points on each respective bone and averaged for both individuals.

Analyses

Several analytical approaches were used to assess variation among groups. Landmarks on each bone underwent a Procrustes superimposition to translate, scale, and rotate the points into alignment. Principal component analyses (PCA) were used to isolate and quantify the observed morphological variation (Zelditch et al., 2012; Klingenberg & McIntyre, 2016). This study is limited to non-phylogenetically-controlled PCA in order to apply the same analyses interpretations from this chapter to the next chapter, which includes Miocene hominoid tarsals from taxa of unknown phylogenetic relationships.

Phylogenetic PCA analyses can be found in the Appendix. ANOVA tests with 10,000 randomizations were run to evaluate whether each PC, a measure of shape, differed among genera and between monkeys and apes in *R* (R Core Team, 2013).

In *WinEDMA* (Cole, 2002), the scaled interlandmark distances that had the highest correlation with axis scores, a proxy of morphological variation of each bone were identified to isolate which specific aspects of morphology varied among groups. The interlandmark distances with the highest correlations for each bone were explored using a phylogenetic generalized least squares (PGLS) regression to explore the relationship between each distance and centroid size and locomotion while taking phylogenetic relationships into account using the tree shown in Figure 9, which was produced using 10kTrees and modified using the *ape* package in R. The PGLS was carried out in R using the *caper* package. These linear distances were also plotted with a linear model regression against bone centroid size where group-specific intercepts were allowed to vary (groups defined in Table 3) to test for among group differences and explore allometric and locomotor trends in related to tarsal morphology in the *geomorph* package in *R*. In addition to the interlandmark distances that were most highly correlated with axis scores, trochlear wedging and cuboid wedging were also included in this bivariate analysis due to previously discussed hypotheses that both morphologies vary based on the manner in which taxa locomote and because interlandmark distances do not capture these morphologies, but a ratio does. Trochlear wedging was estimated as the ratio of the linear distance between the medial and lateral most aspect of the anterior margin of the trochlea and the linear distance between the medial and lateral most aspect of the posterior margin of the trochlea. Higher values indicate more wedging. Cuboid

wedging was measured in a similar manner: a ratio of the linear distance between the medial most point of the proximal and distal articular facets of the cuboid was taken for each specimen and the linear distance between the lateral most point of the proximal and distal articular facets of the cuboid was taken. Higher values indicate more wedging. To correct for multiple comparisons, the adjusted p-values are reported here using the Benjamini & Hochberg (1995) method ("BH") in *R.*

Results:

Landmark Placement Error

The mean error for the talus was 0.20 mm, ranging from 0.055 mm to 0.37 mm. The landmark associated with the highest error was 19. The mean error for the calcaneus was 0.20 mm, ranging from 0.058 mm to 0.55 mm. The landmark associated with the highest error was landmark 15. The mean error for the cuboid was 0.17 mm, ranging from 0.056 mm to 0.42. The landmark with the highest error was 8. The mean error for the navicular was 0.16 mm, ranging from 0.04 mm to 0.50 mm. The landmark with the highest error was 16.

Principal Components Analyses

Talus

Figure 11 shows PC2 plotted against PC1 for the talus, with color separating genus and shape differentiating monkeys and apes. Wireframes are included to illustrate the extremes on either end of the respective axis. PC1 accounts for 25.8% of the variation

and represents relative width/length of the talus, including talar neck length and talar head. PC1 separates by phylogeny, with African apes grouping on the negative end of the axis, Asian apes (*Pongo* and hylobatids) grouping together along PC1, and monkeys falling on the positive end of the x-axis (Figure 11). PC1 separates both between monkeys and apes ($p < 0.01$) and by genus ($p < 0.01$). PC2 describes 9.4% of the variation in talar morphology and captures trochlear height, with *Pongo* exhibiting the relatively flattest trochlear body among apes and hylobatids having relatively taller trochlear bodies, indicating that this morphology does not separate based on locomotion or phylogeny, since *Pongo* and hylobatids are both Asian apes and are both suspensory. PC2 did not separate between monkeys and apes ($p = 0.19$) but did separate by genera ($p < 0.01$).

Figure 12 shows PC4 plotted against PC3 for the talus, with color separating genus and shape differentiating monkeys and apes. PC3 accounts for 8.1% of the morphological variation and appears to show variation in the relative orientation of the posterior subtalar articular facet relative to the trochlear articular surface. This morphology separated genera ($p < 0.01$), between monkeys and apes (0.023), and separates taxonomically within monkey/ape groupings, with platyrrhines (*Sapajus* and atelids) grouping away from cercopithecids and Asian apes separating from African apes. PC4 accounts for 4.6% of the variation and describes the angulation of the posterior subtalar articular surface relative to the trochlea. This PC did not separate between monkeys and apes ($p = 0.73$) but did separate among genera ($p < 0.01$). Subsequent PCs explained very little variation and were therefore not explored.

Calcaneus

Figure 13 shows PC2 plotted against PC1 for the talus, with color separating genus and shape differentiating monkeys and apes. PC1 accounts for 31.5% of the variation and captures the relative width/length of the calcaneus, (i.e., size related shape of the Procrustes-transformed landmarks). PC1 appears to separate by body size, with great apes (*Pongo, Pan*, and *Gorilla*) grouping on the positive end of the axis, hylobatids grouping together, and monkeys heavily grouping on the negative end of the x-axis (Figure 13). PC1 separated both between monkeys and apes ($p < 0.01$) and by genus ($p < 0.01$). PC2 describes 9.8% of the variation in calcaneal morphology and captures tuber length (i.e., the distance between the posterior subtalar articular surface and the posterior end of the calcaneus). PC2 separated among genera ($p < 0.01$) and between monkeys and apes ($p < 0.01$), with *Pongo* and *Hylobates* separating from monkeys and African apes (Figure 13).

Figure 14 shows PC4 plotted against PC3 for the calcaneus. PC3 accounts for 6.7% of the variation and appears to show orientation of the sustentaculum tali. This morphology separated genera ($p < 0.01$), but not monkeys and apes ($p = 0.69$). This PC separates taxonomically within monkeys only, with platyrrhines grouping away from cercopithecids. PC4 accounts for 5.9% of the variation and describes the angulation of the subtalar articular surface relative to the calcaneal tuber. This PC did not separate between monkeys and apes ($p = 0.32$) but did separate among genera ($p < 0.01$). Subsequent PCs explained very little variation and were therefore not explored.

Cuboid

Figure 15 shows PC2 plotted against PC1 for the cuboid, with color separating genus and shape differentiating monkeys and apes. Wireframes are included to illustrate the extremes on either end of the respective axis. PC1 accounts for 23.9% of the variation and captures cuboid breadth and wedging. PC1 appears to separate by body size, with *Gorilla* on the far negative end of the axis, followed by *Pan*, *Pongo*, lesser apes, and monkeys falling on the positive end of the x-axis, but not by phylogeny within monkeys or apes or by locomotion (Figure 15). PC1 separates both between monkeys and apes ($p < 0.01$) and by genus ($p < 0.01$). PC2 describes 12.2% of the variation in cuboid morphology and captures proximodistal length of the cuboid, with *Ateles* and *Colobus* separating from the rest of monkeys on the negative end of the PC scale. PC2 separated between monkeys and apes ($p < 0.01$) and genus ($p < 0.01$).

Figure 16 shows PC4 plotted against PC3 for the cuboid, with color separating genus and shape differentiating monkeys and apes. PC3 accounts for 7.1% of the variation and appears to show differences in the relative orientation of the proximal and distal articular facets, or torsion of the bone. This morphology did not separate between monkeys and apes ($p = 0.081$). PC3 did separate genera ($p < 0.01$) and also separated Asian apes from African apes, but otherwise yields no clear separation patterns. PC4 accounts for 6.8% of the variation and describes the angulation of the proximodistal long axis of the cuboid. There were significant differences among genera ($p < 0.01$) and between monkeys and apes ($p < 0.01$). This PC appears to isolate New World monkeys from Old World monkeys, but has no clear locomotor signal. Subsequent PCs explained very little variation and were therefore not explored.

Navicular

Figure 17 shows PC2 plotted against PC1 for the navicular, with color separating genus and shape differentiating Old World monkeys, New World monkeys, and apes. PC1 accounts for 27.8% of the variation and captures the proximodistal length of the navicular. PC1 separates by genus ($p < 0.01$) and between monkeys and apes ($p < 0.01$) and separates suspensory taxa (*Pongo, Pan, Gorilla, Hylobates, Ateles*) from *Sapajus* and cercopithecids, which stress running or jumping. PC2 describes 12.1% of the variation in navicular morphology and captures projection of the navicular tuberosity. PC2 separates genera ($p < 0.01$) and monkeys from apes ($p < 0.01$) with *Pongo, Lagothrix,* and *Sapajus* exhibiting the least projection and *Hylobates* exhibiting the most tuberosity projection (Figure 17).

Figure 18 shows PC4 plotted against PC3 for the navicular, with color separating genus and shape differentiating monkeys and apes. PC3 accounts for 8.1% of the variation and appears to show variation in the relative length of the talonavicular articular surface compared to the rest of the navicular. This morphology separated genera ($p < 0.01$) and monkeys from apes ($p = 0.017$), notably isolating atelids, which have smaller talonavicular articular surfaces relative to the rest of the navicular compared to the other taxa. PC4 accounts for 7.7% of the variation and describes the relative height of the navicular. This PC did not separate between monkeys and apes ($p = 0.91$) but did isolate New World monkeys from Old World monkeys and African apes from Asian apes. Subsequent PCs explained very little variation and were therefore not explored.

Bivariate Analysis

The PC analyses demonstrated the large-scale shape differences in the morphology of each tarsal. In order to further explore which specific aspects of morphology drive variation in this sample, landmark data were imported into *WinEDMA* and converted into a matrix of linear distances between all landmarks and scaled to the geometric mean for each bone. Correlations between scaled distances and axis scores were calculated for each bone. The highest correlations from those analyses, as well as talar trochlear wedging and cuboid wedging, were explored in bivariate plots of natural log-transformed linear distances plotted against the natural log of each bone's respective centroid size with linear model regressions for each group.

Phylogenetic generalized least squares analysis revealed that when phylogeny is considered, the selected measurements from the EDMA analysis were related to locomotion ($p < 0.01$), except for the two wedging measurements ($p = 0.46$ for trochlear wedging and $p = 0.25$ for cuboid wedging) (Table 4).

Talus

In the talus, four log-transformed interlandmark distances were explored: talar neck length, talar length, talar head breadth, and trochlear wedging. General talar length and breadth were both driving factors of variation in the PC analysis described above, but this secondary analysis allows further exploration of specific distances that are responsible for the variation seen among extant primates. When plotted against log-transformed centroid size, where intercepts are allowed to vary by group (listed in Table

3), talar neck length scales negatively allometrically with centroid size (Table 5). African Apes differed from all groups except hylobatids, and hylobatids were different from *Sapajus*, *Lagothrix* and cercopithecids, but not *Ateles* or African apes (Figure 19; Table 6), which means this morphology may have phylogenetic, size, and slight locomotor signals affecting the variation. Talar length, on the other hand, scales isometrically among primates in this study (Table 5) and largely separates taxa based on size and phylogeny, with platyrrhines separating from cercopithecids and all apes (Figure 20). All catarrhines were indistinguishable from each other.

In the PC analysis, general talar breadth was a driving factor of variation (Figure 21), but this additional interlandmark distance analysis isolated talar head breadth specifically. African apes have the relatively broadest talar heads, followed by Asian apes, then platyrrhines (Figure 21). Cercopithecids display the narrowest talar heads of all specimens studied (Figure 21). This variation can be attributed to phylogeny, size, or both. Trochlear wedging was negatively allometric, but had a very low R-squared value, which suggests little confidence in any allometric trends related to this morphology (Table 5). Although trochlear wedging is hypothesized to be related to increased lateral movements of the talus during locomotion, thought to be associated with increased suspensory locomotion, trochlear wedging does not appear to vary by locomotor type in this study (Figure 22). For example, as can be seen in Figure 22, *Hylobates*, a small, suspensory ape, has a very wedged trochlea, and when plotted, the taxon indeed exhibited among the highest values for trochlear wedging. *Cercopithecus*, a smaller quadrupedal monkey, does exhibit less trochlear wedging than the *Hylobates*. However, *Pongo*, a large, highly suspensory ape exhibits equal if not less wedging than *Cercopithecus*. These

results indicate that trochlear wedging, although it affects foot posture, does not separate taxa by phylogeny, size, or locomotion and therefore is not diagnostic when inferring these characteristics from isolated tarsals.

Calcaneus

In the calcaneus, three measurements were studied: calcaneal height, anterior calcaneal length, and sustentaculum tali projection. Calcaneal height separates highly suspensory African apes, *Pongo*, hylobatids, and atelids from largely arboreal quadrupedal *Sapajus* and cercopithecids (Figure 23; Table 6). Although the regression slope indicates isometry (Table 5), some patterns can still be deduced from this analysis. Since platyrrhines are split, calcaneal height variation does not appear to separate along phylogenetic lines, and since atelid body size overlaps with that of cercopithecids, but the intercepts of those two groups significantly differ ($p < 0.01$), the difference in calcaneal height appears to be affected by locomotor differences. In the PCA, posterior calcaneal length drove variation in the extant sample, but in the bivariate analysis, anterior calcaneal length was isolated as a varying factor among taxa. Anterior calcaneal length and sustentaculum tali morphology drive variation in this sample, but both appear to largely vary based on phylogeny, with apes having relatively anteroposteriorly shorter calcanei than all monkeys, which have relatively longer calcanei with more projecting sustentaculum tali (Figures 24-25; Table 6). However, within each group, there is a locomotor signal, wherein suspensory apes have significantly shorter anterior calcanei than monkeys overall, but within New World monkeys, suspensory atelids have shorter anterior calcanei than quadrupedal *Sapajus* (Figure 24).

Cuboid

In the cuboid, three measures were studied: cuboid length, cuboid breadth, and cuboid wedging. Cuboid length scaled negatively allometrically with body size, but separated taxa based on locomotion (Figure 26; Tables 4-5) with African apes, *Pongo*, hylobatids, and atelids having shorter cuboids than cercopithecids and *Sapajus*. A diagonal line connecting the medial articular surface and the distal lateral articular surface was a significant driver of variation in the EDMA analysis, and this was interpreted to be a proxy for cuboid breadth, but since there was no landmark on the lateral margin of the cuboid at the same proximodistal plane as the medial landmark, cuboid length will also be associated with this interlandmark distance. This morphology scales positively allometrically with centroid size (Table 5). Apes and *Sapajus* appear to separate from the remaining taxa with relatively narrower cuboids, whereas atelids and cercopithecids have relatively wider cuboids (Figure 27). Cuboid wedging appeared to isolate African great apes, which exhibit highly wedged cuboids, which may indicate that this morphology aids in vertical climbing but does not seem to separate non-African great ape taxa by phylogeny, size, or locomotion (Figure 28).

Navicular

In the navicular, two measures were studied after the correlation results from *WinEDMA*: navicular proximodistal length and navicular width. Navicular proximodistal length scales isometrically with centroid size, although the R^2 value is notably low, and so interpretations are made cautiously (Table 5). Apes appear to overall have shorter

naviculars than all monkeys (Figure 29; Table 6) with cebids and some cercopithecids having the longer naviculars. Navicular mediolateral width scaled positively allometrically with apes having slightly wider naviculars than monkeys (Figure 30; Tables 4-5).

Discussion:

The goal of this chapter was to study the variation in tarsal morphology across extant anthropoid primates and test hypotheses about tarsal morphology. This was done using 3D landmarks that were transformed to scaled PC scores in order to quantify shape overall, followed by a series of linear regressions to further explore effects on shape (represented by the Procrustes coordinates) and on interlandmark distances that had the greatest effect on variation. This chapter approached shape variation in tarsal form in two different manners. The PCA provided qualitative but simplified overall shape variation. PCA is also useful, as the same analyses can be performed on fragmentary specimens using subsetted landmark datasets of the same extant sample, as was done in Chapter 4 of this dissertation. In addition to the traditional geometric morphometric analyses, linear models of interlandmark distances focused on specific morphologies that drove variation on each bone rather than overall shape. Contrary to my predictions (listed in Introduction), neither 1) trochlear wedging nor 6) cuboid wedging separated taxa that locomote differently. 2) Trochlear height did vary in the PCA, as predicted, but interlandmark distances were unable to capture variation in this morphology. 3) Talar neck length, though it did appear to somewhat vary by locomotor type, also varied by body size. Talar head breath, contrary to my predictions varied according to body size

and phylogeny, not locomotor type. 4) Orientation of the subtalar articular surface did separate taxa that locomote differently. 7) Proximal peg and socket projection of the cuboid also either was not captured or did not vary in the interlandmark distance analysis. Relative lengths of the 5) calcaneus, 8) cuboid, and 9) navicular did, as hypothesized, all vary based on locomotion. These traits, as well as other morphologies that drove variation are discussed below.

The variation observed from both the PCA and interlandmark distance analyses of this study can be grouped into three categories: phylogeny, size/allometry, and locomotion. These three categories, however, are intertwined. For example, phylogenetically, apes and monkeys are disparate groups, but apes—particularly great apes—are also larger than monkeys in body size, therefore variation along phylogenetic lines may also carry implication of size variation. Similarly, body size affects an organism's locomotion (Jungers, 1985; Langdon, 1986; Biewener, 1989; Ward et al., 2018). Therefore, many morphologies fall into multiple categories. This study does not mean to imply that these morphologies only fall into the category in which it is discussed, only that size, phylogeny, and/or morphology play(s) a role in the morphological variation.

Phylogeny

In the absence of complete fossil specimens, isolated postcranial bones can be the only fossil evidence of extinct taxa. Although phylogeny cannot be inferred from small bones such as the tarsals studied in this chapter, morphological similarities to monkeys or

apes can be helpful in describing fossil taxa. From the PC analysis, significant separators of monkeys from apes are talar neck length/talar length, with monkeys overall having longer necks than apes and anterior calcaneal length, with apes having relatively shorter calcanei. Additionally, PC3 of the navicular, which is associated with the relative size of the talonavicular articular surface isolates atelines from all other taxa, though no allometric, functional, or other phylogenetic conclusions can be drawn from this result. In the bivariate plots, talar length, talar head breadth, anterior calcaneal length, sustentaculum tali projection, and navicular proximodistal length separate monkeys from apes, with apes having relatively shorter tali, broader heads, relatively shorter anterior calcanei, and less-protruding sustentaculum tali than monkeys, which have longer tali, narrower talar heads, relatively longer calcanei, and more sustentaculum protrusion.

Talar head breadth appears to be influenced by phylogeny, as a size gradient is visible in the bivariate plot of this measurement and centroid size, with African apes having much broader talar heads than *Pongo*, which has broader heads than hylobatids, followed by platyrrhines and then cercopithecines with the narrowest heads (Figure 20). Langdon (1986) hypothesized that this was due to loading differences among taxa, with the large African apes requiring greater breadth in order to dissipate the increased force passing through the talar head while the talonavicular joint was loaded, leading to a broader talar head. However, this morphology was negatively allometric with centroid size, so further analysis of talar head breadth and body size is needed. Additionally, the fact that *Sapajus*, *Lagothrix*, and *Ateles*, all platyrrhines of different sizes fall together (Figure 14) indicates that phylogeny also plays a major role in this morphology. The two

factors are difficult to separate due to the fact that body size differences largely also fall along phylogenetic lines.

Size

Due to the large range in primate body size (Jungers, 1985), much of the variation in morphology in this study is due to size. The morphologies where variation appears to be mainly attributable to size are: cuboid breadth, talar head breadth, and calcaneal length. Cuboid breadth is positively allometric with centroid size (Table 5), and the PCA showed a possible size gradient in taxonomic variation (Figure 12). The interlandmark distance analysis did not show such a gradient, but that is likely due to the fact that these landmarks did not strictly capture breadth and other factors, such as cuboid length, which did not scale with body size.

Talar head breadth, as has been discussed previously, appears to separate along a size gradient, with African apes having the broadest heads, followed by Asian apes, then monkeys. This likely has to do with increased forces associated with larger body sizes requiring greater surface area of the talar head as it is loaded longitudinally. However, the amount of force transferred through the talar head will also depend on the form of locomotion, by reducing the need for broad talar heads in highly suspensory taxa, as they would not engage in loaded plantarflexion. This implies that after size, there is a locomotor gradient associated with this morphology.

Calcaneal length appears to be influenced by body size in the current sample, as this measure of calcaneal length in the PCA separated group by body size and the

bivariate plot of calcaneal length also separates along a size gradient. This measure does not separate by phylogeny, as atelids and cercopithecids, which overlap in body size but are phylogenetically disparate, were not significantly different.

Locomotion

Morphologies that vary with primate taxa that locomote in similar manners are: relative orientation of the posterior subtalar facet on the talus, talar neck length, calcaneal tuber height, calcaneal anterior length, cuboid length, and navicular anteroposterior length.

Orientation of the posterior subtalar facet varying among taxa that move differently is consistent with the observations from Chapter 2 of this dissertation and supports hypothesis 4 of this study. Since plantarflexion/dorsiflexion and inversion/eversion are highly correlated with each other at the subtalar joints (Chapter 2), the morphology of this joint, specifically the orientation of the subtalar joint that allows for motion in both planes appears to also vary depending on the type of locomotion an organism engages in. Of note, the PC analysis shows that body size weighs more heavily on talar shape compared to the orientation of the posterior subtalar facet, which is to be expected because the talus also bears much of the body weight, particularly in quadrupedal (including knuckle walking) taxa. Orientation and relative size of the posterior subtalar facet has also been hypothesized to vary by taxa that locomote differently in previous studies. Langdon (1986) hypothesized that the orientation of the posterior subtalar joint in non-human great apes results in less advancement of the talar

head and therefore less close-packing of the joint in a supinated foot position, leading to more stability for taxa that climb and grasp small branches. *Pongo* and atelids (highly suspensory taxa that grasp small branches with their feet) group together in subtalar articular surface orientation. They separate from arboreal quadrupeds cercopithecids and African Apes that engage in terrestrial quadrupedalism and also vertical climbing. Lewis (1980b) attributed this separation between highly suspensory *Pongo* and hylobatids and *Pan* and *Gorilla,* to the fact that both African Apes spend a significant amount of time walking on the ground and therefore differ from the more suspensory hylobatids and *Pongo* (Lewis, 1980b). *Sapajus*, an arboreal quadruped, however also overlaps with *Pongo* and atelids in this analysis, which complicates the hypothesis that this morphology reflects locomotion alone.

Talar neck length appears to be responding to multiple signals, lending partial support for one of the hypotheses for this study. This morphology broadly separates monkeys from apes and along a size gradient. The phylogenetic exception is *Ateles*, which groups with *Pongo*, having shorter necks than cercopithecids, *Sapajus*, and *Lagothrix*, but longer necks than African apes and *Hylobates*. Langdon (1986) hypothesized that larger specimens, like apes, would have shorter talar necks than monkeys to account for greater stresses as a result of body size. *Pongo* and *Ateles* could have elongated necks compared to African Apes and hylobatids partially because these compressive stresses on the foot are decreased in suspensory locomotion (Langdon, 1986). Since *Pongo* rarely travels on the ground, a relatively longer neck can increase excursion of joints in the midfoot in supinated foot postures, which adds a locomotor

signal to this pattern of phylogenetic and size-dependent variation in talar neck morphology.

Calcaneal height at the posterior subtalar articulation, also appears to separate taxa that move differently. Suspensory taxa (African apes, *Pongo*, hylobatids, and atelids) differed from the terrestrial or arboreal quadrupedal cebids and cercopithecids with the suspensory taxa having relatively taller calcanei. Although absolute length of the calcaneus scales with centroid size, the shorter height but longer posterior calcaneus seen in cercopithecines is hypothesized to result from increasing the in lever arm of the triceps surae muscle group for more powerful plantarflexion, which is important in arboreal and terrestrial locomotion, particularly involving running or jumping (Strasser, 1988). The relatively shorter calcaneal body height in cercopithecids seen in this study could also result from the fact that cercopithecids have taller talar trochleae for increased stability during plantarflexion and dorsiflexion and/or leaping (Strasser, 1988, Gebo et al., 2015), and thus this difference in calcaneal height stems from difference in the relative contribution to posterior height of the foot between taxa that locomote differently. Langdon (1986) also noted increased calcaneal height in hominoids and attributed this morphology to the inferior tubercle in gorillas and humans, although noted that a direct measure of the heel process did not yield the same differences separated by calcaneal height. Orangutans, which do not possess a large heel process, also possess tall calcanei.

The general elongation of the lateral foot is evident in both the anterior elongation of the calcaneus and the relative elongation of the cuboid. Although both are unsurprisingly related to size and phylogeny, the shortening of the midfoot region in suspensory taxa would allow the animal to grasp a smaller substrate for the same amount

of midfoot flexion. Apes in particular require lateral foot mobility during grasping and suspensory locomotion, which would not benefit from elongated tarsals (Langdon, 1986; Strasser, 1988).

The proximodistal navicular length separated great apes from arboreal and semi-terrestrial quadrupeds, with a gradient in between those two groups that included suspensory atelids, hylobatids, and *Nasalis* being more similar to great apes and in line with atelids and hylobatids (Figure 14). This distribution of taxa is consistent with Langdon's (1986) observation that *Sapajus* has a relatively long navicular (proximodistal dimension), whereas hominoids have much mediolaterally wider naviculars relative to their length. He associated this disparity with running and leaping taxa requiring a longer load arm for plantarflexion, whereas suspensory taxa have shortened their naviculars to reduce stresses on the bone during supinated foot postures, particularly given the large body size of hominoids (Langdon, 1986). I hypothesize that the intermediate specimens, include smaller suspensory taxa and *Nasalis*, which has been observed to engage in both suspensory behaviors and some vertical climbing (Su & Jablonski, 2009). This gradient, particularly the intermediate group follows this pattern hypothesized by Langdon (1986) in that they would require less shortening of the navicular due to smaller body size than hominoids, which are at risk of injury from placing large loads on their midfoot region during suspensory locomotion and/or vertical climbing. The intermediate group, however, does require more stability during inverted foot posture than the arboreal quadrupedal running/jumping group, therefore falls intermediate to the two extremes.

Limitations

Although there are many benefits of landmark-based GM, it remains possible that aspects of morphology were not quantified due to an absence of landmarks in a particular region. Both measures of wedging yielded little to no detectable patterns in taxa separation, though both have been hypothesized previously to vary among taxa. It remains possible that the manner used in this study to quantify wedging of both the talar trochlea and cuboid body did not aptly capture the aspects of these morphologies that vary among extant anthropoids.

Many of the limitations from this study stem from the fact that size, phylogeny, and locomotion-related differences are confounded by each other in this sample. Inclusion of more non-suspensory New World monkeys would aid in diversifying the locomotor differences analyzed and having better separation between phylogeny and locomotion. Additionally, using body size estimates rather than bone centroid size would be ideal, but is not possible for many museum specimens where body size estimates were not always known. However, in future studies, a proxy for body size that does not include any of the morphologies analyzed in this study ought to be used.

Conclusion:

This chapter was preceded by a study of *in vivo* motions that occur at the talocrural, subtalar, calcaneocuboid, and talonavicular joints. This chapter continued to explore the functional morphology of the anthropoid foot and ankle by analyzing a large sample of tarsals from anthropoid primate taxa that vary in body size, phylogeny, and

locomotion in order to offer the form side of form-function relationships. Tarsals are complicated in shape and difficult to interpret but are often preserved in the fossil record (Sarmiento & Marcus, 2000). As such, it is important to study the diversity in tarsal morphology and what drives that variation in extant taxa before attempting to interpret fossil taxa. This study allowed us to parse out aspects of tarsal morphology that are driven by phylogeny, size, locomotion, or a combination of multiple factors. I also identified specific morphologies related to stability vs. mobility in the midfoot region, subtalar joint orientation, and inversion at the talocrural joint that separate suspensory from quadrupedal taxa. This study showed that the orientation of the posterior subtalar facet on the talus was more oblique in suspensory taxa, talar necks are shorter in suspensory taxa (although this also relates to body size), calcaneal tuber height is greater in suspensory taxa, calcaneal anterior length is greater in quadrupedal taxa, quadrupedal taxa have longer cuboids, and navicular anteroposterior length is also greater in quadrupedal taxa. These morphologies provide a framework to study fossil material based on functional analyses of extant primate diversity.

Figures and Tables for Chapter 3

Figures:

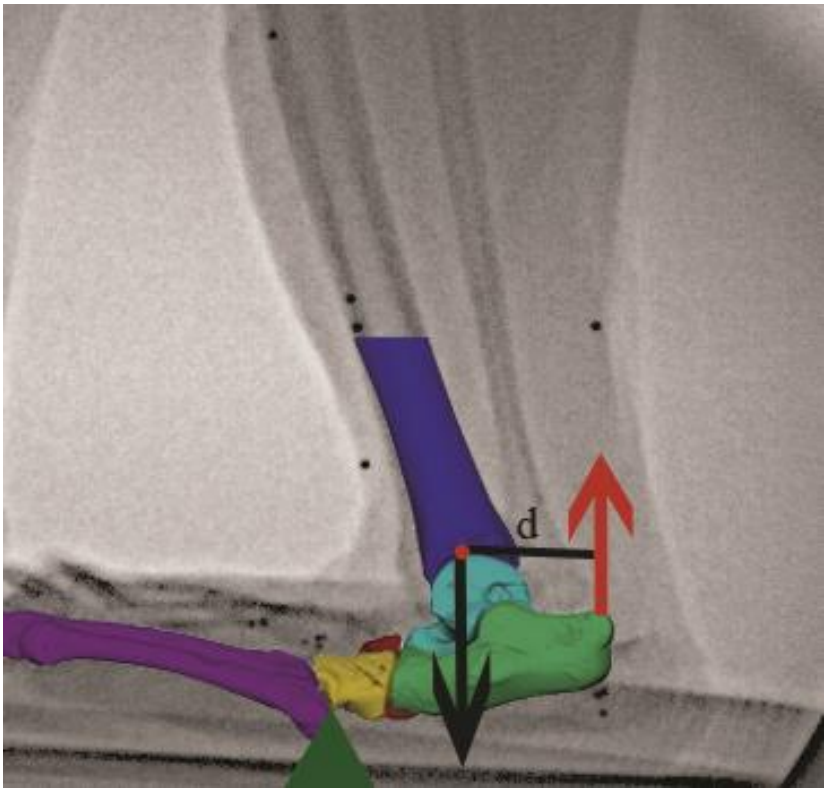

Figure 1: Diagram of the effect of the calcaneal tuber length on ankle plantarflexion. Green triangle is the fulcrum, where the midfoot break occurs (Chapter 2 of this dissertation; DeSilva, 2010). Black arrow shows the load of the body weight on the lever system. Red arrow is the muscular force of the triceps surae muscles on the posterior calcaneus. Increasing the in-lever distance (d) increases the mechanical advantage without increasing muscular effort. Diagram shown on a lateral view of *Macaca mulatta* polygonal model of a foot overlaid onto a uniplanar fluoroscopic image of the same foot.

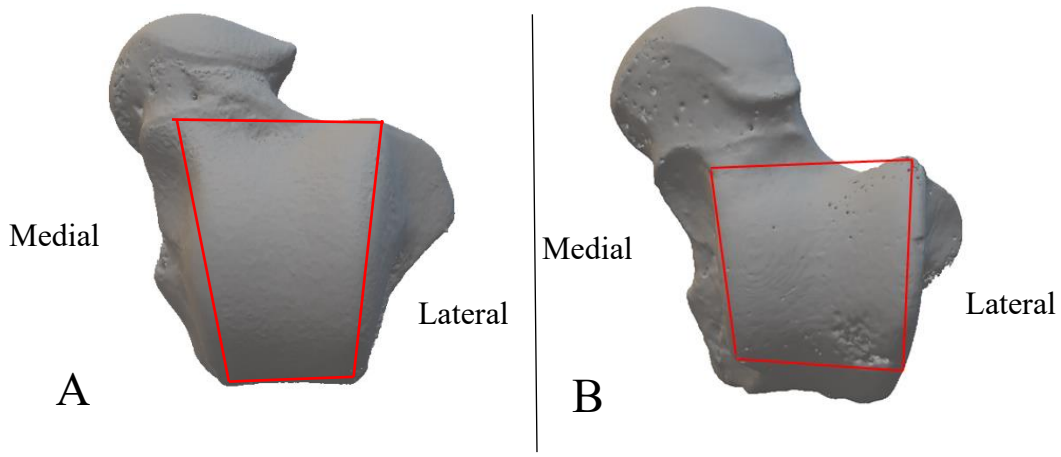

Figure 2: Examples of A) a trapezoidal talar trochlea (*Hylobates klossi*), which tapers posteriorly versus B) a more rectangular talar trochlea (*Cercopithecus mitis*). Note: models are scaled to each other by talar length. Both tali are in dorsal views.

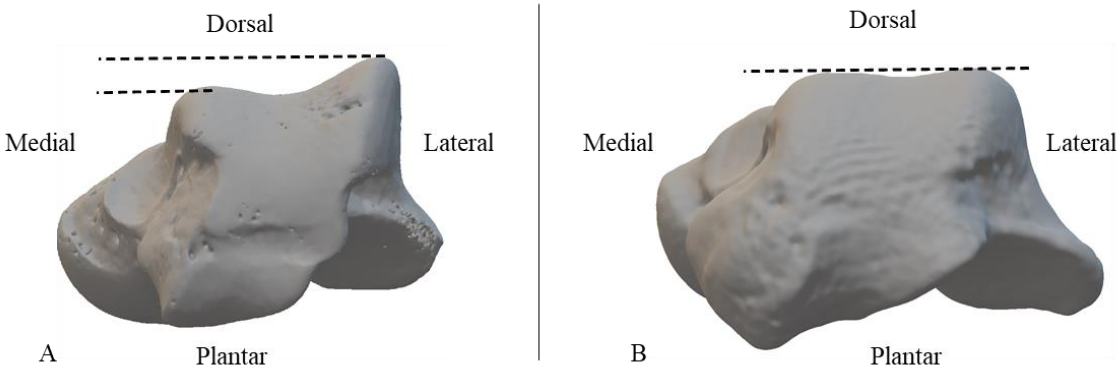

Figure 3: Examples of A) high and asymmetrical talar trochlear crests (*Cercopithecus mitis*) versus B) flat, symmetrical trochlear crests (*Pan troglodytes*). Note: models are scaled to each other by talar height. Both tali are in caudal views.

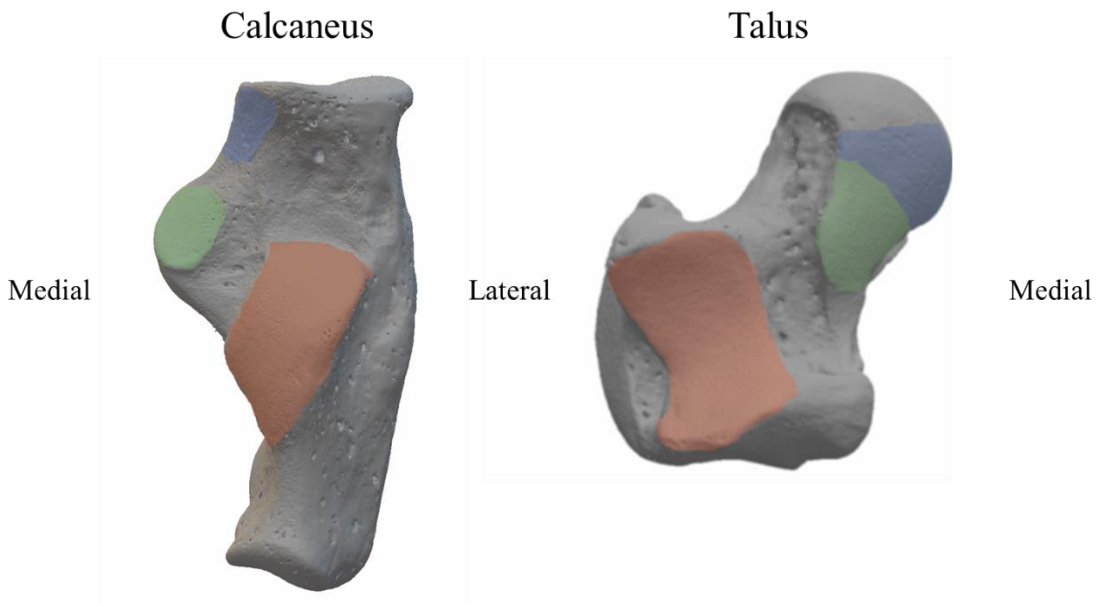

Figure 4: Subtalar articulations on the calcaneus (left, dorsal view) and talus (right, plantar view). Posterior subtalar articular surface colored in red, middle subtalar articular surface in green, anterior subtalar articular surface colored in blue. Shown here in *Cercopithecus ascanius* specimens.

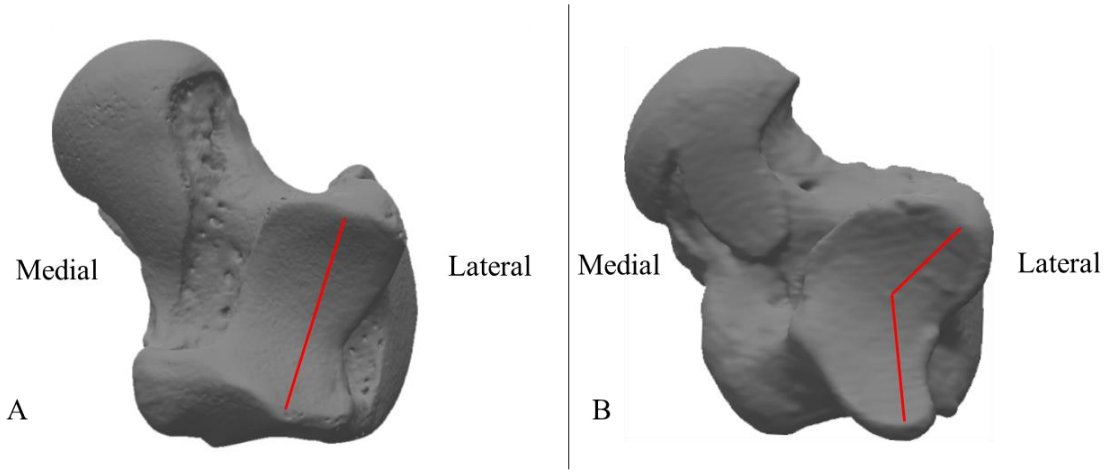

Figure 5: Example of variation in the orientation of the subtalar articular surface in *Cercopithecus alborgularis* (left) and *Pan troglodytes* (right), which is hypothesized to differ between suspensory and non-suspensory taxa. Left tali were scaled to the same length, and thus do not reflect actual talar size relative to each other. Both tali are in plantar views.

A  B 

Figure 6: Examples of A) prominent peg and socket morphology at the calcaneocuboid joint (*Pongo pygmaeus*, plantar view, arrow indicates proximal bony protuberance) versus B) a more planar articulation at the calcaneocuboid joint (*Trachypithecus cristatus* plantar view, arrow indicates proximal bony protuberance). Note: pictures are scaled to each other by cuboid proximodistal length.

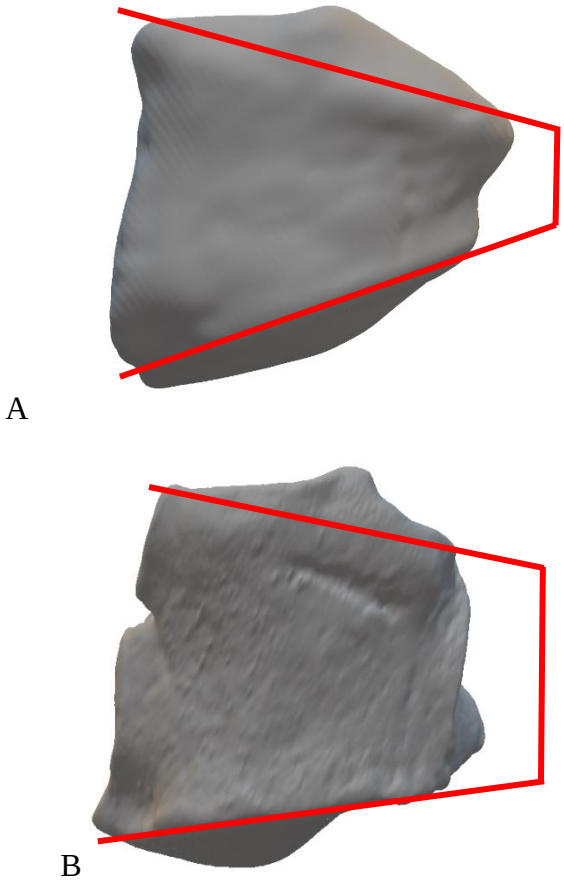

Figure 7: Examples of A) a wedged cuboid (*Gorilla beringei*) and B) a more rectangular cuboid (*Macaca mulatta*). Note: models (dorsal view) scaled to each other by cuboid length.

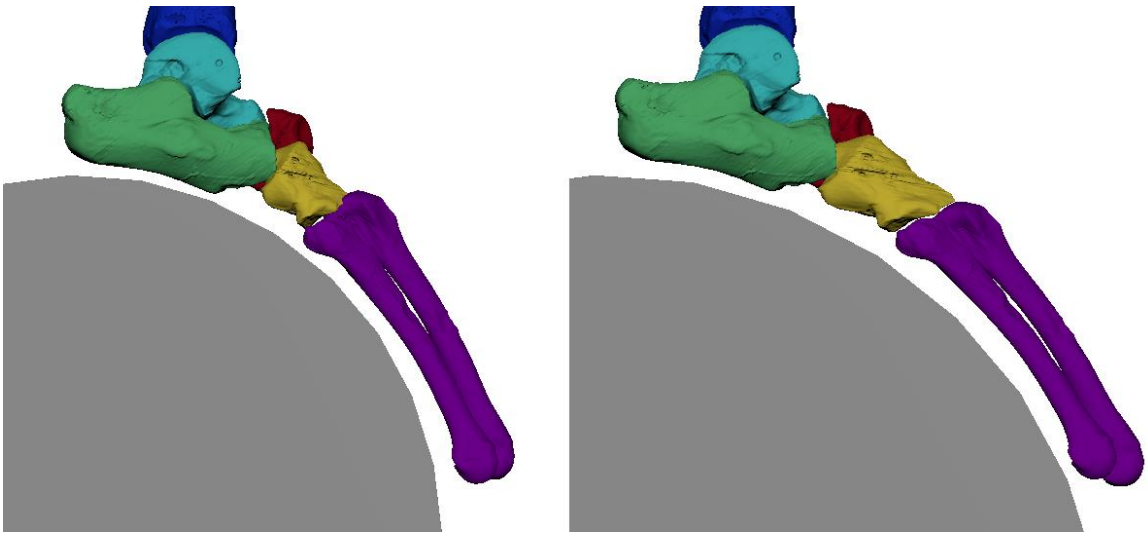

Figure 8: Midfoot length effect on ability to grasp smaller substrates. The image on the right has a longer midfoot than the image on the left. Given the same amount of rotation of the midfoot, the shorter midfoot allows the animal to grasp a smaller substrate without increasing the amount of rotation that occurs between these bones. Lateral view of *Macaca mulatta* right foot.

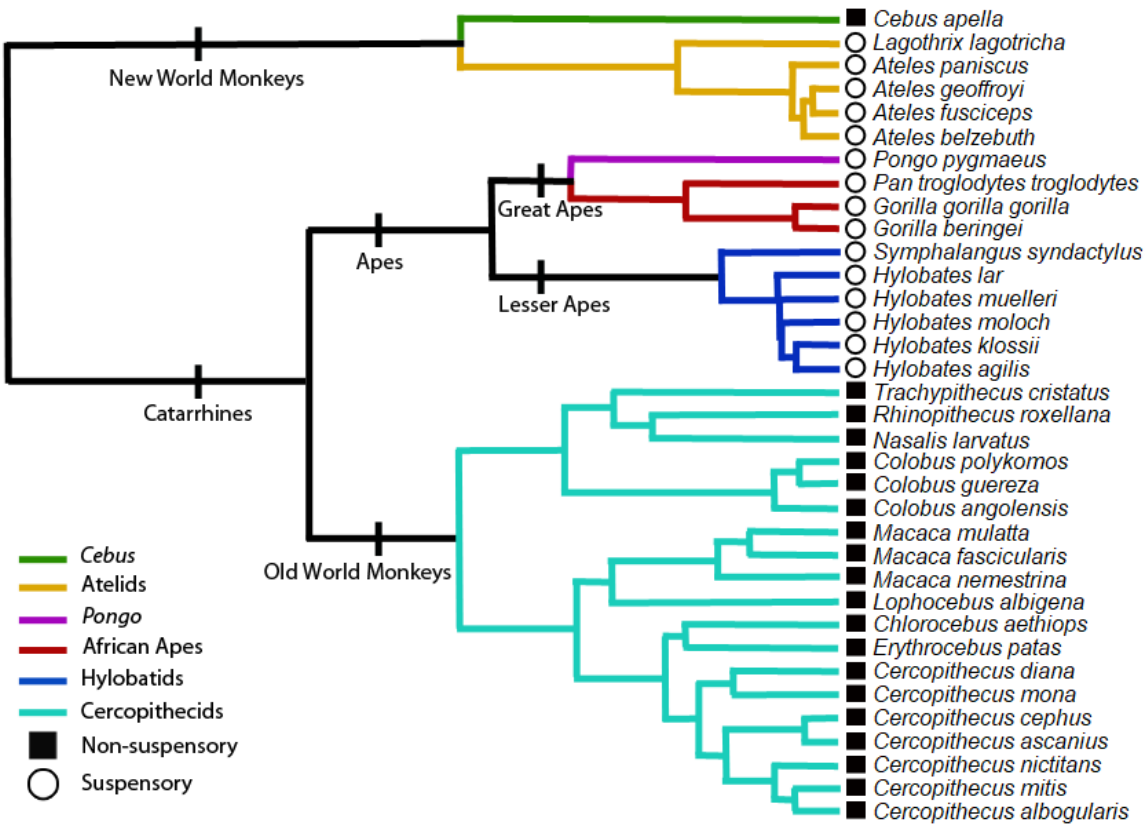

Figure 9: Phylogenetic relationships of the extant sample of anthropoid primates used in this study. Sample sizes listed in Table 1. Branches are colored by Taxonomic Group listed in Table 3. Locomotor category (listed in Table 3) is indicated by a black square (non-suspensory) or hollow circle (suspensory).

Calcaneus

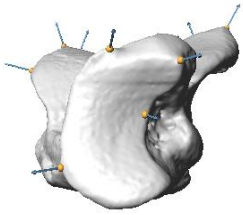

Distal View

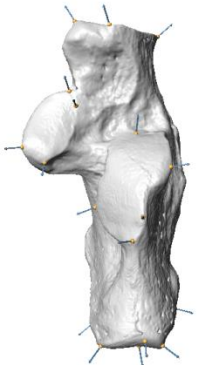

Dorsal View

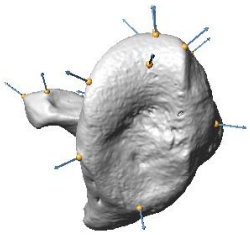

Posterior View

Cuboid

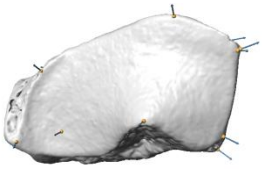

Proximal View

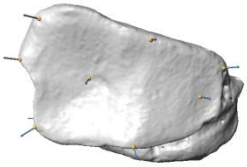

Distal View

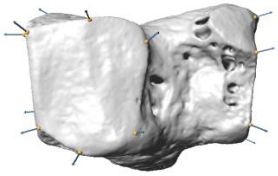

Medial View

Navicular

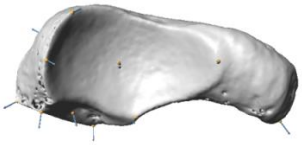

Proximal View

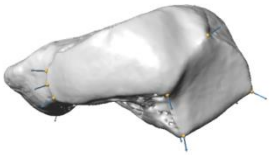

Distal View

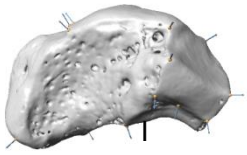

Inferior View

Talus

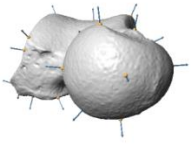

Distal View

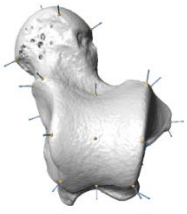

Dorsal View

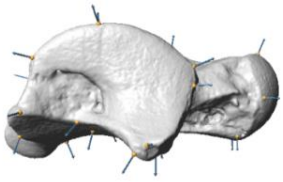

Lateral View

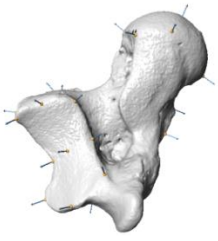

Plantar View

Figure 10: Landmarks to be used in the geometric morphometric analysis of the calcaneus (n = 230), cuboid (n = 282), navicular (n = 254), and talus (n = 238), modified from Harcourt-Smith (2002). Landmarks are listed and described in Table 2.

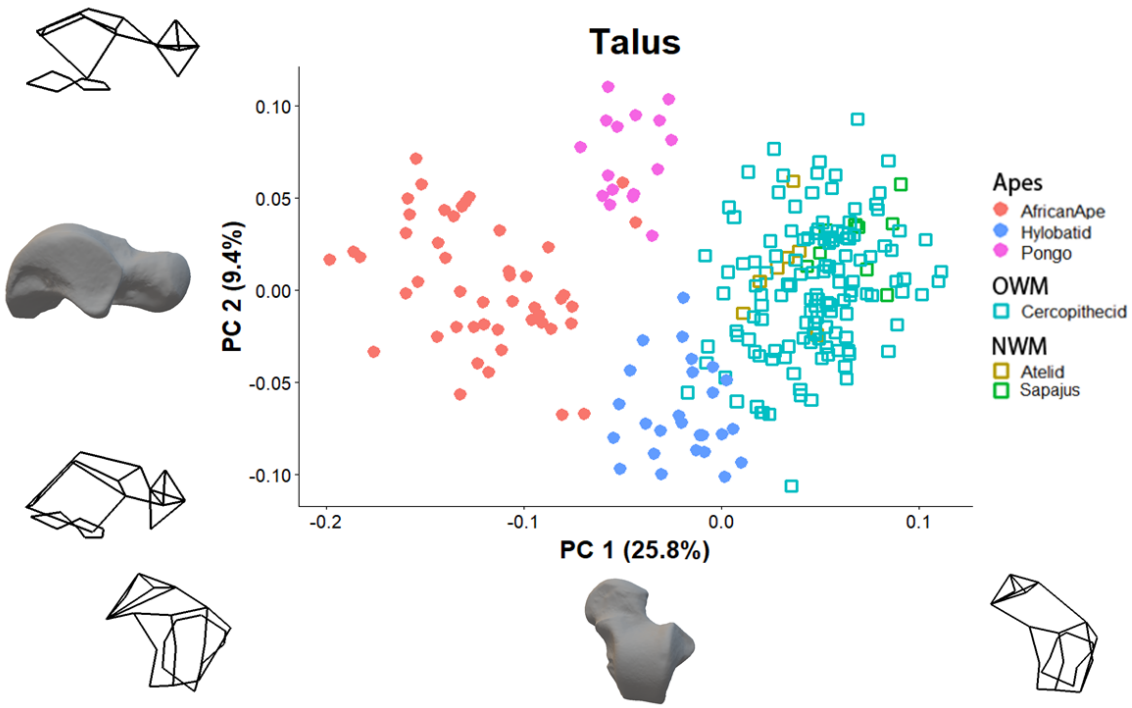

Figure 11: PCs 1 and 2 of the talus. Percent (%) variation explained by each PC is listed along its axis label. Wireframes consisting of connected landmarks of the extreme morphology of the respective ends of each PC provided for visualization of shape changes. Bone models matching the view of the wireframes provided for visualization. Color of data points vary by group, defined in Table 3. Filled circles represent apes, squares represent monkeys. PC 1 captures the relative length and width of the talus, including variation in the talar neck, head. PC 2 captures trochlear height.

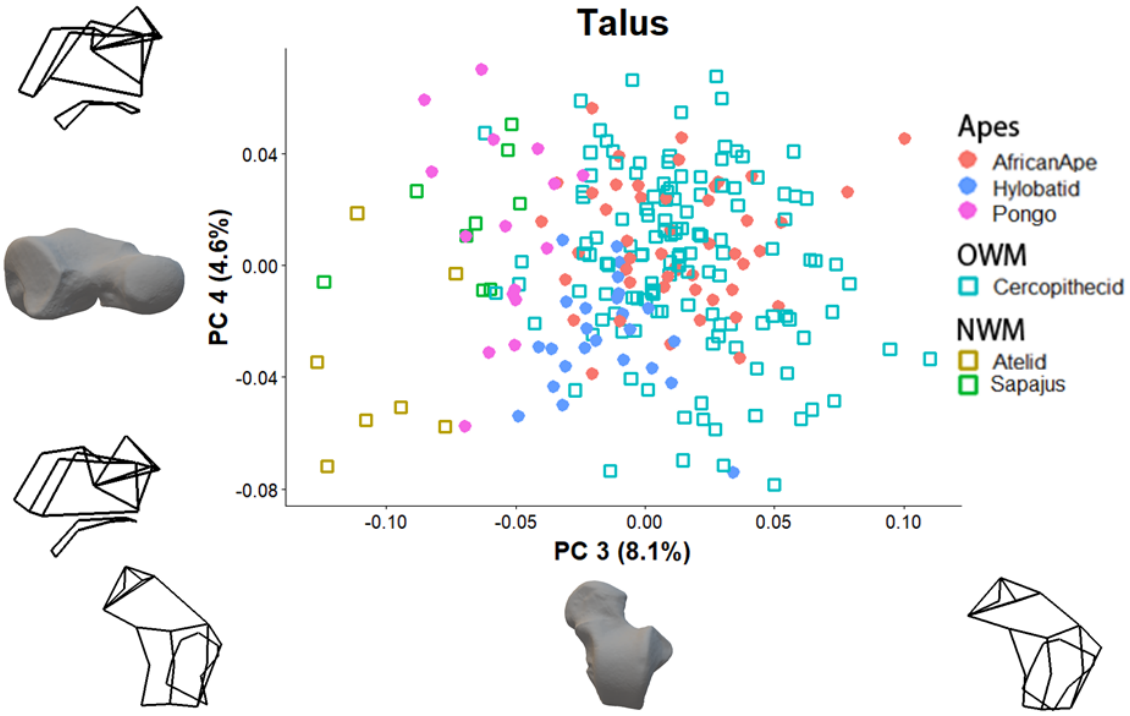

Figure 12: PCs 3 and 4 of the talus. Percent (%) variation explained by each PC is listed along its axis label. Wireframes consisting of connected landmarks of the extreme morphology of the respective ends of each PC provided for visualization of shape changes. Bone models matching the view of the wireframes provided for visualization. Color of data points vary by group, defined in Table 3. Filled circles represent apes, squares represent monkeys. PC 3 captures variation in the curvature of the posterior calcaneal facet relative to the trochlear articular surface. PC 4 describes the angulation of the posterior subtalar articular surface relative to the trochlea in the transverse plane.

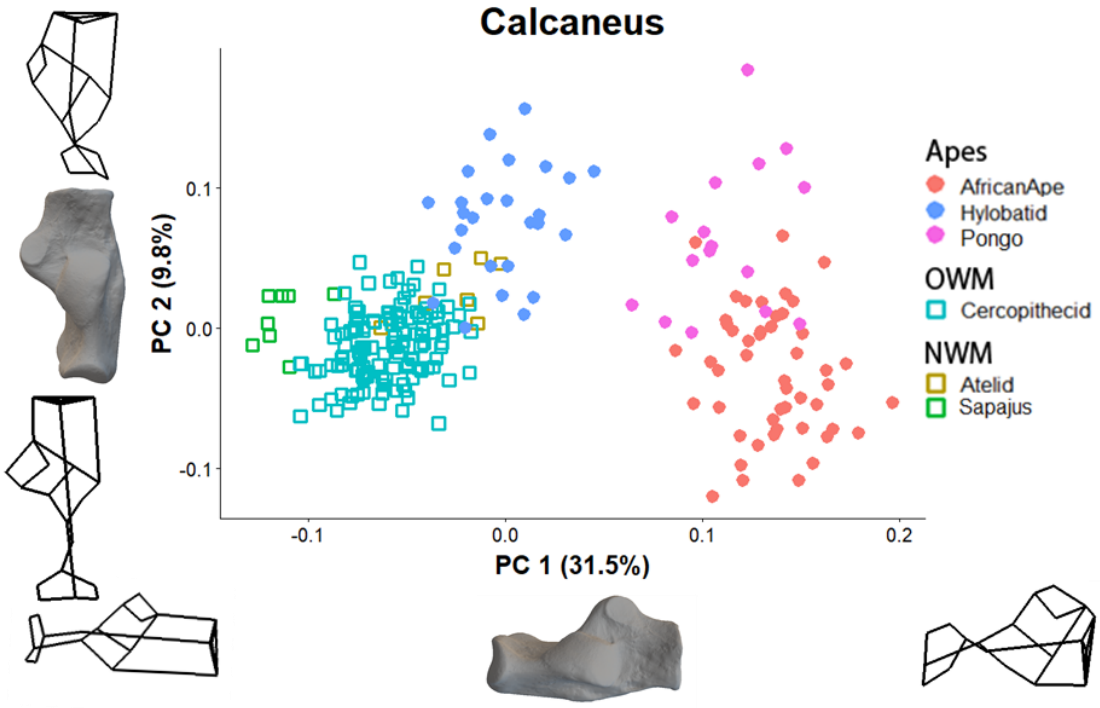

Figure 13: PCs 1 and 2 of the calcaneus. Percent (%) variation explained by each PC is listed along its axis label. Wireframes consisting of connected landmarks of the extreme morphology of the respective ends of each PC provided for visualization of shape changes. Bone models matching the view of the wireframes provided for visualization. Color of data points vary by group, defined in Table 3. Filled circles represent apes, squares represent monkeys. PC 1 captures the relative length and width of the calcaneus. PC 2 captures posterior calcaneal length.

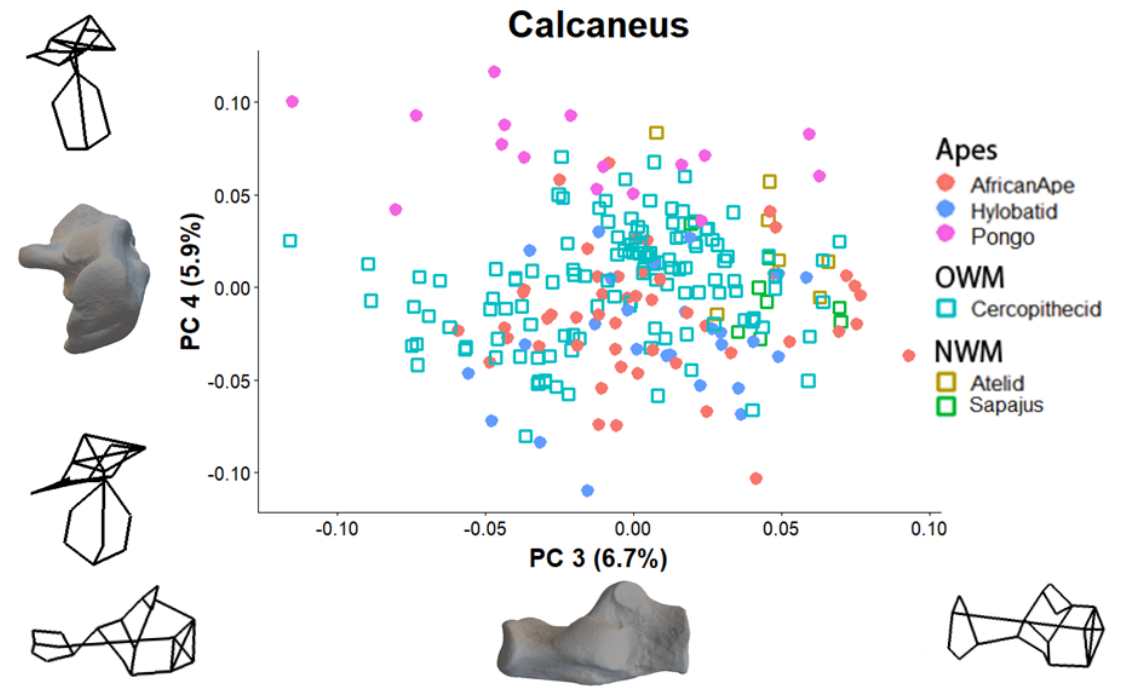

Figure 14: PCs 3 and 4 of the calcaneus. Percent (%) variation explained by each PC is listed along its axis label. Wireframes consisting of connected landmarks of the extreme morphology of the respective ends of each PC provided for visualization of shape changes. Bone models matching the view of the wireframes provided for visualization. Color of data points vary by group, defined in Table 3. Filled circles represent apes, squares represent monkeys. PC 4 describes the angulation of the subtalar articular surface relative to the calcaneal tuber in the transverse plane.

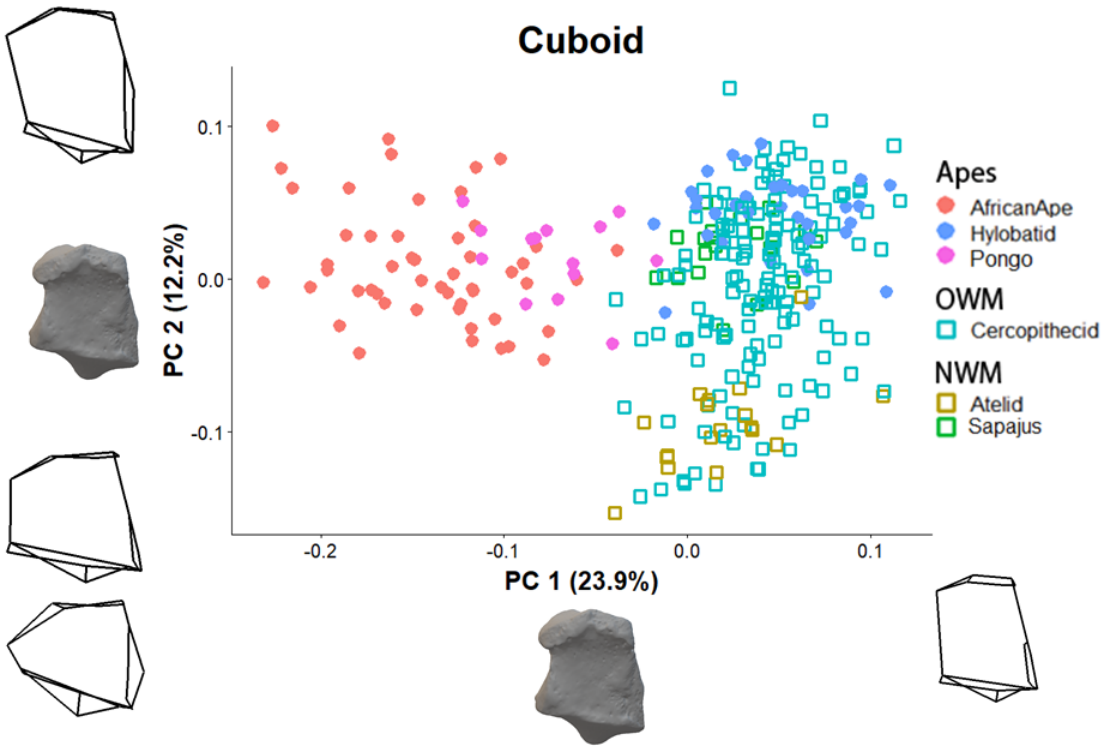

Figure 15: PCs 1 and 2 of the cuboid. Percent (%) variation explained by each PC is listed along its axis label. Wireframes consisting of connected landmarks of the extreme morphology of the respective ends of each PC provided for visualization of shape changes. Bone models matching the view of the wireframes provided for visualization. Color of data points vary by group, defined in Table 3. Filled circles represent apes, squares represent monkeys. PC 1 captures cuboid breadth. PC 2 captures proximodistal length.

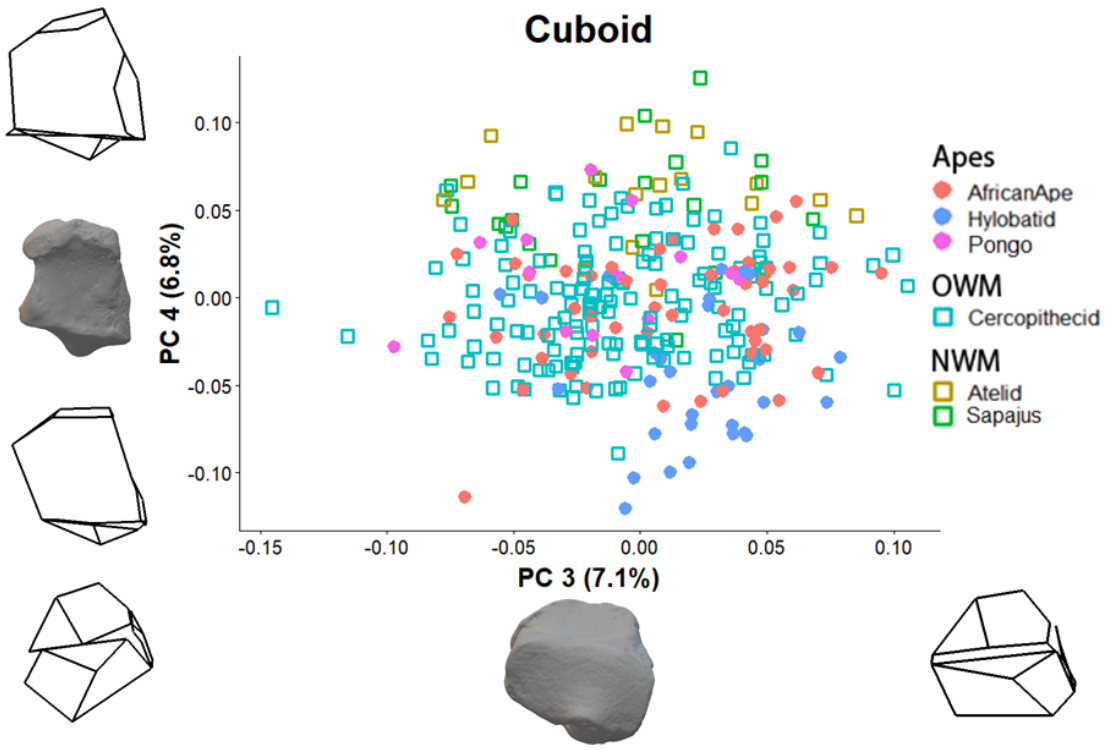

Figure 16: PCs 3 and 4 of the cuboid. Percent (%) variation explained by each PC is listed along its axis label. Wireframes consisting of connected landmarks of the extreme morphology of the respective ends of each PC provided for visualization of shape changes. Bone models matching the view of the wireframes provided for visualization. Color of data points vary by group, defined in Table 3. Filled circles represent apes, squares represent monkeys. PC 3 captures the relative orientation of the proximal and distal articular facets, or torsion of the bone. PC 4 describes the angulation of the proximodistal long axis of the cuboid in the transverse plane.

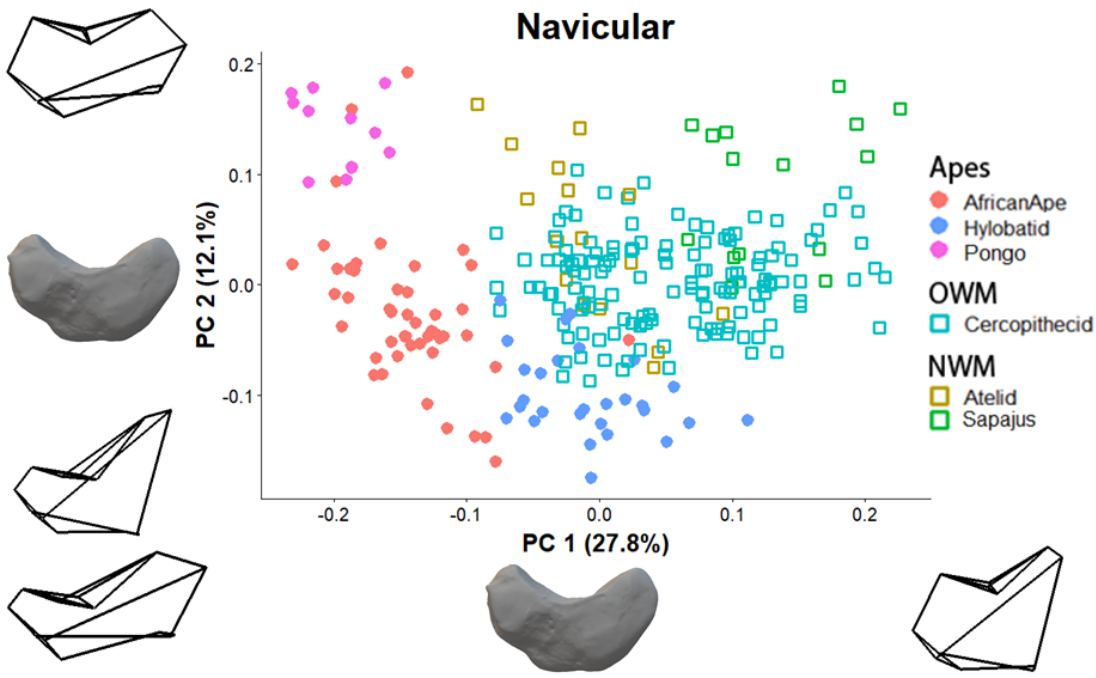

Figure 17: PCs 1 and 2 of the navicular. Percent (%) variation explained by each PC is listed along its axis label. Wireframes consisting of connected landmarks of the extreme morphology of the respective ends of each PC provided for visualization of shape changes. Bone models matching the view of the wireframes provided for visualization. Color of data points vary by group, defined in Table 3. Filled circles represent apes, squares represent monkeys. PC 1 captures the proximodistal length of the navicular. PC 2 captures projection of the navicular tuberosity.

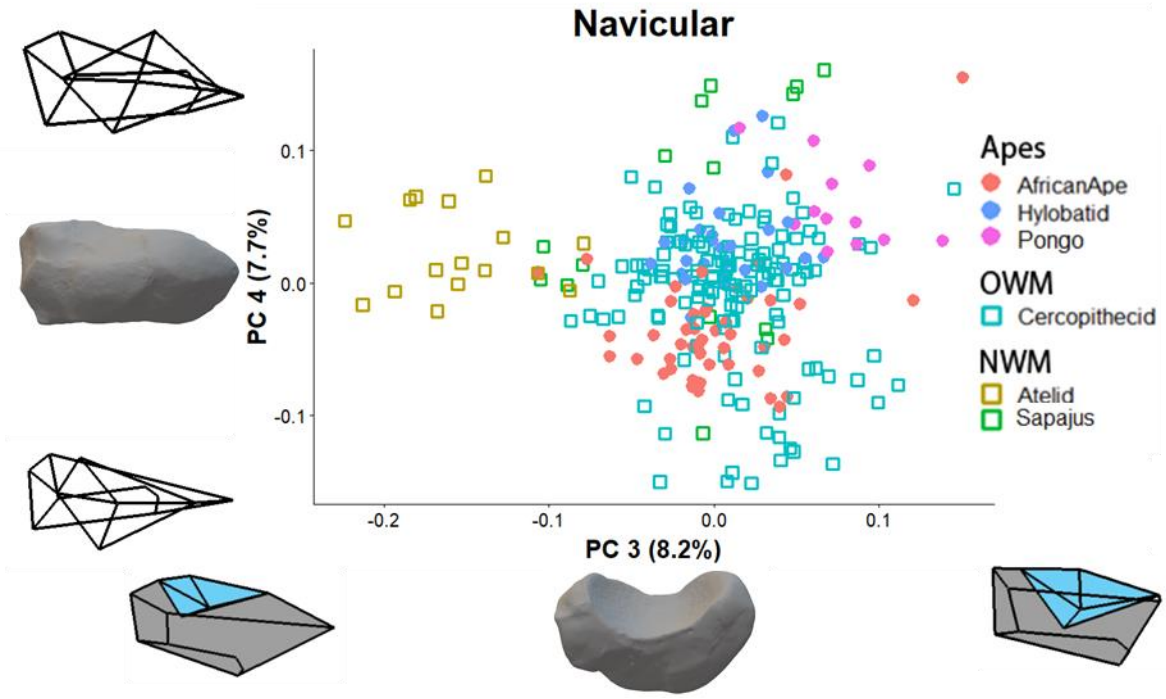

Figure 18: PCs 3 and 4 of the navicular. Percent (%) variation explained by each PC is listed along its axis label. Wireframes consisting of connected landmarks of the extreme morphology of the respective ends of each PC provided for visualization of shape changes. Bone models matching the view of the wireframes provided for visualization. Color of data points vary by group, defined in Table 3. Filled circles represent apes, squares represent monkeys. PC 3 captures variation in the relative length of the talonavicular articular surface (blue in wireframes) compared to the rest of the navicular (grey in wireframes). PC 4 describes the relative dorsoplantar height of the navicular.

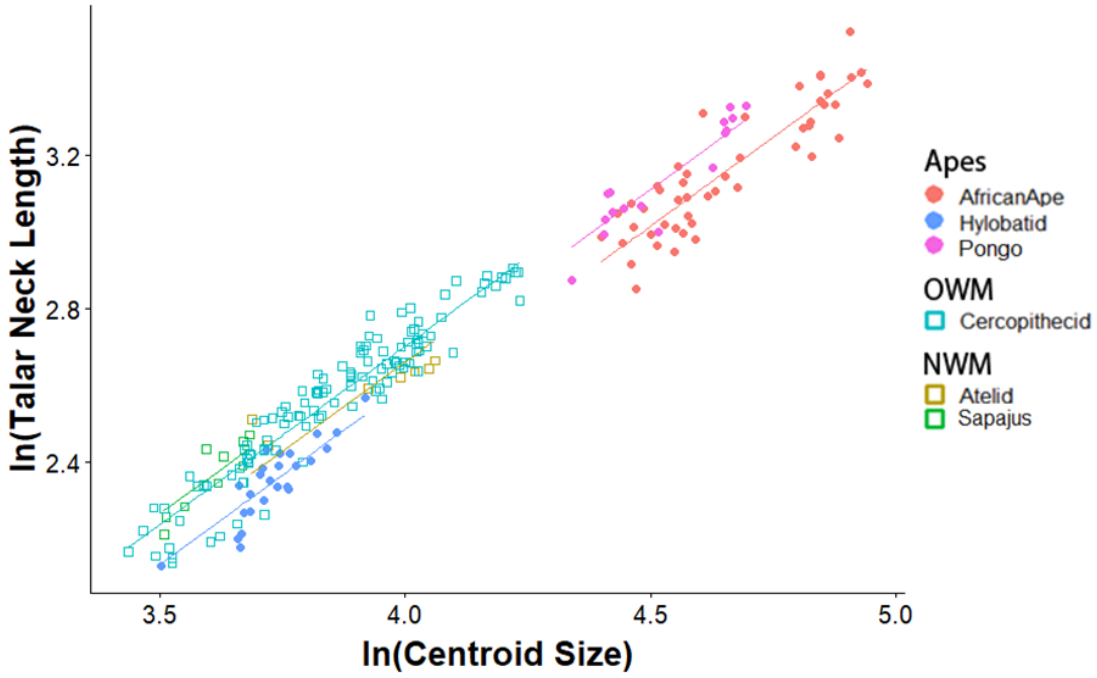

Figure 19: Bivariate plot of ln-transformed linear distance of the base of the talar neck to the distal end of the talar head, or talar neck length to ln-transformed centroid size of the talus. Lines represent linear models fit to grouped anthropoid taxa (colored by group, indicated in Table 3).

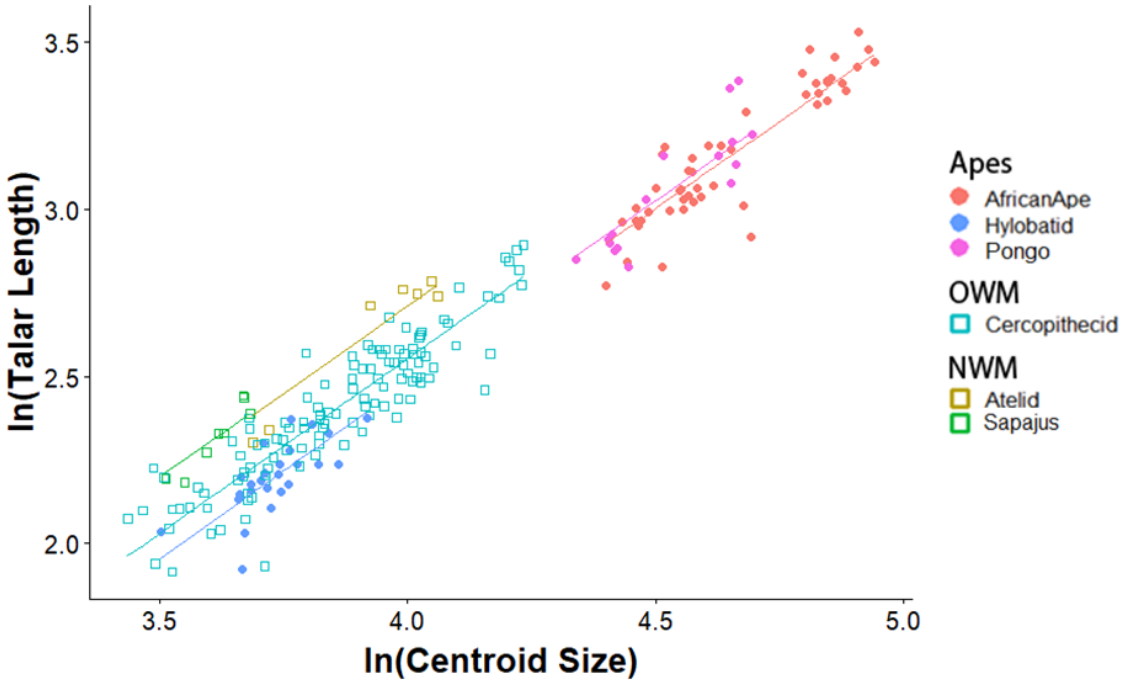

Figure 20: Bivariate plot of ln-transformed linear distance from the posterior subtalar facet to the distal base of the talar head, or talar length to ln-transformed centroid size of the talus. Lines represent linear models fit to grouped anthropoid taxa (colored by group, indicated in Table 3).

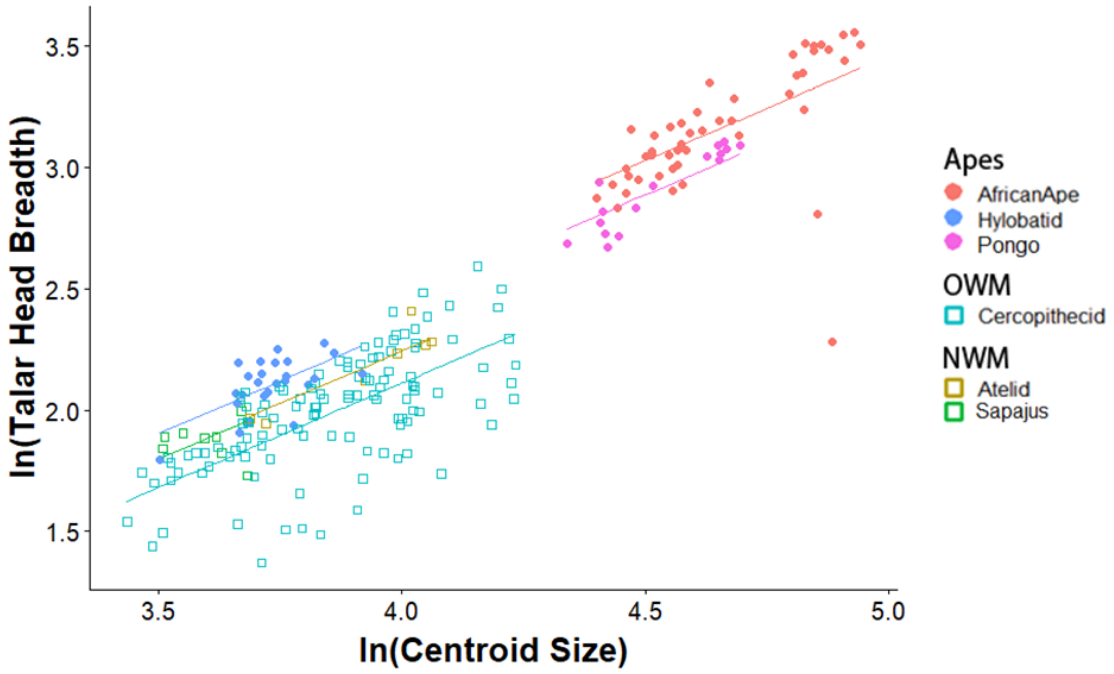

Figure 21: Bivariate plot of ln-transformed linear distance of the medial and lateral points on the talar head, or talar head breadth to ln-transformed centroid size of the talus. Lines represent linear models fit to grouped anthropoid taxa (colored by group, indicated in Table 3).

A

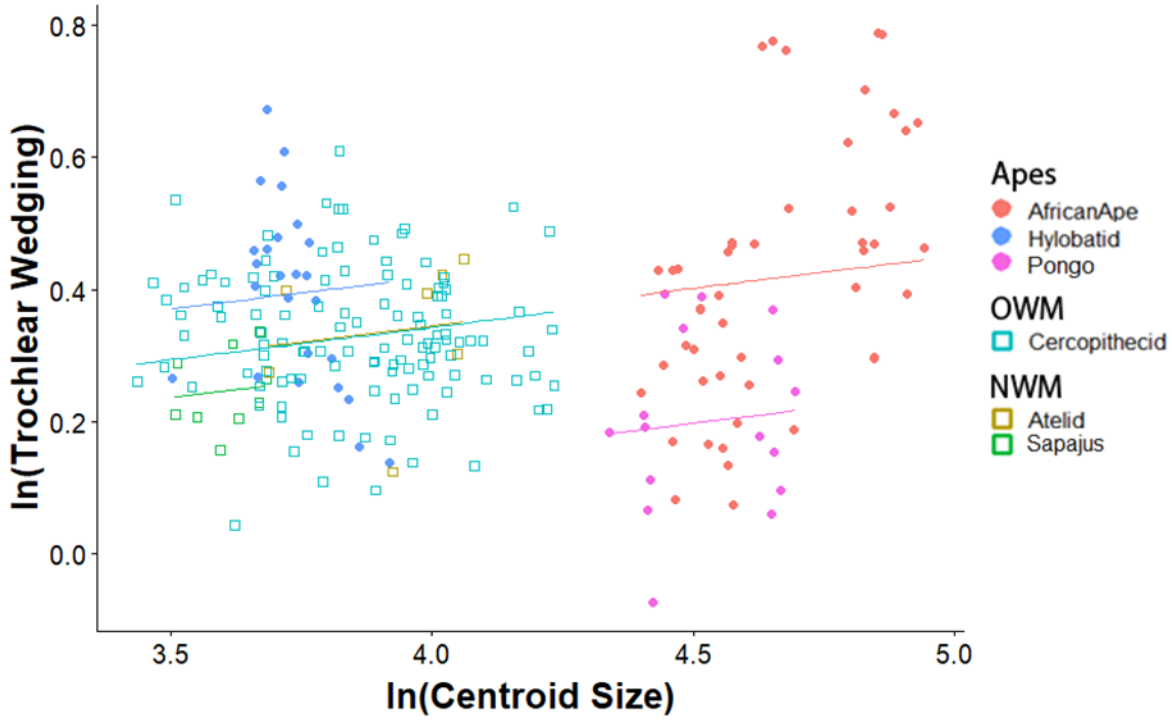

B

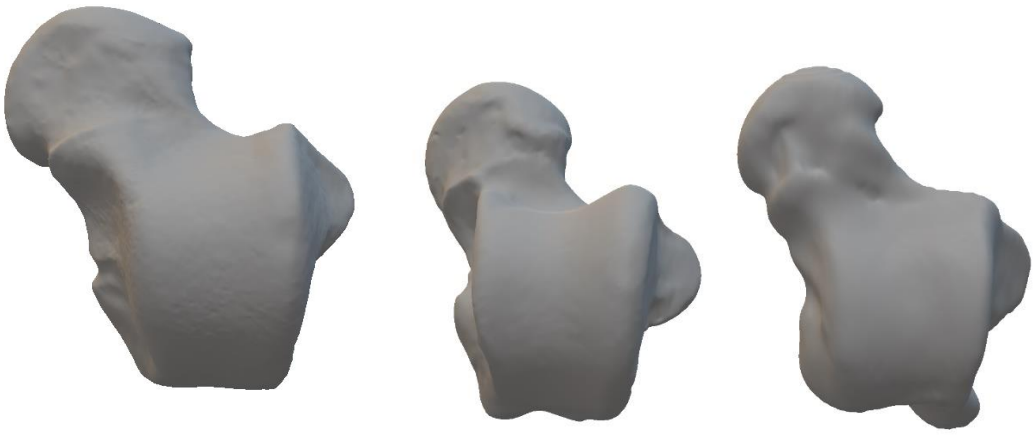

Figure 22: A: Bivariate plot of ln-transformed ratio of the linear distances between the medial and lateral points on the proximal and distal margins of the talar trochlea, or talar

trochlear wedging to ln-transformed centroid size of the talus. Lines represent linear models fit to grouped anthropoid taxa (colored by group, indicated in Table 3).
B: Right tali of (from left to right) *Hylobates, Cercopithecus,* and *Pongo.* Variation in trochlear wedging does not appear to follow phylogenetic, body size, or locomotor patterns. Note: tali (dorsal views) scaled to each other by posterior talar trochlear breadth.

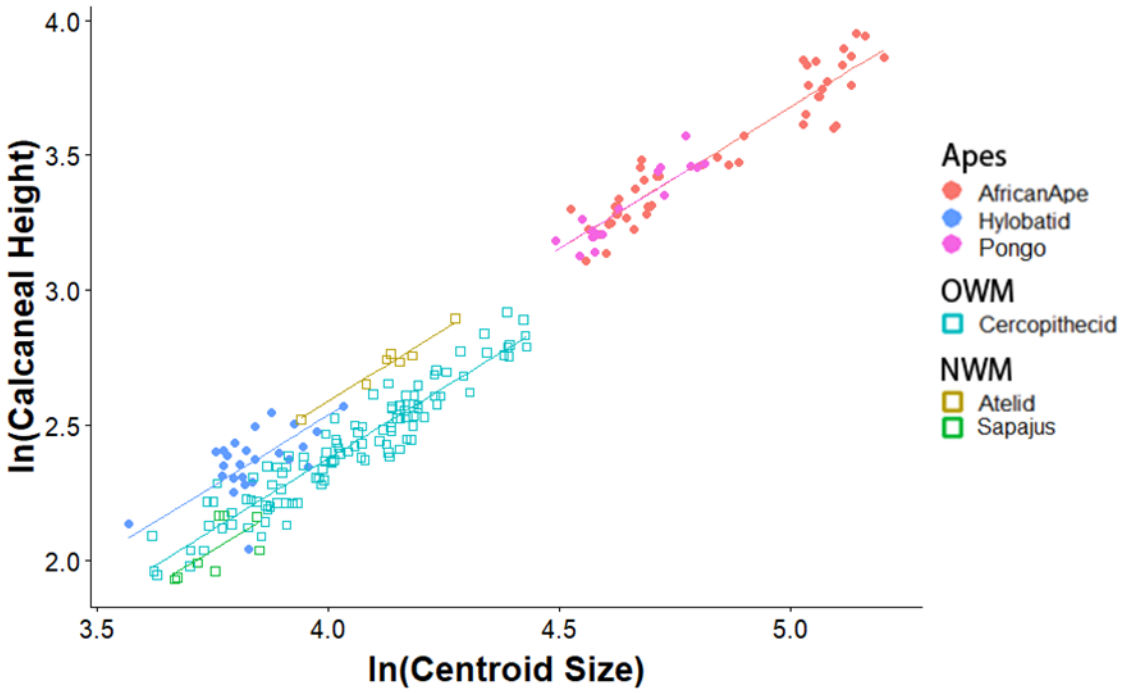

Figure 23: Bivariate plot of ln-transformed linear distance of the posterior subtalar articular surface to the plantar point on the anterior aspect of the medial tubercle of the calcaneus, or calcaneal height to ln-transformed centroid size of the calcaneus. Lines represent linear models fit to grouped anthropoid taxa (colored by group, indicated in Table 3).

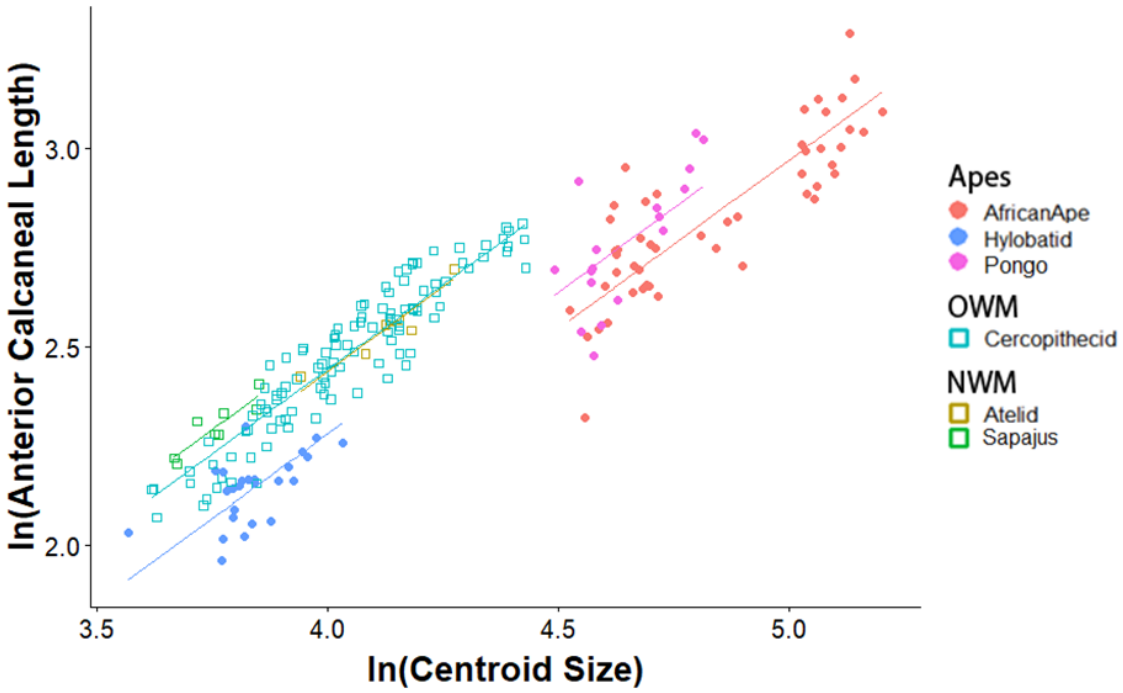

Figure 24: Bivariate plot of ln-transformed linear distance of the anterior point of the posterior subtalar facet to the distal end of the calcaneus, or anterior calcaneal length to ln-transformed centroid size of the calcaneus. Lines represent linear models fit to grouped anthropoid taxa (colored by group, indicated in Table 3).

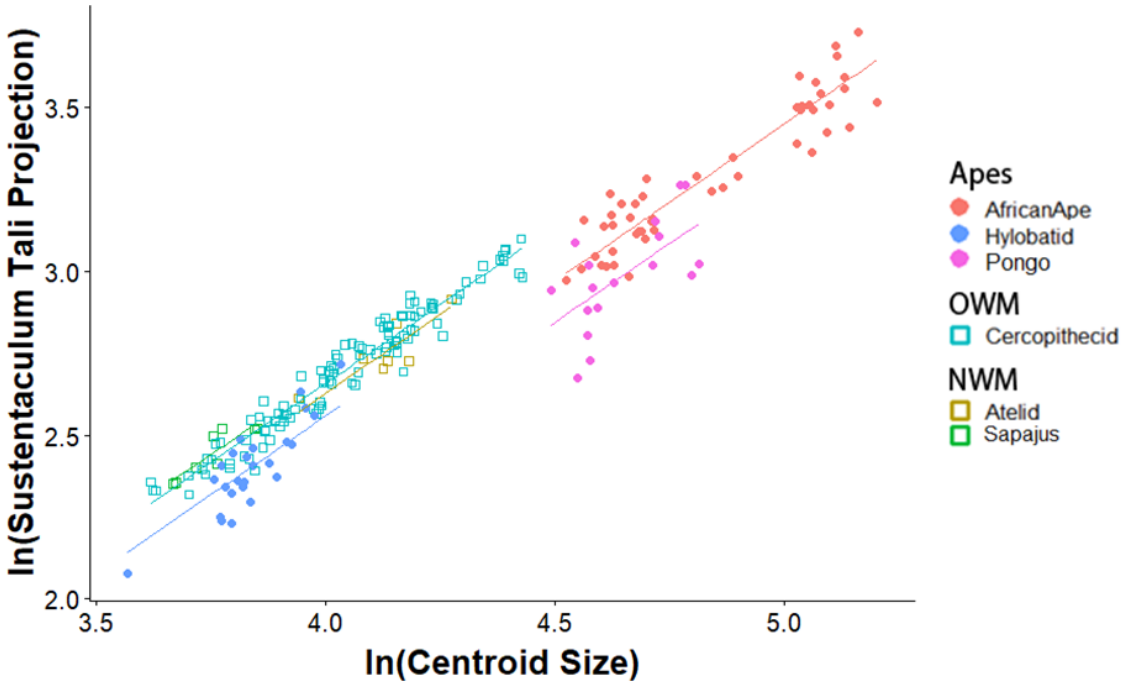

Figure 25: Bivariate plot of ln-transformed linear distance between the sustentaculum tali to a midline point on the distal calcaneus, or sustentaculum tali projection to ln-transformed centroid size of the calcaneus. Lines represent linear models fit to grouped anthropoid taxa (colored by group, indicated in Table 3).

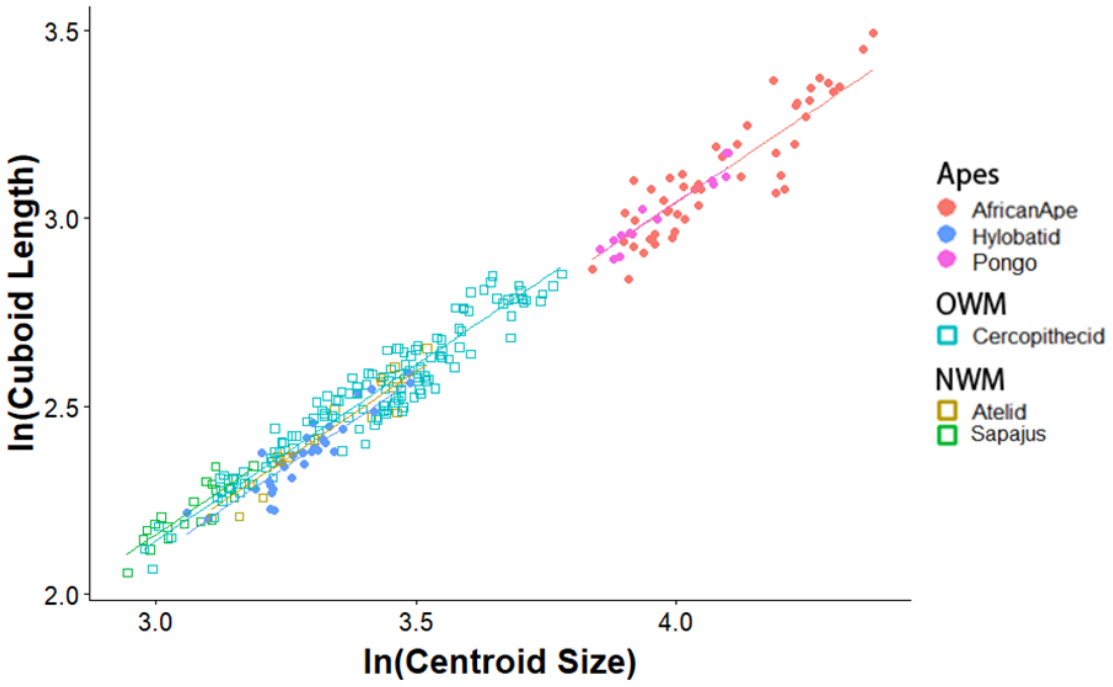

Figure 26: Bivariate plot of ln-transformed linear distance between the proximal and distal articular facets of the cuboid, or cuboid length to ln-transformed centroid size of the cuboid. Lines represent linear models fit to grouped anthropoid taxa (colored by group, indicated in Table 3).

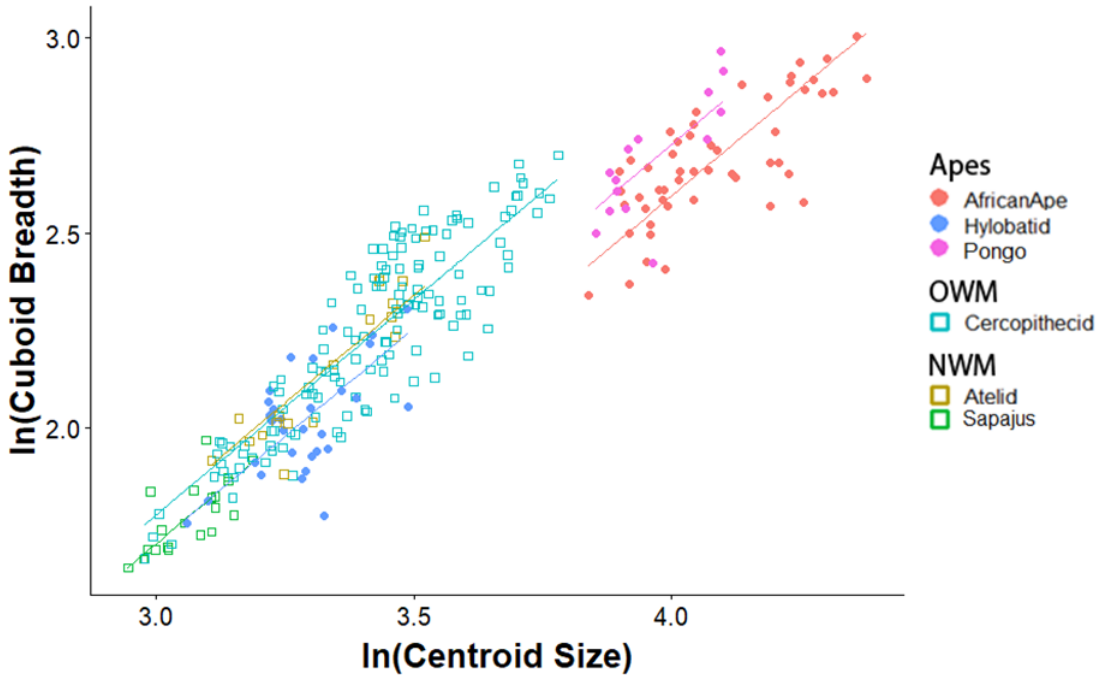

Figure 27: Bivariate plot of ln-transformed linear distance between a point on the distal point of the medial articular facet on the cuboid and a point on the lateral distal articular surface, or cuboid breadth to ln-transformed centroid size of the cuboid. Lines represent linear models fit to grouped anthropoid taxa (colored by group, indicated in Table 3).

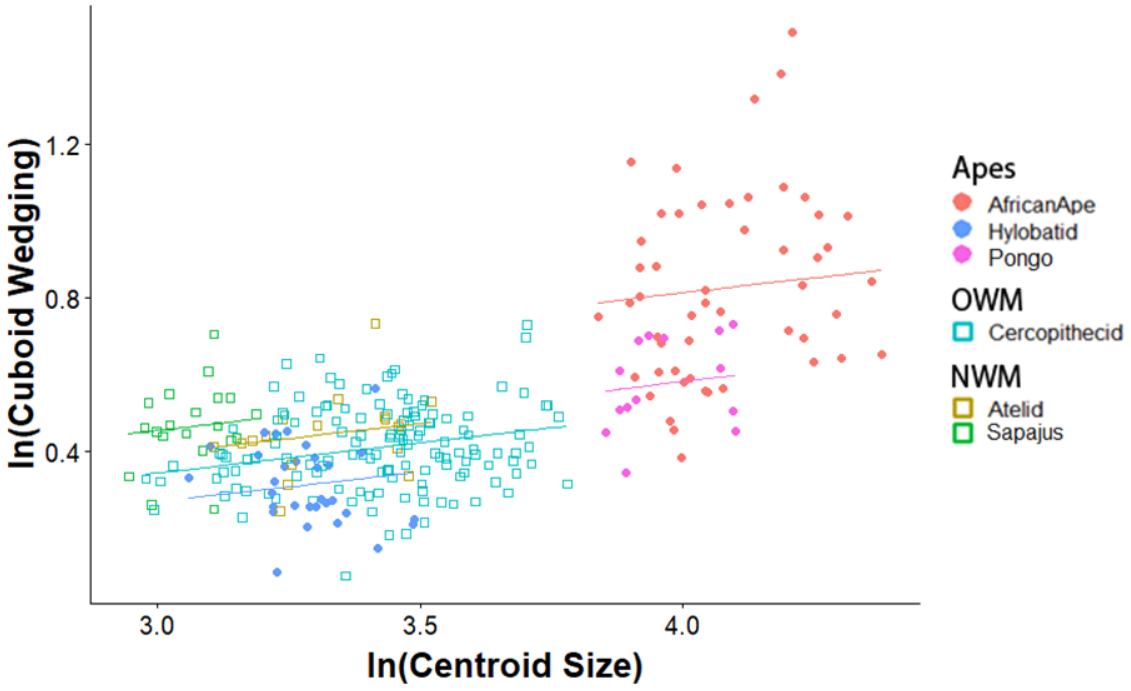

Figure 28: Bivariate plot of ln-transformed ratio of the linear distances between the proximal and distal points on the medial and lateral margins of the cuboid, or cuboid wedging to ln-transformed centroid size of the cuboid. Lines represent linear models fit to grouped anthropoid taxa (colored by group, indicated in Table 3).

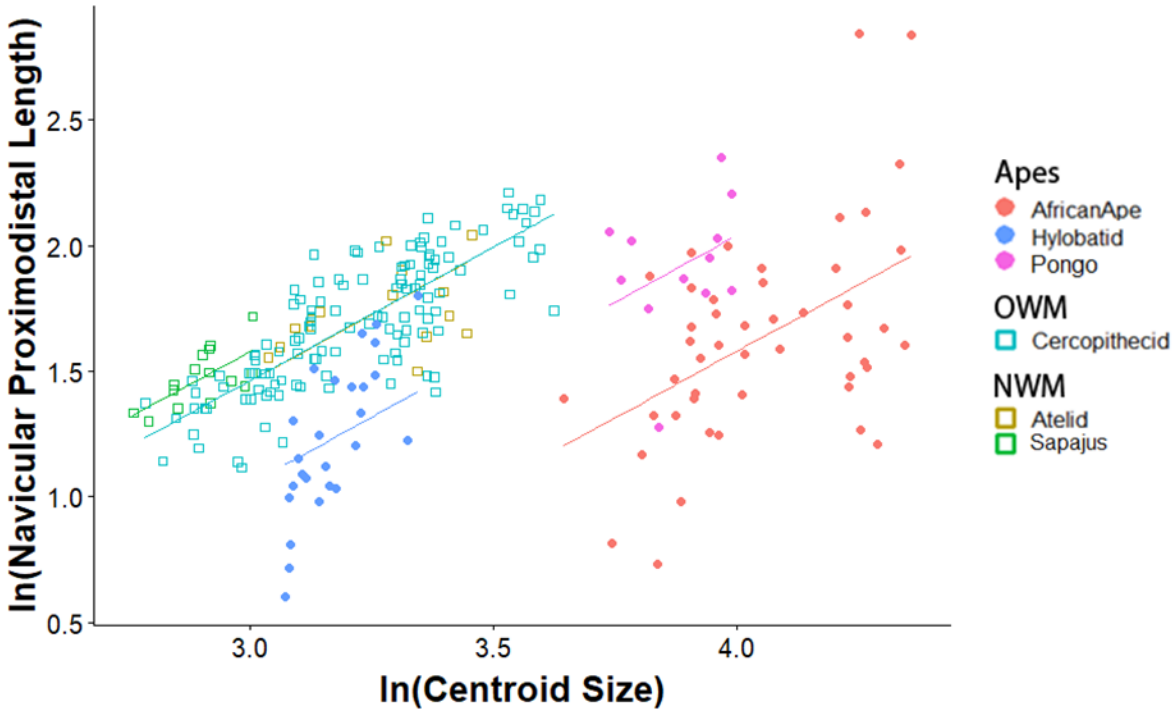

Figure 29: Bivariate plot of ln-transformed linear distance between the proximal and distal articular surfaces, or navicular proximodistal length to ln-transformed centroid size of the cuboid. Lines represent linear models fit to grouped anthropoid taxa (colored by group, indicated in Table 3).

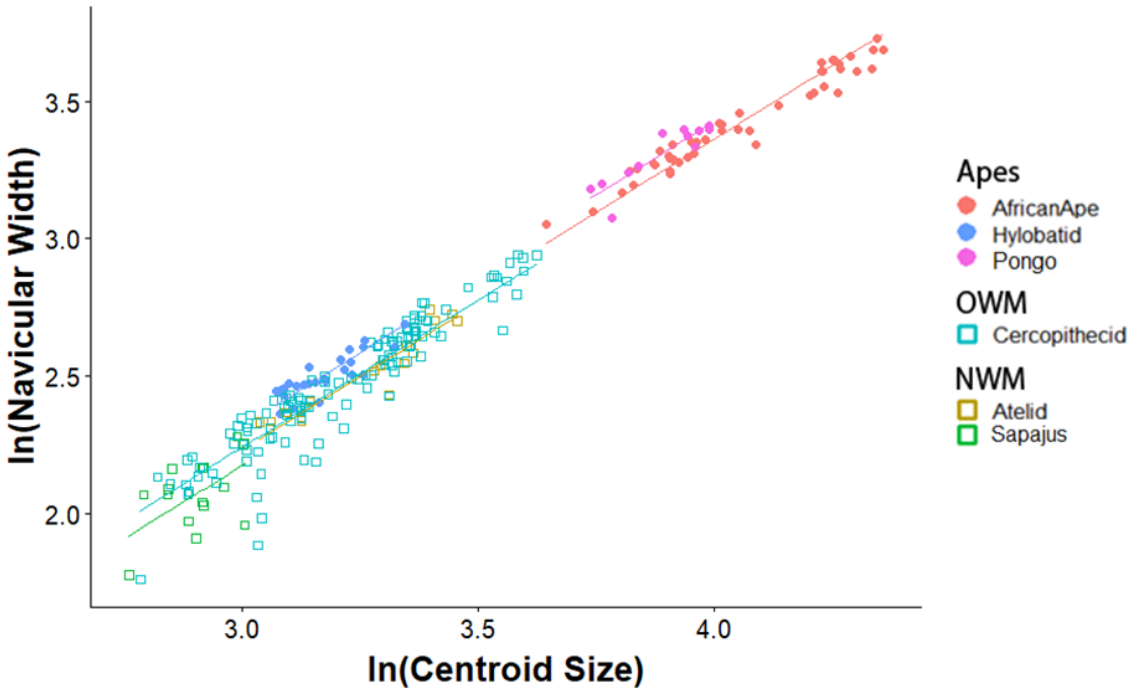

Figure 30: Bivariate plot of ln-transformed linear distance between the medial and lateral aspects of the navicular, or navicular width to ln-transformed centroid size of the cuboid. Lines represent linear models fit to grouped anthropoid taxa (colored by group, indicated in Table 3).

Tables:

Table 1: Specimen list by genus and species for this study.

Genus	Talus	Calcaneus	Cuboid	Navicular	Species	Talus Count	Calcaneus Count	Cuboid Count	Navicular Count
Ateles	5	6	9	8	belzebuth	1	1	3	3
					fusciceps	1	1	1	1
					geoffroyi	3	3	3	3
					marginatus	0	1	1	1
					paniscus	0	0	1	0
Cercopithecus	18	17	18	18	alborgularis	1	1	1	1
					ascanis	3	3	3	3
					cephus	1	1	1	1
					diana	1	1	1	1
					lowei	1	1	1	1
					mitis	7	7	7	7
					mona	3	3	3	3
					nictitans	1	0	1	1
Chlorocebus	11	10	10	11	aethiops	11	10	10	11
Colobus	18	13	23	14	angolensis	4	3	5	4
					guereza	9	5	10	5
					polykomos	5	5	8	5
Erythrocebus	6	6	12	12	patas	6	6	12	12
Gorilla	21	23	22	20	beringei	8	9	9	9
					gorilla	13	14	13	11
Hylobates	21	20	26	22	agilis	0	0	1	1
					concolor	1	1	1	1
					gabriellae	1	1	1	1
					hoolock	2	2	3	2

					klossii	4	3	6	5
					lar	11	11	12	11
					moloch	1	1	1	0
					muelleri	1	1	1	1
Lagothrix	2	1	9	8	lagotricha	2	1	9	8
Lophocebus	5	4	6	5	albigena	5	4	6	5
Macaca	27	26	29	27	fascicularis	13	13	14	13
					mulatta	5	5	6	6
					nemestrina	9	8	9	8
Nasalis	21	22	24	23	larvatus	21	22	24	23
Pan	27	26	29	27	troglodytes	27	26	29	27
Pongo	16	17	14	12	pygmaeus	16	17	14	12
Rhinopithecus	12	11	11	12	roxellana	12	11	11	12
Sapajus	9	8	20	15	apella	9	8	20	15
Symphalangus	5	6	7	6	syndactylus	5	6	7	6
Trachypithecus	14	14	13	14	cristatus	14	14	13	14
Genus Total	**238**	**230**	**282**	**254**					

Table 2: Landmarks used in the geometric morphometric analysis of the calcaneus, talus, cuboid, and navicular, modified from Harcourt-Smith (2002), shown in Figure 10.

Bone	Aspect	Number	Description
Cuboid	Proximal	1	Most proximal point of beak or peg and socket projection
		2	Most dorsal point of the dorsal margin
		3	Most lateral point of the dorsal facet margin
		4	Most lateral point of the plantar facet margin
		5	Most medial point of the dorsal facet margin
		6	Most medial point of the plantar facet margin
		7	Deepest point of the articular facet
	Medial	8	Most distal point of facet margin
		9	Most disto-plantar point of facet margin
		10	Most proximal point of facet margin
		11	Most proximo-plantar point of facet margin
		12	Most dorsal point of facet margin
	Distal	13	Most dorso-medial point
		14	Most medio-plantar point
		15	Most medial point of medial margin
		16	Most dorsal point of the facet margin between articular surfaces for MT4 and MT5
		17	Most plantar point of the facet margin between the articular surfaces for MT4 and MT5
		18	Most lateral point of facet
		19	Deepest point on facet for MT4
		20	Deepest point on facet for MT5
Talus	Trochlea	1	Most anterior point of trochlear groove
		2	Most anterior point of contact between lateral malleolar facet and trochlear surface
		3	Most anterior point of contact between the medial malleolar facet and the trochlear surface
		4	Most anterior point on medial malleolar facet
		5	Most plantar point on medial malleolar facet

		6	Most posterior point of contact between the medial malleolar facet and the trochlear surface
		7	Most posterior point on the trochlear groove
		8	Most posterior point of contact between the lateral malleolar facet and trochlear surface
		9	Most dorsal point of the lateral facet margin
		10	Most dorsal point on the medial facet margin
		11	Most dorsal point on the trochlear groove
		12	Most anterior point on lateral malleolar facet
		13	Most plantar point on lateral malleolar facet
	Posterior calcaneal facet	14	Most anterolateral point
		15	Most lateral point
		16	Most posterolateral point
		17	Most dorsal point on the proximal facet margin
		18	Most posteromedial point
		19	Most medial point
		20	Most anteromedial point
		21	Most dorsal point on the distal facet margin
		22	Most dorsal point on the facet
	Head	23	Most dorsal point
		24	Most plantar point
		25	Most medial point
		26	Most lateral point
		27	Most distal point
		28	Most lateral point of contact between the navicular facet and the distal calcaneal facet
Navicular	Talar facet	1	Most medial point
		2	Most plantar point
		3	Most lateral point
		4	Most dorsal point
		5	Deepest point of facet
	Cuneiform facet	6	Most dorsomedial point
		7	Most medial point
		8	Most medioplantar point
		9	Most dorsal point of margin separating facets for medial and lateral cuneiforms
		10	Most plantar point of margin separating facets for medial and lateral cuneiforms

		11	Most dorsal point of margin separating facets for intermediate and lateral cuneiforms
		12	Most plantar point of margin separating facets for intermediate and lateral cuneiforms
		13	Most dorsolateral point
		14	Most lateral point
		15	Most plantolateral point
	Tuberosity	16	Most medioplantar point of tuberosity
Calcaneus	Posterior talar facet	1	Most posterior point
		2	Most anterior point
		3	Most medial point
		4	Most lateral point
		5	Most superior point
	Anterior talar facet	6	Most posterior point
		7	Most lateral point
		8	Most anterior point
		9	Most medial point
	Posterior	10	Most dorsal point
		11	Most dorsomedial point
		12	Most dorsolateral point
		13	Most posterior point
		14	Most plantar point
		15	Most plantomedial point
		16	Most plantolateral point
		17	Most anterior point on medial tubercle
	Cuboid facet	18	Most posterior point of the beak or peg and socket articulation
		19	Most lateral point
		20	Most dorsal point
		21	Most medial point

Table 3: Classifier groups used to define genera in linear models. Hammond (2013) was used to assign suspensory/non-suspensory behaviors. *Lagothrix* not included in Hammond (2013), but was considered suspensory based on Cant et al., (2003) and Langdon (1986). * indicates that although classified as non-suspensory, *Nasalis* has been observed to engage in both suspensory behaviors and vertical climbing (Su & Jablonski, 2009).

Genus	**Monkey/Ape**	**Group**	**Suspen./Nonsuspen.**
Ateles	Monkey	Atelid	Suspensory
Cercopithecus	Monkey	Cercopithecid	Non-suspensory
Chlorocebus	Monkey	Cercopithecid	Non-suspensory
Colobus	Monkey	Cercopithecid	Non-suspensory
Erythrocebus	Monkey	Cercopithecid	Non-suspensory
Gorilla	Ape	African Ape	Suspensory
Hylobates	Ape	Hylobatid	Suspensory
Lagothrix	Monkey	Atelid	Suspensory
Lophocebus	Monkey	Cercopithecid	Non-suspensory
Macaca	Monkey	Cercopithecid	Non-suspensory
Nasalis	Monkey	Cercopithecid	Non-suspensory*
Pan	Ape	African Ape	Suspensory
Pongo	Ape	*Pongo*	Suspensory
Rhinopithecus	Monkey	Cercopithecid	Non-suspensory
Sapajus	Monkey	*Sapajus*	Non-suspensory
Symphalangus	Ape	Hylobatid	Suspensory
Trachypithecus	Monkey	Cercopithecid	Non-suspensory

Table 4: Regression slope data for phylogenetically controlled generalized least squares analysis. Abbreviations: AP = anteroposterior, PD = proximodistal, ML = mediolateral.

	Centroid Size					Centroid Size and Locomotion			
	Estimate	Standard Error	t	p	Adj R^2	Estimate	Standard Error	t	p
Talar Neck Length	0.89	0.05	16.31	< **0.001**	0.90	-0.071	0.07	-0.99	< **0.001**
Talar AP Length	0.93	0.07	14.16	< **0.001**	0.88	-0.012	0.09	-0.13	< **0.001**
Talar Head Breadth	1.18	0.11	10.34	< **0.001**	0.79	0.079	0.15	0.53	< **0.001**
Trochlear Wedging	0.15	0.11	1.41	0.1701	0.03	0.0038	0.15	0.03	0.3971
Calcaneal Height	1.07	0.07	14.71	< **0.001**	0.88	0.25	0.09	2.76	< **0.001**
Anterior Calcaneal Length	0.71	0.06	11.54	< **0.001**	0.82	-0.12	0.08	-1.42	< **0.001**
Sustentaculum Tali Projection	0.90	0.06	15.08	< **0.001**	0.88	-0.097	0.08	-1.20	< **0.001**
Cuboid PD Length	0.92	0.06	14.40	< **0.001**	0.87	-0.032	0.08	-0.38	< **0.001**
Cuboid Breadth	1.01	0.09	11.08	< **0.001**	0.79	-0.031	0.12	-0.25	< **0.001**
Cuboid Wedging	0.26	0.14	1.89	0.0679	0.10	0.011	0.18	0.06	0.1941
Navicular PD Length	0.94	0.22	4.32	< **0.001**	0.36	-0.37	0.29	-1.29	< **0.001**
Navicular ML Width	1.16	0.08	14.80	< **0.001**	0.87	0.055	0.11	0.51	< **0.001**

Table 5: Regression slope data for each measurement. Bold p-values indicate significant difference from a slope of 1. Lack of significant differences indicate isometry. Slopes significantly greater than 1 indicate positive allometry. Slopes significantly less than 1 indicate negative allometry. Abbreviations: AP = anteroposterior, PD = proximodistal, ML = mediolateral.

Measurement	**Slope**	**S.E.**	**t**	**p**	**Allometry**	**Multiple R^2**
Talar Neck Length	0.93	0.02	-2.80	**<0.001**	-	0.97
Talar AP Length	1.05	0.03	1.33	0.18	Isometric	0.96
Talar Head Breadth	0.86	0.07	-2.02	**0.04**	-	0.90
Trochlear Wedging	0.098	0.053	-17.02	**<0.001**	-	0.18
Calcaneal Height	1.05	0.03	1.92	0.06	Isometric	0.98
Anterior Calcaneal Length	0.85	0.03	-4.73	**<0.001**	-	0.91
Sustentaculum Tali Projection	0.96	0.03	-1.51	0.13	Isometric	0.96
Cuboid PD Length	0.93	0.02	-3.24	**0.001**	-	0.97
Cuboid Breadth	1.10	0.04	2.38	**0.02**	+	0.90
Cuboid Wedging	0.16	0.058	-14.5	**<0.001**	-	0.60
Navicular PD Length	1.06	0.09	0.68	0.50	Isometric	0.54
Navicular ML Width	1.07	0.03	2.42	**0.02**	+	0.98

Table 6: Regression line comparisons of each measurement among taxonomic groups (Table 3). Bold p-values indicate significant difference between the two groups listed in Comparison. Abbreviations: AP = anteroposterior, PD = proximodistal, ML = mediolateral.

	Talar Neck Length				**Talar AP Length**				**Talar Head Breadth**			
Comparison	Estimate	Std. Error	t	Pr(>|t|)	Estimate	Std. Error	t	Pr(>|t|)	Estimate	Std. Error	t	Pr(>|t|)
Atelid - African Ape	0.11	0.03	3.59	**< 0.001**	0.23	0.04	5.41	**< 0.001**	-0.36	0.09	-4.12	**< 0.001**
***Sapajus* - African Ape**	0.18	0.03	5.27	**< 0.001**	0.24	0.05	5.14	**< 0.001**	-0.37	0.1	-3.85	**< 0.001**
Cercopith. - African Ape	0.15	0.02	6.83	**< 0.001**	0.07	0.03	2.39	0.14	-0.49	0.06	-7.76	**< 0.001**
Hylobatid - African Ape	0.05	0.03	1.77	0.45	0	0.04	-0.01	0.99	-0.26	0.08	-3.43	**0.01**
***Pongo* - African Ape**	0.1	0.02	5.36	**< 0.001**	0.02	0.02	1	0.9	-0.14	0.05	-2.8	0.05
***Sapajus* - Atelid**	0.07	0.03	2.21	0.21	0.01	0.04	0.3	0.99	-0.01	0.09	-0.16	0.99
Cercopithecid - Atelid	0.04	0.02	1.77	0.44	-0.16	0.03	-4.73	**< 0.001**	-0.13	0.07	-1.96	0.33
Hylobatid - Atelid	-0.06	0.03	-2.33	0.16	-0.23	0.04	-6.26	**< 0.001**	0.09	0.07	1.23	0.79
***Pongo* - Atelid**	-0.01	0.03	-0.45	0.99	-0.21	0.04	-4.71	**< 0.001**	0.21	0.09	2.42	0.13
Cercopithecid - *Sapajus*	-0.03	0.02	-1.26	0.77	-0.17	0.03	-5.55	**< 0.001**	-0.12	0.06	-1.89	0.37
Hylobatid - *Sapajus*	-0.13	0.02	-5.5	**< 0.001**	-0.24	0.03	-7.34	**< 0.001**	0.11	0.07	1.58	0.57
Pongo* - *Sapajus	-0.08	0.03	-2.46	0.12	-0.22	0.05	-4.62	**< 0.001**	0.23	0.1	2.38	0.15
Hylobatid - Cercopithecid	-0.1	0.01	-7.53	**< 0.001**	-0.07	0.02	-3.87	**< 0.001**	0.22	0.04	5.75	**< 0.001**
***Pongo* - Cercopithecid**	-0.06	0.02	-2.43	0.13	-0.05	0.03	-1.53	0.6	0.35	0.07	5.3	**< 0.001**
***Pongo* - Hylobatid**	0.05	0.03	1.72	0.47	0.02	0.04	0.65	0.98	0.12	0.08	1.57	0.58

	Trochlear Wedging				**Calcaneal Height**				**Anterior Calcaneal Length**			
Comparison	Estimate	Std. Error	t	Pr(>|t|)	Estimate	Std. Error	t	Pr(>|t|)	Estimate	Std. Error	t	Pr(>|t|)
Atelid - African Ape	-0.01	0.07	-0.12	0.99	-0.04	0.04	-1.04	0.88	0.32	0.04	8.03	**< 0.001**

***Sapajus* - African Ape**	-0.07	0.07	-0.92	0.93	-0.33	0.04	-7.84	**<0.001**	0.39	0.05	8.4	**< 0.001**
Cercopith. - African Ape	-0.01	0.05	-0.21	0.99	-0.25	0.03	-9.67	**<0.001**	0.32	0.03	11.4	**< 0.001**
Hylobatid - African Ape	0.07	0.06	1.13	0.84	-0.09	0.03	-2.63	0.08	0.16	0.04	4.34	**< 0.001**
***Pongo* - African Ape**	-0.20	0.04	-5.28	**< 0.001**	0	0.02	0	0.99	0.09	0.02	3.89	**< 0.001**
***Sapajus* - Atelid**	-0.06	0.07	-0.88	0.94	-0.29	0.04	-7.27	**<0.001**	0.07	0.04	1.52	0.61
Cercopithecid - Atelid	0.00	0.05	-0.05	0.99	-0.21	0.03	-7.34	**<0.001**	0.01	0.03	0.18	0.99
Hylobatid - Atelid	0.07	0.06	1.30	0.75	-0.05	0.03	-1.57	0.58	-0.16	0.04	-4.37	**< 0.001**
***Pongo* - Atelid**	-0.20	0.07	-2.90	**0.04**	0.04	0.04	1.03	0.89	-0.23	0.04	-5.66	**< 0.001**
Cercopithecid - *Sapajus*	0.06	0.05	1.22	0.80	0.08	0.03	2.7	0.07	-0.06	0.03	-1.95	0.34
Hylobatid - *Sapajus*	0.13	0.05	2.60	0.09	0.24	0.03	7.89	**<0.001**	-0.22	0.03	-6.75	**< 0.001**
Pongo* - *Sapajus	-0.14	0.07	-1.85	0.39	0.33	0.04	8.05	**<0.001**	-0.29	0.04	-6.56	**< 0.001**
Hylobatid - Cercopithecid	0.08	0.03	2.58	0.09	0.16	0.02	9.25	**<0.001**	-0.16	0.02	-8.51	**< 0.001**
***Pongo* - Cercopithecid**	-0.19	0.05	-3.88	**< 0.001**	0.25	0.03	9.7	**<0.001**	-0.23	0.03	-8.18	**< 0.001**
***Pongo* - Hylobatid**	-0.27	0.06	-4.53	**< 0.001**	0.09	0.03	2.72	0.07	-0.07	0.04	-1.92	0.35

	Sustentaculum Tali Projection				**Cuboid Length**				**Cuboid Breadth**			
Comparison	Estimate	Std. Error	t	Pr(>|t|)	Estimate	Std. Error	t	Pr(>|t|)	Estimate	Std. Error	t value	Pr(>|t|)
Atelid - African Ape	0.14	0.03	4.31	**<0.001**	0.02	0.02	0.87	0.94	0.3	0.04	6.85	**< 0.001**
***Sapajus* - African Ape**	0.19	0.04	5.17	**<0.001**	0.05	0.03	2.08	0.27	0.21	0.05	4.11	**< 0.001**
Cercopith. - African Ape	0.17	0.02	7.32	**<0.001**	0.04	0.02	2.17	0.22	0.29	0.03	8.6	**< 0.001**
Hylobatid - African Ape	0.07	0.03	2.3	0.17	-0.001	0.02	-0.04	0.99	0.21	0.04	5.07	**< 0.001**
***Pongo* - African Ape**	-0.13	0.02	-6.55	**<0.001**	0.001	0.02	0.09	0.99	0.13	0.03	4.08	**< 0.001**
***Sapajus* - Atelid**	0.05	0.04	1.51	0.62	0.03	0.02	1.94	0.34	-0.08	0.04	-2.34	0.16
Cercopithecid - Atelid	0.03	0.03	1.17	0.83	0.02	0.01	1.30	0.75	-0.01	0.03	-0.42	0.99
Hylobatid - Atelid	-0.07	0.03	-2.39	0.14	-0.02	0.02	-1.26	0.77	-0.09	0.03	-2.71	0.06
***Pongo* - Atelid**	-0.26	0.03	-8.15	**<0.001**	-0.02	0.02	-0.74	0.97	-0.17	0.05	-3.56	**0.01**
Cercopithecid - *Sapajus*	-0.02	0.03	-0.92	0.93	-0.02	0.01	-1.19	0.81	0.07	0.03	2.47	0.12
Hylobatid - *Sapajus*	-0.12	0.03	-4.57	**<0.001**	-0.05	0.02	-3.45	**0.01**	0	0.03	-0.02	0.99
Pongo* - *Sapajus	-0.32	0.04	-8.79	**<0.001**	-0.05	0.03	-1.96	0.33	-0.08	0.05	-1.52	0.6

Hylobatid - Cercopithecid	-0.1	0.02	-6.41	**<0.001**	-0.04	0.01	-3.40	**0.01**	-0.07	0.02	-3.38	**0.01**
***Pongo* - Cercopithecid**	-0.29	0.02	-12.81	**<0.001**	-0.03	0.02	-1.83	0.40	-0.15	0.04	-4.09	**< 0.001**
***Pongo* - Hylobatid**	-0.19	0.03	-6.68	**<0.001**	0.002	0.02	0.11	0.99	-0.08	0.05	-1.8	0.42
	Cuboid Wedging				**Navicular PD Length**				**Navicular ML Width**			
Comparison	Estimate	Std. Error	t value	Pr(>|t|)	Estimate	Std. Error	t value	Pr(>|t|)	Estimate	Std. Error	t	Pr(>|t|)
Atelid - African Ape	-0.26	0.06	-4.48	**<0.001**	0.94	0.09	10.08	**<0.001**	-0.06	0.03	-1.99	0.31
***Sapajus* - African Ape**	-0.20	0.07	-2.88	**0.04**	1.06	0.12	8.93	**<0.001**	-0.12	0.04	-2.98	**0.03**
Cercopith. - African Ape	-0.31	0.04	-6.98	**<0.001**	0.94	0.08	11.64	**<0.001**	-0.05	0.03	-1.92	0.36
Hylobatid - African Ape	-0.39	0.06	-6.88	**<0.001**	0.53	0.09	5.72	**<0.001**	0.02	0.03	0.79	0.96
***Pongo* - African Ape**	-0.23	0.04	-5.35	**<0.001**	0.46	0.07	6.21	**<0.001**	0.06	0.02	2.64	0.08
***Sapajus* - Atelid**	0.06	0.05	1.25	0.78	0.12	0.09	1.35	0.72	-0.06	0.03	-1.94	0.35
Cercopithecid - Atelid	-0.05	0.04	-1.39	0.69	0	0.06	0.01	0.99	0.01	0.02	0.51	0.99
Hylobatid - Atelid	-0.13	0.04	-2.98	**0.03**	-0.41	0.07	-5.7	**<0.001**	0.09	0.02	3.62	**< 0.001**
***Pongo* - Atelid**	0.03	0.06	0.48	0.99	-0.48	0.1	-4.78	**<0.001**	0.13	0.03	3.79	**< 0.001**
Cercopithecid - *Sapajus*	-0.11	0.04	-2.79	0.05	-0.12	0.07	-1.73	0.47	0.07	0.02	2.95	**0.03**
Hylobatid - *Sapajus*	-0.19	0.04	-4.37	**<0.001**	-0.53	0.08	-6.89	**<0.001**	0.14	0.03	5.59	**< 0.001**
Pongo* - *Sapajus	-0.03	0.07	-0.43	0.99	-0.6	0.12	-4.96	**<0.001**	0.18	0.04	4.54	**< 0.001**
Hylobatid - Cercopithecid	-0.08	0.03	-2.57	0.09	-0.41	0.05	-8.42	**<0.001**	0.08	0.02	4.71	**< 0.001**
***Pongo* - Cercopithecid**	0.08	0.05	1.58	0.57	-0.48	0.09	-5.45	**<0.001**	0.12	0.03	3.96	**< 0.001**
***Pongo* - Hylobatid**	0.16	0.06	2.58	0.09	-0.07	0.1	-0.73	0.97	0.04	0.03	1.23	0.8

Chapter 4: Foot and ankle functional morphology of Miocene hominoids

Introduction:

The Miocene epoch (23-5 Ma) is of particular interest in paleoanthropology due to the diversity of hominoid taxa, and implications for the resulting diversity seen in extant primates (Conroy & Rose, 1983; Ward et al., 1997; Begun, 2007; Ward, 2007). Most Miocene hominoid taxa exhibit a combination of bony morphologies not seen in extant taxa, confounding inferences about their locomotor adaptations (Rose, 1993, 1994; Ward, 1998). Understanding form function relationships is necessary to reconstruct the evolution of locomotor adaptation in the hominoid clade. Many Miocene hominoid taxa are known from isolated remains that are often fragmentary. However, tarsals are commonly represented in the fossil record and can therefore provide important information about locomotor behavior and inform our understanding of ape locomotor evolution (DeSilva, 2008). Although Miocene hominoid phylogeny is currently unresolved, the hypothesized phylogenetic position of each genus discussed in this chapter is presented in Figure 1.

Many Miocene hominoid taxa do not resemble extant hominoids in overall postcranial morphology, making locomotor reconstructions difficult. This, in turn, confounds the ability of researchers to reconstruct the locomotor evolution leading to extant apes. Additionally, certain taxa, such as *Ekembo* and *Proconsul* are reconstructed

to be above branch quadrupeds (Ward et al., 1991), but are larger than extant above branch quadrupeds (Rafferty et al., 1995). As seen in Chapter 3, extant locomotor differences tend to fall in line with phylogenetic differences, but the Miocene hominoid fossil record provides both a challenge and an opportunity in analyzing specimens that, for example, are phylogenetically apes but are hypothesized to locomote like extant monkeys. Additionally, some Miocene hominoid taxa like *Nacholapithecus* and *Oreopithecus* have contested locomotor reconstructions due to broad comparisons with extant taxa, which they do not resemble. A closer look at the functionally relevant aspects of foot morphology specifically could help resolve some of the confusion over the locomotor behaviors of these taxa. Given that several taxa are known postcranially mainly from tarsal bones, such as the genera *Proconsul* and *Rangwapithecus*, the ability to use isolated tarsals to make accurate inferences about their locomotor adaptations is particularly important.

Ekembo heseloni and *Ekembo nyanzae*

The best represented genus in the Early Miocene is *Ekembo* (20-17 Ma) from Kenya. *Ekembo* is represented by two species, *E. heseloni* and *E. nyanzae* from the Kisingiri sites Rusinga and Mfangano Islands (McNulty et al., 2015). These species appear broadly similar postcranially, although they differ in body size, with *E. heseloni* estimated to have weighed roughly 10.9 kg and *E. nyanzae* up to 36 kg (Rafferty et al., 1995). *Ekembo nyanzae* and *E. heseloni* had a roughly even intermembral index (Dunsworth, 2006) and a long, flexible spine and narrow pelvis (Ward, 1993), implying a narrow thoracic cage, similar to extant above branch quadrupedal monkeys, even though

it lacked a tail (Ward et al., 1991). Unlike extant apes, *Ekembo* displays bony contact between ulna and wrist (Beard et al., 1986; Ward, 2007), further suggesting at least some quadrupedal behavior. Despite the fact that these taxa were most likely pronograde quadrupeds, the elbow appears to be adapted for loading in a wide range of postures (Rose, 1993), and hallucal robusticity also was greater than that of extant monkeys (McNulty et al., 2015). The wrist of *E. heseloni* indicates that it engaged in cautious climbing, with forearm rotation consistent with quadrupedal locomotion on discontinuous supports (Daver & Nakatsukasa, 2015). The skeleton overall, though somewhat resembling an above branch quadruped, suggests a locomotor repertoire unlike that of any living primate, probably involving more varied locomotor behavior including clambering over multiple supports (Beard et al., 1993; Rose, 1994; McNulty et al., 2015). The feet have been not been as thoroughly analyzed as the rest of the skeleton, despite the preservation of multiple tarsals and the utility of a functional analysis of foot use in this taxon.

Proconsul major

Previously grouped with the two *Ekembo* species, *Proconsul major* lived around 20 Ma in modern day Kenya (McNulty et al., 2015) and was estimated to be around 75 kg (Rafferty et al., 1995; Kelley, 1997). *Proconsul* postcranial remains are scarce, but the species is known postcranially from a talus and calcaneus (Lewis, 1980b). *P. major* tali and calcanei have been reconstructed as similar to *Ekembo* skeletally (Leakey et al., 1988; Ward, 1998). *P. major* has been described as cercopithecoid-like and the subtalar joint is said to indicate that stability during dorsiflexion/plantarflexion was prioritized

over mobility (Langdon, 1986; Ward, 1997; Dunsworth, 2006), although comparison to a broad sample of extant with diverse locomotor repertoires taxa is needed.

Rangwapithecus gordoni

Another basal hominoid from about 20 Ma, found in modern day Kenya is *Rangwapithecus gordoni* (Hill et al., 2013). *Rangwapithecus* is also thought to be cercopithecoid-like (Ward, 1997), though appears to have had a flatter, more wedge-shaped trochlea (DeSilva, 2008) and a flatter anterior talar facet on the calcaneus, suggesting to some (DeSilva, 2008) that it may have engaged in vertical climbing and a more ape-like varied locomotor repertoire than *Ekembo* or *Proconsul*.

Nacholapithecus kerioi

The middle Miocene is hypothesized to contain more locomotor diversity among hominoids than the early Miocene based on the fossils from this time period (Benefit & McCrossin, 1995). *Nacholapithecus kerioi* is known from a partial skeleton and isolated postcranial remains that date to around 15 Ma from Baragoi, Kenya (Ishida et al., 1999; Ishida et al., 2004). Torso structure for *Nacholapithecus* is inferred to be similar to that of *Ekembo*, with six lumbar vertebrae, a narrow torso, and no tail, but its limbs differ from both *Ekembo* and extant arboreal quadrupeds (Nakatsukasa et al., 1998; Ishida et al., 1999, 2004; Ward, 2007). The forelimbs are longer than the hind limbs and are heavily built, the phalanges are long, and the shoulder joint appears to have facilitated abduction related to suspensory locomotion when compared to extant monkeys (Nakatsukasa et al., 1998; Nakatsukasa et al., 2003; Ward, 2007). The elbow also indicates that

Nacholapithecus engaged in forelimb-dominated climbing, but its hands and feet resemble those of palmigrade taxa (Ward, 2007). The skeleton preserves a talus and calcaneus, which can clarify the putatively unusual locomotor morphology and function of *Nacholapithecus* (Nakatsukasa et al., 2012). The degree to which this taxon was suspensory or not may be informed by a better understanding of whether its foot was more capable of strong pedal grasping and varied foot postures like extant apes, or more stereotyped foot use like many monkeys.

Oreopithecus bambolii

From the late Miocene, *Oreopithecus bambolii* (Gervais, 1872) is dated to 9-7 Mya (Köhler & Moyà-Solà, 1997) from Italy and is known from a crushed partial skeleton, as well as from many other isolated postcranial elements (Harrison, 1986; Sarmiento, 1987; Rook et al., 1999). *Oreopithecus* has a high intermembral index, a short pelvis, and a reduced lumbar region (Straus, 1963; Russo & Shapiro, 2013). It has been described to have a mediolaterally broad but dorsoventrally shallow trunk, mirroring the hominoid condition as opposed to cercopithecoids and displays an ape-like zona conoidea, which is indicative of varied elbow postures, like those exhibited by suspensory apes (Straus, 1963; Rose 1988; McGechie et al., 2017). The olecranon process is short like a hominoid, with wrists capable of dorsiflexion and relatively short phalanges among apes (Harrison, 1986; Almécija et al., 2014). However, some (Köhler & Moyà-Solà, 1997; Rook et al., 1999; Moyà-Solà et al., 1999) have postulated that *Oreopithecus* was not ape-like in its locomotion, but rather engaged in bipedal locomotion, citing evidence of lumbar lordosis, a short ischium, a hominin-like

diaphyseal angle of the femur, a foot that has a medially-oriented line of leverage similar to what is seen in human feet, and precision grip beyond the ability of extant non-human apes. These hypotheses have been called into question, citing that a reevaluation of the hand of *Oreopithecus* instead reveals power gripping indicative of non-human ape-like locomotion rather than precision gripping (Susman 2004; Susman 2005). A functional reevaluation of the feet will clarify the manner in which this fossil primate moved about its environment.

Locomotor Reconstructions in Miocene Hominoids

The goal of this chapter is to examine available calcaneus, talus, navicular, and cuboid fossils of Miocene hominoids in order to test hypotheses concerning locomotor repertoire of these extinct taxa. I hypothesize that *Ekembo* and *Proconsul* will more closely resemble quadrupedal extant taxa such as cercopithecids or *Sapajus.* I predict *Rangwapithecus* to largely resemble extant cercopithecids, but also show evidence of a more varied locomotor repertoire than other early Miocene taxa. I hypothesize that *Nacholapithecus* will exhibit suspensory foot adaptations, though also to have some adaptations for above branch quadrupedalism. I expect that, unlike some (Köhler and Moyà-Solà, 1997; Rook et al., 1999; Moyà-Solà et al., 1999) have hypothesized, *Oreopithecus* will more closely resemble suspensory taxa such as African apes, hylobatids, *Pongo*, and atelids.

Methods:

Specimens

CT scans of tali, calcanei, cuboids, and naviculars (Table 3.1) were provided by B. Patel (University of Southern California), C. Orr (University of Colorado Denver), S. Almécija (George Washington University), and W. Jungers (Stony Brook University). Each talus, calcaneus, cuboid, and navicular was segmented out of the scans. Monkey tarsals were segmented using MIMICS (Materialise, Leuven, Belgium) and apes were segmented using *Avizo7* (Thermo Fisher Scientific). The resulting polygonal models were cleaned using *Geomagic Wrap 2017* (3D Systems, Inc.). The extant sample comprises taxa chosen to represent an array of locomotor emphases including suspensory taxa and arboreal quadrupeds. Extant taxa were grouped into phylogenetic and locomotor groupings of taxa with different emphases in their locomotor repertoires (Table 3.3). All specimens are from non-pathological, wild-shot individuals. Polygonal models of fossil material (Table 1) were provided by J. DeSilva and E. McNutt (Dartmouth College).

The extant sample of taxa used in this chapter is the same as in the previous chapter (Table 3.1). The calcaneus, talus, navicular, and cuboid of extant anthropoids were analyzed because they comprise the subtalar and transverse tarsal joints, and contribute to the talocrural joint, functionally crucial joints to both suspensory and quadrupedal locomotion (Lewis, 1980 a & b; Chapters 2 and 3). The following specimens from Miocene taxa were included in this study (also listed in Table 1):

Ekembo heseloni and *Ekembo nyanzae*

Ekembo is represented in this study by three calcanei attributed to *E. nyanzae* (KNM-MW 13142B; Figure 2 and KNM-RU 5872; Figure 4) and *E. heseloni* (KNM-RU 2036; Figure 6), and a cuboid attributed to *E. nyanzae* (KNM-RU 5872; Figure 8). All three

calcanei are missing the posterior tuber, and the larger *E. nyanzae* specimen (KNM-RU 5872) has some damage to the superior aspect of the posterior subtalar articular surface. The KNM-RU 5872 *E. nyanzae* cuboid is well-preserved distally, but the proximal end is slightly damaged (Figure 8).

Proconsul major

Proconsul major postcrania attributed to this species were: a right calcaneus pa (KNM-SO 390; Figure 12), partial calcaneus and a complete talus (KNM-SO 389; Figure 11). The calcaneus of *P. major* preserves only the distal part of the bone from just posterior to the posterior subtalar articular surface to the distal end.

Rangwapithecus gordoni

Rangwapithecus is also known from a talus and calcaneus, though both are damaged. The talus (KNM-SO 968; Figure 13) has damage on its inferior aspect, along with the lateral trochlea, so landmarks in those regions could not be collected. The calcaneus of *Rangwapithecus* (KNM-SO 427; Figure 15) is also fragmentary, with the posterior tuber and posterior subtalar articular surface damaged.

Nacholapithecus kerioi

The *Nacholapitheus* calcaneus (KNM-BG 35250; Figure 17) preserves the distal end, including the entire sustentaculum and part of the posterior subtalar articular surface.

Oreopithecus bambolii

Oreopithecus was the genus with the greatest number of tarsal elements represented in this analysis. Two tali (BA 79; Figure 19 and BA 82; Figure 21) were analyzed. Due to damage to the trochlea, BA 79 is represented by talar head landmarks only. BA 82 preserves the talar head and trochlea but the inferior aspect of the talar body, including the posterior calcaneal facet is missing. Two calcanei (BA 155; Figure 25 and BA 79; Figure 23) attributed to *Oreopithecus* were also evaluated. The posterior region of BA 155 past the posterior subtalar articular surface is missing and the sustentaculum tali is damaged. BA 79 is almost complete, with minimal damage to the posterior tuber. Two cuboids (BA 83; Figure 26 and BA 158; Figure 28) attributed to *Oreopithecus* were analyzed in this study. BA 83 is well-preserved and relatively undamaged while BA 155 has some damage distally and is generally more worn than BA 83. The *Oreopithecus* navicular (BA 79; Figure 30) is fully preserved.

Analyses

The same landmark-based 3D geometric morphometric techniques that were used in Chapter 3 were used for these fossils. Landmarks, modified from Harcourt-Smith (2002), were placed on each bone in *Stratovan Checkpoint* (Stratovan, 2018) (Table 3.2). These landmarks have been shown to be successful in quantifying tarsal shape differences related to locomotion and foot posture (Harcourt-Smith, 2002) and were able to be collected with sub-millimeter intraobserver error (Chapter 3). Due to the fragmentary nature of fossils, not every landmark could be collected on every fossil specimen. However, one of the benefits of landmark GM is that partial specimens can be

analyzed by subsetting the landmarks to only include the ones that are able to be taken on the fossil specimen (Table 4.1). In the cases where fossils were subsetted, only the extant variation in the subsetted region was considered in the analysis of the fossil. The x, y, z landmark data collected from polygonal models were imported into *MorphoJ* (Klingenberg & McIntyre, 2016) for visualization and analysis.

In order to quantify shape differences among anthropoid tarsal morphology, landmarks on each bone underwent a Procrustes superimposition to translate, scale, and rotate all the points into alignment for comparison. The subsetted landmark-based 3D geometric morphometric techniques were run for each fossil, as the number of landmarks collected for each one differed. In the event that two or more fossils shared the same landmark preservation, those specimens were grouped into a single analysis.

Principal components analysis (PCA) of the extant taxa, grouped using the same categories listed in Table 3.3 with the fossil specimen as its own group was carried out and plotted to see which group each fossil most closely resembles in morphology. To correct for multiple comparisons, the adjusted p-values are reported here using the Benjamini & Hochberg (1995) method ("BH"). All statistical analyses and visualization were carried out in *R Statistical Programming* (R Core Team, 2014) and *MorphoJ* (O'Higgins & Jones, 1999).

Results:

Ekembo

KNM-MW 13142B (Figure 2) is an *E. nyanzae* calcaneus that preserves 13 landmarks on the anterior part of the calcaneus, because the calcaneal tuber is missing. In the PCA, KNM-MW 13142B fell intermediate between great apes and most monkeys, but most closely resembles hylobatids, and atelids (Figure 3). The KNM-RU 5872 calcaneus (Figure 4) preserved only 10 landmarks on the fossil calcaneus. This fossil falls within the range of atelids and hylobatids along PC1 and within the range of all extant taxa studied except for atelids along PC2 (Figure 5). The anterior calcaneus is wide like an ape and most of the remainder of the bone is damaged. KNM-RU 2036 (Figure 6) represents the only element from *E. heseloni* in this study. KNM-RU 2036 is also missing the posterior part of the calcaneus. This fossil preserves 13 landmarks out of 21, though not the same set as KNM-MW 13142B, so the two cannot be compared. This partial calcaneus fell within the range of both hylobatids and atelids, between great apes and most monkeys (Figure 7).

The cuboid of *E. nyanzae* (KNM-RU 5872; Figure 8) preserves half of the landmarks used for the extant taxa (n = 10 out of 20). For the preserved parts of the bone, this fossil cuboid resembles that of a monkey. In the PCA, the specimen falls outside the range of all great apes and within the ranges of hylobatids, Old World monkeys, and New World monkeys (Figure 9).

Proconsul

KNM-SO 389 (Figure 10) was complete and therefore all talar landmarks were taken (n = 28). The talus also was most similar to hylobatids in the PCA when plotted with extant groups (Figure 11). *P. major* has a broad talar head, much like extant apes, and is overall mediolaterally wider. The broad, ape-like head combined with a longer

talar neck compared to extant apes likely drove this similarity with hylobatids, which, as shown in the previous chapter (Chapter 3), also have broad talar heads but a relatively longer talar neck compared to African apes.

KNM-SO 390 (Figure 12) is a calcaneus that preserves 13 landmarks out of 21 and fell within the range of hylobatids and atelids, but outside the range of all other extant taxa (Figure 7). This calcaneus was also extremely similar to the KNM-RU 2036 calcaneus in the PCA (Figure 7).

Rangwapithecus

The *Rangwapithecus* talus (KNM-SO 968; Figure 13) preserved 16 out of 28 talar landmarks. This talus was most similar to cercopithecids and outside of the range of all apes and atelids along PC1. The tall trochlea and similarity to cercopithecids suggest that the talus was engaged in significant plantar/dorsiflexion, much like extant cercopithecids (Figures 13 & 14).

The calcaneus (KNM-SO 427; Figure 15; Figure 40) preserves only nine landmarks that could be collected due to the damage to the fossil. The calcaneus fell within the range of hylobatids, cercopithecids, atelids, and African apes (Figure 16).

Nacholapithecus

Nine out of the 21 calcaneal landmarks were taken on the *Nacholapithecus* calcaneus (KNM-BG 36550O; Figure 17). The same nine landmarks were also taken on

the *Oreopithecus* specimen BA 155, so the two were grouped into a single PC analysis. *Nacholapithecus* falls within the range of hylobatids, cercopithecids, and atelines along PC1, though was most similar to hylobatids and atelids (Figure 18). *Nacholapithecus* fell similarly to the *Oreopithecus* specimen along PC1, but differed greatly along PC2, where the *Oreopithecus* fell outside the range of all extant taxa except for *Pongo* (Figure 18).

Oreopithecus

BA 79 only had six landmarks that were limited to the talar head (Figure 19). PCA of the talar head landmarks placed the *Oreopithecus* specimen most morphologically similar to hylobatids and atelids, though still within the range of variation of *Sapajus*, cercopithecids, and African apes (Figure 20). The more complete BA 82 talus had 17 of 28 talar landmarks preserved (Figure 21). BA 82 falls among hylobatids, *Pongo,* and atelids along PC1 (Figure 22).

The BA 79 calcaneus preserved 14 out of 21 total calcaneal landmarks (Figure 23). BA 79 fell outside the range of cercopithecids, atelids, *Sapajus*, and hylobatids along PC1, but was most morphologically similar to African apes and *Pongo* (Figure 24). Along PC2, the BA 79 specimen fell within the range of *Pongo* and hylobatids (Figure 24). The other *Oreopithecus* BA 155 specimen preserved only nine landmarks (Figure 25). When the preserved part of the bone was analyzed using PCA, it was most similar to hylobatids, atelids, and *Pongo* (Figure 18).

Both *Oreopithecus* cuboids (BA 83 and BA 158) preserved 18 and 16 landmarks, respectively, out of 20 total cuboid landmarks. BA 83 (Figure 26) fell outside the range

of African apes, but fell within the range of all other extant taxa analyzed (Figure 27). BA 158 (Figure 28) fell intermediate between great apes and smaller taxa, within the statistical range of *Pongo* along PC1 (Figure 29).

The navicular of *Oreopithecus* preserved all 16 navicular landmarks used in this study (Figure 30). The navicular fell within the range of African apes and outside the range of variation of all monkeys except for suspensory atelids (Figure 31).

Discussion:

The goal of this chapter was to examine tarsals of Miocene hominoids in order to test hypotheses concerning locomotor repertoire of these extinct taxa. Fossilized tarsals (n = 16) from *Ekembo, Proconsul, Rangwapithecus, Nacholapithecus,* and *Oreopithecus,* were landmarked (subsets of landmarks were used when not all landmarks were able to be taken due to the fragmentary nature of many of these fossils). The functional interpretation for each genus is presented below:

Ekembo

When compared to extant anthropoid primates, all three *Ekembo* specimens exhibit relatively elongated anterior calcanei, similar to cercopithecids, although relatively wider than cercopithecids, likely due to a larger body size. This feature was determined to be related to locomotor differences in Chapter 3, with quadrupedal taxa having relatively longer anterior calcanei and suspensory taxa having relatively shorter calcanei, like the pictured *Gorilla* calcaneus (Figure 32). The sustentaculum of KNM-

MW 13142B strongly resembles a quadrupedal monkey both in morphology and projection angle, the sustentaculum of the other *E. nyanzae* specimen (KNM-RU 5872) more closely resembles that of suspensory apes, being less bulbous in dorsal view, and the sustentaculum of the *E. heseloni* specimen is damaged (Figure 32). The calcaneal morphology is consistent with that of an above branch arboreal quadruped, though it does share some similarities with extant apes, as evidenced by its intermediate position between monkeys and apes in the PCA (Figure 3).

A left cuboid from *Ekembo nyanzae* is also analyzed in this study. Overall, the PCA revealed that the cuboid most closely resembled monkeys and hylobatids (Figure 4). However, damage to the lateral side of the proximal aspect of the bone is severe (Figure 33), and therefore that region was not landmarked; thus, the overall morphological interpretations were made cautiously. Features such as cuboid wedging and proximal articular surface morphology could not be evaluated due to the damage. In his analysis of this specimen DeSilva (2008) was also cautious in his interpretations of this fossil specimen due to the damage. Based on the remaining fossil, however, this specimen more closely resembles arboreal quadrupeds like *Macaca* and *Cercopithecus* than it does suspensory taxa like *Pan* and *Ateles*, regardless of the phylogenetic and body size affinities between *Ekembo* and extant apes (Figure 33). The KNM-RU 5872 cuboid is proximodistally elongated (Figure 16) and dorsoventrally tall, similar to *Macaca* and *Cercopithecus*, and unlike the relatively shorter (proximodistally), broader (mediolaterally), and flatter (dorsoplantarly) *Pan*, *Hylobates*, and *Ateles* (Figures 33-34). This elongation of the cuboid in arboreally quadrupedal cercopithecids and *Ekembo* is hypothesized to provide a mechanical advantage during push off phase of plantarflexion

for taxa that engage in more quadrupedal walking (Lovejoy et al., 2009) as opposed to suspensory locomotion, where an elongated cuboid would limit midfoot mobility during grasping.

This reconstruction is consistent with the hypothesis that *Ekembo* was an above branch quadruped. *E. nyanzae* provides an example of a large-bodied above branch quadrupedal ape, which is not represented in extant primates, which makes the study of their locomotor behaviors crucial to a more complete view of primate locomotion.

Proconsul

The *P. major* talus fell outside the range of extant monkeys in the PCA analyses and most closely resembled hylobatids and *Pongo* along PC1. The ape-like appearance likely is related to the fact that *P. major* is larger than extant monkeys, and the talus bears the body weight of the animal during locomotion. The talar neck, however, is relatively longer than it is in extant great apes (Figure 35). The *P. major* trochlear ridge is also taller and the trochlear ridges are more pronounced, similar to an arboreal quadruped such as *Macaca* (Figure 36). These more pronounced and taller trochleae are thought to aid in stability during plantarflexion/dorsiflexion and reduce lateral movements of the talus (Chapter 3 PCA results). On flat surfaces, there is minimal movement besides plantarflexion/dorsiflexion in cercopithecids, which adds to the stability of the ankle joint (Chapter 2). However, this anatomy is not ideal for highly suspensory taxa, as high trochleae would impede foot inversion during climbing or grasping small branches. This morphology therefore suggests that *P. major* was a large above branch quadruped with limited suspensory abilities.

The anterior calcaneus of *P. major* is mediolaterally wide, reflecting the large body size of *P. major*, but relatively longer than great apes (*Gorilla* pictured in Figure 37). The elongated anterior calcaneus is more reminiscent of arboreal quadrupeds and leapers like *Colobus* and *Cercopithecus*, which gain a mechanical advantage from an elongated midfoot region during propulsive plantarflexion (Anemone & Nachman, 2003, Prang, 2019). This is consistent with my hypothesis as well as previous reconstructions by Langdon (1986) and Ward (1997) that *P. major* is an above branch quadruped that engaged in quadrupedalism.

Rangwapithecus

Due to the paucity of postcranial material attributed to *Rangwapithecus* and the damage to both the talus and calcaneus, little is known about the locomotor repertoire of *Rangwapithecus*. The talus of *Rangwapithecus* resembles extant great apes in the orientation and breadth of the talar head (Figure 38). *Rangwapithecus,* however, fell most closely to quadrupedal cercopithecids in the PC analysis. The talus also has a relatively longer neck than extant great apes, and the talar trochleae, though slightly damaged, are also taller, much like extant cercopithecids (Figures 38 & 39). The tall trochleae with minimal wedging may indicate that it engaged in more dorsiflexion/plantarflexion at the talocrural joint with less emphasis on inversion/eversion, which would make its locomotion more like extant cercopithecids. This mixed locomotor signal has been noted previously and interpreted an indication that *Rangwapithecus* engaged in a variety of types of locomotion including above branch quadrupedalism and vertical climbing (Ward, 1997; DeSilva, 2008).

The calcaneus of *Rangwapithecus* also carries a mixed locomotor signal. The preserved anterior aspect of the calcaneus is wide like extant modern apes, but relative longer than extant modern apes with a less laterally protruding sustentaculum tali than cercopithecids (Figure 40). The talus and calcaneus both indicate that *Rangwapithecus* shared traits with both suspensory great apes as well as arboreal quadrupedal monkeys, but more fossil material from this taxon could aid in the functional interpretations of its locomotion.

Nacholapithecus

Nacholapithecus is another Miocene hominoid with contested locomotor repertoire. It exhibits traits that both resemble arboreal quadrupeds as well as suspensory taxa. The calcaneus of *Nacholapithecus* fell in the range of cercopithecids, hylobatids, and atelids in the PCA. The *Nacholapithecus* specimen only preserves the distal end (Figure 41), including the sustentaculum tali. Anterior calcaneal length is preserved as it was quantified in Chapter 3. The *Nacholapithecus* is relatively wider than monkeys, and more closely resembles apes. The sustentaculum tali is also rounded, and less projecting relative to the width of the anterior calcaneus, and more closely resembling apes. Within monkeys, atelids has the least projecting sustentaculum, likely due to the fact that the sustentaculum tali holds the talar head and neck and atelids have shorter necks than other monkeys, much like apes have relatively shorter necks than monkeys. Given the limited material available in this study, the calcaneus of *Nacholapithecus* most closely resembles that of a suspensory ape, though some morphological features do overlap with cercopithecids, confirming previous studies that suggest a mixed locomotor repertoire,

which included pronograde quadrupedalism (Rose, 1996, Senut et al., 2004; DeSilva, 2008). This reconstruction is also consistent with my hypothesis that *Nacholapithecus* would exhibit suspensory foot adaptations but also to have some adaptations for above branch quadrupedalism.

Oreopithecus

Oreopithecus is one most heavily-contended fossil specimens in terms of locomotion, with hypotheses that it was bipedal (Moyá-Solá et al., 1999; Rook et al., 1999). Although bipedal humans were not included in this study, attribution to bipedal capabilities of the foot of *Oreopithecus* were made based on monkey-ape comparisons and inferences of morphologies being poorly adapted for grasping with the foot, such as limited motion at the calcaneocuboid and metatarsocuboid joint, which they inferred from flat joint surfaces. However, I know from Chapter 2 of this dissertation that even cercopithecoid calcaneocuboid and cuboid/MT5 joints undergo plantarflexion/dorsiflexion and inversion/eversion. Additionally, when PC scores plotted using the extant sample used in Chapter 3, that the tarsals of *Oreopithecus* most closely resemble apes, most often *Pongo*, a suspensory ape or extant atelids, which are suspensory monkeys.

The talar heads of both *Oreopithecus* tali are broad relative to a quadrupedal monkey like *Cercopithecus* (Figures 42 & 43). Talar head breadth is a feature that was found in Chapter 3 to separate monkeys and apes. The trochleae are lower and broader, much like apes and unlike the tall, sharper-crested trochleae of cercopithecids (Figures 42 & 43). The talus overall is relatively short anteroposteriorly, with a lack of an elongated

talar neck (Figure 43). The ape talar neck is relatively shorter than monkeys (see Chapter 3), but within apes, hylobatids and *Pongo* have relatively longer necks than African apes, which is hypothesized to be driven by locomotion, since compressive stresses that constrain talar neck length in African apes are reduced in highly suspensory locomotion that rarely engage in terrestrial, hindlimb weight bearing locomotion (Langdon, 1986). The *Oreopithecus* talus grossly resembles an ape, and within apes more closely resembles *Pongo*, suggesting that *Oreopithecus* also engaged in suspensory locomotion.

The anterior length of the *Oreopithecus* calcaneus resembles extant apes and looks dissimilar to extant monkeys (Figure 44). Apes have broader, relatively shorter anterior calcanei and are relatively flatter anteriorly (Figure 45) and taller posteriorly (Figure 46). This morphology separated taxa by locomotor group in Chapter 3, with suspensory taxa having taller, relatively narrower calcanei posteriorly. Obligate bipeds, on the other hand, have posterior calcaneal tubers that are very wide inferiorly to account for absorbing forces of heel strike (Latimer & Lovejoy, 1989; Bramble & Lieberman, 2004; DeSilva et al., 2018). Even if *Oreopithecus* did not heel strike like modern humans, which is likely given the retention of a divergent hallux (Köhler & Moyà-Solà), the calcaneus has no indication of any plantar morphology that would dissapate the forces of a roughly 32 kg (Jungers, 1987) animal walking only on its hindlimbs. From a posterior view of the *Oreopithecus* with the calcaneal tuber intact, the inferior aspect of the calcaneal tuber is slightly wider inferiorly, but not to the degree expected if the plantar surface of the foot were to be bearing the weight of the entire organism as a biped (Figure 46). The orientation of the posterior subtalar facet is also more aligned with the long axis of the bone in suspensory taxa, unlike arboreal quadrupeds. This disparity is thought to

increase subtalar stability during climbing (Langdon, 1986; Chapter 3), and *Oreopithecus* displays the suspensory condition (Figure 44).

Two cuboids attributed to *Oreopithecus* were analyzed in this study. Both were clearly mediolaterally broad (Figure 47), dorsoplantarly flattened (Figure 48), and proximodistally short (Figure 47). The flattening of the cuboid resembles hylobatid and atelid cuboid morphology (Figure 48), whereas the mediolaterally broad, proximodistally short, wedged cuboid is similar to *Gorilla beringei* and *Pan* cuboids. Cuboid wedging is thought to place position the metacarpals in a more abducted position in arboreal taxa compared to terrestrial taxa to allow for better grasping. Arboreal quadrupeds and obligate bipeds, on the other hand, have dorsoventrally expanded cuboids that are rectangular rather than wedged in order to better facilitate push off during plantarflexion.

The sole navicular analyzed in this study is attributed to *Oreopithecus*. The navicular of *Oreopithecus* strongly resembles an ape navicular, in dorsal view (Figure 49) in proximodistal dimensions as opposed to the proximodistally elongated naviculars of quadrupedal taxa. Proximodistally long navicular are thought to be related to running and above branch locomotion requiring a longer load arm for plantarflexion, whereas shorter naviculars benefit suspensory taxa to reduce stresses on the navicular during supinated foot postures in suspensory locomotion (Chapter 3). A shallower talonavicular facet with a less defined articular surface rim in *Oreopithecus* (Figure 50) may also allow for greater mobility at the talonavicular joint, where significant inversion/eversion occur during locomotion (Chapter 2). Apes, which are suspensory also exhibit a more gently curved articular surface at the talonavicular joint, which allow the talar head to be more mobile

during inversion and eversion, whereas arboreal quadrupeds show a priority for stability at the talonavicular joint during propulsive plantarflexion.

There is therefore little to no support for a bipedal reconstruction of *Oreopithecus.* The fossil tarsals studied here share features with suspensory, large bodied apes. Additionally, they display none of the features that are consistent with habitual arboreal or terrestrial quadrupedalism that were identified in extant monkeys and some Miocene hominoids. Unlike Moyá-Solá and colleagues (1999) and Rook and colleagues (1999) hypothesized, *Oreopithecus* is most similar to a suspensory ape.

Limitations

Although phylogenetic reconstruction was not one of the goals of this study, nor ought such relationships between taxa be determined by locomotor similarities since convergence upon similar locomotion is common, one of the major hindrances of studying Miocene taxa is that the phylogenetic relationships of many Miocene species are unclear (Begun et al., 2007; Hammond, 2013), and a resolved cladogram does not currently exist. This lack of understanding leads to a context deficit when discussing these taxa and also prevents phylogenetically-controlled analyses of morphology.

Another consistent obstacle in the study of Miocene hominoid locomotion is low sample size. Although some tarsals are well-preserved, analyses are still limited to a low number (often n = 1) of each element represented, often with some associated taphonomic damage. This precludes study of variability within a species and also forces researchers to allow a single specimen to represent a whole taxon. More specimens and a better understanding of how these taxa are related are sorely needed.

Conclusion:

The goal of this dissertation was to better understand motion and morphology of the joints of the foot in order to better interpret the functional morphology of the foot and ankle in Miocene hominoids. The goal of this chapter was to apply the results of the previous chapters to interpret isolated tarsals of key Miocene taxa and test hypotheses about their locomotor repertoires. This goal was successful and I was able to confirm previous hypotheses about how these taxa navigated their environment, and also was able to provide more insights than previous studies based on functionally-relevant features of isolated tarsals. This study supported the hypothesis that early Miocene hominoids like *Ekembo*, *Proconsul*, and *Rangwapithecus* were predominantly above branch quadrupeds but that *Rangwapithecus* also likely engaged in more varied locomotor behaviors than the other two taxa. Conversely, *Nacholapithecus* was reconstructed to be mostly suspensory but also showed evidence for a mixed locomotor repertoire, including pronograde quadrupedalism. Finally, the tarsals attributed to *Oreopithecus* exhibit adaptations for suspensory locomotion, leading us to believe that it was not primarily bipedal, as previously hypothesized (Moyá-Solá et al., 1999; Rook et al., 1999).

This chapter provided a thorough analysis of some Miocene hominoid tarsals in order to better understand the locomotion of some key and contested fossil taxa. Parsing out features of isolated tarsal bones related to size, phylogeny, and locomotion in the previous chapter was important for the interpretation of this chapter. Using gross similarities with extant monkeys and apes alone are cautioned against when interpreting Miocene fossils because they differ in overall body size and proportions from extant taxa. Therefore, a closer look at individual bones and joint surfaces was warranted. The lack of

an extant large-bodied monkey complicates our understanding of these taxa, and creates the risk of categorizing, for example, an arboreal quadruped that moves like a monkey as an ape due to phylogenetic or size-related morphologies rather than functional ones. A more thorough understanding of the features driving morphological variation in extant samples was applied to these fossils and these same methods can be applied to more fossil taxa for a more thorough understanding of how Miocene hominoids moved.

Figures for Chapter 4

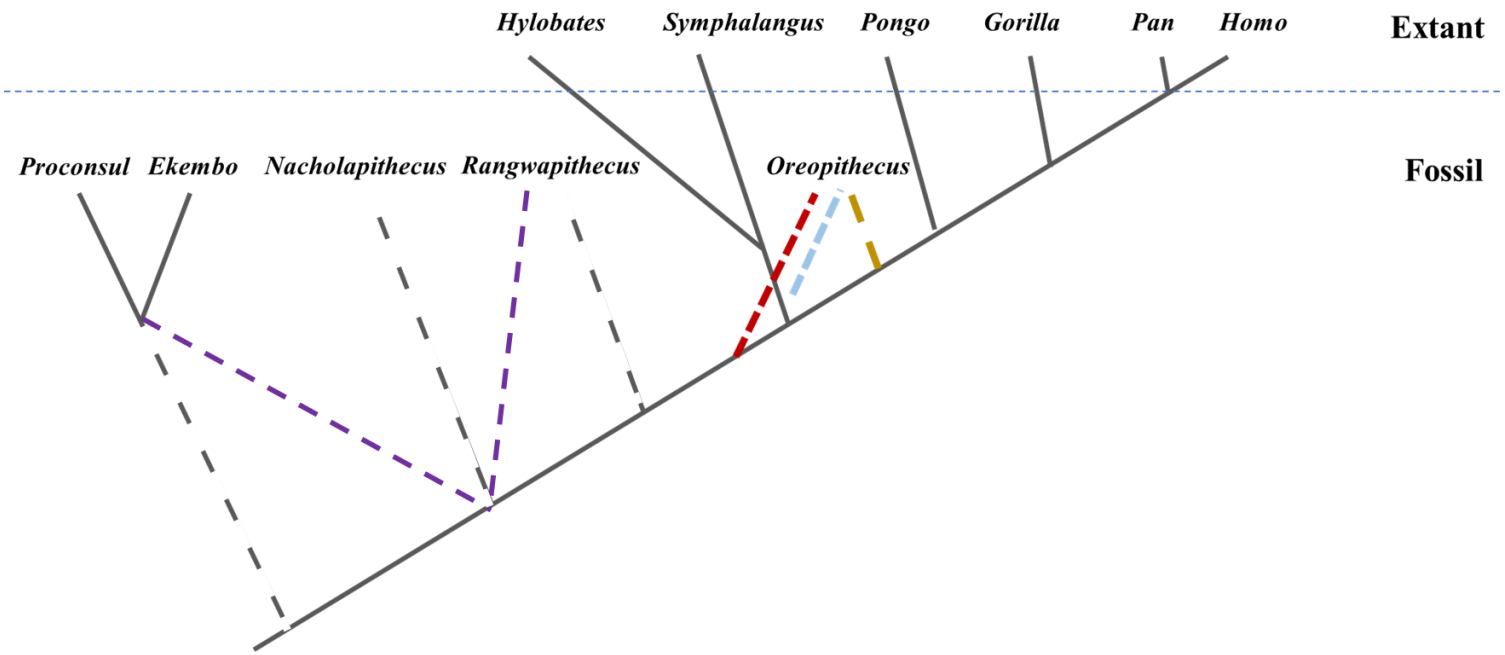

Figure 1: Composite hypothesized phylogeny of fossil hominoids in relation to extant apes. Extant ape phylogeny is from Begun, 2007. *Proconsul* and *Ekembo* phylogeny based on Nengo et al., 2017 and Rasmussen et al., 2019. *Nacholapithecus* phylogeny based on Nengo et al., 2017. *Rangwapithecus* phylogeny based on Nengo et a., 2017. *Oreopithecus* phylogenetic position based on Young & Maclatchy, 2002 (yellow), Begun, 2007 (blue), Thompson & Almécija, 2017 (red and yellow), and Nengo et al., 2017 (red). Extant taxa are above the dotted line, whereas fossil taxa are below the dotted line.

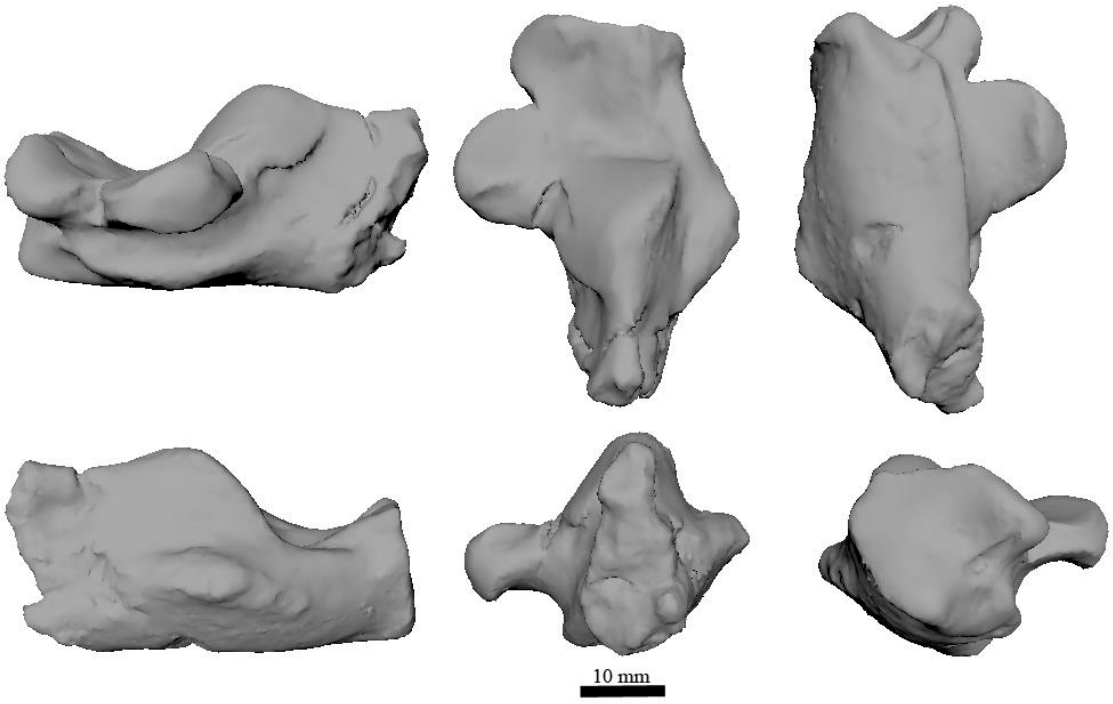

Figure 2: KNM-MW 13142B right calcaneus attributed to *Ekembo nyanzae*. Top row views: medial, proximal, plantar. Bottom row views: lateral, caudal, distal.

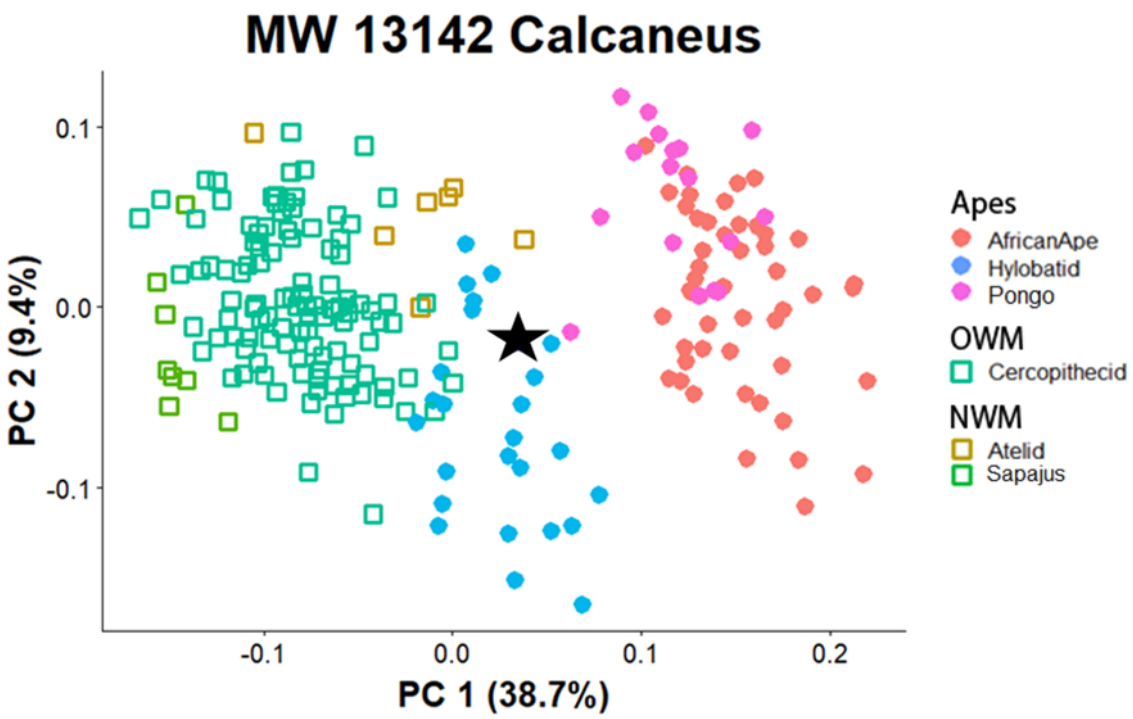

Figure 3: PCA of extant sample of calcanei from anthropoid primates using the same groups as in Chapter 3 (Table 3.3) with the *Ekembo* (KNM-MW 13142) calcaneus indicated by the black star.

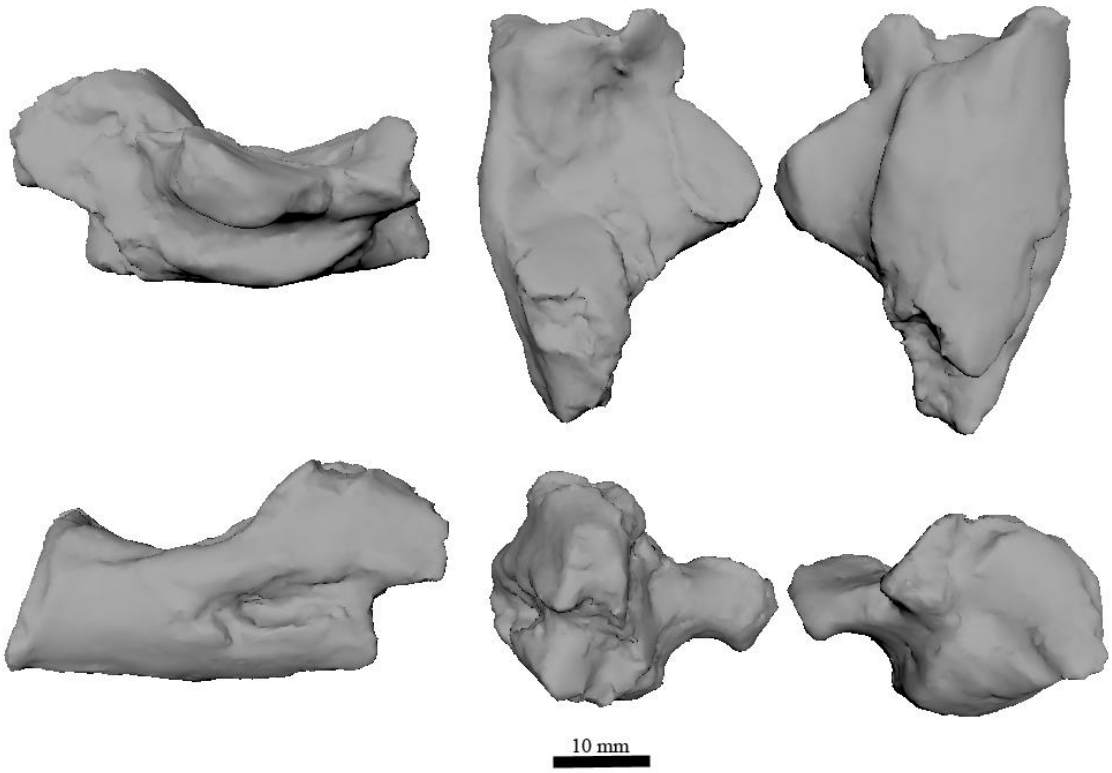

Figure 4: KNM-RU 5872 left calcaneus attributed to *Ekembo nyanzae*. Top row views: medial, proximal, plantar. Bottom row views: lateral, caudal, distal.

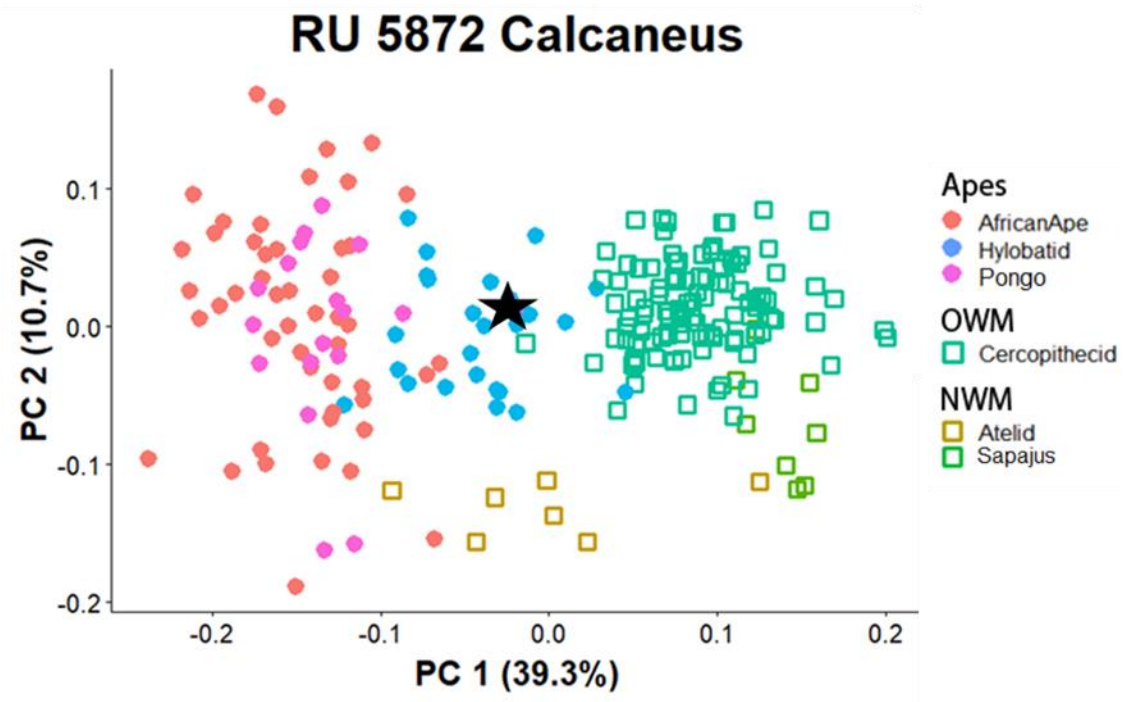

Figure 5: PCA of extant sample of calcanei from anthropoid primates using the same groups as in Chapter 3 (Table 3.3) with the *Ekembo* (KNM-RU 5872) calcaneus indicated by the black star.

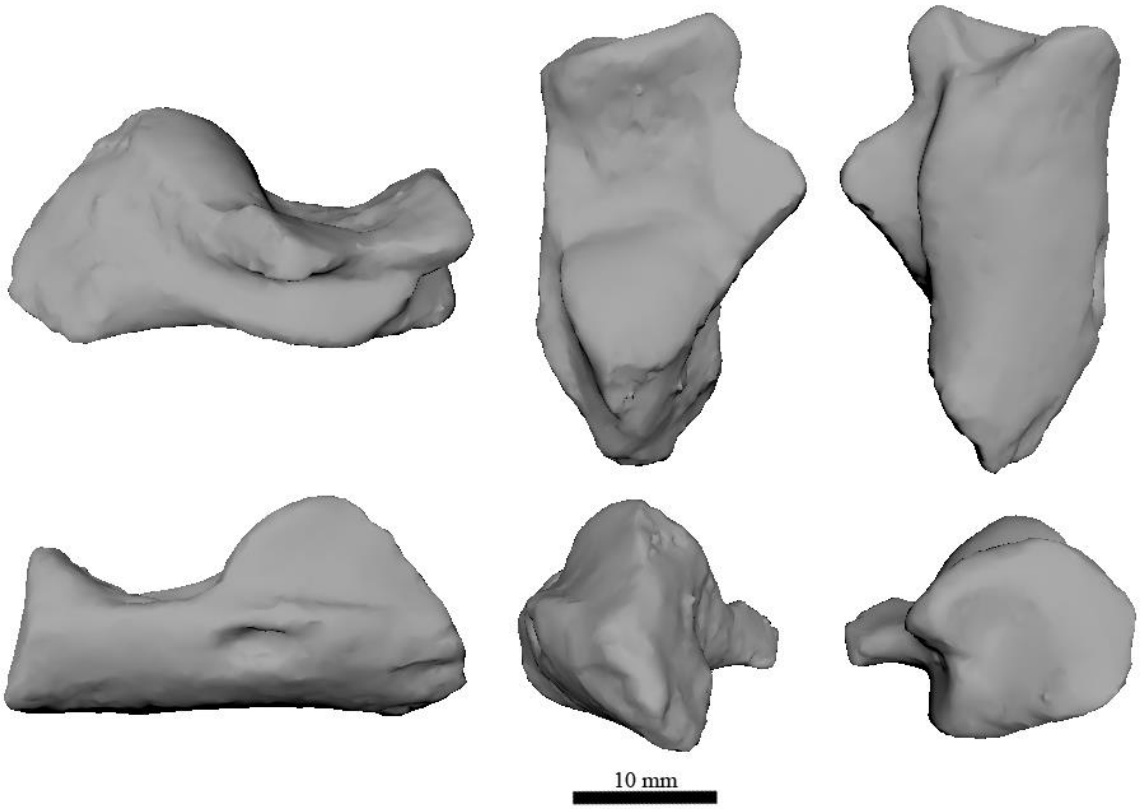

Figure 6: KNM-RU 2036 left calcaneus attributed to *Ekembo heseloni*. Top row views: medial, proximal, plantar. Bottom row views: lateral, caudal, distal.

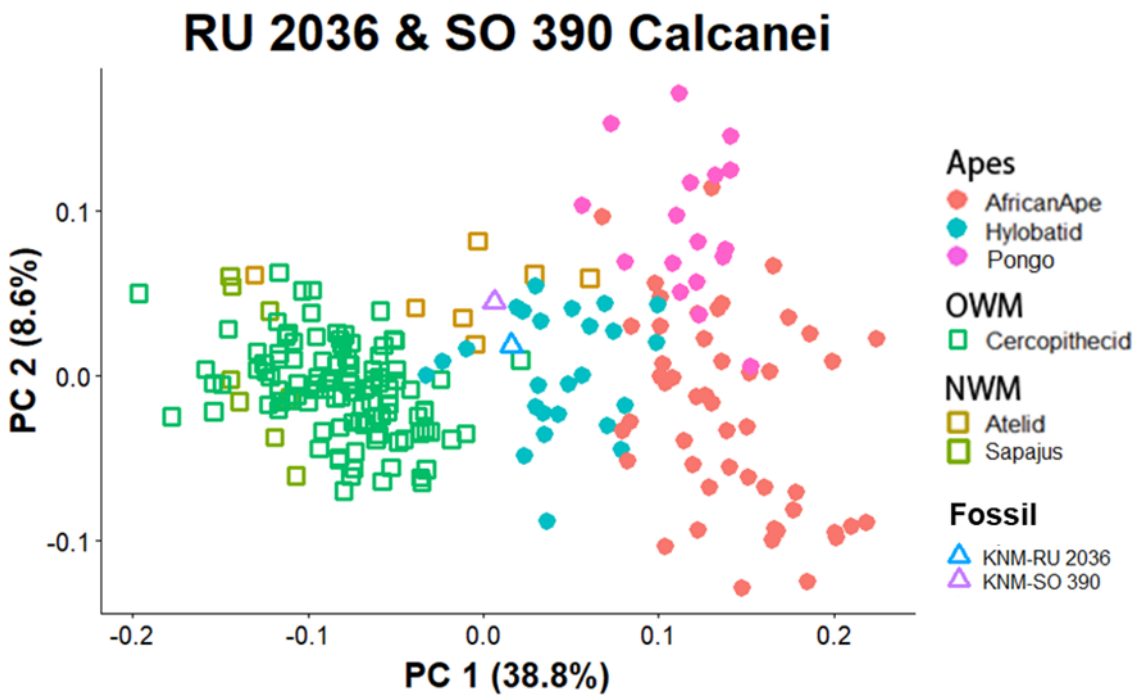

Figure 7: PCA of extant sample of calcanei from anthropoid primates using the same groups as in Chapter 3 (Table 3.3) with *Ekembo* (KNM-RU 2036) and *Proconsul* (KNM-SO 390) calcanei, which shared the same preserved landmarks.

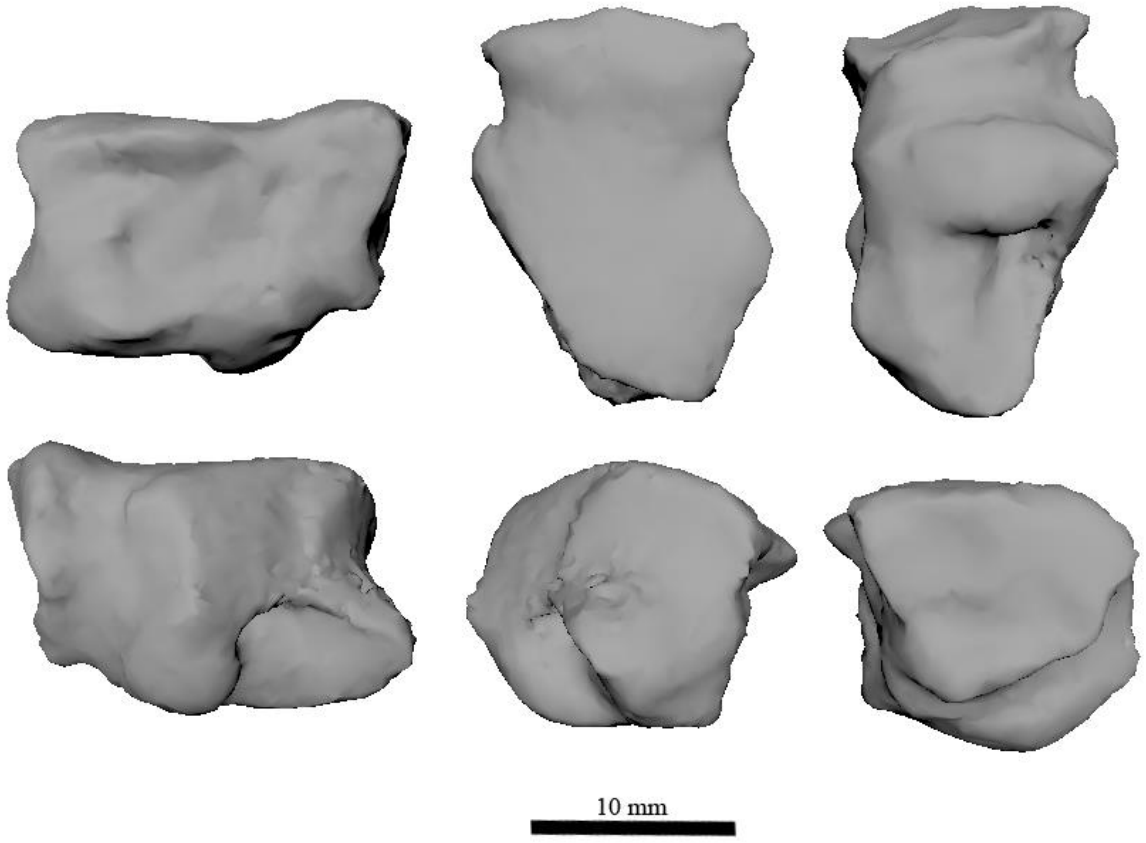

Figure 8: KNM-RU 5872 left cuboid attributed to *Ekembo nyanzae*. Top row views: medial, dorsal, plantar. Bottom row views: lateral, proximal, distal.

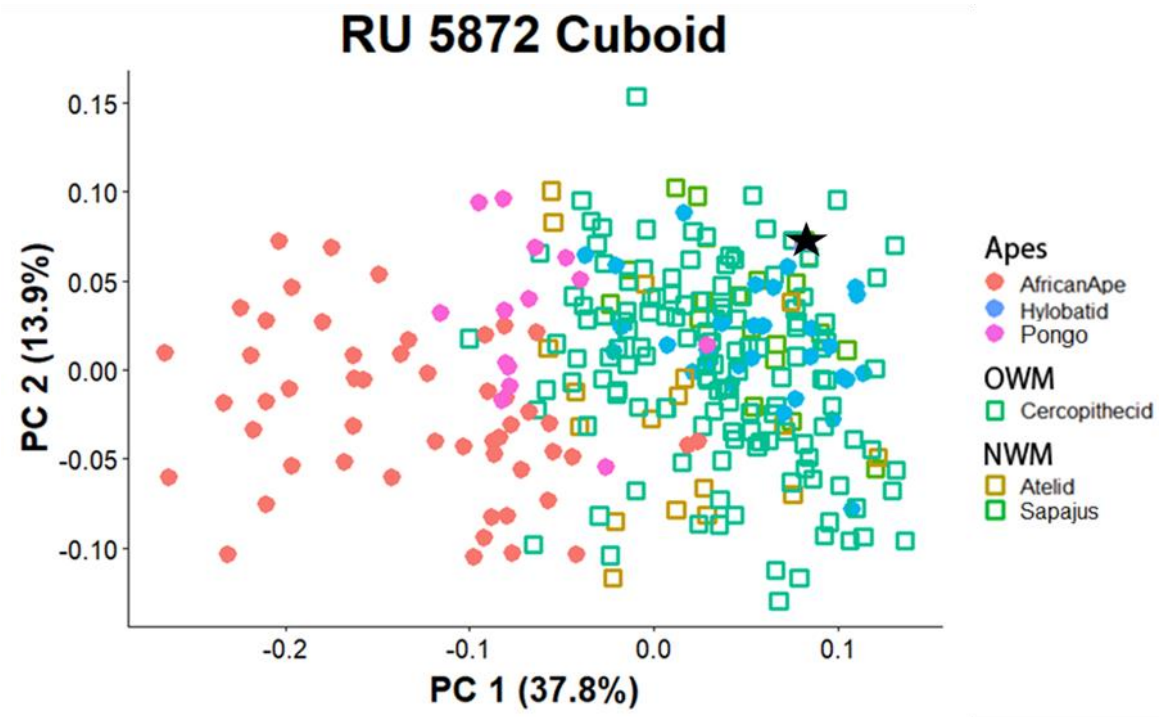

Figure 9: PCA of extant sample of cuboids from anthropoid primates using the same groups as in Chapter 3 (Table 3.3) with the *Ekembo* (KNM-RU 5872) cuboid indicated by the black star.

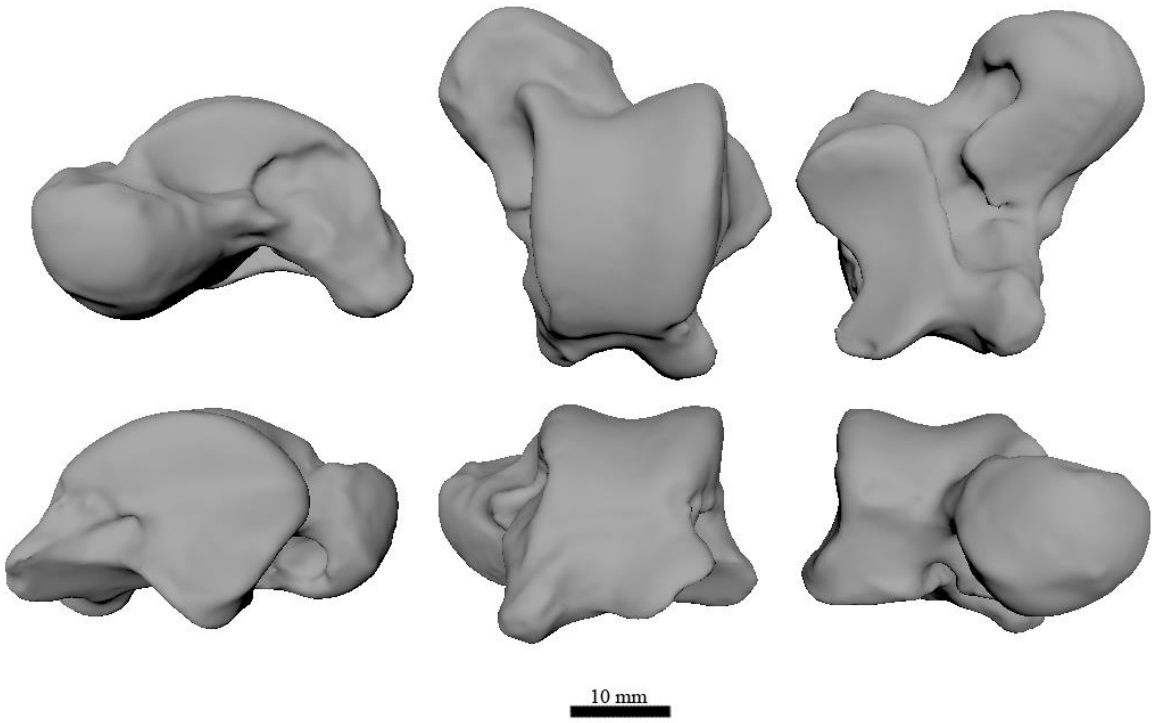

Figure 10: KNM-SO 389 right talus attributed to *Proconsul major*. Top row views: medial, proximal, plantar. Bottom row views: lateral, caudal, distal.

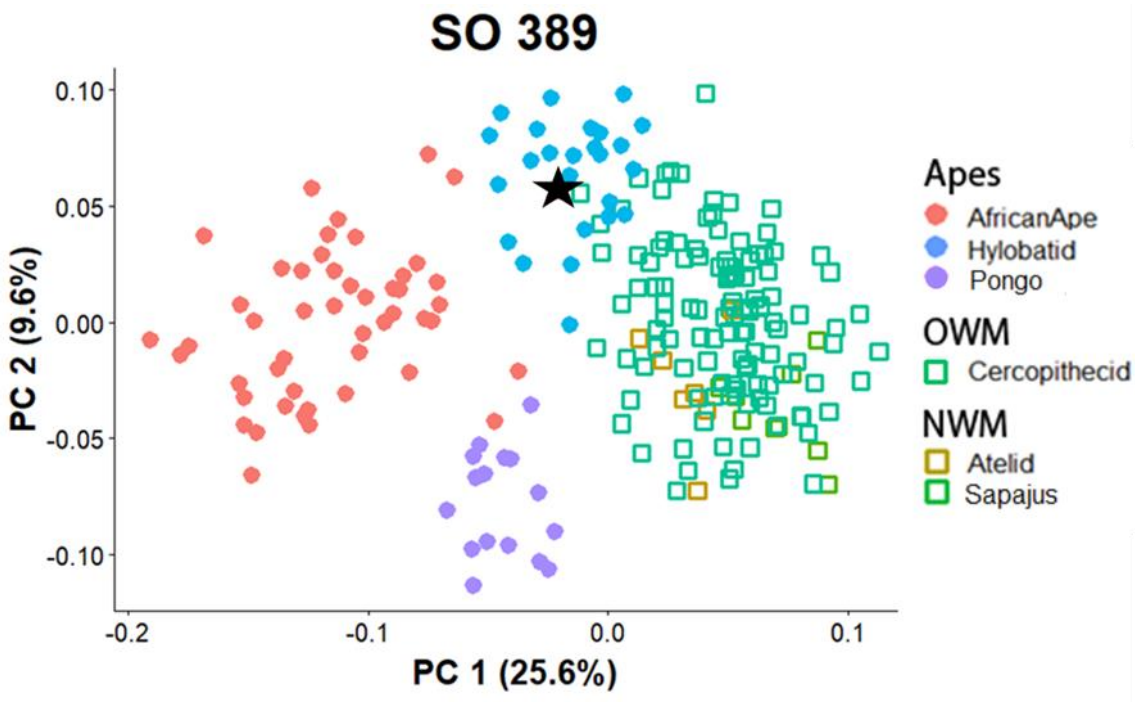

Figure 11: PCA of extant sample of tali from anthropoid primates using the same groups as in Chapter 3 (Table 3.3) with *Proconsul* (KNM-SO 389) talus indicated by the black star.

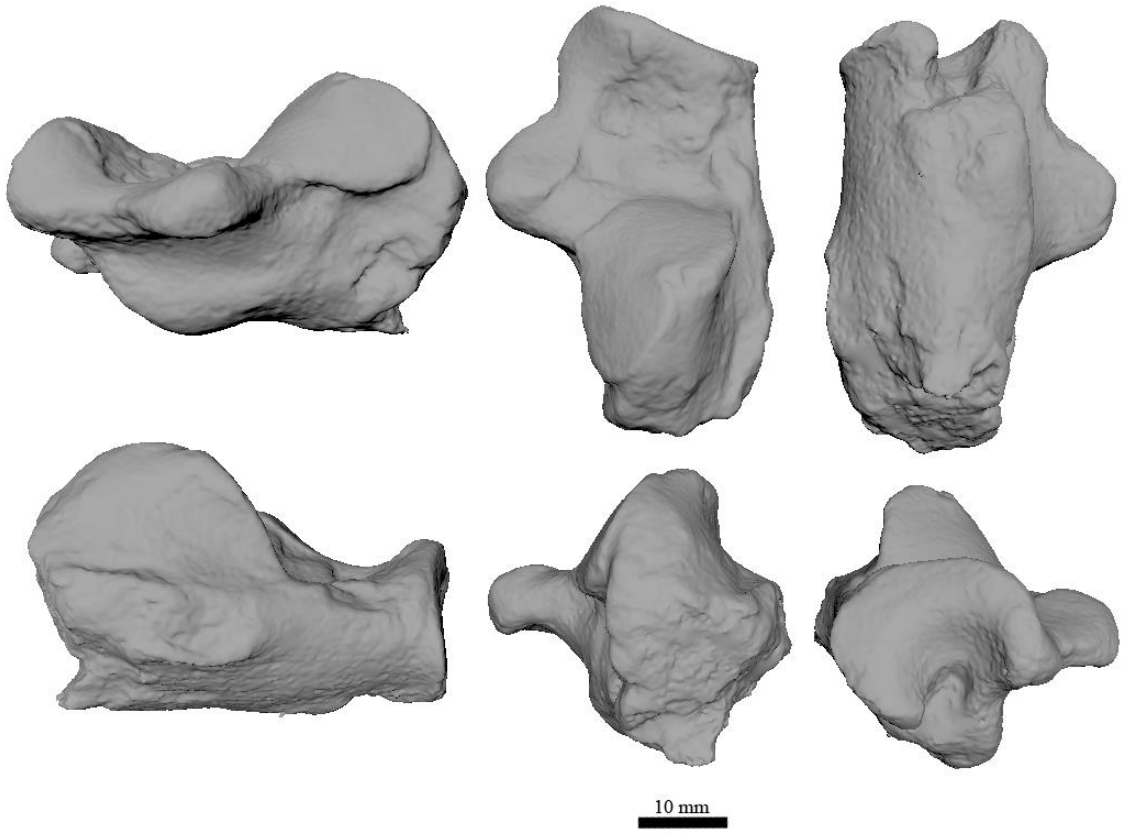

Figure 12: KNM-SO 390 right calcaneus attributed to *Proconsul major*. Top row views: medial, proximal, plantar. Bottom row views: lateral, caudal, distal.

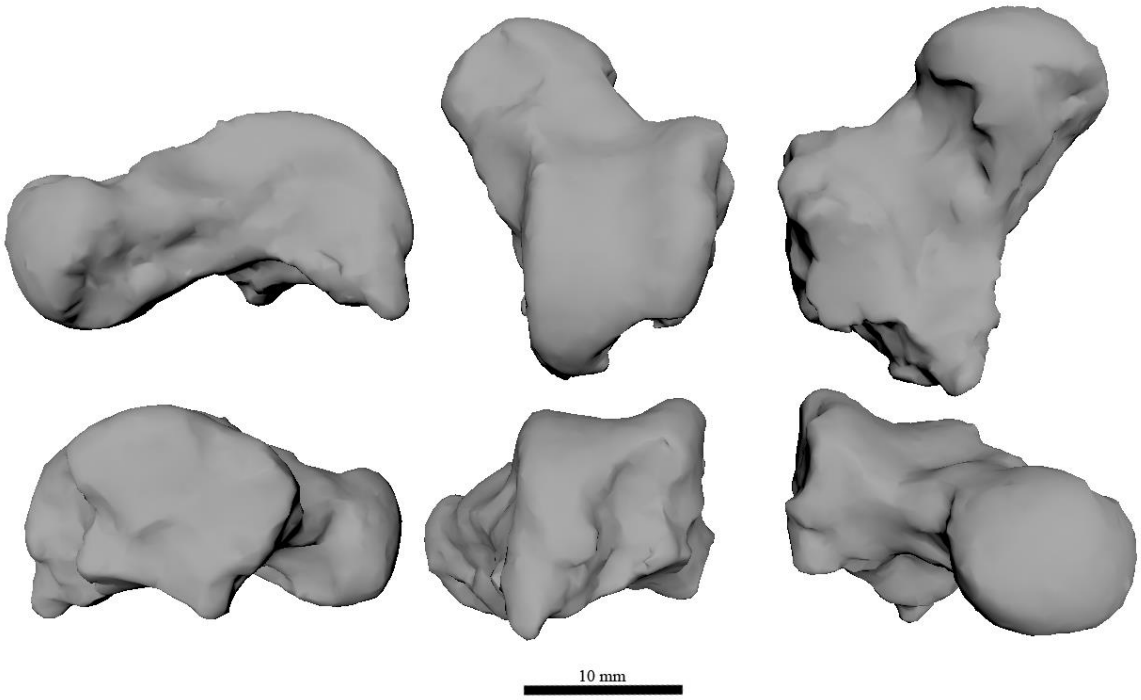

Figure 13: KNM-SO 968 right talus attributed to *Rangwapithecus gordoni*. Top row views: medial, proximal, plantar. Bottom row views: lateral, caudal, distal.

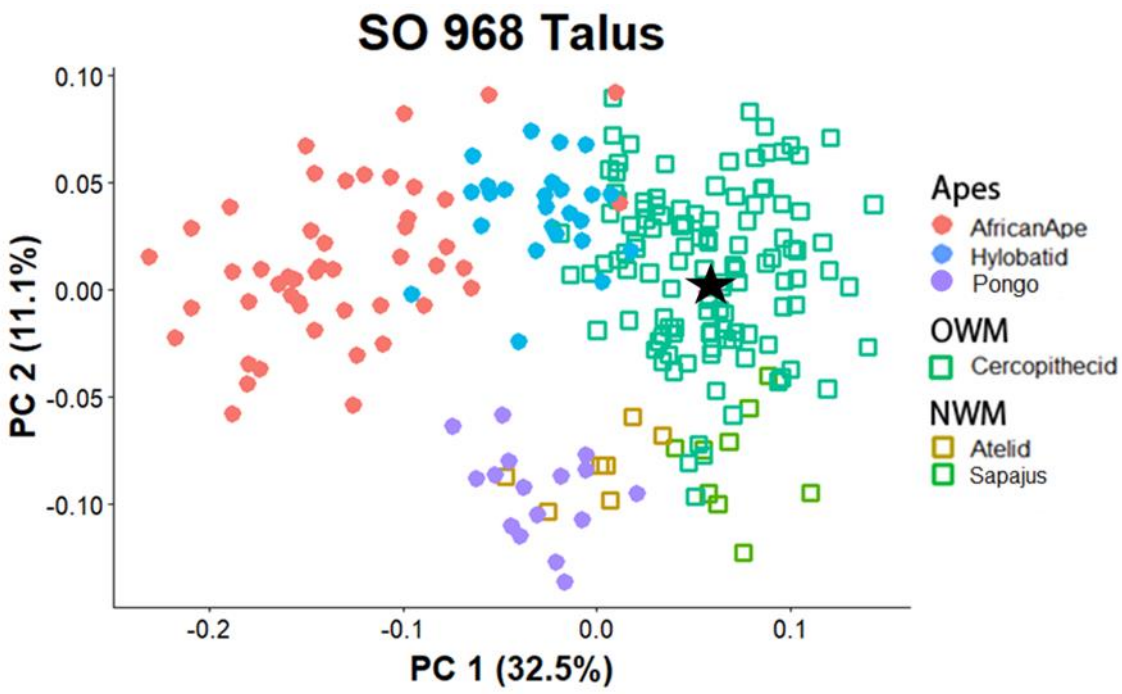

Figure 14: PCA of extant sample of tali from anthropoid primates using the same groups as in Chapter 3 (Table 3.3) with *Rangwapithecus* (KNM-SO 968) talus indicated by the black star.

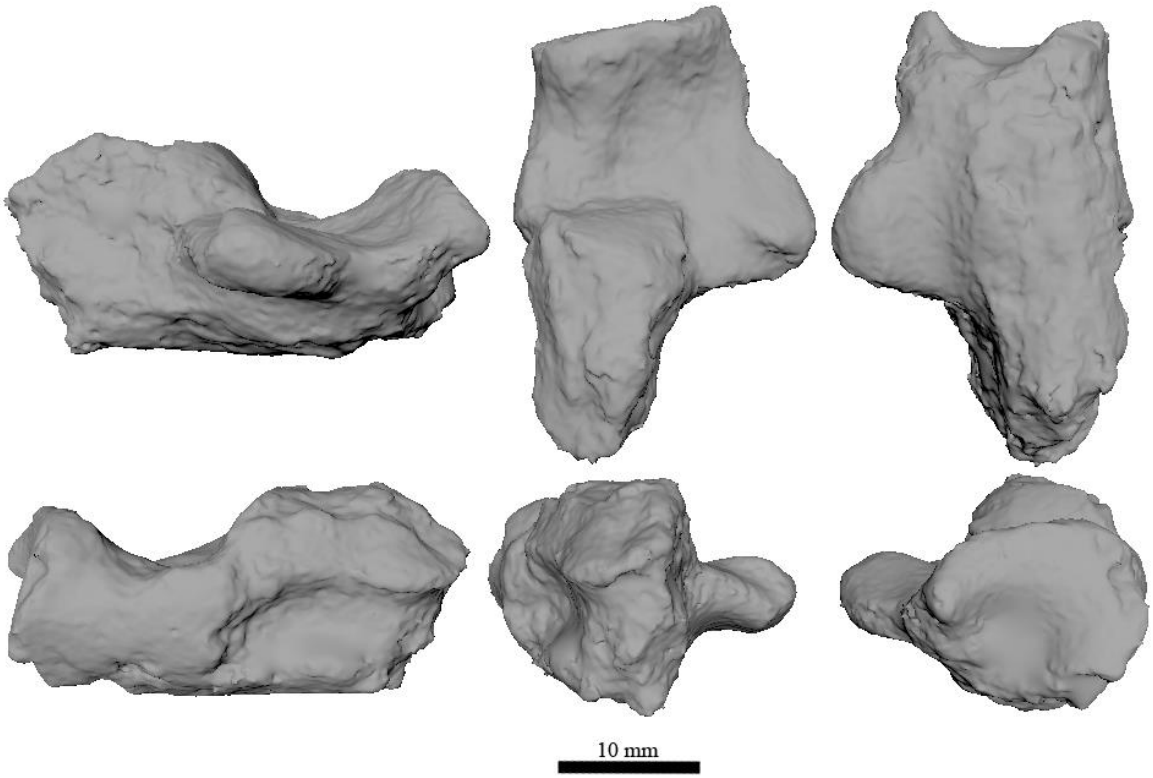

Figure 15: KNM-SO 427 left calcaneus attributed to *Rangwapithecus gordoni*. Top row views: medial, proximal, plantar. Bottom row views: lateral, caudal, distal.

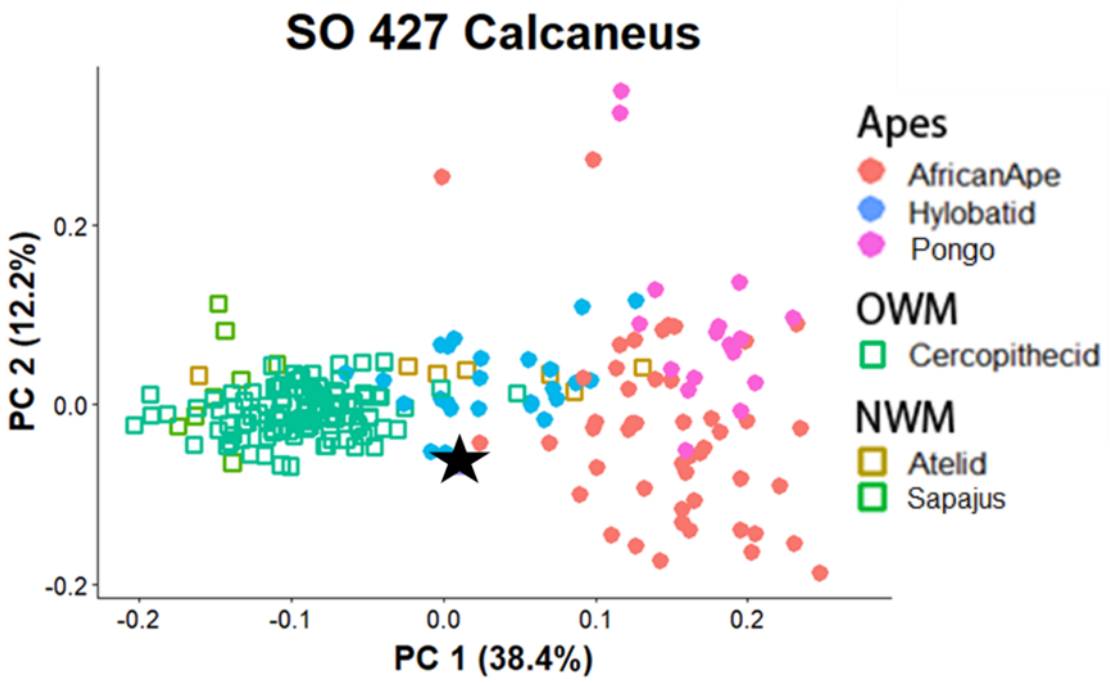

Figure 16: PCA of extant sample of calcanei from anthropoid primates using the same groups as in Chapter 3 (Table 3.3) with *Rangwapithecus* (KNM-SO 427) calcaneus indicated by the black star.

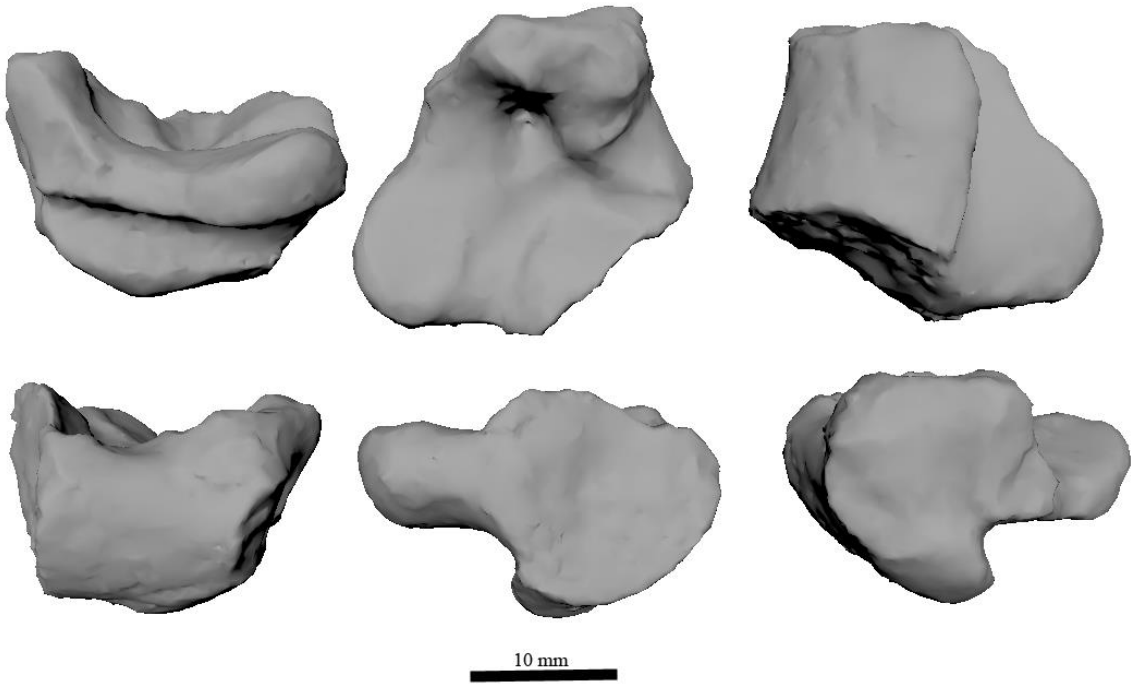

Figure 17: KNM-BG 35250 right calcaneus attributed to *Nacholapithecus kerioi*. Top row views: medial, proximal, plantar. Bottom row views: lateral, caudal, distal.

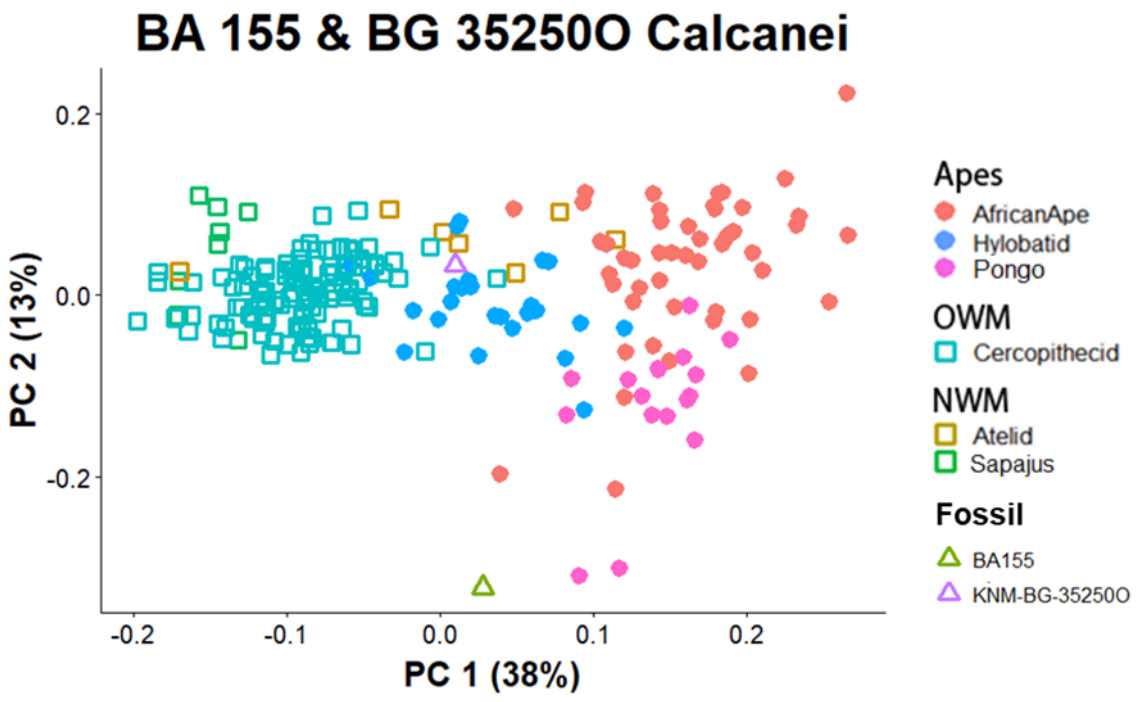

Figure 18: PCA of extant sample of calcanei from anthropoid primates using the same groups as in Chapter 3 (Table 3.3) with *Nacholapithecus* (KNM-BG 35250O) and *Oreopithecus* (BA 155) calcanei, which shared the same preserved landmarks.

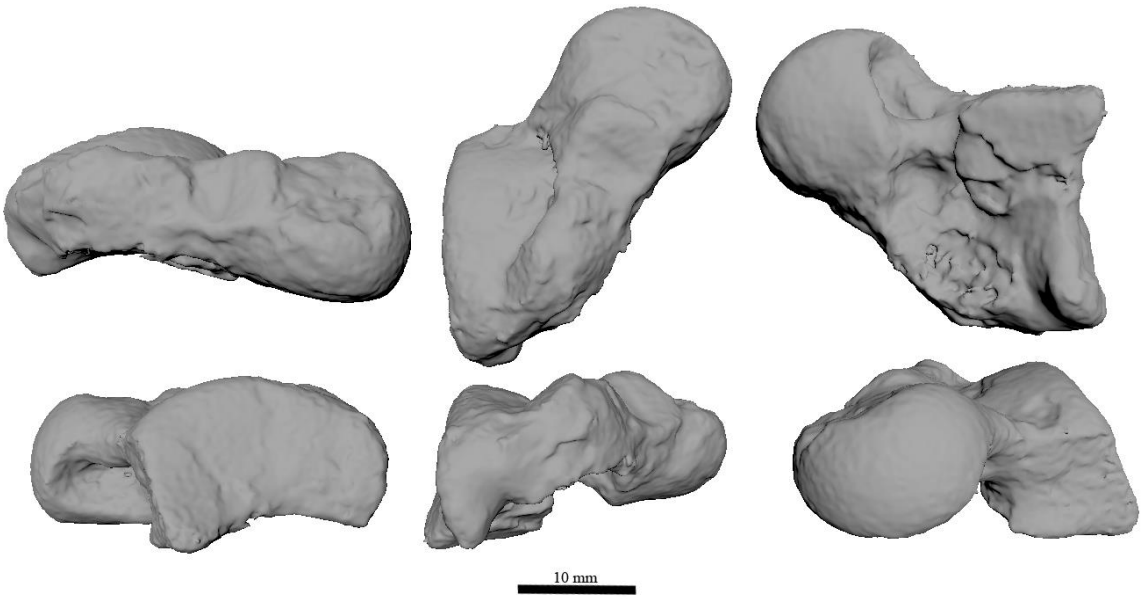

Figure 19: BA 79 left talus attributed to *Oreopithecus bambolii*. Top row views: medial, proximal, plantar. Bottom row views: lateral, caudal, distal.

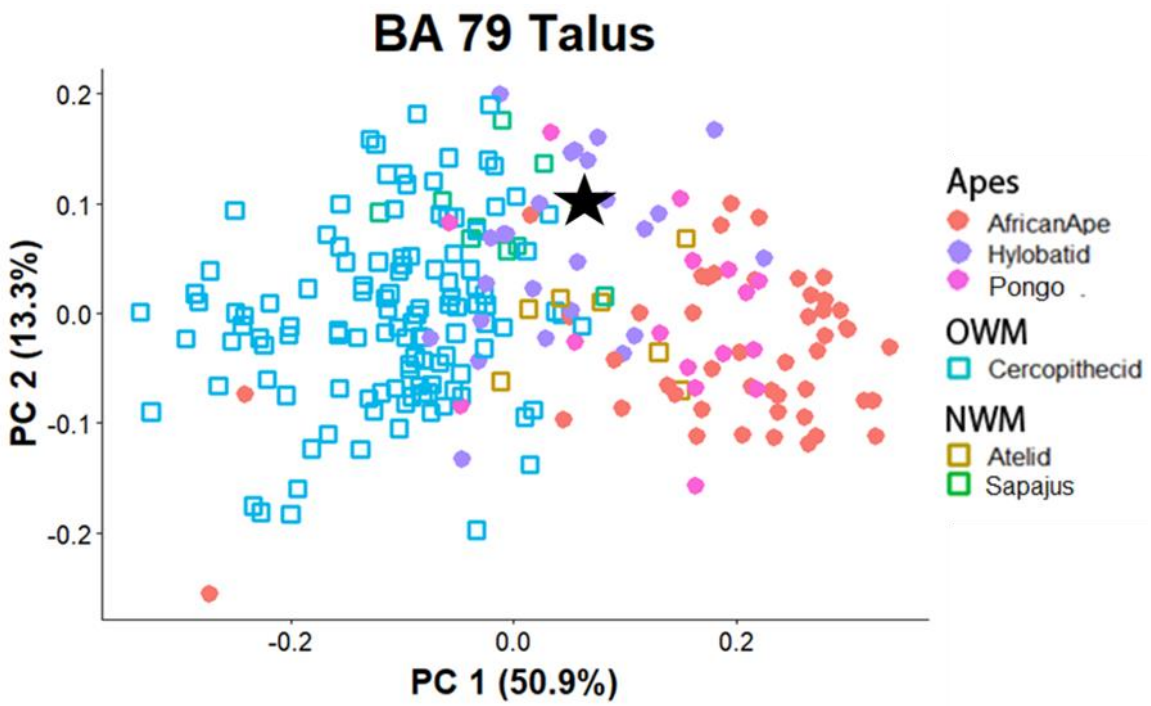

Figure 20: PCA of extant sample of tali from anthropoid primates using the same groups as in Chapter 3 (Table 3.3) with *Oreopithecus* (BA 79) talus indicated by the black star.

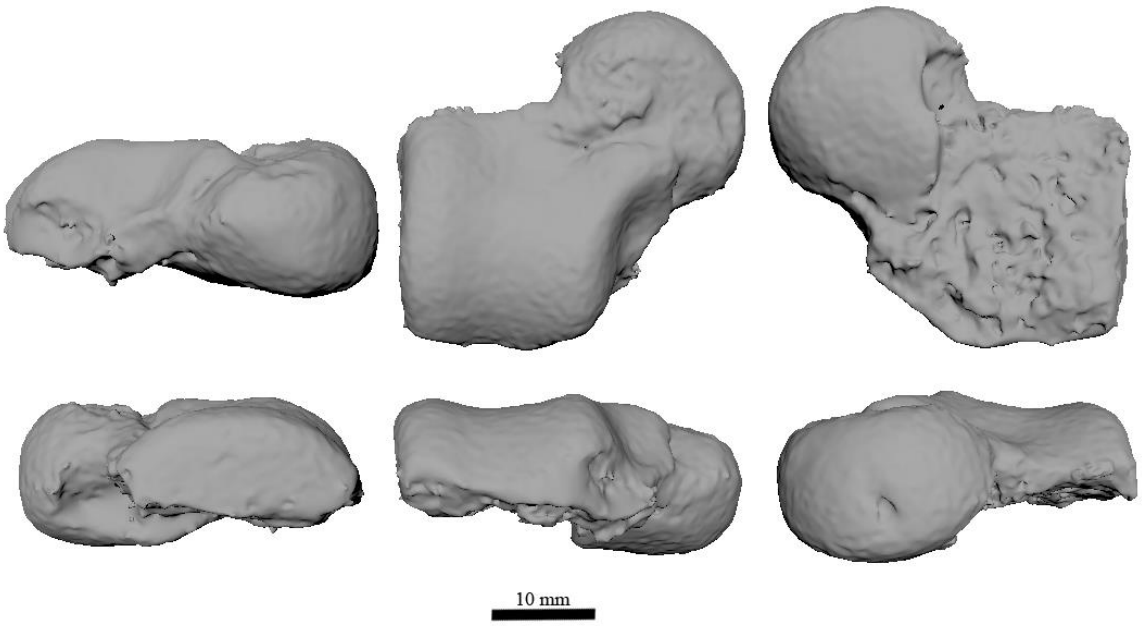

Figure 21: BA 82 left talus attributed to *Oreopithecus bambolii*. Top row views: medial, proximal, plantar. Bottom row views: lateral, caudal, distal.

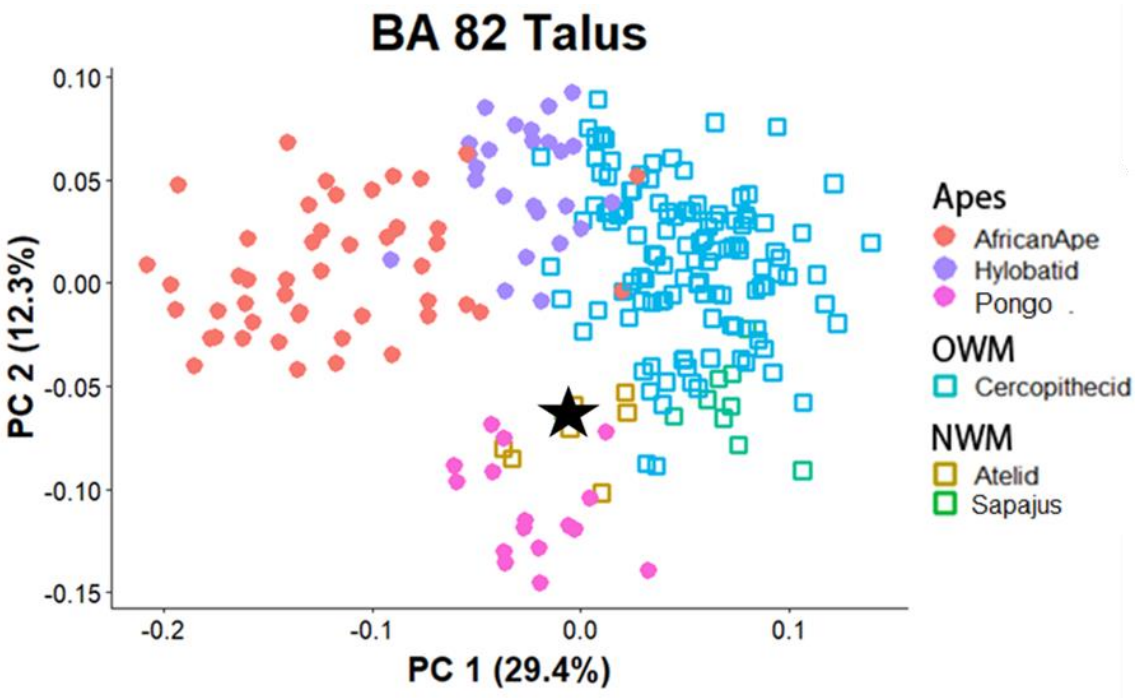

Figure 22: PCA of extant sample of tali from anthropoid primates using the same groups as in Chapter 3 (Table 3.3) with *Oreopithecus* (BA 82) talus indicated by a black star.

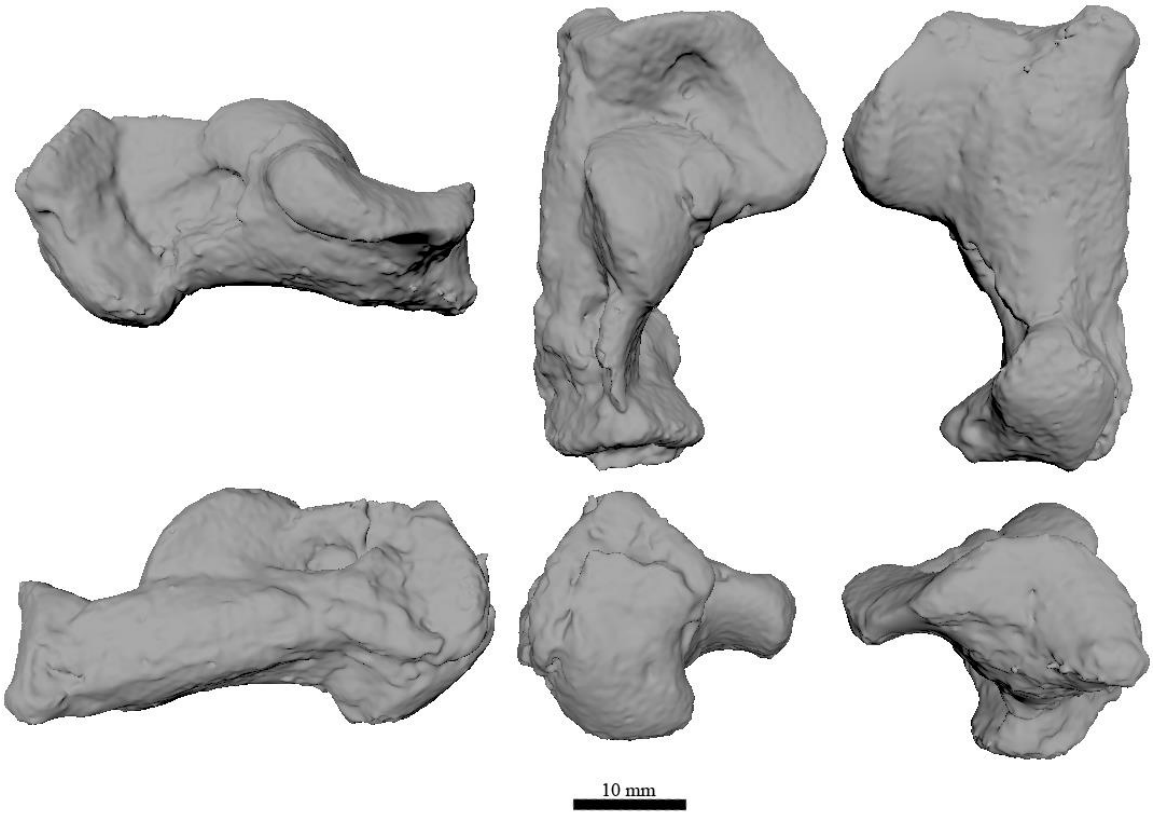

Figure 23: BA 79 left calcaneus attributed to *Oreopithecus bambolii*. Top row views: medial, proximal, plantar. Bottom row views: lateral, caudal, distal.

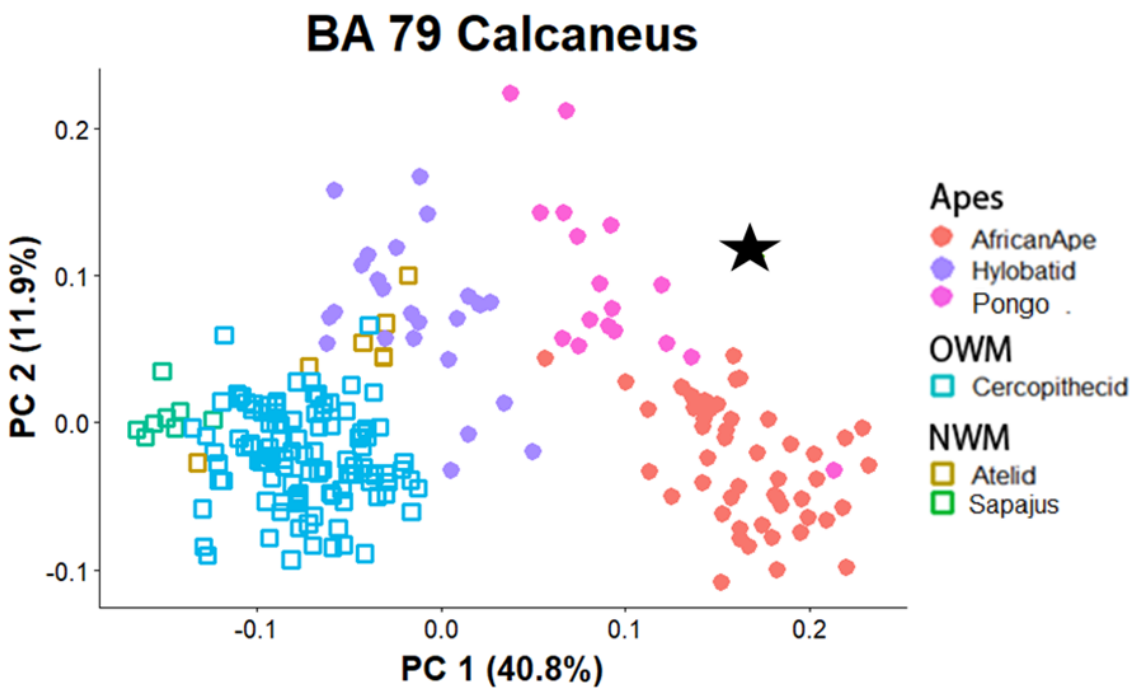

Figure 24: PCA of extant sample of calcanei from extant anthropoid primates using the same groups as in Chapter 3 (Table 3.3) with *Oreopithecus* (BA 79) calcaneus indicated by a black star.

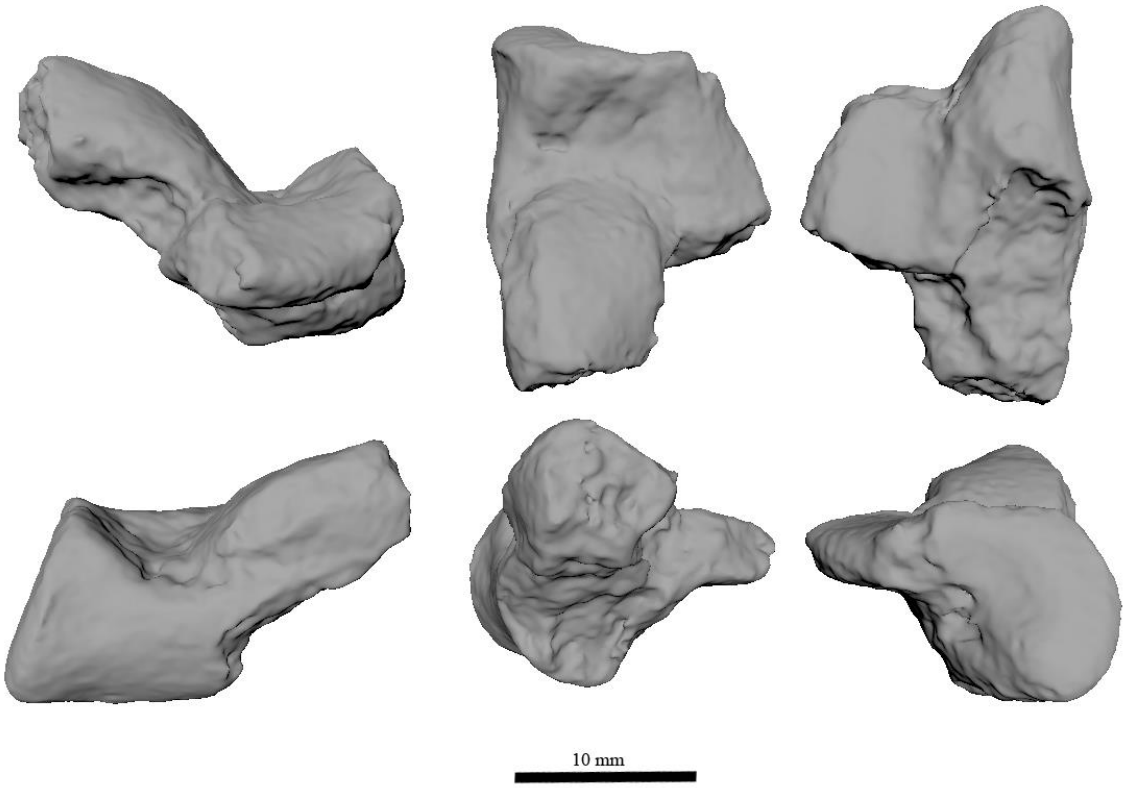

Figure 25: BA 155 left calcaneus attributed to *Oreopithecus bambolii*. Top row views: medial, proximal, plantar. Bottom row views: lateral, caudal, distal.

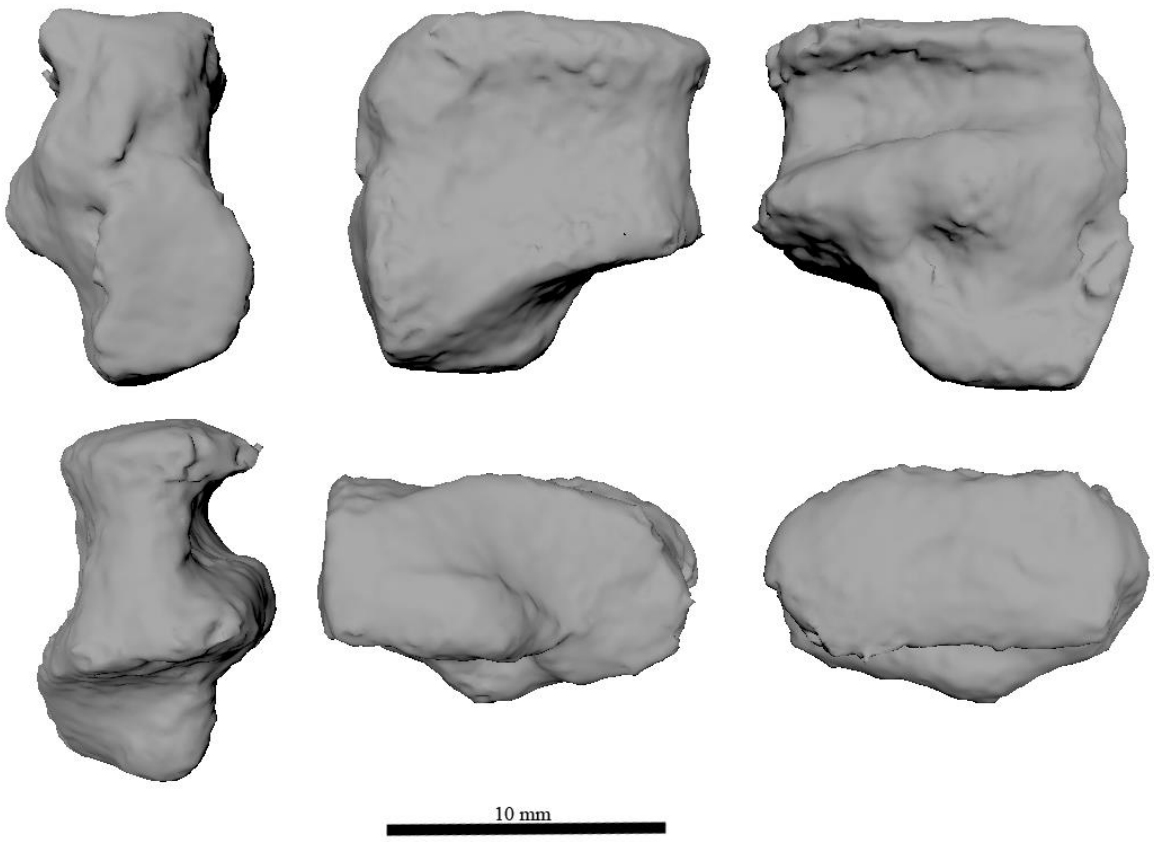

Figure 26: BA 83 right cuboid attributed to *Oreopithecus bambolii*. Top row views: medial, dorsal, plantar. Bottom row views: lateral, proximal, distal.

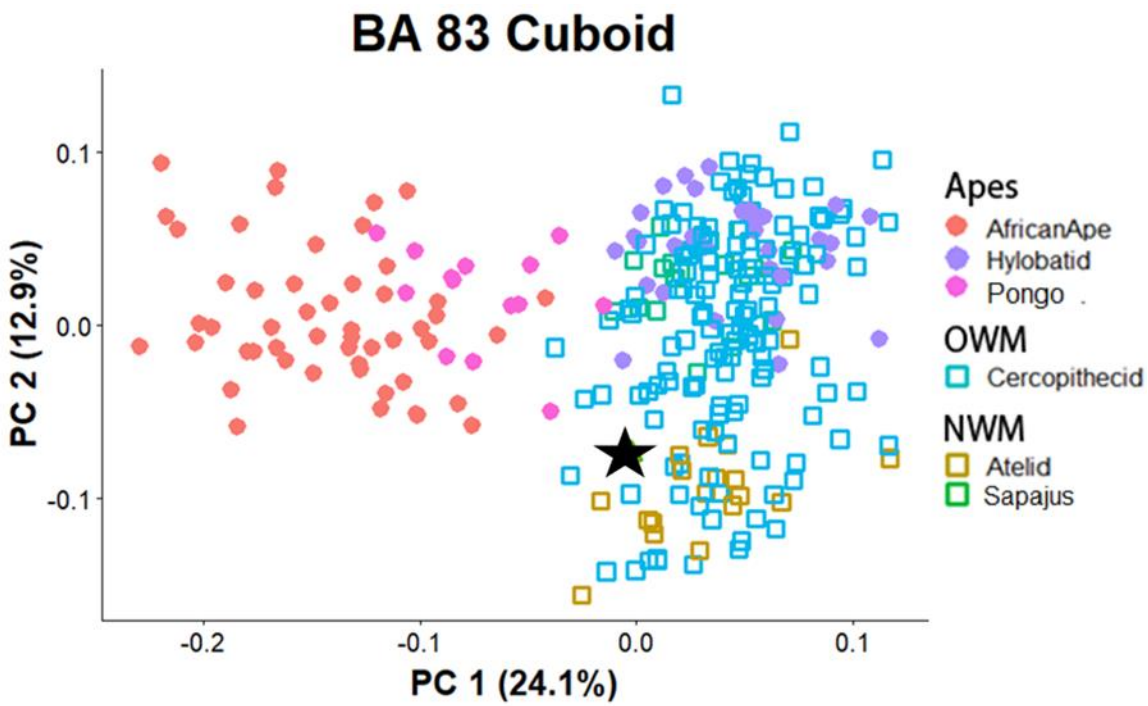

Figure 27: PCA of extant sample of cuboids from anthropoid primates using the same groups as in Chapter 3 (Table 3.3) with *Oreopithecus* (BA 83) cuboid indicated by a black star.

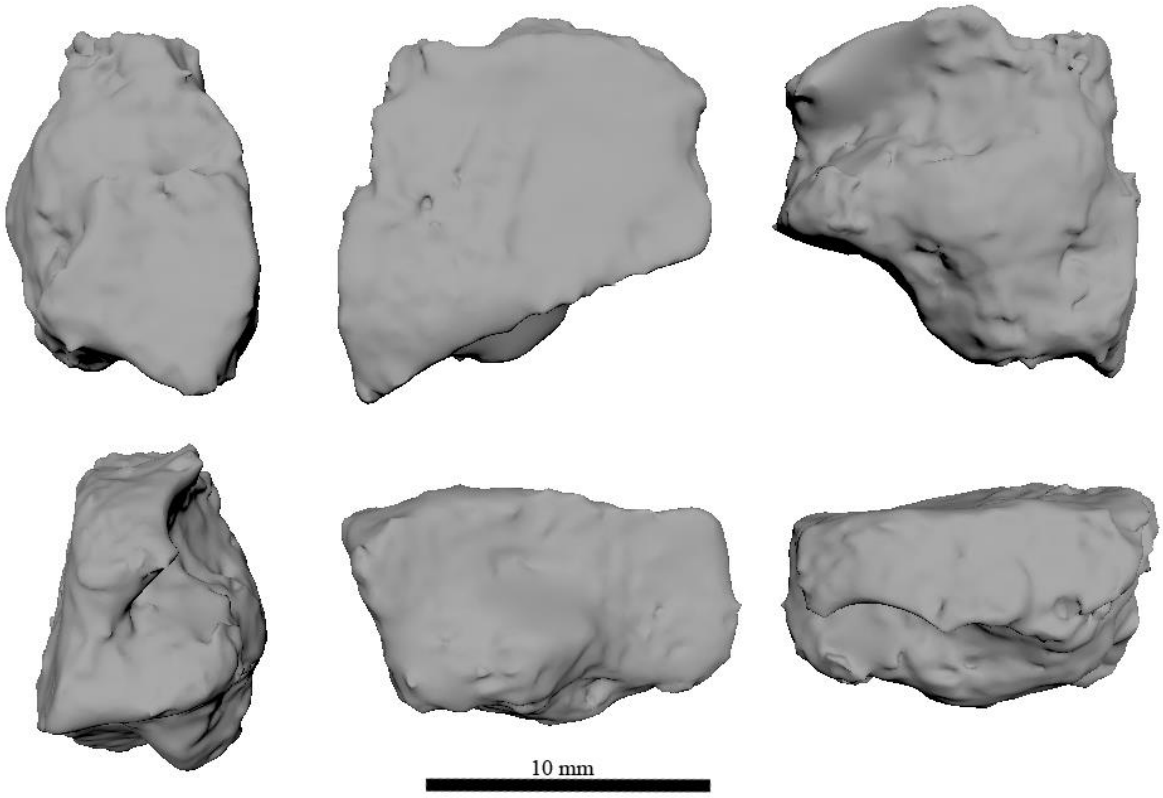

Figure 28: BA 158 right cuboid attributed to *Oreopithecus bambolii*. Top row views: medial, dorsal, plantar. Bottom row views: lateral, proximal, distal.

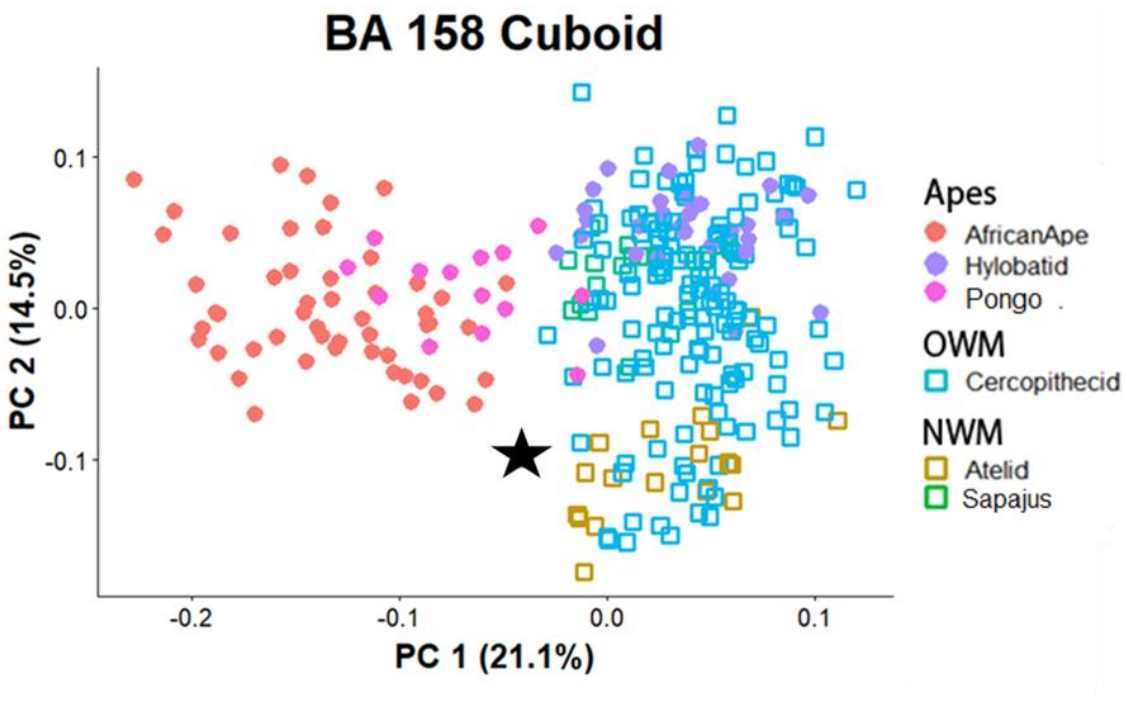

Figure 29: PCA of extant sample of cuboids from anthropoid primates using the same groups as in Chapter 3 (Table 3.3) with *Oreopithecus* (BA 158) cuboid indicated by a black star.

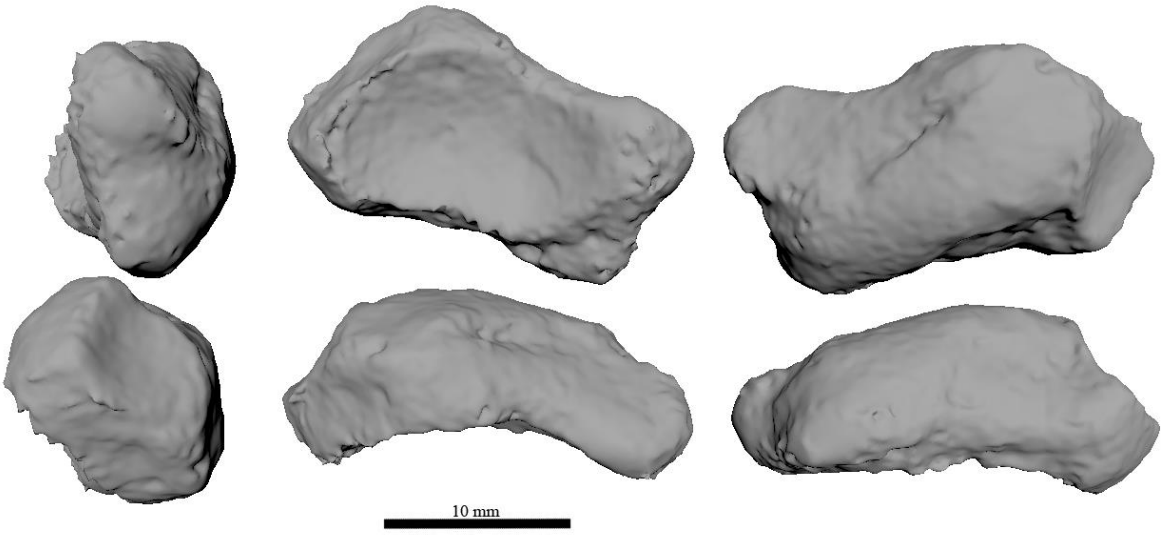

Figure 30: BA 79 left navicular attributed to *Oreopithecus bambolii*. Top row views: medial, proximal, distal. Bottom row views: lateral, dorsal, plantar.

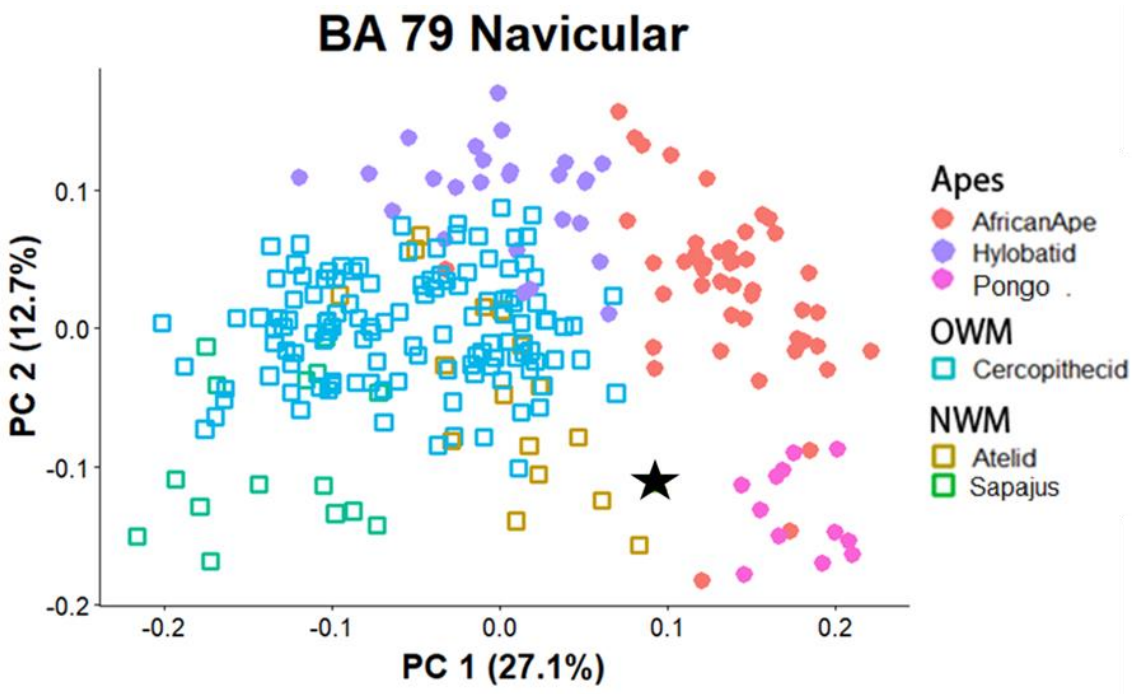

Figure 31: PCA of extant sample of naviculars from anthropoid primates using the same groups as in Chapter 3 (Table 3.3) with *Oreopithecus* (BA 79) navicular indicated by a black star.

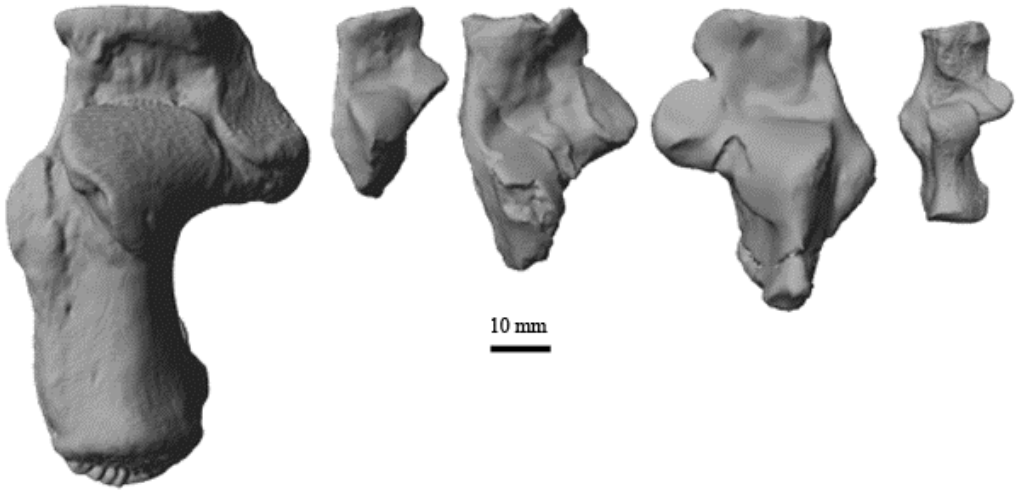

Figure 32: Proximal view of *Ekembo* calcaneus with extant comparisons. From left to right: *Gorilla*, *Ekembo heseloni* (KNM-RU 2036), *Ekembo nyanzae* (KNM-RU 5872), *Ekembo nyanzae* (KNM-MW 13142B), *Cercopithecus*.

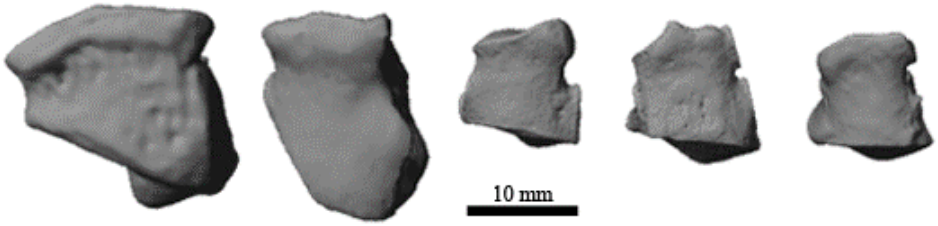

Figure 33: Dorsal view of *Ekembo* cuboids with extant comparisons. From left to right: *Pan, Ekembo* (KNM-RU 5872), *Ateles, Macaca, Cercopithecus.* Note that KNM-RU 5872 is damaged along the proximal lateral margin, giving it a wedged appearance.

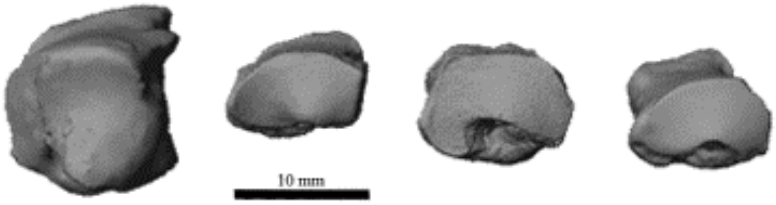

Figure 34: Proximal view of *Ekembo* cuboids with extant comparisons. From left to right: *Hylobates, Ekembo* (KNM-RU 5872), *Macaca, Ateles, Cercopithecus.*

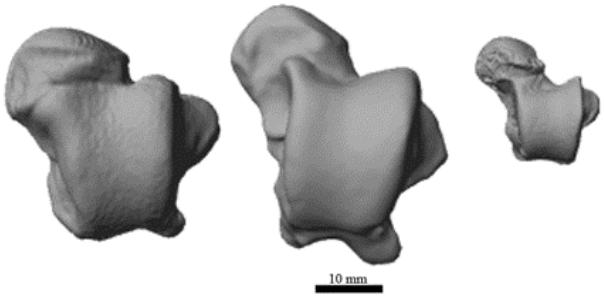

Figure 35: Proximal view of *Proconsul* talus with extant comparisons. From left to right: *Pan, Proconsul* (KNM-SO 389), *Macaca*.

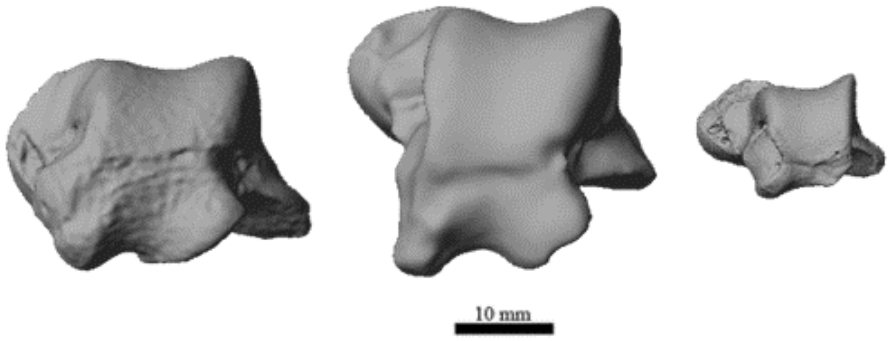

Figure 36: Posterior view of *Proconsul* talus with extant comparisons. From left to right: *Pan*, *Proconsul* (KNM-SO 389), *Macaca*.

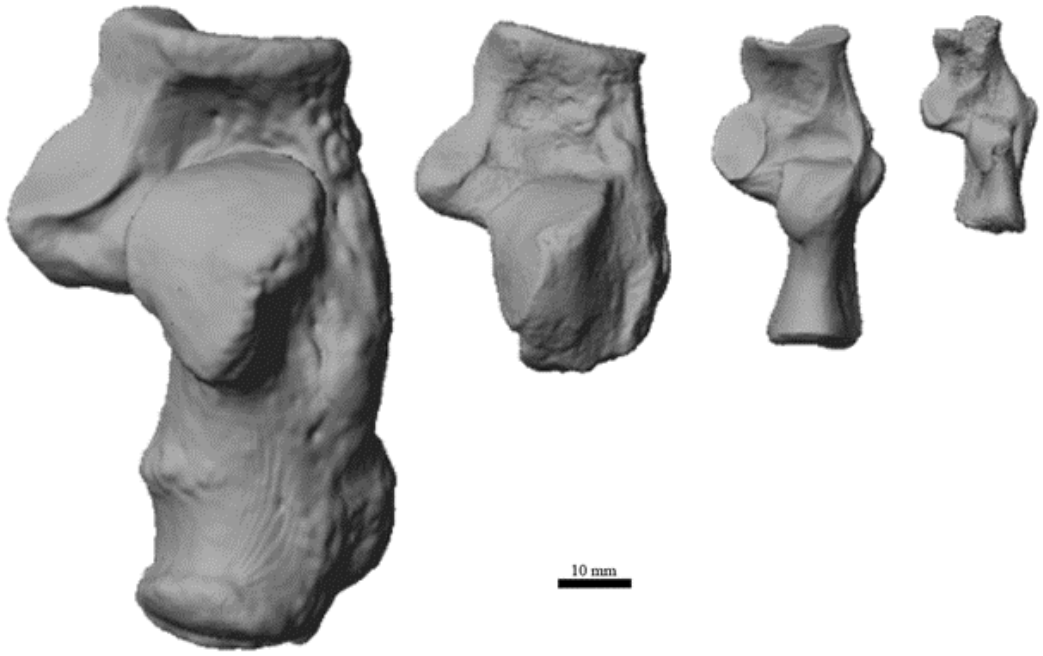

Figure 37: Proximal view of *Proconsul* calcaneus with extant comparisons. From left to right: *Gorilla*, *Proconsul* (KNM-SO 390), *Colobus*, *Sapajus*.

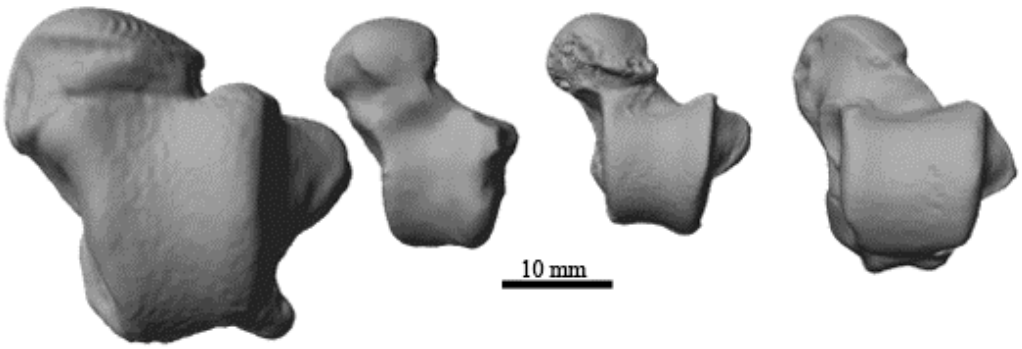

Figure 38: Proximal view of *Rangwapithecus* tali with extant comparisons. From left to right: *Pan, Rangwapithecus* (KNM-SO 968), *Macaca, Colobus*.

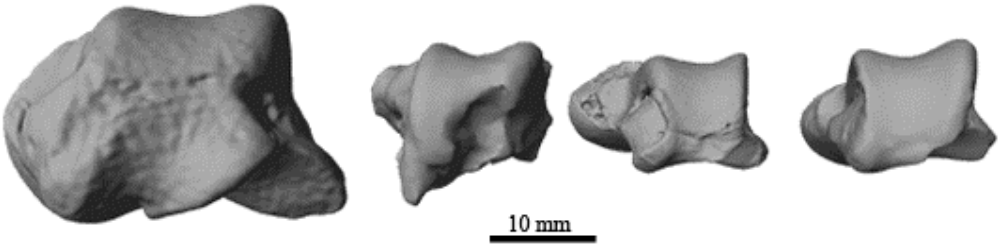

Figure 39: Posterior view of *Rangwapithecus* tali with extant comparisons. From left to right: *Pan, Rangwapithecus* (KNM-SO 968), *Macaca, Cercopithecus*.

Figure 40: Proximal view of *Rangwapithecus* calcaneus with extant comparisons. From left to right: *Gorilla*, *Rangwapithecus* (KNM-SO 427), *Cercopithecus*.

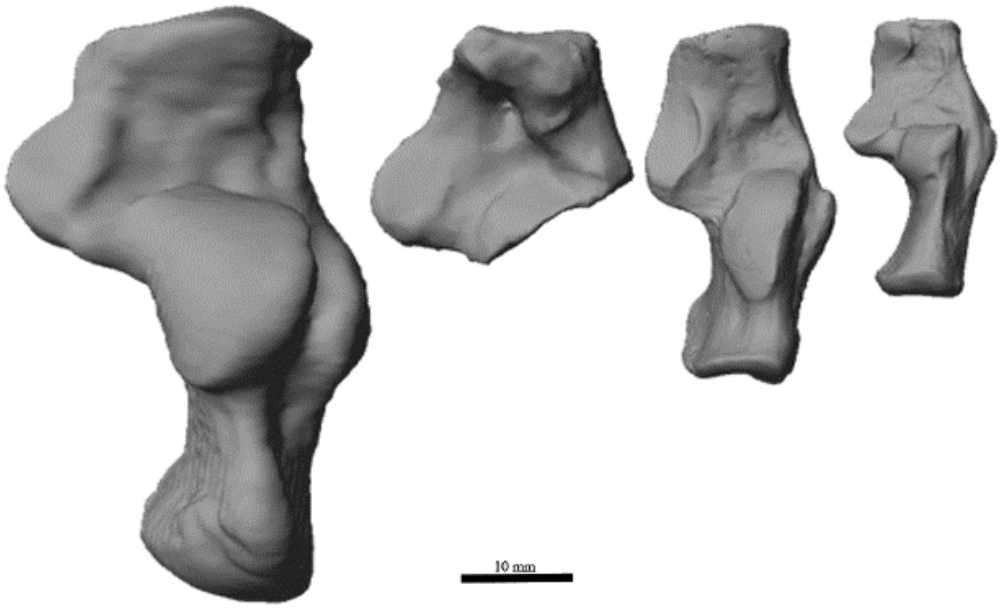

Figure 41: Proximal view of *Nacholapithecus* calcaneus with extant comparisons. From left to right: *Pongo*, *Nacholapithecus* (KNM-BG 35250O), *Ateles*, *Cercopithecus*.

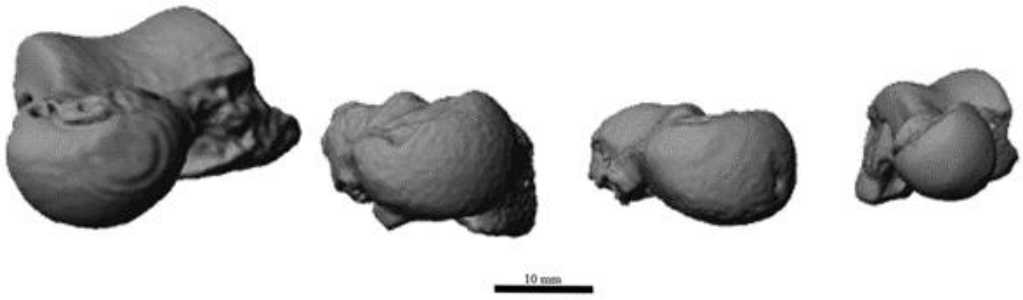

Figure 42: Anterior view of *Oreopithecus* talar heads with comparative tali. From left to right: *Pongo*, *Oreopithecus* (BA 79), *Oreopithecus* (BA 82), *Cercopithecus*.

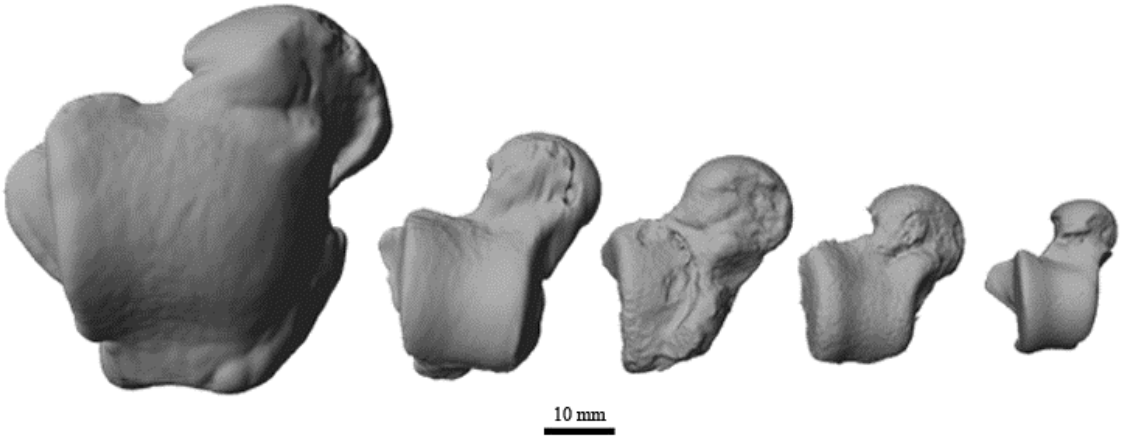

Figure 43: Proximal view of *Oreopithecus* tali with extant comparisons. From left to right: *Gorilla*, *Pongo*, *Oreopithecus* (BA 79), *Oreopithecus* (BA 82), *Cercopithecus*.

Figure 44: Proximal view of *Oreopithecus* calcanei with extant comparisons. From left to right: *Gorilla*, *Oreopithecus* (BA 79), *Oreopithecus* (BA 155), *Sapajus.*

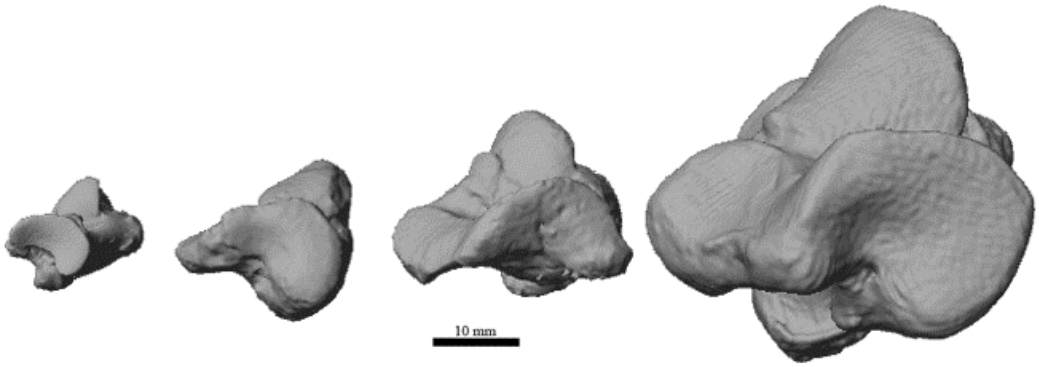

Figure 45: Distal view of *Oreopithecus* calcanei with extant comparisons. From left to right: *Sapajus*, *Oreopithecus* (BA 155), *Oreopithecus* (BA 79), *Gorilla.*

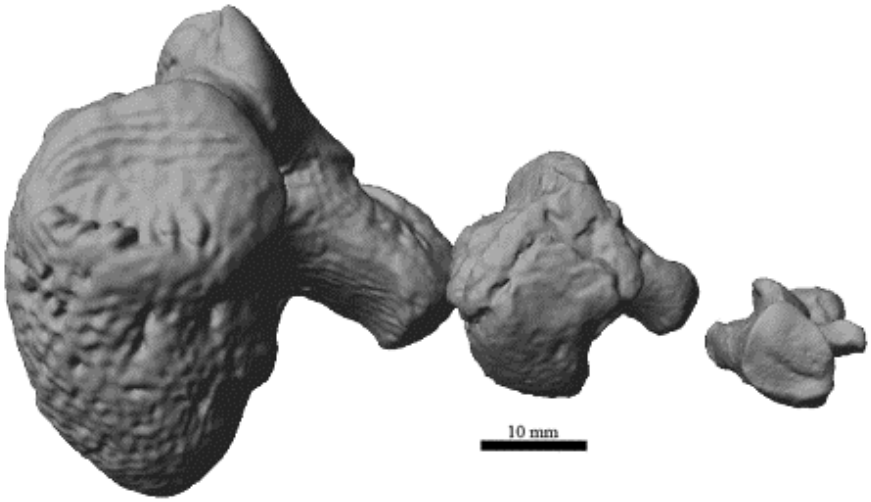

Figure 46: Posterior view of intact *Oreopithecus* calcanei with extant comparisons. From left to right: *Gorilla*, *Oreopithecus* (BA 79), *Sapajus.*

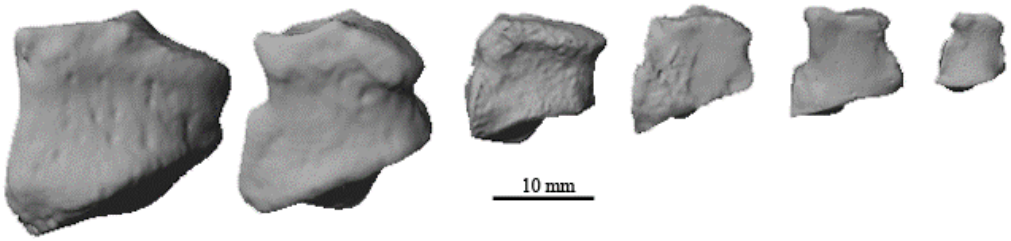

Figure 47: Dorsal view of *Oreopithecus* cuboids with extant comparisons. From left to right: *Gorilla, Pan, Oreopithecus* (BA 83), *Oreopithecus* (BA 158), *Ateles, Sapajus.*

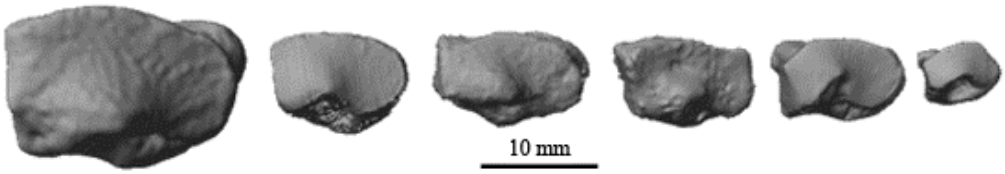

Figure 48: Proximal view of *Oreopithecus* cuboids with extant comparisons. From left to right: *Pan, Symphalangus, Oreopithecus* (BA 83), *Oreopithecus* (BA 158), *Ateles, Sapajus.*

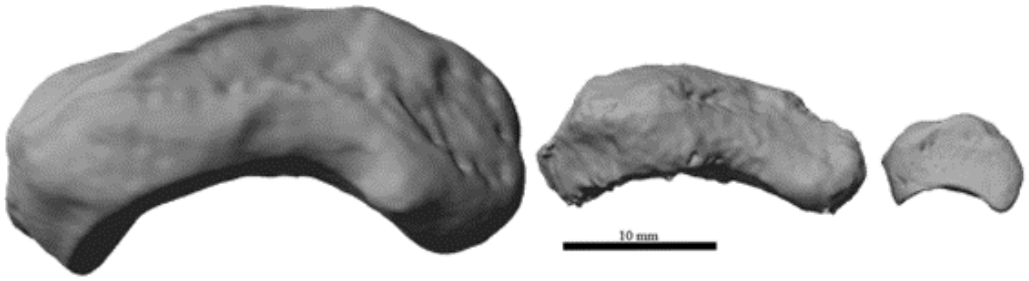

Figure 49: Proximal view of *Oreopithecus* naviculars with extant comparisons. From left to right: *Pan, Oreopithecus* (BA 79), *Sapajus.*

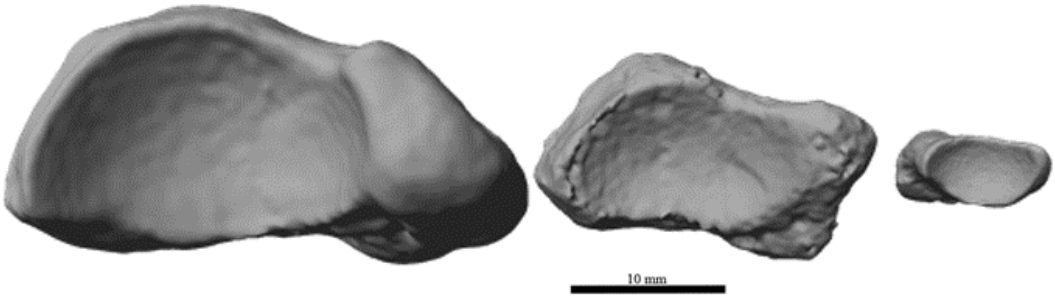

Figure 50: Proximal view of *Oreopithecus* naviculars with extant comparisons. From left to right: *Pan, Oreopithecus* (BA 79), *Sapajus.*

Tables:

Table 1: Fossil sample used in this study.

Element	Specimen	Genus	Species	Side	Landmarks taken	nlandmarks
Calcaneus	KNM-RU 2036	*Ekembo*	*heseloni*	Left	1, 2, 3, 4, 5, 6, 7, 8, 9, 18, 19, 20, 21	13
	KNM-MW 13142B	*Ekembo*	*nyanzae*	Right	1, 2, 3, 4, 5, 6, 7, 8, 9, 17, 18, 19, 21	13
	KNM-RU 5872	*Ekembo*	*nyanzae*	Left	1, 2, 3, 4, 6, 7, 8, 9, 18, 20	10
	KNM-BG 35250O	*Nacholapithecus*	*kerioi*	Right	2, 6, 7, 8, 9, 18, 19, 20, 21	9
	BA 155	*Oreopithecus*	*bambolii*	Left	2, 6, 7, 8, 9, 18, 19, 20, 21	9
	BA 79	*Oreopithecus*	*bamboili*	Left	1, 2, 3, 4, 5, 6, 7, 8, 9, 13, 18, 19, 20, 21	14
	KNM-SO 390	*Proconsul*	*major*	Right	1, 2, 3, 4, 5, 6, 7, 8, 9, 18, 19, 20, 21	13
	KNM-SO 427	*Rangwapithecus*	*gordoni*	Left	2, 3, 6, 7, 8, 9, 18, 20, 21	9
Cuboid	KNM-RU 5872	*Ekembo*	*nyanzae*	Left	1, 2, 13, 14, 15, 16, 17, 18, 19, 20	10
	BA 158	*Oreopithecus*	*bambolii*	Right	1, 2, 3, 4, 5, 6, 7, 8, 9, 10, 11, 12, 16, 17, 19, 20	16

	BA 83	*Oreopithecus*	*bambolii*	Right	1, 2, 3, 4, 5, 6, 7, 8, 9, 10, 11, 12, 13, 14, 15, 18, 19, 20	18
Navicular	BA 79	*Oreopithecus*	*bambolii*	Left	all	16
Talus	BA 79	*Oreopithecus*	*bambolii*	Left	23, 24, 25, 26, 27, 28	6
	BA82	*Oreopithecus*	*bambolii*	Left	1, 2, 3, 4, 5, 6, 7, 8, 9, 10, 11, 23, 24, 25, 26, 27, 28	17
	KNM-SO 389	*Proconsul*	*major*	Right	all	28
	KNM-SO 968	*Rangwapithecus*	*gordoni*	Right	1, 3, 4, 5, 6, 9, 10, 11, 12, 13, 23, 24, 25, 26, 27, 28	16

Chapter 5: Summary and Conclusions

Introduction

Locomotion is one of the most crucial aspects of survival for many organisms, but a major issue in the study of the evolution of locomotion is how to interpret function from bony morphology. This is particularly true in anthropoid primates, where understanding the evolution of locomotor diversity is intertwined with reconstructing locomotor adaptations of fossil taxa that have no living analogs. As such, reconstructing their locomotor behavior requires careful consideration of the functional anatomy of each joint. Sound locomotor reconstructions are critical to interpreting many of the key transitions in hominoid evolutionary history, not the least of which is the evolution of suspensory locomotion in Miocene hominoids.

Foot morphology is particularly useful in inferring locomotor repertoire, as feet interact directly with the substrate on which an animal is moving (Vereecke et al., 2005a; Boyer et al., 2013). The orientation and shape of joints were shown in this dissertation to reflect foot movements and posture and, therefore, how the foot was used. The functional morphology of the foot and ankle, a complicated anatomical region, has now been quantified in extant macaques *in vivo* for the first time and has been compared across extant anthropoid primates. Reconstructions based on isolated bones therefore now have a foundation in biomechanics and soft tissue contributions, resulting in a stronger tie between bony morphology and *in vivo* locomotion. Understanding how foot bone morphology reflects locomotion in extant primates has allowed for the interpretation of

the many tarsal bones known from Miocene fossil hominoids and improve our understanding of the locomotor repertoires of these fossil taxa. For some Miocene taxa, like *P. major* and *R. gordoni*, the majority of postcranial remains that have been discovered are tali and calcanei.

A more accurate connection between tarsal form and locomotor behavior is especially important but their functional relationship have traditionally not been well understood, as there were few validated biomechanical models on which to base locomotor interpretations. Bony morphology was previously hypothesized to reflect habitual posture and motion during key behaviors; however, we were limited by our lack of understanding of form-function relationships in the foot and ankle of primates. This has impeded our knowledge of how tarsals are affected by locomotion and our reconstructions of locomotion in fossil taxa.

Movements at the intertarsal joints had long been hypothesized to vary among anthropoids to reflect their suspensory, quadrupedal, arboreal and/or terrestrial locomotor specializations (Close et al., 1967; Inman, 1976; Chester et al., 2015; Holowka et al., 2017). This dissertation focused on the talocrural, subtalar, calcaneocuboid, and talonavicular of the foot, as they are thought to be primarily responsible for plantarflexion, dorsiflexion, inversion, eversion, and midfoot flexibility (Manter, 1941; Close et al., 1967; Holowka et al., 2017). In addition, the cuboid/MT5 joint was evaluated in Chapter 2 in order to answer questions about the midtarsal/midfoot flexibility.

Many hypotheses concerning *in vivo* movements at these joints were largely untested. This deficit was partially due to the difficulty in quantifying tarsal movements and relative positions during locomotion to relate this information to bone morphology.

By evaluating morphological variation among anthropoids at these intertarsal joints and using *in vivo* data to confirm and quantify differences in joint rotation, we now better understand the foot as a functional unit and have applied these ties between form and function to fossils.

Quantification of Rotations at the Talocrural, Subtalar, Calcaneocuboid, Talonavicular, and Lateral Tarsometatarsal Joints in Macaca mulatta *Using XROMM*

In Chapter 2, I quantified the amount of plantarflexion/dorsiflexion and inversion/eversion that occurred at the talocrural, subtalar, calcaneocuboid, cuboid/MT5, and talonavicular joints in macaques using markered XROMM. To my knowledge, this study was the first to visualize and quantify catarrhine intertarsal rotations using markered XROMM. This study confirmed previous hypotheses that the midfoot break occurs distal to the cuboid through direct measures of intrinsic foot movements. It also confirmed that plantarflexion/dorsiflexion predominantly occurred at the talocrural joint on a flat surface, which implies that species that mainly engage in propulsive quadrupedalism will have morphologies that emphasize stability in this parasagittal motion. This study confirmed that on a flat substrate, inversion and eversion occur at the subtalar joint and that inversion/eversion and plantarflexion/dorsiflexion are highly correlated with each other during locomotion. The transverse tarsal joint was found to not function as a single joint complex and should thus be treated as independent joints. Chapter 2 of the dissertation provided the basis of function for the evaluation of form in the rest of the dissertation. It served as a lens for functional interpretation of bony tarsal morphology and acted as a vehicle to assess whether bony variation among taxa that

locomote differently reflect the basic motions quantified in this chapter. Thus, the results of this study aid to better understand locomotor diversity among primates.

Analysis of Morphological Diversity in the Talus, Calcaneus, Cuboid, and Navicular Across Anthropoid Primate Taxa

Chapter 3 of this dissertation built upon the study of *in vivo* motions that occur at the talocrural, subtalar, calcaneocuboid, and talonavicular joints. The XROMM study, though it provided valuable information about intertarsal rotations, lacked the ability to infer phylogenetic, allometric, and locomotor patterns across taxa due to the use of a single species in a laboratory setting. Chapter 3 offered a broad analysis of a large sample of tarsals from 17 anthropoid primate taxa that vary in body size, phylogeny, and locomotion. Tarsals are complicated in shape and difficult to interpret, but are often preserved in the fossil record (Sarmiento & Marcus, 2000). As such, it is important to study tarsal morphology and what drives that variation in extant taxa before attempting to interpret fossil taxa. This study allowed me to parse out aspects of tarsal morphology that are driven by phylogeny, size, locomotion, or a combination of multiple factors. Although many aspects of tarsal morphology are driven by size and phylogeny, I also identified specific morphologies related to stability vs. mobility in the midfoot region, subtalar joint orientation, and inversion at the talocrural joint that separate suspensory from quadrupedal taxa: relative orientation of the posterior subtalar facet on the talus, talar neck length, calcaneal tuber height, calcaneal anterior length, cuboid length, and navicular anteroposterior length. This chapter provided a framework to study fossil material based on functional analyses of extant primate diversity.

Analysis of Morphological Indicators of Locomotion in Miocene Hominoids

Finally, in Chapter 4, I applied the results of Chapters 2 and 3 to Miocene hominoid tarsal fossils. I was able to confirm previous hypotheses about how these taxa navigated their environment, and also was able to provide more insights than previous studies based on functionally-relevant features of isolated tarsals. This study confirmed that early Miocene hominoids like *Ekembo*, *Proconsul*, and *Rangwapithecus* were predominantly above branch quadrupeds, all possessing tall trochleae for stability during plantarflexion, relatively long talar necks, and elongated anterior calcanei for more effective push off during quadrupedal locomotion. *Rangwapithecus,* however, also likely engaged in more varied locomotor behaviors than the other two early Miocene taxa, with a talar head and sustentaculum tali that are better suited for a variety of foot postures, much like extant apes. This led me to believe that *Rangwapithecus* was not only an above branch quadruped. *Nacholapithecus* also displayed mixed locomotor signals. *Nacholapithecus* was reconstructed to be mostly suspensory based on its relatively wider anterior calcaneus and less projecting sustentaculum tali, but also showed evidence for a mixed locomotor repertoire, including pronograde quadrupedalism in the CV plot. Finally, the tarsals attributed to *Oreopithecus* exhibit adaptations for suspensory locomotion including a flat, broad talar trochlea, a talar neck resembling that of *Pongo*, a relatively short anterior calcaneus, a less transverse posterior subtalar articular facet, and a tall and narrow posterior calcaneus, all characteristics of a suspensory ape, leading me to believe that it was not bipedal, as previously hypothesized.

Synthesis

The goal of this study was to understand form function relationships in the anthropoid primate foot. I wanted to better understand motion and morphology of the foot and better interpret the functional morphology of fossil taxa. Previous studies of this nature typically evaluated function without also considering the effect on bony form, or only evaluated form in the absence of kinematic function.

This began with a better understanding of the movements that occur at the intertarsal joints, which informed our understanding of foot function. This chapter was necessary to form the baseline of inferring function from form. Rather than basing morphological variation on hypothesized movements at the joints in question, XROMM analysis of the foot allowed me to test hypotheses about the motion that occurs between tarsals and to quantify the actual *in vivo* movement, which is rare in morphometrics studies and almost unheard of in primate foot locomotion morphometrics studies. This crucial first step grounded the remaining morphometrics analyses in a biomechanically-based reality.

Once intertarsal rotations had been calculated and interpreted in one taxon, a broad morphometrics analysis could be applied to different taxa. Geometric morphometrics allowed me to quantify bone shape in order to test hypotheses about shape variation in tarsals among anthropoid primate taxa. Parsing out features of isolated tarsal bones related to size, phylogeny, and locomotion in the previous chapter was important for the interpretation of this chapter. Gross similarities alone are cautioned against when interpreting Miocene fossils because many features of their tarsals stem from the fact that they are large hominoids. The lack of an extant large-bodied monkey

complicates our understanding of these taxa, and creates the risk of categorizing, for example, an arboreal quadruped that moves like a monkey as an ape due to phylogenetic or size-related morphologies rather than functional ones. A more thorough understanding of the features driving morphological variation in extant samples was applied to these fossils and these same methods can be applied to more fossil taxa for a more thorough understanding of primate locomotion.

Lastly, I applied these results to Miocene hominoid fossils. The information gained from the broad geometric morphometric analysis of extant tarsals, grounded in the quantification of foot movements during locomotion allowed me to interpret specific bony morphologies tied to locomotor differences. This aim provided new information about Miocene hominoid taxa, some of which lack complete postcranial skeletons, thereby limiting the interpretation of their locomotor repertoire to a functional morphological analysis of tarsal bones.

The three aims of this dissertation set out to characterize form and function relationships in the anthropoid primate foot. They answer the central question: how does bone morphology (i.e., form) reflect the manner in which an organism navigated its environment (i.e., function)? This central question stems from the ultimate goal of studying the evolution of primate locomotion coupled with a historical inability to infer function from form in the foot and ankle. The central question was then broken down into three questions. The first question was: how do primates move? The first aim of this study set the baseline of understanding the movements that occur in the region of interest. The second question was: how are these movements reflected the bones of taxa that move differently? The second aim of this study explored variation in morphological indicators

of locomotion in a wide array of primates. The third question was: how did extinct Miocene hominoids move? The third aim sought to answer this question by evaluating tarsals from the Miocene, a key time period in the evolution of locomotion in primates, especially of our own ape ancestors.

After isolating specific movements at intertarsal joints, such as the predominance of dorsi/plantarflexion at the talocrural joint, the importance of correlated movements at the subtalar joint, and the functional separation of the transverse tarsal joint, the effect of these movements were studied in bony specimens to provide the morphological input into understanding form function relationships in the anthropoid primate foot. This not only facilitated the analysis of the fossils discussed in Chapter 4, but also allowed for an exploration of how these movements differ among various taxa that vary in size, phylogeny, and locomotion. After identifying which aspects of morphology that vary phylogenetically and which are a product of the animal's size, aspects of morphology associated with locomotor differences were isolated. I found that the orientation of the subtalar facet on the talus varies with locomotion, which is not surprising given the importance of conjunct motions at this joint. The degree to which an animal requires inversion/eversion and dorsi/plantarflexion will vary based on their dependence on small-substrate grasping or foot inversion, which is evidenced in the articular facet orientation relative to the body of the talus. Calcaneal height differences were attributed to the difference in relative contribution to posterior foot height, with cercopithecids having taller trochleae related to their need to for stable plantarflexion at the talocrural joint. This talocrural plantarflexion was quantified in a cercopithecid in Chapter 2, showing that, although there was variation in how much movement occurred, it was the predominant

motion at this joint. Anterior calcaneal length and the elongation of the cuboid are both related to differences in midfoot flexion that occur during locomotion. Midfoot motion was found to be very important on the lateral side of the foot, at the calcaneocuboid joint, where roughly equal inversion/eversion and plantar/dorsiflexion occurred in the *in vivo* trials. Similarly in the isolated tarsals, midfoot length affects an animal's ability navigate either a small-branch environment or a flat surface. This was evidenced in the separation of suspensory versus non-suspensory taxa when this bony morphology was assessed. The medial midfoot also displayed elongation related to differences related to differences in substrate use. The differences among taxa were more pronounced in the navicular than the cuboid, which, makes sense in the context of the movements observed in Chapter 2. The increased movement of the navicular relative to the talus in the last part of the step, likely due to the pull of tibialis posterior muscle on the navicular tuberosity was observed during macaque locomotion.

These findings were then applied to some Miocene hominoids in order to reconstruct foot use. Early Miocene taxa share common bony features that suggest that they were generally above branch quadrupeds. *Nacholapithecus* showed a short, rounded sustentaculum tali and wide anterior calcaneus, similar to suspensory taxa, but also overlapped with above branch quadrupedalism, indicating a mixed or varied locomotor behavior. *Oreopithecus* was shown to not be bipedal, as previously hypothesized, but rather was suspensory.

Together, these three aims quantify detectable movement occurs in the foot, identify bony indicators of locomotor differences among primate taxa, and test hypotheses concerning the locomotor repertoires of Miocene hominoids, leading to a

more comprehensive understanding of form function relationships in anthropoid primate feet.

Future Directions

This dissertation creates multiple future research opportunities in order to expand upon the results presented here. Continuous rotations between steps can be analyzed in addition to the maximum rotations assessed in this dissertation in order to study not only the extreme movements that drives morphological differences, but also the rotations of the step overall. The increased prevalence of XROMM access and methodological advances provide the opportunity to vastly broaden the data collected for this study. In order to assess intraindividual variation in intertarsal mobility, more steps from the same two monkeys must be tracked and analyzed in a similar manner to this study and more of each step. This will provide a baseline for variability that a single individual exhibits in laboratory-controlled settings, which is reasonably assumed to result in less step variability than locomotion in a wild setting. These results will invariably affect our interpretation of primate kinematics based on a small sample size for a single individual, as well as our interpretation of fossil taxa kinematic variability, but it will also reduce possible the effect of error associated with noise, tracking error, and errant steps in this study. Furthermore, in order to assess interindividual variation, more macaques must be assessed using the same methods. This will allow us to assess how much of this dissertation was affected by the use of only two individuals. It would address concerns that the results of this study are based on pathological animals or those that would otherwise walk differently from other macaques.

The next logical step is to carry out XROMM procedures on more primates outside of macaques. The odds of performing XROMM on a non-human ape are, in my opinion, small so it is likely that future anthropoid primate XROMM studies would still be limited to monkeys. Monkeys, however, display a large range of locomotor behaviors, and there is great utility in comparing intertarsal mobility in a wide range of taxa. This study would allow us to better understand intertarsal mobility and foot function across many taxa, rather than being limited to one taxon and applying it to a broad range of taxa. Using a small taxon may necessitate the use of small tantalum beads in order to fit at least three markers per bone, but would allow us to collect data through the entire step, rather than only the second half.

In order to assess morphological diversity associated with differences in foot use in primates, particularly within the framework of suspensory versus non-suspensory locomotion, XROMM studies of primates that have different substrate preference (ideally a terrestrial quadruped versus a suspensory monkey of close phylogenetic similarity and of similar body size) moving on different substrates is an eventual goal of this line of research. Comparing rotations on a flat versus a branch-like substrate would provide even more information about intertarsal rotations in the primate foot. The ideal experimental design would be to have animals from a terrestrially quadrupedal species and a highly suspensory species each walk on a flat surface and a rope. I would compare the entire time series of rotations (not only maximum rotations) for multiple steps for each monkey. Multiple consecutive steps would allow us to better study gait mechanics associated with locomotion, rather than looking at parts of steps taken at different times.

The morphometrics study presented here shows the importance of many aspects of bone shape in differentiating taxa by phylogeny, body size, and locomotion. Many of the locomotor differences in the PCA were associated with relative orientation of the articular surfaces. Landmark data was not ideal for further exploring these aspects of morphology, a future study could further delve into this line of research. Fitting planes or surface meshes to articular surfaces and solely focusing on articular surface orientation can reveal even more patters of form-function relationships in the foot. Of course, expanding the sample of extant tarsals both in number within a taxon and number of taxa studied would be ideal in future studies.

One of the major problems associated with studying fossils is the fragmentary nature of many preserved specimens. This analysis used subsets of landmarks in order to account for parts of the fossils being missing, but future studies can impute the missing data using regression analyses from an extant reference sample (Richtsmeier et al., 1992). This would allow for the inclusion of all landmarks for each fossil rather than using subsetted data, which changes the distribution of variation in geometric morphometric studies.

Future studies of Miocene hominoid locomotion will include more taxa. Of particular interest would be analyzing the foot of the late Miocene genus *Ardipithecus,* which, like *Oreopithecus* in this study, has had multiple conflicting hypotheses about the manner in which it walked based on the foot alone (Lovejoy et al. 2009). A stiff lateral foot has been used to indicate that it walked bipedally, but an abducted hallux and mobile medial foot indicate that it engaged in climbing behaviors. A biomechanically-based analysis of the foot of *Ardipithecus* could shed light on its locomotion.

The further exploration of large bodied Miocene hominoids, such as *Sivapithecus* (Pilbeam et al. 1990), which strongly resembles an extant *Pongo* cranially and exhibits distal humeral morphology that indicates varied forearm postures, much like suspensory taxa (Rose 1994; Madar et al. 2002; Ward 2007; Morgan et al. 2016; McGechie et al., 2017), however, has a narrow torso and exhibits many postcranial features of a quadrupedal monkey (Rose, 1994; Madar et al., 2002). The reconstruction of *Sivapithecus* as an orangutan head on a monkey body is puzzling given the highly specialized suspensory locomotion of modern orangutans paired with the size of the animal and the lack of highly suspensory adaptations postcranially (Andrews and Cronin, 1982; Pilbeam et al., 1990; Madar et al., 2002). There are no large-bodied arboreal monkey taxa, so this presents the exciting opportunity to further explore allometric effects on locomotion in a body morphotype that does not exist today.

With the addition of human tarsals to the extant sample, this study can also be expanded into the study of Pliocene hominins to answer questions about foot stiffness. One of the major questions about the evolution of hominin locomotion in the Pliocene is when hominin feet stiffened, leading to one of the hallmarks of hominins: efficient bipedalism (DeSilva 2010; DeSilva & Throckmorton 2010; Ward et al. 2011). A reevaluation of hominin feet with a more in-depth knowledge of morphologies tied to foot stiffness, based on a comprehensive study of intertarsal rotations in a diverse sample of monkeys with varying foot stiffness, could expand our knowledge of the evolution of foot stiffness in the hominin fossil record.

References

Adams, D. C., Collyer, M. L., and Kaliontzopoulou, A. 2019. Geomorph: Software for geometric morphometric analyses. R package version 3.1.0. https://cran.r-project.org/package=geomorph.

Agoada, D., Kramer, P. A. 2019. The relationship between angular osteologic and radiographic measurements of the human talus and calcaneus. Journal of the American Podiatric Medical Association, 109(5), 327-344.

Alexander, R. M. 1982. *Locomotion of animals*, Vol. 163. Glasgow: Blackie.

Almécija, S., Moyà-Solà, S., Alba, D. M. 2010. Early origin for human-like precision grasping: a comparative study of pollical distal phalanges in fossil hominins. PLoS One, 5(7), e11727.

Almécija, S., Shrewsbury, M., Rook, L., Moyà-Solà, S. 2014. The morphology of *Oreopithecus bambolii* pollical distal phalanx. American Journal of Physical Anthropology, 153(4), 582-597.

Andrews, P., Cronin, J. E. 1982. The relationships of *Sivapithecus* and *Ramapithecus* and the evolution of the orang-utan. Nature, 297(5867), 541.

Anemone, R. L., Nachman, B. A. 2003. Morphometrics, Functional Anatomy. Tarsiers: past, present, and future, 97.

Arnold, C., Matthews, L. J., Nunn, C. L. 2010. The 10kTrees website: A new online resource for primate phylogeny. Evolutionary Anthropology, 19(3), 114-118.

Astley, H. C., Roberts, T. J. 2012. Evidence for a vertebrate catapult: elastic energy

storage in the plantaris tendon during frog jumping. Biology Letters, 8, 386–9.

Baier, D. B., Gatesy, S. M. 2013. Three-dimensional skeletal kinematics of the shoulder girdle and forelimb in walking *Alligator*. Journal of Anatomy, 223, 462–473.

Baier, D. B., Gatesy, S. M., Dial, K. P. 2013. Three-dimensional, high-resolution skeletal kinematics of the avian wing and shoulder during ascending flapping flight and uphill flap-running. PLoS ONE, 8(5), e63982.

Beard, K. C., Teaford, M. F., Walker, A. 1986. New wrist bones of *Proconsul africanus* and *P. nyanzae* from Rusinga Island, Kenya. Folia primatologica, 47(2-3), 97-118.

Beard, K. C., Teaford, M. F., Walker, A. 1993. New hand bones of the early Miocene hominoid *Proconsul* and their implications for the evolution of the hominoid wrist. In: Hands of Primates, pp. 387–403.

Begun, D. R. 1988. Catarrhine phalanges from the late Miocene (Vallesian) of Rudabánya, Hungary. Journal of Human Evolution, 17(4), 413-438.

Begun, D. R. 2007. Fossil record of Miocene hominoids. In: Henke, W.,Tattersall, I. (Eds.), Handbook of paleoanthropology. Heidelberg: Springer Verlag, pp. 921-977.

Beimers, L., Tuijthof, G. J. M., Blankevoort, L., Jonges, R., Maas, M., van Dijk, C. N. 2008. In-vivo range of motion of the subtalar joint using computed tomography. Journal of Biomechanics, 41(7), 1390-1397.

Benefit, B. R., McCrossin, M. L. 1995. Miocene hominoids and hominid origins. Annual Review of Anthropology, 24, 237–256.

Benjamini, Y., Hochberg, Y. 1995. Controlling the false discovery rate: a practical and powerful approach to multiple testing. Journal of the Royal Statistical Society: series B (Methodological), 57(1), 289-300.

Bennett, E. L., Davies, A. G. 1994. The ecology of Asian colobines. Colobine monkeys: Their ecology, behaviour and evolution, 129-171.

Bergeson, D. J. 1998. Patterns of Suspensory Feeding in *Alouatta palliata*, *Ateles geoffroyi*, and *Cebus capucinus*. In: Primate Locomotion. Springer, pp. 45–60.

Biewener, A. A. 1989. Mammalian terrestrial locomotion and size. Bioscience, 39(11), 776-783.

Biewener, A.A., Patek, S. 2018. *Animal locomotion*. Oxford University Press.

Bloch, J. I., Boyer, D. M. 2002. Grasping primate origins. Science, 298(5598), 1606-1610.

Bojsen-Møller, F. 1979. Calcaneocuboid joint and stability of the longitudinal arch of the foot at high and low gear push off. Journal of Anatomy, 129, 165–176.

Bonnan, M. F., Shulman, J., Varadharajan, R., Gilbert, C., Wilkes, M., Horner, A., Brainerd, E. 2016. Forelimb kinematics of rats using XROMM, with implications for small eutherians and their fossil relatives. PLoS ONE, 11, 1–21.

Boyer, D. M., Seiffert, E. R., Gladman, J. T., Bloch, J. I. 2013. Evolution and allometry of calcaneal elongation in living and extinct primates. PLoS One, 8(7), e67792.

Brainerd, E. L., Baier, D. B., Gatesy, S. M., Hedrick, T. L., Metzger, K. A., Gilbert, S. L., Crisco, J. J. 2010. X-ray reconstruction of moving morphology (XROMM): precision, accuracy and applications in comparative biomechanics research.

Journal of Experimental Zoology. Part A, Ecological Genetics and Physiology, 313, 262–279.

Brainerd, E. L., Moritz, S., Ritter, D. A. 2016. XROMM analysis of rib kinematics during lung ventilation on the green iguana, *Iguana iguana*. Journal of Experimental Biology, 219, E15–E15.

Bramble, D. M., Lieberman, D. E. 2004. Endurance running and the evolution of *Homo*. Nature, 432(7015), 345.

Byron, C. D., Covert, H. H. 2004. Unexpected locomotor behaviour: brachiation by an Old World monkey (*Pygathrix nemaeus*) from Vietnam. Journal of Zoology, 263, 101–106.

Camp, A. L., Brainerd, E. L. 2015. Reevaluating musculoskeletal linkages in suction-feeding fishes with X-Ray Reconstruction of Moving Morphology (XROMM). Integrative and Comparative Biology, 55, 36–47.

Cant, J. G.H., Youlatos, D., Rose, M. D. 2001. Locomotor behavior of *Lagothrix lagothricha* and *Ateles belzebuth* in Yasunı National Park, Ecuador: general patterns and nonsuspensory modes. Journal of Human Evolution, 41(2), 141-166.

Cant, J. G. H., Youlatos, D., Rose, M. D. 2003. Suspensory locomotion *of Lagothrix lagothricha* and *Ateles belzebuth* in Yasuni National Park, Ecuador. Journal of Human Evolution, 44, 685–699.

Cartmill, M. 1974. Pads and claws in arboreal locomotion. In: Jenkins, F.A. J. (Ed.), Primate Locomotion. Academic Press, New York, pp. 45–83.

Channon, A. J., Günther, M. M., Crompton, R. H., D'Août, K., Preuschoft, H., Vereecke,

E. E., 2011. The effect of substrate compliance on the biomechanics of gibbon leaps. The Journal of Experimental Biology, 214, 687–96.

Chester, S. G., Bloch, J. I., Boyer, D. M., Clemens, W. A. 2015. Oldest known euarchontan tarsals and affinities of Paleocene Purgatorius to Primates. Proceedings of the National Academy of Sciences, 112(5),1487-1492.

Close, J., Inman, V., Poor, P., Todd, F. 1967. The function of the subtalar joint. Clinical Orthopaedics and Related Research, 50, 159–179.

Cole, T. M. 2002. *WinEDMA*: Software for Euclidean distance matrix analysis. Kansas City: University of Missouri, Kansas City School of Medicine.

Conroy, G. C., Rose, M. D. 1983. The evolution of the primate foot from the earliest primates to the Miocene hominoids. Foot & ankle, 3(6), 342-364.

Cornwall, M. W. 2002. Motion of the Calcaneus, Navicular and First Metatarsal During the Stance Phase of Walking. Journal of the American Podiatric Medical Association, 92, 67–76.

Currier, A. F. 1911. The Foundation Library. New York, NY: The Educational Society.

Dagosto, M., Gebo, D. L. 1998. Methodological Issues in Studying Positional Behavior. In: Primate Locomotion. Springer, pp. 5–29.

D'Août, K., Aerts, P., De Clercq, D., De Meester, K., Van Elsacker, L. 2002. Segment and joint angles of hind limb during bipedal and quadrupedal walking of the bonobo (*Pan paniscus*). American Journal of Physical Anthropology, 119:37–51.

D'Août, K., Vereecke, E., Schoonaert, K., De Clercq, D., Van Elsacker, L., Aerts, P.

2004. Locomotion in bonobos (*Pan paniscus*): Differences and similarities between bipedal and quadrupedal terrestrial walking, and a comparison with other locomotor modes. Journal of Anatomy, 204, 353–361.

D'Août, K., Aerts, P. 2008. The evolutionary history of the human foot. Advances in plantar pressure measurements in clinical and scientific research. Maastricht: Shaker Publishing, 44-68.

Daver, G., Nakatsukasa, M. 2015. *Proconsul heseloni* distal radial and ulnar epiphyses from the Kaswanga Primate Site, Rusinga Island, Kenya. Journal of Human Evolution, 80, 17-33.

Delson, E. 1986. An anthropological enigma: Historical introduction to the study of *Oreopithecus bambolii*. Journal of Human Evolution, 15:523–531

DeSilva, J. M. 2008. Vertical climbing adaptations in the anthropoid ankle and midfoot: implications for locomotion in Miocene catarrhines and Plio-Pleistocene hominins. University of Michigan.

DeSilva, J. M. 2010. Functional morphology of the ankle and the likelihood of climbing in early hominins. Proceedings of the National Academy of Sciences of the United States of America, 106, 6567–6572.

DeSilva, J. M., Gill, S. V. 2013. Brief communication: a midtarsal (midfoot) break in the human foot. American Journal of Physical Anthropology, 151(3), 495-499.

DeSilva, J. M., Throckmorton, Z. J., 2010. Lucy's flat feet: The relationship between the ankle and rearfoot arching in early hominins. PLoS ONE. 5.

DeSilva, J. M., Bonne-Annee, R., Swanson, Z., Gill, C. M., Sobel, M., Uy, J., Gill, S.

2015. Midtarsal break variation in modern humans: Functional causes, skeletal correlates, and paleontological implications. American Journal of Physical Anthropology, 156, 543–552.

DeSilva, J., McNutt, E., Benoit, J., Zipfel, B. (2019). One small step: A review of Plio-Pleistocene hominin foot evolution. American Journal of Physical Anthropology, 168, 63-140.

Di Fiore, A., Campbell, C. J. 2007. The atelines: variation in ecology, behavior, and social organization. In: Primates in Perspective, pp. 155–185.

Disotell, T. R. 1996. The phylogeny of Old World monkeys. Evolutionary Anthropology: Issues, News, and Reviews, 5(1), 18-24.

Doran, D. M. 1997. Ontogeny of locomotion in mountain gorillas and chimpanzees. Journal of Human Evolution, 32(4), 323-344.

Dunn, R. H., Tocheri, M. W., Orr, C. M., Jungers, W. L. 2014. Ecological divergence and talar morphology in gorillas. American Journal of Physical Anthropology, 153, 526–541.

Dunsworth, H. M. 2006. *Proconsul heseloni* feet from Rusinga Island, Kenya. Pennsylvania State University.

Elftman, H., Manter, J. 1935. Chimpanzee and human feet in bipedal walking. American Journal of Physical Anthropology, 20, 69–79.

Engsberg, J. R., Andrews, J. G. 1987. Kinematic analysis of the talocalcaneal/talocrural joint during running support. Medicine and Science in Sports and Exercise, 19(3), 275-284.

Fleagle, J. G. 1976. Locomotion and Posture of the Malayan Siamang and Implications for Hominoid Evolution. Folia Primatologica, 26, 245–269.

Fleagle J. G. 1984. Primate Locomotion and Diet. In: Chivers D. J., Wood B. A., Bilsborough A. (Eds.), Food Acquisition and Processing in Primates. Springer, Boston, MA

Fleagle, J. G. 1985. Size and adaptation in primates. In: Size and Scaling in Primate Biology, (pp. 1-19). Springer, Boston, MA.

Gatesy, S. M., Baier, D. B., Jenkins, F. A., Dial, K. P. 2010. Scientific rotoscoping: a morphology-based method of 3-D motion analysis and visualization. Journal of Experimental Zoology. Part A, Ecological Genetics and Physiology, 313, 244–261.

Gebo, D. L. 1986. Anthropoid origins-the foot evidence. Journal of Human Evolution, 15, 421–430.

Gebo, D. L. 1988. Foot morphology and locomotor adaptation in Eocene primates. Folia Primatologica, 50, 3–41.

Gebo, D. L. 1989. Locomotor and phylogenetic considerations in anthropoid evolution. Journal of Human Evolution, 18, 201–233.

Gebo, D. L. 1992. Plantigrady and foot adaptation in African apes: implications for hominid origins. American Journal of Physical Anthropology, 89(1), 29-58.

Gebo, D. L. 1992b. Locomotor and postural behavior in *Alouatta palliata* and *Cebus capucinus*. American Journal of Primatology, 26(4), 277-290.

Gebo, D. L. 1993. Postcranial anatomy and locomotor adaptation in early African

anthropoids. In: Postcranial Adaptation in Nonhuman Primates, pp. 220–234.

Gebo, D. L. 2010. Locomotor function across primates (including humans). A Companion to Biological Anthropology, Wiley-Blackwell, pp. 530-544.

Gebo, D. L., Schwartz, G. T., 2006. Foot bones from Omo: Implications for hominid evolution. American Journal of Physical Anthropology, 129, 499–511.

Gebo, D. L., Dagosto, M., Beard, K. C., Qi, T. 2001. Middle Eocene primate tarsals from China: implications for haplorhine evolution. American Journal of Physical Anthropology, 116(2), 83-107.

Gebo, D. L., Simons, E. L., 1987. Morphology and locomotor adaptations of the foot in early Oligocene anthropoids. American Journal of Physical Anthropology, 74, 83–101.

Gebo, D. L., Smith, R., Dagosto, M., Smith, T. 2015. Additional postcranial elements of *Teilhardina belgica*: The oldest European primate. American Journal of Physical Anthropology, 156(3), 388-406.

Gervais, P. 1872. Sur un singe fossile, d'espèce non encore décrite, qui a été découvert au Monte Bamboli. Comptes Rendus Hebdomadaires des Séances de l'Académie des Sciences de Paris, 74, 1217-1223.

Gidmark, N. J., Konow, N., Lopresti, E., Brainerd, E. L. 2013. Bite force is limited by the force-length relationship of skeletal muscle in black carp, *Mylopharyngodon piceus*. Biology Letters, 9, 20121181.

Gidmark, N. J., Tarrant, J. C., Brainerd, E. L. 2014. Convergence in morphology and masticatory function between the pharyngeal jaws of grass carp,

Ctenopharyngodon idella, and oral jaws of amniote herbivores. The Journal of Experimental Biology, 217, 1925–1932.

Gomberg, D. N. 1985. Functional differences of three ligaments of the transverse tarsal joint in hominoids. Journal of Human Evolution, 14(6), 553-562.

Granatosky, M. C., Laird, M. F., Kuo, S., Alemseged, Z., Ross, C. F. 2018. An XROMM analysis of midfoot mobility in non-human primates. American Journal of Physical Anthropology, 165(S66), 104.

Grand, T. I. 1968. The functional anatomy of the lower limb of the howler monkey (*Alouatta caraya*). American Journal of Physical Anthropology, 28, 163–181.

Gregory, W. K. 1912. Notes on the principles of quadrupedal locomotion and on the mechanism of the limbs in hoofed animals. Annals of the New York Academy of Sciences, 22(1), 267-294.

Greiner, T. M., Ball, K. A. 2014. Kinematics of primate midfoot flexibility. American Journal of Physical Anthropology, 155, 610–620.

Griffin, N. L., Miller, C., Schmitt, D., D'Août, K. 2015. Understanding the evolution of the windlass mechanism of the human foot from comparative anatomy: insights, obstacles, & future directions. American Journal of Physical Anthropology, 156, 1–10.

Grueter, C. C., Li, D., Ren, B., Li, M. 2013. Substrate use and postural behavior in free-ranging snub-nosed monkeys (*Rhinopithecus bieti*) in Yunnan. Integrative Zoology, 8(4), 335-345.

Hamel, A. J., Sharkey, N., Buczek, F. L., Michelson, J. 2004. Relative motions of the

tibia, talus, and calcaneus during the stance phase of gait: A cadaver study. Gait and Posture, 20, 147–153.

Hammond, A. S. 2013. 3D analysis of hip joint mobility and the evolution of locomotor abilities in Miocene hominoids. University of Missouri.

Harcourt-Smith, W. 2002. Form and function in the hominoid tarsal skeleton. University College London.

Harrison, T. 1986. A reassessment of the phylogenetic relationships of *Oreopithecus bambolii gervais*. Journal of Human Evolution, 15, 541–583.

Hesse, B., Nyakatura, J. A., Fischer, M. S., Schmidt, M. 2015. Adjustments of limb mechanics in cotton-top tamarins to moderate and steep support orientations: Significance for the understanding of early primate evolution. Journal of Mammalian Evolution, 22, 435–450.

Hill, A., Odhiambo Nengo, I., Rossie, J. B. 2013. A *Rangwapithecus gordoni* mandible from the early Miocene site of Songhor, Kenya. Journal of Human Evolution, 65, 490–500.

Hintermann, B., Nigg, B. M., Sommer, C. 1994. Foot movement and tendon excursion: an in vitro study. Foot & Ankle International, 15, 386–395.

Holowka, N. B., O'Neill, M. C. 2013. Three-dimensional moment arms and architecture of chimpanzee (*Pan troglodytes*) leg musculature. Journal of Anatomy, 223, 610–628.

Holowka, N. B., O'Neill, M. C., Thompson, N. E., Demes, B. 2017. Chimpanzee ankle and foot joint kinematics: Arboreal versus terrestrial locomotion. American

Journal of Physical Anthropology, 104, 23–31.

Hunt, K. D., Cant, J. G., Gebo, D. L., Rose, M. D., Walker, S. E., Youlatos, D. 1996. Standardized descriptions of primate locomotor and postural modes. Primates, 37(4), 363-387.

Hunt, A. E., Smith, R. M., Torode, M. 2001. Extrinsic muscle activity, foot motion and ankle joint moments during the stance phase of walking. Foot & Ankle International. 22, 31–41.

Inman, V. T. 1976. The joints of the ankle. Williams and Wilkins, Baltimore.

Ishida, H., Kunimatsu, Y., Nakatsukasa, M., Nakano, Y. 1999. New Hominoid Genus from the Middle Miocene of Nachola, Kenya. Anthropological Science, 107, 189–191.

Ishida, H., Kunimatsu, Y., Takano, T., Nakano, Y., Nakatsukasa, M. 2004. *Nacholapithecus* skeleton from the Middle Miocene of Kenya. Journal of Human Evolution, 46, 69–103.

Jenkins, F. A. J. 1972. Chimpanzee bipedalism: cineradiographic analysis and implications for the evolution of gait. Science, 178, 877–879.

Jungers, W. L. 1985. Body size and scaling of limb proportions in primates. In: Size and scaling in primate biology (pp. 345-381). Springer, Boston, MA.

Jungers, W. L. 1987. Body size and morphometric affinities of the appendicular skeleton in *Oreopithecus bambolii* (IGF 11778). Journal of Human Evolution, 16(5), 445-456.

Jungers, W. L., Susman, R. L. 1984. Body size and skeletal allometry in African apes.

In The pygmy chimpanzee (pp. 131-177). Springer, Boston, MA.

Kambic, R. E., Roberts, T. J., Gatesy, S. M. 2015. Guineafowl with a twist: asymmetric limb control in steady bipedal locomotion. Journal of Experimental Biology, 218, 3836–3844.

Kanamoto, S., Ogihara, N., Nakatsukasa, M., 2011. Three-dimensional orientations of talar articular surfaces in humans and great apes. Primates, 52, 61–68.

Kelley, J. 1997. Paleobiological and phylogenetic significance of life history in Miocene hominoids. In: Function, Phylogeny, and Fossils. Springer, pp. 173–208.

Kimura, T. 2002. Primate limb bones and locomotor types in arboreal or terrestrial environments. Zeitschrift für Morphologie und Anthropologie, 201-219.

Klingenberg, C. P. 2011. MorphoJ: An integrated software package for geometric morphometrics. Molecular Ecology Resources, 11, 353–357.

Klingenberg, C. P., McIntyre, G. S. 2016. Geometric Morphometrics of Developmental Instability : Analyzing Patterns of Fluctuating Asymmetry with Procrustes Methods. Evolution, 52, 1363–1375.

Knigge, R. P., Tocheri, M. W., Orr, C. M., Mcnulty, K. P. 2015. Three-dimensional geometric morphometric analysis of talar morphology in extant gorilla taxa from highland and lowland habitats. The Anatomical Record, 298(1), 277-290.

Knörlein, B. J., Baier, D. B., Gatesy, S. M., Laurence-Chasen, J. D., Brainerd, E. L. 2016. Validation of XMALab software for marker-based XROMM. The Journal of Experimental Biology, 145383.

Köhler, M., Moyà-Solà, S. 1997. Ape-like or hominid-like? The positional behavior of

Oreopithecus bambolii reconsidered. Proceedings of the National Academy of Sciences of the United States of America, 94, 11747–11750.

Langdon, J. 1986. Functional morphology of the Miocene hominoid foot. Yale University.

Larson, S. G., Stern, J. T. 2006. Maintenance of above-branch balance during primate arboreal quadrupedalism: Coordinated use of forearm rotators and tail motion. American Journal of Physical Anthropology, 129, 71–81.

Latimer, B., Lovejoy, C. O. 1989. The calcaneus of *Australopithecus afarensis* and its implications for the evolution of bipedality. American Journal of Physical Anthropology, 78(3), 369-386.

Latimer, B., Ohman, J. C., Lovejoy, C. O. 1987. Talocrural joint in African hominoids: implications for *Australopithecus afarensis*. American Journal of Physical Anthropology, 74, 155–175.

Leardini, A., Benedetti, M. G., Catani, F. 1999. An anatomically based protocol for the description of foot segment kinematics during gait. Clinical Biomechanics, 14, 528.

Leardini, A., Stagni, R., O'Connor, J. J. 2001. Mobility of the subtalar joint in the intact ankle complex. Journal of Biomechanics, 34(6), 805-809.

Leardini, A., Benedetti, M. G., Berti, L., Bettinelli, D., Nativo, R., Giannini, S. 2007. Rear-foot, mid-foot and fore-foot motion during the stance phase of gait. Gait and Posture, 25, 453–462.

Lewis, O. J. 1980a. The joints of the evolving foot. Part II. The intrinsic joints. Journal of

Anatomy, 130(Pt 4), 833.

Lewis, O. J. 1980b. The joints of the evolving foot. Part III. The fossil evidence. Journal of Anatomy, 131(Pt 2), 275.

Lovejoy, C. O., Latimer, B., Suwa, G., Asfaw, B., White, T. D., 2009. Combining prehension and propulsion: the foot of *Ardipithecus ramidus*. Science (New York, N.Y.), 326, 72e1-e8.

Lundberg, A., 1989. Kinematics of the ankle and foot. *In vivo* roentgen stereophotogrammetry. Acta orthopaedica Scandinavica. Supplementum, 233, 1–24.

Lundberg, A., Svensson, O. K., Nemeth, G., Selvik, G. 1989. The axis of rotation of the ankle joint. Journal of Bone & Joint Surgery, British Volume, 71–B, 94–99.

Lycett, S. J., Collard, M. 2005. Do homoiologies impede phylogenetic analyses of the fossil hominids? An assessment based on extant papionin craniodental morphology. Journal of Human Evolution, 49(5), 618-642.

MacLatchy, L., Gebo, D. L., Kityo, R., Pilbeam, D. 2000. Postcranial functional morphology of *Morotopithecus bishopi*, with implications for the evolution of modern ape locomotion. Journal of Human Evolution, 39, 159–183.

Madar, S. I., Rose, M. D., Kelley, J., MacLatchy, L., Pilbeam, D. 2002. New *Sivapithecus* postcranial specimens from the Siwaliks of Pakistan. Journal of Human Evolution, 42, 705–52.

Manduell, K. L., Harrison, M. E., Thorpe, S. K. 2012. Forest structure and support availability influence orangutan locomotion in Sumatra and Borneo. American

Journal of Primatology, 74(12), 1128-1142.

Manter, J. T. 1941. Movements of the subtalar and transverse talar joints. The Anatomical Record, 80, 397–409.

McGechie, F., Kuo, S., Ward, C. V. 2017. Three-dimensional analysis of the distal humerus in catarrhines with implications for Miocene locomotor diversity. American Journal of Physical Anthropology, 162(S64), 282-283.

McGraw, W. S. 1998. Comparative locomotion and habitat use of six monkeys in the Tai Forest, Ivory Coast. American Journal of Physical Anthropology, 105(4), 493-510.

McNulty, K. P., Begun, D. R., Kelley, J., Manthi, F. K., Mbua, E. N. 2015. A systematic revision of *Proconsul* with the description of a new genus of early Miocene hominoid. Journal of Human Evolution, 84, 42–61.

McNutt, E. J., Zipfel, B., DeSilva, J. M. 2018. The evolution of the human foot. Evolutionary Anthropology: Issues, News, and Reviews, 27(5), 197-217.

Meldrum, D. J. 1991. Kinematics of the cercopithecine foot on arboreal and terrestrial substrates with implications for the interpretation of hominid terrestrial adaptations. American Journal of Physical Anthropology, 84, 273–289.

Menegaz, R. A., Baier, D. B., Metzger, K. A., Herring, S. W., Brainerd, E. L. 2015. XROMM analysis of tooth occlusion and temporomandibular joint kinematics during feeding in juvenile miniature pigs. Journal of Experimental Biology, 218, 2573– 2584.

Metz-Schimmerl, S. M., Bhatia, G., Vannier, M. W. 1994. Visualization and quantitative

analysis of talocrural joint kinematics. Computerized medical imaging and graphics, 18(6), 443-448.

Mittermeier, R. A. 1978. Locomotion and posture in *Ateles geoffroyi* and *Ateles paniscus*. Folia Primatologica, 30(3), 161-193.

Moore, K. L., Agur, A. M. R., Dalley, A. F. 2011. Essential Clinical Anatomy. 4th ed. Baltimore: Lippincott Williams & Wilkins.

Morgan, M. E., Lewton, K. L., Kelley, J., Otárola-castillo, E., Barry, J. C., Flynn, L. J. 2015. A partial hominoid innominate from the Miocene of Pakistan : Description and preliminary analyses. Proceedings of the National Academy of Sciences, 112, 82–87.

Morton, D. J. 1922. Evolution of the human foot. American Journal of Physical Anthropology, 5, 305–336.

Morton, D. J. 1924. Evolution of the human foot II. American Journal of Physical Anthropology, 7(1), 1-52.

Muybridge, E. 1887. *Animal locomotion*. Da Capo Press.

Naas, Paul. 2012. Autodesk Maya 2013 Essentials. Hoboken, NJ: Sybex.

Nakatsukasa, M., Kunimatsu, Y. 2009. Nacholapithecus and Its Importance for Understanding Hominoid Evolution. Evolutionary Anthropology, 18, 103–119.

Nakatsukasa, M., Yamanaka, A., Kunimatsu, Y., Shimizu, D., Ishida, H. 1998. A newly discovered *Kenyapithecus* skeleton and its implications for the evolution of positional behavior in Miocene East African hominoids. Journal of Human Evolution, 34, 657–664.

Nakatsukasa, M., Kunimatsu, Y., Nakano, Y., Takano, T., Ishida, H. 2003. Comparative and functional anatomy of phalanges in *Nacholapithecus kerioi*, a Middle Miocene hominoid from northern Kenya. Primates, 44(4), 371-412.

Nakatsukasa, M., Ward, C. V., Walker, A., Teaford, M. F., Kunimatsu, Y., Ogihara, N. 2004. Tail loss in Proconsul heseloni. Journal of Human Evolution, 46(6), 777-784.

Nakatsukasa, M., Kunimatsu, Y., Shimizu, D., Nakano, Y., Kikuchi, Y., Ishida, H. 2012. Hind limb of the *Nacholapithecus kerioi* holotype and implications for its positional behavior. Anthropological Science, 120731.

Napier, J. R., Davis, P. R. 1959. The forelimb skeleton and associated remains of *Proconsul africanus*. In: Fossil Mammals of Africa. British Museum of Natural History, pp. 1–69.

Netter, F. H. 2010. Atlas of Human Anatomy. Philadelphia, PA : Saunders/Elsevier.

O'Higgins, P., Jones, N. 1999. *Morphologika*. Tools for shape analysis. University College London, London, United Kingdom.

Orsbon, C. P., Gidmark, N. J., Ross, C. F. 2018. Dynamic musculoskeletal functional morphology: integrating diceCT and XROMM. The Anatomical Record, 301(2), 378-406.

Ouzounian, T. J., Shereff, M. J., 1989. In vitro determination of midfoot motion. Foot and Ankle. 10, 140–146.

Oxnard, C. E. 1973. Functional Inferences from Morphometrics: Problems Posed by Uniqueness and Diversity among the Primates. Systematic Biology, 22 (4), 409–

424.

Parr, W. C. H., Chatterjee, H. J., Soligo, C. 2012. Calculating the axes of rotation for the subtalar and talocrural joints using 3D bone reconstructions. Journal of Biomechanics, 45(6), 1103-1107.

Patel, B. A. 2010. Functional morphology of cercopithecoid primate metacarpals. Journal of Human Evolution, 58(4), 320-337.

Patel, B. A., Wallace, I. J., Boyer, D. M., Granatosky, M. C., Larson, S. G., Stern Jr, J. T. 2015. Distinct functional roles of primate grasping hands and feet during arboreal quadrupedal locomotion. Journal of Human Evolution, 88, 79-84.

Perelman, P., Johnson, W. E., Roos, C., Seuánez, H. N., Horvath, J. E., Moreira, M. A., Kessing, B., Pontius, J., Roelke, M., Rumpler, Y., Schneider, M. P. C. 2011. A molecular phylogeny of living primates. PLoS genetics, 7(3), e1001342.

Pilbeam, D., Rose, M. D., Barry, J. C., Shah, S. M. 1990. New *Sivapithecus* humeri from Pakistan and the relationship of *Sivapithecus* and *Pongo*. Nature, 348, 237–239.

Polly, P. D., Lawing, A. M., Fabre, A. C., Goswami, A. 2013. Phylogenetic principal components analysis and geometric morphometrics. Hystrix, the Italian Journal of Mammalogy, 24(1), 33-41.

Pontzer, H., Wrangham, R. W. 2004. Climbing and the daily energy cost of locomotion in wild chimpanzees: implications for hominoid locomotor evolution. Journal of Human Evolution, 46(3), 315-333.

Prang, T. C. 2016. Conarticular congruence of the hominoid subtalar joint complex with implications for joint function in Plio-Pleistocene hominins. American Journal of

Physical Anthropology, 160(3), 446-457.

Prang, T. C. 2019. The African ape-like foot of *Ardipithecus ramidus* and its implications for the origin of bipedalism. eLife, 8, e44433.

Prost, J. H. 1965. A definitional system for the classification of primate locomotion. American Anthropologist, 67, 1198–1214.

Puech, Pierre-François. 2018. Songhor hominoid holotype *Rangwapithecus maxilla* KNM-SO 700. Photo from: https://www.researchgate.net/publication/328807667_Songhor_hominoid_holotype_Rangwapithecus_maxilla_KNM-SO_700

R Core Team. 2013. R: A language and environment for statistical computing. R Foundation for Statistical Computing, Vienna, Austria. URL http://www.R-project.org.

Rafferty, K. L., Walker, A., Ruff, C. B., Rose, M. D., Andrews, P. J. 1995. Postcranial estimates of body weight in *Proconsul*, with a note on a distal tibia of *P. major* from Napak, Uganda. American Journal of Physical Anthropology, 97, 391–402.

Rasmussen, O., Tovborg-Jensen, I. 1982. Mobility of the ankle joint: recording of rotatory movements in the talocrural joint in vitro with and without the lateral collateral ligaments of the ankle. Acta Orthopaedica Scandinavica, 53(1), 155-160.

Remis, M. J. 1998. The gorilla paradox. In Primate locomotion (pp. 95-106). Springer, Boston, MA.

Revell, L. J. 2012. Phytools: an R package for phylogenetic comparative biology (and

other things). Methods in Ecology and Evolution, 3(2), 217-223.

Richtsmeier, J. T., Cheverud, J. M., Lele, S. 1992. Advances in anthropological morphometrics. Annual Review of Anthropology, 21(1), 283-305.

Riegger, C. L. 1988. Anatomy of the ankle and foot. Physical therapy, 68(12), 1802-1814.

Ripley, S. 1967. The leaping of langurs: A problem in the study of locomotor adaptation. American Journal of Physical Anthropology, 26, 149–170.

Rockar, Jr., P. A. 1995. The subtalar joint: anatomy and joint motion. Journal of Orthopaedic & Sports Physical Therapy, 21(6), 361-372.

Rollinson, J., Martin, R. D. 1981. Comparative aspects of primate locomotion, with special reference to arboreal cercopithecines. Symposia of the Zoological Society of London, 48.

Rome, K. 1996. Ankle joint dorsiflexion measurement studies. A review of the literature. Journal of the American Podiatric Medical Association, 86, 205–211.

Rook, L., Bondioli, L., Köhler, M., Moyà-Solà, S., Macchiarelli, R. 1999. *Oreopithecus* was a bipedal ape after all: evidence from the iliac cancellous architecture. Proceedings of the National Academy of Sciences, 96(15), 8795-8799.

Rose, M. D. 1973. Quadrupedalism in primates. Primates, 14(4), 337-357.

Rose, M. D. 1986. Further hominoid postcranial specimens from the Late Miocene Nagri formation of Pakistan. Journal of Human Evolution, 15, 333–367.

Rose, M. D. 1993. Locomotor anatomy of miocene hominoids. In: Postcranial Adaptation in Nonhuman Primates, pp. 252–272.

Rose, M. D. 1994. Quadrupedalism in some Miocene catarrhines. Journal of Human Evolution, 26, 387–411.

Russo, G. A., Shapiro, L. J. 2013. Reevaluation of the lumbosacral region of *Oreopithecus bambolii*. Journal of Human Evolution, 65, 253–265.

Sarmiento, E. E. 1987. The phylogenetic position of *Oreopithecus* and its significance in the origin of the Hominoidea. American Museum Novitates, 10024, 1–44.

Sarmiento, E. E., Marcus, L. F. 2000. The os navicular of humans, great apes, OH 8, Hadar, and *Oreopithecus*: function, phylogeny, and multivariate analyses. American Museum Novitates, 1-38.

Sarrafian, S. K. 1993. Biomechanics of the subtalar joint complex. Clinical Orthopaedics and Related Research, 17–26.

Schmidt, M. 2011. Locomotion and postural behaviour. Advances in Science and Research, 5(1), 23-39.

Schmitt, D. 2003. Substrate size and primate forelimb mechanics: implications for understanding the evolution of primate locomotion. International Journal of Primatology, 24(5), 1023-1036.

Schmitt, D., Rose, M. D., Turnquist, J. E., Lemelin, P. 2005. Role of the prehensile tail during ateline locomotion: Experimental and osteological evidence. American Journal of Physical Anthropology, 126, 435–446.

Senut, B., Nakatsukasa, M., Kunimatsu, Y., Nakano, Y., Takano, T., Tsujikawa, H., Shimizu, D., Kagaya, M., Ishida, H. 2004. Preliminary analysis of *Nacholapithecus* scapula and clavicle from Nachola, Kenya. Primates, 45(2), 97-

104.

Simons, E. A., Turley, K., Frost, S. R. 2019. Phylogenetic perspectives on catarrhine talo-crural joint phenotypic plasticity. The Anatomical Record, 302 (11), 1977-1984.

Smith, R. J., Cheverud, J. M. 2002. Scaling of sexual dimorphism in body mass: a phylogenetic analysis of Rensch's rule in primates. International Journal of Primatology, 23(5), 1095-1135.

Sondaar, P. Y., Van der Geer, A. A. E. 2002. Arboreal and terrestrial traits as revealed by the primate ankle joint. Hellenic Journal of Geosciences 87–98.

Strasser, E. 1988. Pedal evidence for the origin and diversification of cercopithecid clades. Journal of Human Evolution, 17, 225–245.

Stratovan Corporation. Stratovan Checkpoint. Version 2018.08.07. 2018. URL: https://www.stratovan.com/products/checkpoint.

Straus, W. L. 1940. The posture of the great ape hand in locomotion, and its phylogenetic implications. American Journal of Physical Anthropology, 27, 199–207.

Straus, W. L. 1963. The classification of *Oreopithecus*. In: Classification and Human Evolution, pp. 146–177.

Su, D. F., Jablonski, N. G. 2009. Locomotor behavior and skeletal morphology of the odd-nosed monkeys. Folia Primatologica, 80, 189–219.

Susman, R. L. 1984. The locomotor behavior of *Pan paniscus* in the Lomako forest. In: The Pygmy Chimpanzee. Springer, pp. 369–393.

Susman, R. L. 1987. Pygmy chimpanzees and common chimpanzees: models for the

behavioral ecology of the earliest hominids. The evolution of human behavior: Primate models, 72-86.

Susman, R. L. 2004. *Oreopithecus bambolii:* an unlikely case of hominidlike grip capability in a Miocene ape. Journal of Human Evolution, 46(1), 105-117.

Susman, R. L. 2005. *Oreopithecus*: still apelike after all these years. Journal of Human Evolution, 49(3), 405-411.

Swartz, S. M., Bertram, J. E., Biewener, A. A. 1989. Telemetered *in vivo* strain analysis of locomotor mechanics of brachiating gibbons. Nature, 342(6247), 270-272.

Taylor, G., Triantafyllou, M. S., Tropea, C. 2010. *Animal locomotion*. Springer Science & Business Media.

Theodor, J. M. 2001. Artiodactyla (Even-Toed Ungulates Including Sheep and Camels). eLS.

Thompson, N. E., Holowka, N. B., O'Neill, M. C., Larson, S. G. 2014. Brief communication: Cineradiographic analysis of the chimpanzee (*Pan troglodytes*) talonavicular and calcaneocuboid joints. American Journal of Physical Anthropology, 154, 604–608.

Thorpe, S. K., Crompton, R. H. 2006. Orangutan positional behavior and the nature of arboreal locomotion in Hominoidea. American Journal of Physical Anthropology 131(3), 384-401.

Thorpe, S. K. S., Crompton, R. H., Alexander, R. M. 2007. Orangutans use compliant branches to lower the energetic cost of locomotion. Biology Letters, 3(3), 253-

256.

Turley, K., Frost, S. R. 2014. The appositional articular morphology of the talo-crural joint: The influence of substrate use on joint shape. The Anatomical Record, 297(4), 618-629.

Vereecke, E. E., D'Août, K., Payne, R., Aerts, P. 2005a. Functional analysis of the foot and ankle myology of gibbons and bonobos. Journal of Anatomy, 206(5), 453-476.

Vereecke, E. E., D'Août, K., Van Elsacker, L., De Clercq, D., Aerts, P. 2005b. Functional analysis of the gibbon foot during terrestrial bipedal walking: Plantar pressure distributions and three-dimensional ground reaction forces. American Journal of Physical Anthropology, 128, 659–669.

Vereecke, E. E., Aerts, P. 2008. The mechanics of the gibbon foot and its potential for elastic energy storage during bipedalism. Journal of Experimental Biology, 211(23), 3661-3670.

Walker, A. 1974. Locomotor adaptations in past and present Prosimian primates. In: Jenkins, F.A.J. (Ed.), Primate Locomotion. Elsevier, pp. 349–382.

Walker, A. 1997. *Proconsul*: Function and Phylogeny. In: Begun, D. R., Ward, C. V., Rose, M. D. (Eds.), Function, Phylogeny, and Fossils. Plenum Press, New York, pp. 209–224.

Walker, A. C., Pickford, M. 1983. New Postcranial Fossils of *Proconsul africanus* and *Proconsul nyanzae*. In: Ciochon R. L., Corruccini R. S. (Eds.) New Interpretations of Ape and Human Ancestry. Advances in Primatology. Springer,

Boston, MA.

Wan, L., De Asla, R. J., Rubash, H. E., Li, G. 2006. Determination of *in-vivo* articular cartilage contact areas of human talocrural joint under weightbearing conditions. Osteoarthritis and Cartilage, 14(12), 1294-1301.

Ward, C. V. 1993. Torso morphology and locomotion in *Proconsul nyanzae*. American Journal of Physical Anthropology, 92, 291–328.

Ward, C. V. 1997. Functional anatomy and phyletic implications of the hominoid trunk and hindlimb. In: Function, Phylogeny, and Fossils. Miocene Hominoid Evolution and Adaptations, pp. 101–130.

Ward, C. V. 1998. *Afropithecus, Proconsul,* and the primitive hominoid skeleton. In: Primate locomotion, (pp. 337-352). Springer, Boston, MA.

Ward, C. V. 2007. Postcranial and Locomotor Adaptations of Hominoids. In: Handbook of Paleoanthropology. Springer, Berlin, pp. 1011–1030.

Ward, C. V., Begun, D. R., Rose, M. D. 1997. Function and Phylogeny in Miocene Hominoids. In: Function, Phylogeny, and Fossils. Miocene Hominoid Evolution and Adaptations, pp. 1-12.

Ward, C. V., Kimbel, W. H., Johanson, D. C., 2011. Complete fourth metatarsal and arches in the foot of *Australopithecus afarensis*. Science, 331, 750–753.

Ward, C. V., Maddux, S. D., Middleton, E. R. 2018. Three-dimensional anatomy of the anthropoid bony pelvis. American Journal of Physical Anthropology, 166(1), 3-25.

Ward, C. V., Walker, A., Teaford, M. F. 1991. *Proconsul* did not have a tail. Journal of

Human Evolution, 21, 215–220.

Webb, J. E., Wallwork, J. A., Elgood, J. H. 1977. Artiodactyles. In: Guide to Living Mammals. Classification guides, Palgrave, London.

Wright, D. G., Desai, S. M., Henderson, W. H. 1964. Action of the Subtalar and Ankle Joint Complex During Stance Phase of Walking. Journal of Bone & Joint Surgery. 46A, 361–464.

Wright, K. A. 2007. The relationship between locomotor behavior and limb morphology in brown (*Cebus apella*) and weeper (*Cebus olivaceus*) capuchins. American Journal of Primatology: Official Journal of the American Society of Primatologists, 69(7), 736-756.

Youlatos, D. 2003. Calcaneal features of the Greek Miocene primate *Mesopithecus pentelicus* (Cercopithecoidea: Colobinae). Geobios, 36(2), 229-239.

Youlatos, D., Koufos, G. D. 2010. Locomotor evolution of *Mesopithecus* (Primates: Colobinae) from Greece: evidence from selected astragalar characters. Primates, 51(1), 23.

Young, J. W., Heard-Booth, A. N. 2016. Grasping primate development: ontogeny of intrinsic hand and foot proportions in capuchin monkeys (*Cebus albifrons* and *Sapajus apella*). American Journal of Physical Anthropology, 161(1), 104-115.

Zelditch, M. L., Swiderski, D. L., Sheets, H. D. 2012. Geometric morphometrics for biologists: a primer. Academic Press.

Appendix

Phylogenetic analyses are often informative when studying bony morphology, as it removes analytical bias from the relatedness of taxa (Smith & Cheverud, 2001; Lycett & Collard, 2005; Polly et al., 2013). Phylogenetic PCA takes the non-independence of a sample into account and can reveal the functional aspects of morphological variation that are not solely due to phylogenetic proximity (Polly et al., 2013). However, a common issue when applying phylogenetic methods to anthropoid primate locomotion and foot use is that extant primates locomotor and phylogenetic patterns fall along similar lines (See Figure 1-11 for phylogenetic and locomotor relationships among the taxa studied here). Simons and colleagues cautioned against using morphological aspects of the talocrural joint for phylogenetic purposes, stating "when analyzing adult [talocrural joint] morphology, it is difficult to disentangle the signal of substrate usage from the phylogenetic information" (Simons et al., 2019, p. 1981). Although isolating function from phylogeny, the phylogenetic signal and locomotor signal in anthropoid primates mirror each other, and accounting for one in an alalysis may inadvertently remove the other.

In order to explore whether a phylogeneitc PCA would reveal results that were less biased but still carried a functional signal, phylogenentic PCA was run on the talus, calcaneus, cuboid, and navicular of the extant sample used in Chapters 3 and 4 (Figure 1-11; Table 3-1). Mean species values of procrustes-corrected landmarks for each bone were run using the tree shown in Figure 1-11 with the phyl.pca function in *Phytools*

(Revell, 2012) in R. The resulting phylogenetic PC scores were plotted in R.

PC 1 and PC 2 of the talus (Figure 1), calcaneus (Figure 2), cuboid (Figure 3), and navicular (Figure 4) show no meaningful separation or discernable patterns among extant anthropoid taxa. These results suggest that removing phylogeny from the PC analyses may have removed the parallel locomotor functional signal. Additional taxa, for example strepsirrhine primates, may allow for better separation of locomotor signal from phylogeny.

Figures for Appendix:

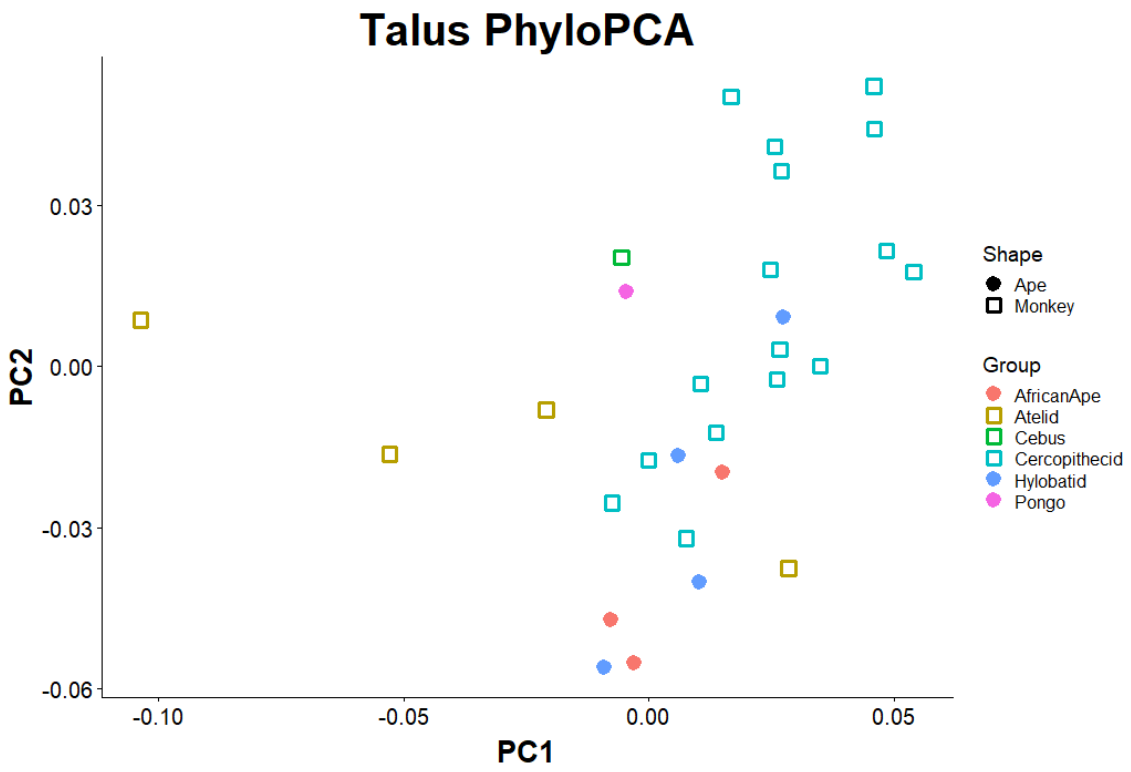

Figure 1: Phylogenetically-controlled PCA of the tali of extant taxa included in this dissertation.

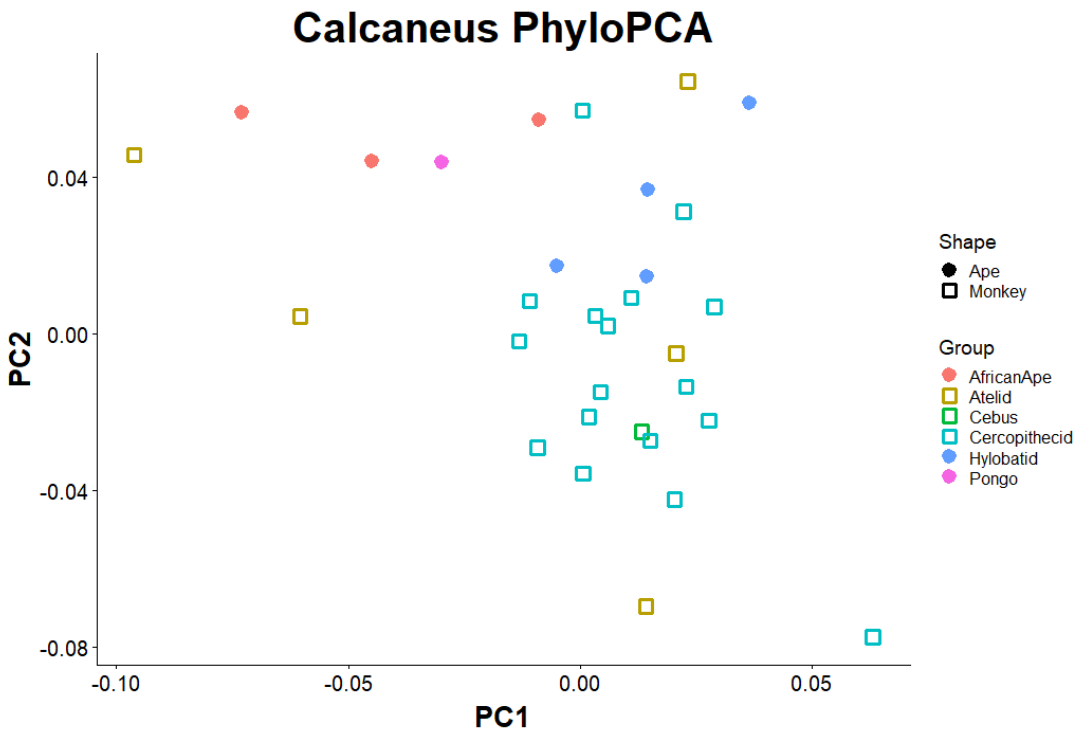

Figure 2: Phylogenetically-controlled PCA of the calcanei of extant taxa included in this dissertation.

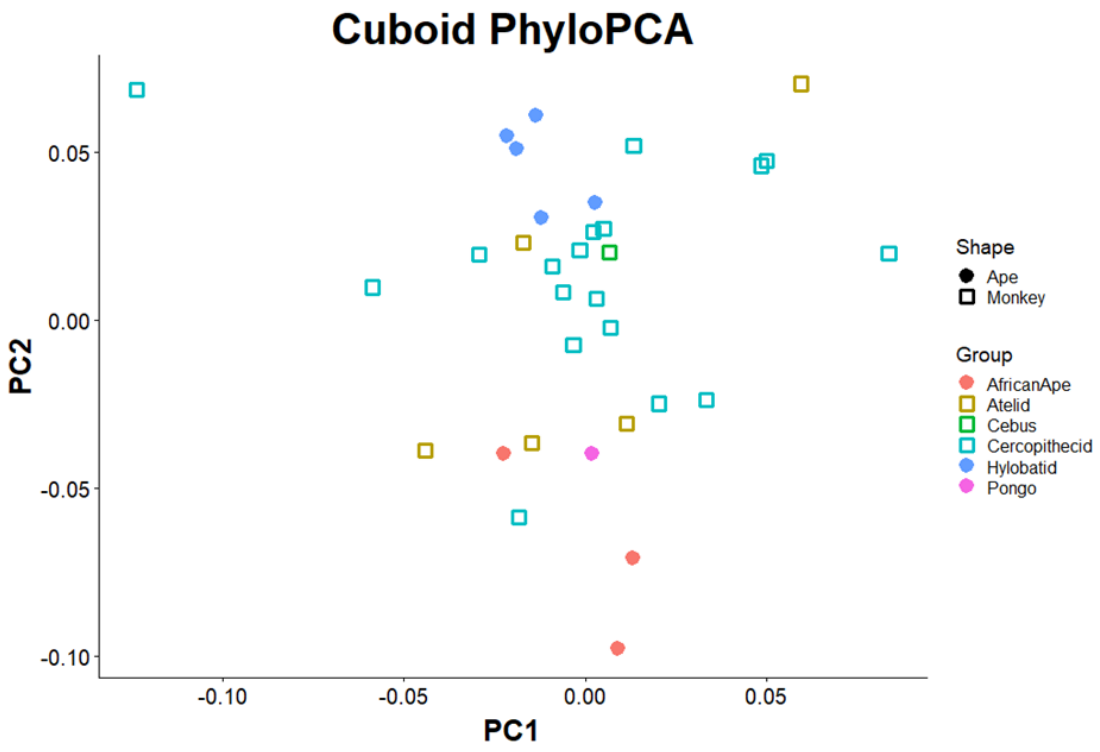

Figure 3: Phylogenetically-controlled PCA of the cuboids of extant taxa included in this dissertation.

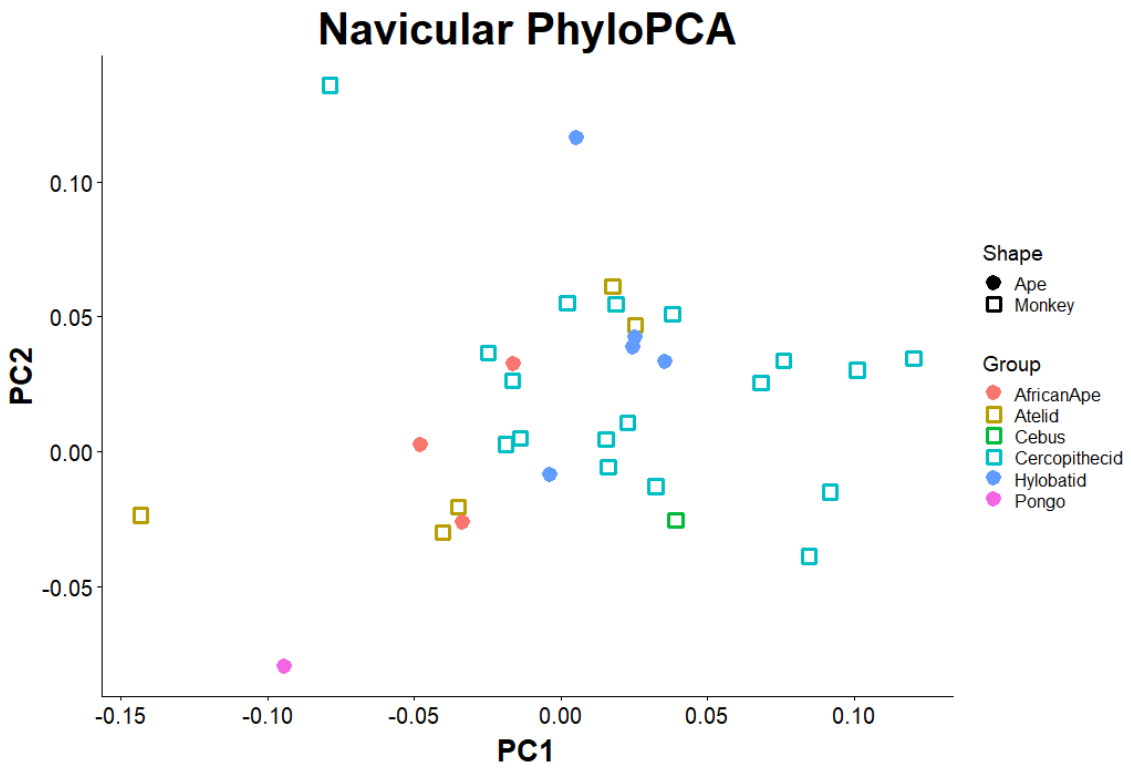

Figure 4: Phylogenetically-controlled PCA of the naviculars of extant taxa included in this dissertation.

Vita

Sharon grew up outside of San Francisco, CA and went to college at Boston University, where she discovered her interest in Biological Anthropology. A fortuitous meeting discussing research opportunities with Dr. Jeremy DeSilva led to a senior thesis on trabecular bone properties in the calcanei of primates, which solidified a strong interest in primate locomotion, anatomy, and funcitonal morphology that has driven her research ever since. Sharon graduated *magna cum laude* from BU with a major in Anthropology and a minor in Russian Language. She received practical training in forensic anthropology and an M.S. degree in Biological and Forensic Anthropology from Mercyhurst University in Erie, PA before beginning her doctorate studies at the University of Missouri. As a graduate student in the Integrative Anatomy department, she was able to further pursue her interest in anatomy and functional morphology, as well as teach gross anatomy, participate in paleoanthropological fieldwork in Kenya, and consult as a forensic anthropologist locally. She will continue her research endeavors as a Postdoctoral Scholar at Pennsylvania State University in the Department of Anthropology under the direction of Dr. Timothy Ryan.